



University
of Glasgow

Ismail, Rainah (2013) *Vibration analysis of a plate with an arbitrarily orientated surface crack*. PhD thesis.

<http://theses.gla.ac.uk/4002/>

Copyright and moral rights for this thesis are retained by the author

A copy can be downloaded for personal non-commercial research or study, without prior permission or charge

This thesis cannot be reproduced or quoted extensively from without first obtaining permission in writing from the Author

The content must not be changed in any way or sold commercially in any format or medium without the formal permission of the Author

When referring to this work, full bibliographic details including the author, title, awarding institution and date of the thesis must be given



VIBRATION ANALYSIS OF A PLATE WITH AN ARBITRARILY ORIENTATED SURFACE CRACK

Rainah Ismail

Submitted in fulfilment of the requirement for the
Degree of Doctor of Philosophy (PhD)

School of Engineering,
College of Science and Engineering,
University of Glasgow

December 2012

Abstract

This research presents a vibration analysis for a thin isotropic plate containing an arbitrarily orientated surface crack. The work has been motivated by the well known applicability of various vibrational techniques for structural damage detection in which the detection and localisation of damage to thin plate structures at the earliest stage of development can optimise subsystem performance and assure a safer life, and is intended to be an enhancement to previous work on cracked plates for which the orientation of the crack angle was not included. The novelty of this research activity has been in the assimilation of a significantly enhanced crack model within the analytical model of the plate, in modal space, and taking the form of a specialised Duffing equation. The governing equation of motion of the plate model with enhanced crack modelling is proposed to represent the vibrational response of the plate and is based on classical plate theory into which a developed crack model has been assimilated. The formulation of the angled crack is based on a simplified line-spring model, and the cracked plate is subjected to transverse harmonic excitation with arbitrarily chosen boundary conditions. In addition, the nonlinear behaviour of the cracked plate model is investigated analytically from the amplitude-frequency equation by use of the multiple scales perturbation method. For both cracked square and rectangular plate models, the influence of the boundary conditions, the crack orientation angle, crack length, and location of the point load is demonstrated. It is found that the vibration characteristics and nonlinear characteristics of the cracked plate structure can be greatly affected by the orientation of the crack in the plate.

The dynamics and stability of the cracked plate model are also examined numerically using dynamical systems tools for representing the behaviour of this system for a range of parameters. Finally the validity of the developed model is shown through comparison of the results with experimental work and finite element analysis in order to corroborate the effect of crack length and crack orientation angle on the modal parameters, as predicted by the analysis. The results show excellent predictive agreement and it can be seen that the new analytical model could constitute a useful tool for subsequent investigation into the development of damage detection methodologies for generalised plate structures.

Table of Contents

Abstract	iii
Table of Contents	iv
List of Tables.....	viii
List of Figures	ix
Acknowledgement.....	xii
Nomenclature	xiv
Chapter 1	17
Introduction	17
1.1 Motivation	17
1.2 Research Aims and Objectives.....	18
1.3 Thesis Overview	19
Chapter 2.....	21
Literature Review.....	21
2.1 Plate Structures.....	21
2.1.1 Vibration Problems in Plates.....	22
2.2 Nonlinearities	26
2.2.1 Nonlinear Plate Theory	26
2.2.2 Nonlinear Vibration of Plates.....	28
2.3 Damage Identification Methods in Plate Structures.....	32
2.4 Cracked Plate Structures	36
2.4.1 Vibration Analysis of a Cracked Plate Based on an Analytical Approach....	37
2.4.2 Vibration Analysis of a Cracked Plate based on the FE approach.....	40
2.4.3 Vibration Analysis of a Plate with a Variably Orientated Crack.....	42
2.4.4 Line-Spring Model (LSM).....	43

2.5	Perturbation Methods	46
2.5.1	Method of Multiple Scales	48
2.6	Routes to Chaos in Nonlinear Systems	51
Chapter 3	54
A Plate with a Surface Crack of Variable Angular Orientation	54
3.1	Introduction	54
3.2	Cracked Plate Modelling	54
3.3	The Classical Dynamic Equation of a Plate with Variably Orientated Crack.....	55
3.4	The equation of motion of a cracked plate including relevant forces in the middle plane of the plate	61
3.5	The Variably Orientated Crack Term Formulations	64
3.6	Application of Galerkin's Method	70
3.7	Application of the Berger Formulation	74
3.8	Enhanced Cracked Plate Simulation	79
3.8.1	A plate with a horizontally located centre crack, $\beta = 0^\circ$	79
3.8.2	A plate with a variably orientated surface crack	82
3.8.3	Factors which influence changes in the natural frequency	86
3.9	Chapter Conclusions.....	90
Chapter 4	91
Approximate Solution Methods	91
4.1	Introduction	91
4.2	Approximate Analytical Method: First Order Multiple Scales Method.....	91
4.2.1	Linear and Nonlinear frequency response curves	100
4.2.2	Factors that influence nonlinearity.....	100
4.3	Direct Integration Method	105

4.4	Numerical Solution Technique: FE Method (ABAQUS/CAE 6.9.1)	107
4.4.1	The sequence of steps required to perform the FE Analysis	108
4.4.2	Numerical Results	110
4.5	Chapter Conclusions	119
Chapter 5		120
Dynamical Systems Analysis		120
5.1	Introduction	120
5.2	Equation of Motions for Dynamical System Analysis	120
5.3	Numerical Methods: Mathematica™ code	122
5.4	Bifurcation Analysis	124
5.5	Lyapunov Exponents	125
5.6	Bifurcations as Functions of Normalised Excitation Acceleration	126
5.7	Time Plots, Phase Planes, and Poincaré Maps	140
5.7.1	Figures 5-11(a) to 5-25(a), showing Period-1 motion	141
5.7.2	Figures 5-11(b) to 5-25(b), showing Period-2 motion	142
5.7.3	Figures 5-11 (c) to 5-25(c), showing Period-4 motion	142
5.7.4	Figures 5-11(d) to 5-25(d), showing Chaotic motion	143
5.8	Chapter Conclusions	174
Chapter 6		175
Experimental Validation		175
6.1	Introduction	175
6.2	Plate Specimens	175
6.3	Experimental Setup and Procedure	176
6.4	Experimental results	178
6.5	Chapter Conclusions	179

Chapter 7	182
Comparative Study and Discussion	182
7.1 Introduction	182
7.2 Comparative Assessment	182
7.3 Discussions of Results.....	184
7.3.1 Analytical Results	184
7.3.2 Numerical Results	188
7.3.3 Experimental Results	189
Chapter 8	191
Conclusions	191
8.1 Summary and Conclusions.....	191
8.2 Recommendations for further work.....	193
List of References	195
Publications	215
Appendices.....	216

List of Tables

Table 3-1 : Natural frequencies of the intact and cracked plate models with a horizontal crack	81
Table 3-2 : Natural frequencies of the intact and cracked plate models with a variably orientated surface crack for the simply supported (SSSS) boundary condition, at various orientation angles.	82
Table 3-3 : Natural frequencies of the intact and cracked plate models with a variably orientated surface crack for the clamped-clamped simply supported (CCSS)	83
Table 3-4 : Natural frequencies of the intact and cracked plate models with a variably orientated surface crack for the clamped-clamped free-free (CCFF) boundary condition, at various orientation angles	84
Table 4-1 : Properties of the aluminium rectangular plate model for FE analysis	109
Table 4-2 : Frequency extraction analysis for 1 st , 2 nd , and 3 rd modes of vibration	112
Table 4-3 : Vibration mode shapes of cracked plates for half-crack length of 3 mm.....	115
Table 4-4 : Vibration mode shapes of cracked plates for half-crack length of 7.5 mm.....	117
Table 4-5 : Amplitude responses from the FE analysis	118
Table 5-1 : Data used for numerical simulations for the SSSS boundary condition.....	123
Table 5-2 : Data used for numerical simulations for the CCSS boundary condition.....	123
Table 5-3 : Data used for numerical simulations for the CCFF boundary condition.....	124
Table 5-4 : Period doubling bifurcation of cracked plate for the SSSS boundary condition and 0.003 m half-crack length.....	131
Table 5-5 : Period doubling bifurcation of cracked plate for the CCFF boundary condition.	140
Table 6-1 : Experimental results for the first three modes of vibration	179
Table 7-1 : Comparison of the frequency and amplitude response results	183
Table 7-2 : Comparison between the experimental and theoretical results	184

List of Figures

Figure 2-1: Position of the Vibration-Based Identification Methods.....	32
Figure 3-1 : A rectangular plate with a surface crack of length $2a$ orientated at an angle β to the horizontal x -axis and showing the bending and tensile stresses	56
Figure 3-2 : A plate structure loaded by uniform pressure with a variably orientated crack located at the centre of the plate.....	57
Figure 3-3 : In-plane forces acting on a plate with an arbitrarily orientated crack of length $2a$ located at the centre of the plate.....	61
Figure 3-4 : Boundary condition with two edges fixed and two edges free and subsequent deformation of the plate having an arbitrarily orientated crack at the centre of the plate (after Israr, 2008)	63
Figure 3-5 : A plate with an arbitrarily orientated surface crack loaded in tension and with a bending moment.....	65
Figure 3-6 : A cracked plate subjected to an arbitrarily located load, \bar{q}_z (Israr, 2008)	72
Figure 3-7: First mode natural frequency as a function of half-crack length.....	85
Figure 3-8: First mode natural frequency as a function of crack orientation angle	86
Figure 3-9 : β for maximum natural frequency as a function of half-crack length.....	87
Figure 3-10 : β for maximum natural frequency as a function of plate thickness	88
Figure 3-11 : β for maximum natural frequency as a function of plate aspect ratio	89
Figure 3-12 : β for maximum natural frequency as a function of Poisson Ratio	89
Figure 3-13 : β for maximum natural frequency as a function of (a) Density	90
Figure 4-1 : Linear and nonlinear response curves for the cracked square plate.....	101
Figure 4-2 : Linear and nonlinear response curves for the cracked rectangular plate	102
Figure 4-3 : Frequency response curves for a rectangular plate with a variably orientated surface crack for different locations of the applied load.....	103

Figure 4-4 : The influence of the excitation amplitude on the nonlinearity of the rectangular plate with a surface crack of variable orientation	104
Figure 4-5 : Comparison of nonlinear response curves for the cracked rectangular plate model with an aspect ratio of 1:2 between numerical integration and the method of multiple scales, for different crack orientation angles (Dotted line: NI, Solid line: MMS).	106
Figure 4-6 : 1 st , 2 nd and 3 rd vibration mode shapes for the intact plate	113
Figure 5-1 : An illustration of the divergence of trajectories (after Israr, 2008)	125
Figure 5-2 : Intact plate and the enlarged view of A1.....	128
Figure 5-3 : Bifurcation diagrams for SSSS boundary condition	129
Figure 5-4 : Bifurcation diagrams for SSSS boundary condition	131
Figure 5-5 : Intact plate and the enlarged view of A1.....	132
Figure 5-6 : Bifurcation diagrams for CCSS boundary condition	133
Figure 5-7 : Bifurcation diagrams for CCSS boundary condition	135
Figure 5-8 : Intact plate and the enlarged view of A1.....	136
Figure 5-9 : Bifurcation diagrams for CCFF boundary condition	137
Figure 5-10 : Bifurcation diagrams for CCFF boundary condition	139
Figure 5-11 : Dynamical systems analysis for an intact plate with SSSS boundary condition	145
Figure 5-12 : Dynamical systems analysis for a cracked plate with half-crack length of 0.003.....	147
Figure 5-13 : Dynamical systems analysis for a cracked plate with half-crack length of 0.003.....	149
Figure 5-14 : Dynamical systems analysis for a cracked plate with half-crack length of .151	
Figure 5-15 : Dynamical systems analysis for a cracked plate with half-crack length of .153	
Figure 5-16 : Dynamical systems analysis for an intact plate with CCSS boundary condition.....	155

Figure 5-17 : Dynamical systems analysis for a cracked plate with half-crack length of 0.003.....	157
Figure 5-18 : Dynamical systems analysis for a cracked plate with half-crack length of 0.003.....	159
Figure 5-19 : Dynamical systems analysis for a cracked plate with half-crack length of .	161
Figure 5-20 : Dynamical systems analysis for a cracked plate with half-crack length of .	163
Figure 5-21 : Dynamical systems analysis for an intact plate with CCF boundary condition.....	165
Figure 5-22 : Dynamical systems analysis for a cracked plate with half-crack length of 0.003.....	167
Figure 5-23 : Dynamical systems analysis for a cracked plate with half-crack length of 0.003.....	169
Figure 5-24 : Dynamical systems analysis for a cracked plate with half-crack length of .	171
Figure 5-25 : Dynamical systems analysis for a cracked plate with half-crack length of .	173
Figure 6-1 : Classification of experimental crack orientations, dark dot denoting excitation location point.....	176
Figure 6-2 : Layout of the experimental setup.....	177
Figure 6-3 : The experimental test rig.....	178
Figure 6-4 : Frequency responses for the first three modes of vibration	181

Acknowledgement

All praise is due to Allah. May Allah's peace and blessings be upon the one after whom there is no other prophet.

It takes more than determination and hard work for the completion of this dissertation. Supports I received from many people throughout my years here at University of Glasgow undeniably played an important role.

First of all, I express my profound sense of reverence to my amazing supervisor, James Watt Professor Matthew Phillip Cartmell, of University of Glasgow. His encouragement helped me to keep focused throughout the process, providing guidance and motivation that often meant progress rather than stagnation, challenging me to think critically and outside my comfort zone, and honing my research skills. The insightful comments, inspiration and superior knowledge undoubtedly resulted in significant contributions to the development of this dissertation. I forever indebted for his understanding and support to help me go through difficult and challenging times of being full time student as well as mother of two young children. The good advice and support of Professor Margaret Lucas, who apart from helping me cross the finish line, has also been invaluable which I am extremely grateful.

Very special thanks to the Ministry of Higher Education of Malaysia and University Technical Malaysia Melaka (UTeM) for opportunity as well as financial support in this study.

In addition, my sincere gratitude is reserved for Dr. Olga A. Ganilova, whom not only becomes a close friend over these years, but also a wise adviser to me. Without her technical advice, guidance, and invaluable assistance to technical aspect, this dissertation would not been a success. Needless to mention, experimental obstacles might not able to be coped without the assistances of technical staffs. Hereby I would like to express my sincere appreciation to Mr. Brian Robb and Mr. Bernard Hoey, Mr. Ken McColl, and Mr. Walter Robinson for their help and patience in providing me the resources in completing this dissertation.

To my family and friends, my greatest treasures and gifts in my life, thank you. I am forever grateful to my parents, sibling and my in-laws for instilling in me a desire to achieve my goals and a commitment to finish what I start, to the best of my ability, no

matter what it takes. This dissertation was definitely a challenge and did not eventuate without many sacrifices. To my beloved husband Masrullizam Mat Ibrahim, thank you for your patience and support. He has been a constant source of strength and inspiration, a rock in my life. Finally, I would like to express my deepest appreciation and love to my lovely son Muhammad Amir Najwan and my beautiful daughter Aliyah Damia. Thank you for blessing me with your presence, wisdom, patience and good humour. You have kept my life in perspective and taught me the lessons in life of what really matter.

With all my heart, I would like to thank my sweetest friends Rosazra Roslan, Norilmi Amalia Ismail, Zaleha Mustafa, Rafidah Hasan, Saodah Mohamed, Rosnita Tamjis and Siti Amaliah Tun Shaleha Mohd Yasin very warmly for their continuous help, permanent enthusiasm, friendship, and for being with me on this long journey of contemplation, tears and sweat.

For myself, this dissertation has been a personal accomplishment which I hope will benefit others as much as it has to me.

Nomenclature

Symbols	Description
D	Flexural rigidity
E	Modulus of Elasticity
ν	Poisson's ratio
ρ	Density of the plate
w	Transverse deflection
n_x, n_y, n_{xy}, n_o	In-plane forces per unit length
h	Thickness of the plate
Q_x, Q_y	Forces per unit length acting on the plate element
q_z	Load per unit area
M_x, M_y, M_{xy}, M_o	Bending moments per unit length
$\sigma_x, \sigma_y, \tau_{xy}$	Bending and shear stresses
\bar{M}_y, \bar{M}_{xy}	Bending moment due to crack, per unit length
\bar{n}_y, \bar{n}_{xy}	In-plane force due to crack, per unit length
$\bar{\sigma}_{mn}, \bar{m}_{mn}$	Nominal tensile and bending stresses at the crack location
$\bar{\sigma}_{pq}, \bar{m}_{pq}$	Tangential tensile and bending stresses at the crack location
σ_{mn} and m_{mn}	Nominal tensile and bending stresses at the far sides of the plate
σ_{pq} and m_{pq}	Tangential tensile and bending stresses at the far sides of the plate
\bar{n}_{mn}	Force per unit length in the y-direction
\bar{M}_{mn}	Moment per unit length in the y-direction
\bar{n}_{pq}	Force per unit length in the x-y-direction
\bar{M}_{pq}	Moment per unit length in the x-y-direction
a	Half crack length
β	Crack orientation angle

α_{tt}, C_{tt}	Nondimensional stretching compliance coefficients
α_{bb}, C_{bb}	Nondimensional bending compliance coefficients
$\alpha_{bt} = \alpha_{tb}, C_{bt} = C_{tb}$	Nondimensional stretching-bending compliance coefficients
X_i, Y_j	Characteristic or modal functions of the cracked plate
A_{ij}	Arbitrary amplitude
$\psi_{ij}(t)$	Time dependent modal coordinate
l_1, l_2	Lengths of the edges of the plate
$\lambda_{m,n}, \gamma_{m,n}$	Mode shape constants
m, n	Mode numbers
ϵ_x, ϵ_y	Middle surface strains
P_{1ij}, P_{2ij}	Complex in-plane force functions
M_{ij}	Complex modal component-1
K_{ij}	Complex modal component-2
G_{ij}	Complex modal component-3
P_{ij}	Complex modal component-4
ω_{ij}	Natural frequency of the cracked plate
γ_{ij}, C_3	Nonlinear cubic spring stiffness
$P_o(t)$	Harmonic or periodic load
μ, C_1	Damping coefficient
Ω_{ij}	Excitation frequency
ϵ	Perturbation parameter
$T_n = \epsilon^n t$	$n=0$; fast time scale, $n=1$; slow time scale
$\epsilon\sigma_{ij}$	Detuning parameter
b	Real amplitude
α	Phase angle

b_{peak}	Peak amplitude
MMS	Method of Multiple Scales
NI	Numerical integration
CCFF	Clamped-clamped-free-free
CCSS	Clamped-clamped-simply supported-simply supported
SSSS	All edges simply supported
FEM	Finite element method

Chapter 1

Introduction

1.1 Motivation

In recent years the dynamic behaviour of thin isotropic rectangular plates has received considerable attention due to its wide technical importance. Thin plate structures have very many broad applications, ranging from those of automotive and structural engineering, up to space technology. The demand for this type of structure has rapidly increased due to industrial stringency, especially in aerospace vehicles in which light weight is essential. However, this type of structure can lead to unwanted instances of high vibration. Over time, vibrational effects can have long-term as well as short-term damaging effects on the structure. Such phenomena are potentially dangerous as they can create a complete unbalance of the structure which can then ultimately fail. Therefore, the detection and localisation of damage to thin plate structures at the initial stage of development can optimise system performance and safety.

Two plate theories are widely accepted and used in engineering problems, namely the Kirchhoff plate theory, or classical plate theory, and the Mindlin – Reissner plate theory. A comprehensive background on plates has been provided by Timoshenko and Woinowsky-Krieger (1959) in which methods were introduced that can be used in various derivative systems. At the end of the 19th century plate theory was routinely applied to engineering problems involving vibration and noise in structures (Szilard, 2004) and there are many published papers offering vibration analyses of cracked plates. Based on the literature which has been reviewed for the vibration analysis of a cracked plate, it is seen that most of the published papers have analysed vibrations in plates with part-through surface cracks, part-through finite length cracks, all over part-through cracks, and internal cracks. All of these cracks have tended to be located at the side or edge of the plate, or have been centrally located cracks parallel to one side of the plate. Only a few papers (Maruyama and Ichinomiya (1989); Wu and Law (2004); Huang and Leissa (2009); Huang *et al.* (2011)) have investigated the vibration analysis of a plate with a crack which is not horizontally or vertically aligned along one side of the plate. However, until now, none of this research has provided clarification of the modelling necessary to accommodate a surface crack of variable angular orientation which could then be used for nonlinear vibration analysis.

Therefore, one of the motivations for this thesis is to provide an extension to the development of currently available analytical models for the vibration analysis of a cracked plate. A new analytical model of an aircraft panel structure, in the form of a thin flat plate with enhanced crack modelling and various boundary conditions, is provided in the form of an isotropic cracked plate. This plate is then subjected to a transverse harmonic load and is considered for nonlinear vibration analysis. As is known, the different behaviour in the vibration characteristic and the nonlinear responses of cracked plates are both dependent on several factors, such as plate geometry, external forces and locations, prevailing damping coefficients, and the geometry, location and orientation of the crack itself. Thus, it is instructive to compare and analyse the effect of orientation of a crack in a plate, in order to improve the overall performance of the structure.

1.2 Research Aims and Objectives

It is necessary still to develop a deep understanding of the derivation of the model of a cracked plate, especially for the nonlinear case. Much research work has been undertaken on the linear model, and there are restricted nonlinear models available for vibration problems in cracked plates. A detailed derivation of the differential equation based on classical plate theory for modelling a crack in a plate for a nonlinear model was initiated by Israr (2008) and Israr *et al.* (2009). In these works, the concept of a line-spring model based on Kirchhoff's plate bending theories, as first introduced by Rice and Levy (1972), was used for the crack formulation. The idea behind this concept was to reduce the problem of a three-dimensional surface crack to a quasi-two-dimensional problem. The type of crack considered by these authors was a part-through crack located at the centre and parallel to one side of the plate. Hence, the aim of this research is to extend the vibration analysis of the cracked plate discussed in paper by Israr (2008) and Israr *et al.* (2009) by considering an alternative geometry whereby the crack orientation is variable. Therefore, the work in this thesis seeks to:

- i. Develop the mathematical model of an aircraft panel structure which takes the form of a specialised Duffing equation. An aircraft panel structure is modelled as an isotropic thin flat plate with an arbitrarily orientated surface crack, subjected to transverse harmonic excitation with arbitrarily chosen SSSS, CCSS and CCFB boundary conditions based on classical plate theory.

- ii. Investigate the nonlinear behaviour of the cracked plate model from the amplitude-frequency equation by use of the multiple scales perturbation method and to compare the results of this with those obtained from direct numerical integration.
- iii. Study the influence of the orientation of the crack angle on the nonlinear vibration characteristics of the plate.
- iv. Perform an appropriate finite element analysis in order to corroborate the effect of crack length and crack orientation angle on the modal parameters and vibrational amplitude of the cracked plate.
- v. Undertake a dynamical systems analysis of the cracked plate model.
- vi. Verify the developed model through comparison of the results with experimental work.

1.3 Thesis Overview

Chapter 2 presents a critical review of the literature of thin plate structures and plates with cracks, particularly for vibration problems.

Chapter 3 provides a derivation of the equation of motion for the forced vibration of a plate containing an arbitrarily orientated surface crack, and based on three different boundary conditions. The derivation method is based on classical plate theory. Numerical results are presented for the natural frequency of the first mode of the intact plate and for the cracked plate, for various aspect ratios and crack orientation angles. The physical parameters that control the orientation of the crack angle are also investigated.

Chapter 4 proposes an analytical solution to the nonlinear governing equation of motion for the cracked plate by use of the perturbation method of multiple scales. In this chapter the amplitude-frequency equation obtained is used to investigate the nonlinear behaviour of square and rectangular plates containing a surface crack of known orientation. The influences of the boundary conditions, the crack orientation angle, crack length, and location and magnitude of the point load are all demonstrated. In addition, for purposes of comparison, numerical results are also calculated by directly integrating the derived nonlinear ordinary differential equation. This chapter also summaries a finite element

model of an intact plate and a cracked plate both with CCFF boundary conditions, within ABAQUS, for a further modal analysis in order to corroborate the effect of crack length and crack orientation angle on the modal parameters, particularly the natural frequency as predicted by the analysis. The finite element analysis is also performed in order to study the effects of parameter changes on the vibrational amplitude of the cracked plate.

Chapter 5 presents a dynamical systems analysis of the plate with a variably orientated surface crack, and includes time domain plots, phase plane representations, Poincaré maps, and bifurcation diagrams. The transitions to chaos are analysed using the dynamical tools provided within MathematicaTM.

Chapter 6 gives experimental measurements in order to verify the theoretical cracked plate model. The response of intact and cracked plates with various surface crack orientation angles is investigated. The tested plates are subjected to a transverse harmonic excitation at a selected point with arbitrarily chosen CCFF type boundary conditions.

Chapter 7 provides the comparative studies between the theoretical modelling and FE approaches, and the theoretical modelling with experimental measurements and to extend the discussion where appropriate regarding the results obtained from Chapters 3 to 6 including the method of multiple scales, direct numerical integration method within MathematicaTM, and a numerical study into the system's dynamics.

Chapter 8 concludes this PhD research and provides suggestions for potential future work.

Chapter 2

Literature Review

2.1 Plate Structures

Flexible structures are extensively used particularly in many aerospace applications. Plates, beams, frames and shells are basic elements for structural analysis and are of great practical significance to civil, mechanical, marine, aerospace engineering and other areas of practical interest, such as slabs on columns, flexible satellite manipulators, printed circuit boards, and solar panels supported at a few points. Flexible plates are initially flat structural elements where the thickness is much smaller than the other dimensions. Plates can be classified into three groups; thin plates with small deflections, thin plates with large deflections, and thick plates. Two plate theories are widely accepted and used in engineering problems, namely the Kirchhoff plate theory, or Classical plate theory, and the Mindlin–Reissner plate theory. These two main theories can be applied to plate problems depending on the value of the plate thickness. Classical plate theory must be employed for thin plates when ignoring the effect of shear deformation through the plate thickness, while for thick plates Mindlin-Reissner plate theory must be applied so that the effects of shear force can be taken into account. A comprehensive background on plates has been provided by Timoshenko and Woinowsky-Krieger (1959) in which methods were introduced that could be used in various derivative engineering systems.

This research is focused on thin plate structures in order to develop enhanced modelling for reliable, light and efficient structures. Plate materials now lead to designs that are thinner, lighter and larger than before. According to the criterion often applied to define a thin plate, the ratio of the thickness to the smaller span length should be less than $1/20$. If the ratio is more than that, then transverse shear deformation must be accounted for and the plate is then said to be definitionally thick (Ugural, 1999). However, thin, light and large structures lead potentially to high vibration. Vibration of flexible structures causes generally reduced system effectiveness, structural fatigue, and possible human discomfort or reduced safety. With their potential applications and problems, the vibration of plates undergoing installations with complex boundary conditions has received considerable attention from researchers.

2.1.1 Vibration Problems in Plates

The vibration of plates has been studied extensively since 1787, due to its importance in the design of plate structures, and many of the important studies in this field were documented in Leissa's monograph (Zhou and Zheng, 2006). At the end of the 19th century, plate theory and its resultant behaviour was applied to engineering problems involving vibration and noise in structures (Szilard, 2004). According to Szilard (2004), initial mathematical solutions to the free vibration problem based on the membrane theory of plates was formulated by Euler (1776) and Bernoulli (1789), and then in 1813, Lagrange developed the governing equation for the free vibration analysis of plates. Subsequently, Navier (1836) derived a differential equation for plates subjected to distributed static lateral loads, and Kirchhoff (1887) obtained a similar differential equation for plate problems through the use of a different energy approach.

Corrections for rotary inertia and shear were first applied by Timoshenko in 1921 for the case of beams. Following Timoshenko, Reissner, in 1944 and 1945, improved the equation for vibration of thick plates by including the effects of shear and rotary inertia through a complementary energy principle. Afterwards, Mindlin in 1951 also developed an equation including these effects with a different approach by utilising a modified theorem and assumptions. In this study, he generalised the Timoshenko one dimensional theory of beams to the plate and showed a more comprehensive two dimensional theory of flexural motions of plates which could be deduced directly from the three dimensional equations of elasticity (Tomar, 1962). According to Ugural (1999), analysis methods for plates are strongly dependent on their boundary conditions and geometrical shape. It is widely recognised that closed-form solutions are possible only for a limited set of simple boundary conditions and geometries.

Warburton (1954) proposed the first comprehensive collection of solutions for rectangular plates. In this useful work he obtained the approximate natural frequency formulas for plates with all possible boundary conditions for all modes of vibration, by use of Rayleigh's method. All 21 types of boundary condition problem were obtained from a combination of free, freely-supported, and fixed edge boundary conditions. The approximate natural frequency formula was obtained in term of the boundary conditions, the nodal pattern, the plate dimensions, and the material properties. Tomar (1962) studied the flexural vibrations of an isotropic elastic plate according to Mindlin's theory by including the effects of shear and rotary inertia. A numerical solution for the equation for a

simply supported thin square plate with various ratios of thickness to the side has been obtained, and then the results were compared with those from fundamental classical plate theory. In 1973, Leissa presented a comprehensive study of the free vibration of all the 21 combinations of classical boundary conditions for rectangular plates. Accurate frequency parameters have been presented for a range of aspect ratios, and comparisons were made with useful approximate formulas by Warburton (1954). Dawe and Roufaeil (1980) examined the use of the Rayleigh-Ritz method to predict the natural frequencies of flexural vibration of isotropic plates based on Mindlin theory, and Bhat (1985) investigated the vibration problem of rectangular plates by using a set of characteristic orthogonal polynomials within the Rayleigh-Ritz method generated from a Gram-Schmidt process in order to express the bending deflection of rectangular plates under static loads. The method showed superior results for lower modes and particularly for plates with some free edges. Kitipornchai *et al.* (1993) have also carried out the free vibration analysis of thick rectangular plates using the Rayleigh-Ritz method. The energy function derived using Mindlin's plate theory was minimised using the Rayleigh-Ritz method which leads to the governing eigenvalue equations. Sets of reasonably accurate vibration frequencies were presented for a wide range of plate aspect ratios and relative thickness ratio for the first ten modes of 21 sets of boundary conditions involving all possible combinations of clamped, simply supported and free edges. They found that the Rayleigh-Ritz method can show substantial success in the vibration analysis of thick plates.

The Galerkin method is one of the more powerful numerical methods for the solution of differential equations, and is comparable in ability to other numerical techniques for related stability problems such as the differential quadrature method (Saadatpour *et al.*, 2000). The Galerkin method involves direct use of the governing differential equation, so it does not assume the existence of a functional that is usually minimised as in other methods. In 1989, Ng and Araar solved the fourth order differential equation for the problem of free vibration and buckling of isotropic clamped rectangular plates of variable thickness by use of the Galerkin method. In 1997 and 1998, Azhari and Saadatpour, and Saadatpour and Azhari, respectively, used the Galerkin method for the dynamic and static analysis of simply supported plates of general shapes. Later, in 2000 Saadatpour *et al.* extended their work for the vibration analysis of general plates. By making use of the Galerkin method, a theoretical formulation for the free vibration analysis of simply supported quadrilateral plates having intermediate line or point supports was presented. The results for the natural frequency of trapezoidal, rhombic, skew, and continuous rectangular plates, with line supports i.e. one-span, two-span, three-span and etc., and a

plate with a central support have been obtained and compared with results of other researchers. Close agreement has been obtained for all cases. The Galerkin method was also applied by Kopmaz and Telli in 2002 to obtain the eigenfrequencies of a rectangular plate carrying a uniformly distributed mass. Using the Galerkin procedure, the equation of motion was reduced to a set of ordinary differential equations and then used to obtain the frequency equation.

Gorman, in 1995 and 2005, obtained a series of solutions for the free vibration frequencies and mode shapes of thin orthotropic cantilever plates by the superposition method. In his study the natural modes were expressed in the form of trigonometric and hypermetric series, and the number of terms in the series depended on the requirements of precision. Before that, Bardell in 1991 applied a new approach from developments in the finite element method called the hierarchical finite element method (HFEM) in order to determine the natural frequencies and modes of a flat, rectangular plate for ten different boundary conditions. According to Bardell, the finite element method can generally be regarded as a special case of the classical Rayleigh-Ritz method with the main difference between the two lying in the choice of admissible functions used in the series of representation of the solution. The basic finite element approach consists of dividing the domain of interest into a number of smaller subdomains called finite elements and then the solution is approximated by locally admissible polynomial functions. The HFEM, known as the p -version of the finite element method, is one of the techniques needed to improve the accuracy of the finite element approximation. The HFEM involves keeping the element mesh constant, and letting the degree of the approximating polynomial functions tend to infinity. In Bardell's (1991) study of HFEM, the results obtained have shown good agreement with the work of other researchers and any combination of edge condition can be incorporated in this analysis.

Subsequently, Han and Petyt, 1996 (a) studied the linear vibrations of symmetrically laminated rectangular plates with clamped boundary conditions by using the HFEM. Their results showed that the solutions converged rapidly with the increase in the number of polynomials used, and this required far fewer degree of freedom than when using the conventional finite element method. In the same year of 1996, Han and Petyt (b) extended their study to the forced vibration problems using the same method of HFEM. The loads were considered as harmonic acoustic plane waves applying on the plate surface in a normal direction and at grazing incidence. The results for the natural frequencies of five layer, symmetrically laminated, rectangular plates for different grazing incidents were

obtained and they found a decreasing trend of frequencies with the increase of incidence. Furthermore, they found that the maximum surface bending strains might not occur at the middle of the edges due to distorted mode shapes. Besides FEM, partial differential equation models (PDEs) also can be solved by using the finite difference method (FDM) and the differential quadrature method (DQM). However, these methods face difficulties when applied to problems with complex domains due to the non-coincidence of mesh lines and boundaries. According to Shu *et al.* (2007), in order to eliminate this problem the so-called meshless methods have been developed including the moving least-square (MLS) approximation, the reproducing kernel particle methods (RKPM), the least-square-based finite difference method (LSFD), the element-free Galerkin method (EFG), and the differential cubature method (DCM) etc. In Shu *et al.*'s (2007) study, the meshless LSFD method was employed to solve the free vibration problems of isotropic, thin, arbitrarily shaped plates with simply supported and clamped edge boundary conditions, in which the governing equation for this plate problem was in the form of a fourth order PDE. The chain rule was used in the approximation of the higher-order derivatives due to the efficiencies of this rule for approximating higher-order derivatives in the LSFD discretisation. They found that the present approach of LSFD showed many advantages over the traditional methods such as FDM and DQM. For example, numerical errors caused by discretising derivatives in the boundary conditions can be completely avoided in the case of clamped edges, and considerably reduced in the case of simply supported boundary conditions.

Wu *et al.* (2007) proposed a Bessel function method to obtain the exact solutions for the free vibration analysis of rectangular thin plates for three different boundary conditions, namely fully simply supported, fully clamped, and two opposite edges simply supported with the other two edges clamped. According to Xing and Liu (2009), the Hamilton dual method was applied by Ouyang and Zhong (1993), Bao and Deng (2005), and Zhong and Zhang (2006) for analyses of the modes and natural frequencies of thin plates, in which the natural modes in these solutions were expressed in the form of symplectic eigenfunction expansions rather than in closed form, and Cen *et al.* (2004) gave some Hamiltonian dual differential equations for thin plates. In a paper by Xing and Liu (2009) the Hamiltonian symplectic dual method was adopted and the separation of variables used in order to solve the transverse free vibration problems of rectangular thin plates. The first ten frequencies and mode shapes for the SSCC, SCCC and CCCC cases were obtained and validated with the FEM results. Xing and Liu (2009) concluded that these exact normal modes and frequency equations can be used to obtain results for any combination of separable simply-

supported and clamped boundary conditions which can thus be taken as a benchmark for verifying the different approximate approaches.

2.2 Nonlinearities

Nonlinear problems are of interest to the scientific and engineering communities because most physical systems such as structures are inherently nonlinear in nature. No physical system is strictly linear and hence linear models of physical systems have limitations of their own in which these linear models are only applicable in a very restrictive domain, for instance when the vibration amplitude is very small. Nonlinearities exist in an equation of motion when some product of variables, or their derivatives, exists. Nonlinear equations are difficult to solve and yet give rise to interesting phenomena such as jumps, saturations, sub-harmonics, super-harmonics, combination resonances, self-excited oscillations, modal interactions, periodic doubling, and chaos. Detailed explanations about the various types of nonlinearities, with examples, can be found in the books by Nayfeh and Mook (1979), Moon (1987), Cartmell (1990) and Thomsen and Stewart (2002).

2.2.1 Nonlinear Plate Theory

The sources of nonlinear behaviour can be classified into three main categories i.e. geometric nonlinearity, material nonlinearity and boundary condition nonlinearity. The geometric nonlinearity category is important to systems with large deflections, or systems that may fail due to buckling. When plates are deflected beyond a certain magnitude, linear theory loses its validity and produces incorrect results. The deflection of the plate may then exceed the original dimensions of the plate and can be predicted by linear theory, but it is generally unrealistic. Thus, geometric nonlinearity must necessarily be taken into account. In plates geometric nonlinearity may arise because of two reasons, namely the nonlinear strain-displacement relationship, and the nonlinearity in the governing differential equation due to the coupling of inplane and transverse displacement fields. As a result, mid-plane stretching of the plate may occur. When the deflection of the plate increases, the stretching effect becomes more pronounced than the bending effect, particularly when the edges of the plate are restricted. However for beams the nonlinear moment-curvature relationship becomes significant when large deflections without stretching are considered.

Another important category of nonlinearity relates to material properties. Such nonlinearities would render the stress strain relationship of the material of the structure

nonlinear, so that Hooke's law is therefore invalid. In the case of nonlinear material behaviour, linearity occurs up to the yield point and this region called the elastic region of the material, in which the slope of the linear region can be defined as the Young's modulus, but beyond that point it deviates from a linear to a nonlinear response. Nonlinear systems are also caused by nonlinear boundary conditions. Examples of such phenomena include the use of a nonlinear spring or damper on the edge of a plate, or the case of a nonlinear spring in a mass-spring-damper system. Duffing's equation is a special case of a cubic nonlinear spring in a mass-spring-damper system. Besides these categories, inertia, impacts, backlash, fluid effects and damping are also capable of categorising other types of nonlinearities which exist in structures (Malatkar, 2003).

According to Malatkar (2003) and Israr (2008), plate structures undergoing transverse deflection can be classified into three numerous regimes that describe the nature of their behaviour and thus the characteristics of the mathematical problem, namely; (1) small deflection theory (linear), (2) moderately large deflection theory (nonlinear), and (3) very large deflection theory (highly nonlinear). This behaviour can generally be classified by observation of the amount of deflection in comparison to the plate dimensions. Small deflection theory can typically be used for deflections less than twenty percent of the thickness. Moderately large deflection theory is applied when the deflection is a multiple of the plate thickness but much less than the plate side length, whereas very large deflection theory is applied when the deflection of the plate is similar in order of magnitude of the plate side length. Depending on the plate classification the solution to these problems can be relatively simple or highly complex, and typically impossible without the implementation of approximating techniques. Problems of linear and moderately nonlinear deflection will be discussed in this review, but very large deflections are currently not significant to this work and subsequently will not be covered.

It is interesting to note that the majority of physical systems belong to the class of weakly nonlinear (or quasi-linear) systems. For certain phenomena, these systems exhibit behaviour only slightly different to that of their linear counterparts. In addition they also exhibit phenomena which do not exist in the linear domain. Therefore, for weakly nonlinear structures, the usual starting point is still the identification of the linear natural frequencies and mode shapes. Then, in the analysis, the dynamic response is usually described in terms of its linear natural frequencies and mode shapes. The effect of the small nonlinearities is seen in the equations governing the amplitude and phase of the structures response.

2.2.2 Nonlinear Vibration of Plates

A selective history of the nonlinear vibration of plates is given below. The credit for the discovery of nonlinear theory, that accounts for both bending and stretching of a plate, is generally given to G. Kirchhoff (1824-1887). These problems also can be found in the book of Nayfeh and Mook (1979). Two highly cited literature reviews on nonlinear vibrations are by Chia (1980) and Sathyamoorthy (1998). Chia published a compilation of information on nonlinear plates, with methods for approaching the different plate problems, in his book, *Nonlinear Analysis of Plates*, whereas Sathyamoorthy summarised work on the nonlinear vibrations of plates from 1983 to 1986. After Kirchhoff established the classical linear plate theory, von Kármán (1910) developed the nonlinear plate theory. In his study the final form of the nonlinear differential equations governing the moderately large deflection behaviour of a statically deflected plate was developed. Solutions for these sets of nonlinear equations have been examined extensively in the literature. Following an approximation by Berger in 1955, the coupled von Kármán equations were replaced by a simplified set of equations describing the large deflection of plates. Berger solved several problems in the static deflection of plates and concluded that his simplified theory gave results in substantial agreement with more elaborate methods. The Berger formulation can be used to investigate nonlinear vibrations when the strain energy due to the second strain invariant in the middle surface can justifiably be ignored. This then results in decoupling and linearisation of the governing equations. The applicability and simplicity of this approximation to the nonlinear vibration analysis of plates makes it a very useful approach. Wah (1963) used the simplified Berger equation by imposing the condition that the in-plane displacements u and v can be assumed to disappear at the external boundaries, and therefore applied this equation for the vibration analysis of rectangular plates with large amplitudes, and with various boundary conditions. Vendhan (1975) considered the Berger equation for the nonlinear vibration analysis of elastic plates. Research works on geometrically nonlinear vibration of thick plate problems are relatively frequent, however only some of them are given here because thick plates are not considered in this research. In Leissa's monograph (1993) other techniques are illustrated which extend the Berger technique to include the vibrational behaviour of these nonlinear plates. Part of this approach is to assume a solution based on the spatial modes and on some function in time. This has been shown, in this thesis, to reduce to the well known Duffing oscillator problem.

Nonlinear plate dynamics were studied by Chu and Herrmann (1956) who began with an investigation into the effects of large deflections on the free flexural vibration of rectangular plates. They used the von Kármán equations in order to study the problem of an isotropic plate simply supported on all edges with fixed and hinged edges. The general solution of these equations is unknown, but first approximations to the solutions have been obtained by these authors using a perturbation method and the principle of conservation of energy. Afterwards, in 1961, Yamaki obtained solutions for isotropic rectangular plates for simply supported and clamped plates by use the Galerkin Method. Srinivasan (1965) applied a Ritz-Galerkin technique to obtain the nonlinear free vibration response of hinged-hinged beams and plates for different boundary conditions. In 1968, Stanišić and Payne introduced a technique based on the Galerkin approach for determining the natural frequencies of rectangular plates with discrete masses added for simply supported and clamped boundary conditions. Their results indicated the expected trend that natural frequencies decreased with added mass whereas the deflections and stresses of the plate increased. Next, calculation of the nonlinear natural frequencies of beams and plates for large amplitude free vibrations was presented by Mei (1973) using the Finite Element Method. In this study, the nonlinearity considered was due to large deflections, and not due to nonlinear stress-strain relationships. Mei derived the stiffness matrix formulation for a plate element based on a modification of Berger's hypothesis. As a result, the nonlinear behaviour of the hard spring type for the large amplitude lateral oscillations was shown clearly as the dimensionless amplitude increases. During the same period Rehfield (1973) applied Hamilton's principle and a perturbation approach for analysing the nonlinear free vibration of elastic structures including plates and beams. In 1978 Prathap and Pandalai incorporated the effects of transverse shear and rotary inertia in their study of the nonlinear vibration of transversely isotropic rectangular plates using the von Kármán field equations. The three generalised coordinates together with the Galerkin technique were used to define the state of deformation of the plate. Sathyamoorthy (1979) also applied a Galerkin method for the large amplitude free flexural vibration of orthotropic rectangular plate problems. Dumir and Bhaskar (1988) studied the large amplitude forced vibrations of orthotropic thin rectangular plates using the orthogonal point collocation method. Plates with all edges clamped or simply supported and fixed edges have been considered in this work.

Benamar *et al.* (1993) developed a theoretical model based on Hamilton's principle and spectral analysis for the study of large amplitudes in fully clamped isotropic rectangular plates. This investigation was an extension of their previous work on fully clamped symmetrically laminated rectangular plates published in 1990, and for simply supported

and clamped-clamped beams in 1991. Numerical results for various plate aspect ratios and vibration amplitudes were obtained and showed that the mode shapes were amplitude dependent. The general trends of the mode shape change were an increase of the displacement, or curvature, near the clamps, and flattening near the centre of the plate. A good agreement was obtained between theoretical predictions and experimental measurements, however the theoretical models employed in these studies considered transverse displacements only and neglected the effects of in-plane displacements. Bencharif and Ng (1993) conducted a nonlinear analysis of thick rectangular plates by using the finite difference method in order to transform the partial differential equations into an algebraic system of equations to yields the solutions. Han *et al.* (1994) applied the HFEM for the geometrically nonlinear static analysis of thin laminated rectangular plates with clamped boundary conditions. After successfully applying this method, Han and Petyt (1996) continued their work in order to study the nonlinear vibration analysis of thin, isotropic rectangular plates with the same boundary conditions. They employed the von Kármán nonlinear strain-displacement relationship, and the harmonic balance method, for formulating the mathematical model and obtaining eigenvalue-like equations, respectively. A modified form of Berger's hypothesis was also employed to study the in-plane membrane force averaging effect on the geometrically nonlinear behaviour. In Han and Petyt's (1996) studies, the influences of large vibration amplitude on the frequency and mode shape of the fundamental mode have been presented and the results have been compared with other results from the published literature.

The Galerkin method was also used by Leung and Mao in 1995. In that paper the geometrically nonlinear free vibration of thin plate and beam problems were studied by Hamilton's formalism instead of using the familiar approaches of the Newtonian or Lagrangian formulations. The Galerkin method was applied to discretise the continuous Lagrangian in order to obtain the discrete Hamilton equations. Ribeiro and Petyt (1999) analysed the steady state, geometrically nonlinear, periodic vibration of rectangular thin plates under harmonic external excitations by use of the HFEM and the harmonic balance methods. Again in 1999 the theoretical model based on Hamilton's principle and spectral analysis proposed by Benamar *et al.* (1991 and 1993) was used by Kadiri *et al.* to calculate the second nonlinear mode of a fully clamped rectangular plate. The large vibration amplitude problem was reduced to a set of nonlinear algebraic equations and was solved numerically. They found that the nonlinear mode showed a higher bending stress near to the clamps at large deformations compared with that predicted by linear theory. This model was extended by Kadiri and Benamar (2002) in order to study the geometrically nonlinear

free vibration of fully clamped rectangular plates, with some improvement observed in allowing a direct and easy calculation of the first, second, and higher nonlinear mode shapes, associated with the nonlinear natural frequencies and nonlinear bending stress patterns. In Kadiri and Benamar's study, the nonlinear free vibration problem was reduced to the solution of a set of nonlinear algebraic equations and was performed numerically using appropriate algorithms in order to obtain a set of nonlinear mode shapes for the structure. In 2003 these authors proposed an improved form for determining the geometrically nonlinear response of rectangular plates which were excited by concentrated or distributed harmonic forces. This approach was applied to the cases of fully clamped (CCCC), simply supported and clamped-clamped-simply supported (SCCS) rectangular plates. The results showed that the relative natural frequency was a function of the ratio of the amplitude and thickness of the plate. Bikri *et al.* (2003) also extended the work by Benamar *et al.* (2003) based on Hamilton's principle and spectral analysis to the case of clamped-clamped-simply supported-simply supported (CCSS) rectangular plates. In this study the effects of large vibration amplitudes on the first nonlinear mode shape, the fundamental natural frequency, and the associated flexural stress distribution have all been determined. Bikri *et al.* found that the nonlinear natural frequency increases with increasing vibration amplitudes for the hardening type nonlinearity, and the geometrical nonlinearity was also characterised by a deformation of the first mode shape when the vibration amplitude increased. Consequently this was seen to induce a variable rate of increase in the maximum flexural stresses when the maximum non-dimensional amplitude, obtained in the vicinity of the plate centre, increases, whereas this rate remains constant in the linear theory.

The use of HFEM to study the nonlinear free and forced vibration analyses of skew and trapezoidal plates for the clamped boundary condition was presented by Leung and Zhu (2004), by considering the effects of transverse shear deformation and rotary inertia. Only weak nonlinearity without bifurcation was considered in their study. A new methodology that could be employed for plate structure problems with any combination of boundary conditions to determine the nonlinear natural frequencies and mode shapes was proposed by Saha *et al.* in 2005. In their study (Saha *et al.*), the static analysis served as a basis for the subsequent dynamic problems, and both these problems were formulated through the energy method. The solution methodology was employed as an iterative numerical scheme using the technique of successive relaxation. In 2006, Amabili theoretically and experimentally investigated the large amplitude vibrations of rectangular plates with geometric imperfections subjected to harmonic excitation. Recently, in 2011 Mitra *et al.*

presented a large amplitude free vibration analysis for stiffened plate problems subjected to uniformly distributed transverse loading with a single free edge and also associated with different combinations of clamped and simply supported boundary conditions. In 2012, Mitra *et al.* extended their work for the large amplitude forced vibration analysis of stiffened plates subjected to transverse harmonic excitation. The governing equations in both the forced and free vibration cases were derived based on the energy principle method, and solved by employing an iterative direct substitution method with an appropriate relaxation technique. Results were given as frequency response curves in the nondimensional frequency-amplitude plane, and were accompanied by backbone curves for the system. Mitra *et al.* (2012) found that when the amplitude of excitation reduced, the nonlinear response of the system tended to attain the shape of a backbone curve.

2.3 Damage Identification Methods in Plate Structures

Damage identification techniques, particularly in structures, have received increasing effort from many researchers over the last few years. Generally damage identification techniques are categorised into local/visual and global methods as shown in Figure 2-1.

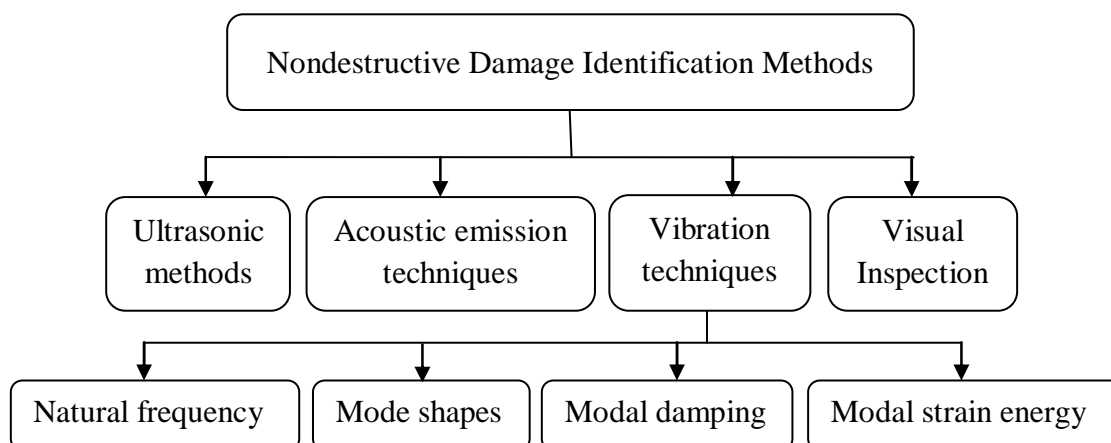


Figure 2-1: Position of the Vibration-Based Identification Methods with respect to other damage identification methods (Loendersloot *et al.*, 2010).

Local damage identification techniques comprise experimental technique such as ultrasonic methods, magnetic field methods, radiography testing, eddy-current methods or thermal field methods, and require that the location of damage must be known *a priori* and that the structure being inspected is readily accessible. Global damage identification methods, such as the vibration-based damage detection method, refer to numerical methods and experimental techniques which can be applied to complex structures by examining

changes in the vibration characteristics of the structure. These have led to developments which overcome local damage identification method limitations in which such experimental methods can only detect damage on or near the surface of the structure (Doebbling *et al.*, 1998).

A comprehensive review of the vibration-based damage identification methods has been reported by several researchers (Doebbling *et al.*, 1998; Wang and Chan, 2009; Fan and Qiao, 2011). The basic principle behind this technology is that modal parameters i.e. frequencies, mode shapes, and modal damping, are all functions of the physical properties of the structure, namely mass, damping, and stiffness. Therefore, changes in such physical properties, for example reductions in stiffness which result from the onset of a crack, will cause detectable changes in the modal properties. Vibration-based damage detection methods are especially attractive because they are global monitoring methods in the sense that no *a priori* information for the location of the damage is needed and immediate access to the damaged part is not required. These features are especially important when the objects of monitoring are large or complex structures, and when some parts of these structures are either inaccessible or very problematically located for taking measurements. Doebbling *et al.*, in 1998 reported a summary review of vibration-based damage identification methods. They provided an overview of methods to detect, locate, and characterise damage in structural and mechanical systems by examining changes in the measured vibration response. The methods are categorised according to various criteria, such as the level of damage detection provided, model-based vs. non-model-based methods, and linear vs. nonlinear methods. Besides that, Fan and Qiao (2011) presented a comprehensive review of modal parameter-based damage identification methods specifically for beam or plate type-structures.

Many structures or major components in civil, aerospace, and mechanical engineering can be simplified to a plate or a beam. However there are relatively few references related to damage identification methods for plate-type structures. In 1999, Cornwell *et al.* applied a strain energy method to detect damage in plate-like structures. This method was based on the changes in the strain energy of the structure and required only the mode shapes of the structure before and after damage. The developed algorithm was found to be effective in locating areas with stiffness reductions as low as 10% using relatively few modes. Hu *et al.* (2005) developed a damage index using modal analysis and strain energy methods in order to detect a surface crack in a laminated plate. Modal analysis was firstly performed to obtain the mode shapes from experimental and finite element analysis results, then the

mode shapes obtained were used to calculate the strain energy of the laminated plate before and after damage by using the differential quadrature method (DQM) and they subsequently defined a damage index. They found that the damage index successfully identified the surface crack location, as shown by the peak value of the damage index. However, some peak values also emerged at other undamaged areas due to irregularities of the mode shapes. Loendersloot *et al.* (2010) studied a vibration based damage identification of a composite plate with stiffeners as are frequently applied in aircraft components. They found that the modal strain energy damage index (MSE-DI) algorithm is a suitable method for detection and localisation of a delamination of the stiffener.

Yan and Yam (2002) detected damage in composite plates using the energy variation of the structural vibration response decomposed by wavelet analysis. The study shows that the proposed technique is capable of detecting extremely small cracks in composite plates. Paget *et al.* (2003) examined the amplitude change of the wavelet coefficients to characterise successfully the interactions of Lamb waves with damage in a plate. A versatile numerical approach for the analysis of wave propagation and damage detection within cracked plates was applied by Krawczuk *et al.* (2003 and 2004). They considered the spectral plate element as a tool for the investigation of such phenomena and showed that when a propagating wave runs to the crack location of the plate it divides itself into two signals, which can show an indication of the damage section. The use of a spatial wavelet based approach for damage detection of a rectangular plate has also been discussed by Chang and Chen (2004). In that study they obtained spatially distributed signals of the damaged rectangular plate by using the finite element method and then analysed this by using wavelet transformation. These spatially distributed signals can exist in terms of mode shapes or displacements. Chang and Chen (2004) found that the distributions of the wavelet coefficients can identify the damage position in a rectangular plate by showing a peak at the position of the damage and that they have a high sensitivity to the damage size. However, some indications of damage were also observed at the clamped edges of the rectangular plate. Therefore, it was concluded that it was very hard to detect the crack position at the edges. The work by Rucka and Wilde in 2006 is also devoted to wavelet based damage detection techniques for estimating the damage location in beam and plate structures. In their study, the wavelet transform was applied to the fundamental mode shape of the beam and plate, and the estimated mode shapes of the steel plate with four fixed boundary conditions were analysed by use of the two dimensional (2D) continuous wavelet transform. The location of the damage is indicated by a peak in the spatial variation of the transformed response.

More recently data-based damage detection in the time domain has been investigated by several researchers. In this method, the idea was to use a measured dynamic response in terms of time series analysis for damage diagnosis in vibrating structures. Basically the time series is a sequence of data points, measured typically at successive times, spaced at time intervals. Space-time series are the sets of multiple time series that are location-related. In 2005, Trendafilova used nonlinear time series based dynamic characteristics for the purpose of damage detection and quantification of a reinforced concrete plate. Later in 2007, Trendafilova and Manoach developed two viable methods for damage detection and localisation in a thin rectangular plate by use of large amplitude vibrations which are based on a state space representation of the time domain structural response. One of the methods uses the statistical distribution of state space points on the attractor of a vibrating structure, while the other one is based on the Poincaré map of the state space projected dynamic response. Hu *et al.* (2011) developed a method for detecting damage in plate structures based on space-time series analysis. All of the proposed damage detection methodologies based on time series and space-time series show a capability for the detection and localisation of damage, however noise sensitivity has a great influence on the results and can even destroy the detection.

Trendafilova *et al.* (2005) have suggested a damage detection methodology based on the analysis of the vibration response in an aircraft wing scaled model. In this study localised and distributed damage was considered, and a simplified FEM in ANSYS was used to model the problem for the vibration response. The wing was split into five volumes for the purpose of analysing the damage detection for the first ten natural frequencies. It was shown that cracks of length less than half of the wing width are undetectable in the case of localised damage, whilst in the case of distributed damage less than 30% in any of the volumes was not detectable using natural frequencies. The authors proposed in their concluding remarks that changes in the lower modal frequencies were affected by damage close to the wing root, and these changes decreased when the damage moved towards the wing tip, or conversely the higher frequencies were more affected by damage close to the wing tip and those changes increased when damage moved from the wing root towards the tip. Subsequently in 2006, Trendafilova *et al.* applied a similar technique for vibration based damage detection in aircraft panels modelled as isotropic plates with a crack at some specified location. It has been found that the method can produce extremely good results. In 2009, Trendafilova *et al.* applied frequency-based methods for the development of a viable vibration health monitoring system (VHM) for thin circular plates. The sensitivity of the lower natural frequencies to certain types of damage has been examined and the

authors attempted to establish the type and size of defects which maybe detectable using these frequencies. Their results show that the sensitivity of the first several natural frequencies to damage is rather limited. It is well known that small damage is easier to detect by examining large amplitude vibrations, which are much more affected by the nonlinearities in a structure. Moore *et al.* (2011) developed and implemented a Bayesian approach for crack identification in a freely vibrating plate using dynamic impulse response data. The Bayesian framework is used for identifying the size, location, and orientation of a single crack. This parameter estimation process was then implemented by means of a simulated time series. The results demonstrated that the credible intervals (Bayesian confidence intervals) are extremely small and do not show any definitive trends with crack orientation, crack length, etc.

2.4 Cracked Plate Structures

Failures can occur for many reasons, including uncertainties in the loading or environment, defects in the materials or damage in a structures, inadequacies in design, and deficiencies in construction or maintenance. The types of damage that happen in structures are cracks, fatigue, loosening of bolted joints, and corrosion. Thin plate structures can lead to unwanted instances of high vibration. Over time, vibrational effects can have long-term as well as short-term damaging effects on the structure. Cracks can form and propagate catastrophically with very little warning. Such phenomena are potentially dangerous as they can create a complete imbalance of the structure which can then ultimately fail. Failure of a structure can result in terrible consequences, economically and most probably and importantly in terms of loss of life. Therefore, the detection and localization of damage to thin plate structures at the initial stage of development can optimize system performance and safety.

The dynamic responses of rectangular plates with cracks, or minor irregularities under different loading conditions, have been investigated in the past by many researchers for different boundaries conditions, and various methods have been proposed to deal with the problem (Israr, 2008). The length, position, and orientation of a crack will affect the vibration characteristics of any host structure, in addition to the effects of material properties, plate geometry, and boundary conditions. Cracks in plate elements necessarily cause local changes in plate stiffness (Irwin, 1957). Existing methods for the study of

vibration analysis in cracked plates can be categorised into three general techniques namely analytical, numerical and experimental investigations.

2.4.1 Vibration Analysis of a Cracked Plate Based on an Analytical Approach

Vibration analysis of a cracked plate was firstly investigated by Lynn and Kumbasar in 1967. They used the Green's function approach to obtain a homogeneous Fredholm integral equation of the first kind which satisfied the mixed edge condition along a fictitious line partially formed by the crack. The result of free vibration analysis of thin rectangular plates with narrow cracks for simply supported edges boundary condition was presented in terms of variations of frequencies with respect to different crack lengths and the relative moment distributions along the uncracked segments. These results (Lynn and Kumbasar, 1967) have been used as a comparison by Stahl and Keer (1972), who investigated the vibration and stability of a simply supported rectangular plate with; i) a crack emanating from one edge, and ii) a centrally located internal crack. In their study dual series equation solution methods proposed by Keer and Sve in 1970 were applied by taking the stress singularity at the crack tips into account. The dual series equations were then converted by the use of certain integral representations to a homogeneous Fredholm integral equation of the second kind in which the natural frequencies and the auxiliary function to calculate the mode shapes were determined. Studies by Lynn and Kumbasar (1967), Keer and Sve (1970) and Stahl and Keer (1972) showed that their methods limited the crack to a position along the symmetry axis. In addition, the antisymmetric vibration of cracked plate has also been presented by Stahl and Keer, and the result in terms of frequency factors as functions of crack length was plotted and compared with the work of Lynn and Kumbasar (1967) for which the maximum differences was about 11 %.

Trying to overcome this existing restriction in which the crack was limited to a position along the symmetry axis, Solecki in 1975 and 1980 developed a method that would allow the study of isotropic, elastic, simply supported rectangular plates with arbitrarily located cracks based on a combination of a finite Fourier transformation and a generalised Green-Gauss theorem. Fundamental frequencies of natural vibration were obtained for a square plate with centrally located but arbitrarily inclined cracks of any length. The results showed that the crack parallel to one edge of the plate or diagonal crack reaching the corners of the plate show very good agreement with other researches. Hirano and Okazaki (1980) investigated the free vibrations of a rectangular plate having line cracks parallel to

its edge while the two opposite edges perpendicular to the line of the crack are assumed to be simply supported (Levy's form of solution). The Fourier expansion and the weighted residual methods were used in order to formulate the mixed boundary conditions on the line of the crack. Neku (1982) analysed the free vibration of a simply-supported rectangular plate with a straight notch which simulates a through-crack in a plate by establishing the Green's functions proposed by Lynn and Kumbasar (1967) via Levy's form of solution. Subsequently, in 1983, Solecki presented the natural flexural vibration of a simply supported rectangular plate with an arbitrarily located crack parallel to one edge. This problem was analysed by means of a finite Fourier transformation of discontinuous functions representing the displacement and the slope across the crack. In his study the case of the crack centrally located and off-centre was taken as an example. The results obtained were not sufficiently accurate for a crack extending almost to the edges. Basically, all of these papers (Solecki, 1975, 1980 and 1983; Hirano and Okazaki, 1980; Neku, 1982) applied a finite Fourier transform to the differential equation governing their own problems. These authors obtained a system of integral equations which possessed the unknown discontinuities of the deflection and slope across the crack. The unknown quantities then were expanded into a Fourier series, however this method was restricted to plates in which one pair of opposite sides, perpendicular to the line of the crack, was simply supported. This has come to be called the Levy plate.

The use of the Rayleigh method, with a simple subsectioning technique to determine the fundamental frequency of annular plates with internal cracks, was presented by Lee (1992). This method can be applied to annular plates with various boundary conditions, but the results were limited to the first natural frequency. In 1993 Lee and Lim proposed a numerical method based on the Rayleigh principle to obtain the natural frequencies of a simply supported rectangular plate with a centrally located crack, including the effects of transverse shear deformation and rotary inertia, by use of the dynamic equivalent of the simplified Reissner theory. Numerical results were presented for cracked isotropic and orthotropic rectangular plates. It was found that for cracked orthotropic plates the effect of rotary inertia could be neglected because the additional reduction in natural frequency caused by this effect was relatively small compared with the effect of transverse shear deformation, while for thick isotropic plates with a long crack, the effect of rotary inertia reduced the fundamental frequency by a certain amount comparable to the amount caused by the effect of shear deformation alone. This method was claimed as a simple alternative to the existing analytical and finite element method as the computation only involves the integration of simple trigonometric functions. The decomposition method was used by

Liew *et al.* (1994) to determine the vibration frequencies of cracked plates with any combination of boundary conditions. In 1996, a comprehensive review of the vibration analysis of cracked structures, including plates, has been reported by Dimarogonas. Next, a new technique for the vibration analysis of cracked plates by considering the effect of compliance due to bending was introduced by Khadem and Rezaee in 2000 (a). Later in 2000 (b), the same authors established an analytical approach for damage in the form of a crack in a rectangular plate under the application of an external load for different boundary conditions by employing modified comparison functions using the Rayleigh-Ritz method. Khadem and Rezaee, 2000 (b) concluded from their results that the presence of a crack at a specific depth and location would affect each of the natural frequencies differently. Chen and Bicanic (2000) introduced a method in which the incomplete natural frequencies and vibration modes could be used to detect damage within a cantilever plate. Lee *et al.* (2003) then derived the equation of motion for a thin uniform plate with crack-like local damages. They presented local damage in terms of the effective orthotropic elastic stiffness based on the theory of continuum damage mechanics.

By applying Galerkin's method to Von Kármán plate theory, Wu and Shih (2005) theoretically analysed the dynamic instability and nonlinear response of simply supported plates with an edge crack subjected to a periodic in-plane load along two opposite edges. The incremental harmonic balance method was then applied to solve the nonlinear temporal model. The results indicated that the stability behaviour and the response of the system were governed by the crack location of the plate, the aspect ratio, conditions of in-plane loading, and the amplitude of vibration. Wu and Shih also explained that increasing the crack ratio (the ratio of the crack length to the length of the edge along the direction of the crack) and/or the static component of the in-plane load, decreases the natural frequency of the system. The nonlinear equations for a moderate thickness rectangular plate with a transverse surface penetrating crack on the two-parameter foundation were derived by Xiao *et al.* (2005) based on the Reissner plate theory and the Hamilton variational principle. In this study, the Galerkin method and the harmonic balance method were employed to obtain the solution to the nonlinear vibration equations. The influences of the position and depth of the crack, the geometric parameters of the plate and the different physical parameters of the foundation on the nonlinear amplitude frequency response curves of the plate were carried out for free boundary conditions. The results showed that for a given vibration amplitude the nonlinear vibration frequency of the plate decreases with an increase of the crack depth, and when the crack position was near the symmetry plane of the plate. In addition, the nonlinear vibration frequency increases, as the thickness

of the plate increases or the aspect ratio of the plate decreases. In 2009, Israr *et al.* proposed an analytical model for the vibrations analysis of an isotropic aluminium plate containing a crack in the form of a continuous line with its centre located at the centre of the plate, and running parallel to one edge of the plate. The plate was subjected to a point load on its surface for three different possible boundary conditions. Galerkin's method was applied to reformulate the governing equation of the cracked plate into time dependent modal coordinates, and the nonlinearity was introduced by applying Berger's method. The results are presented in terms of natural frequency versus crack length and plate thickness, and the nonlinear amplitude response of the plate is calculated for one set of boundary conditions and three different load locations, over a practical range of external excitation frequencies. Based on Mindlin plate theory, Hosseini-Hashemi *et al.* (2010) proposed a method for free vibration analysis of moderately thick rectangular plates with all over-part through cracks for different classical boundary conditions. This solution was presented for the case where the crack was open, non-propagating and perpendicular to two opposite simply-supported edges. It was shown that the crack which was very close to the clamped edge, results in a considerable reduction in the natural frequencies of the cracked plate.

2.4.2 Vibration Analysis of a Cracked Plate based on the FE approach

A finite element model for a cracked plate was established by Qian *et al.* in 1991 for the investigation of the vibration characteristics of a simply supported and a cantilevered square plate with a crack. According to Qian *et al.*, the additional strain energy of a crack is related to the stress intensity factor (SIF) which expresses the flexibility coefficient that can be used to obtain the stiffness matrix of the plate element with the crack. Therefore, in Qian *et al.*'s study the element stiffness matrix was derived from an integration of the stress intensity factor estimated for a finite plate with a through crack under bending, twisting and shearing. Qian *et al.* compared their results with the model of Solecki (1983) with good agreement and claimed that their model provided a more efficient computational technique requiring a shorter numerical computation time due to the fact that mesh subdivision in the neighbourhood of the crack tip is unnecessary. Later, in 1993, the method of the formation of the stiffness matrix for a rectangular plate with a through crack was presented in closed form by Krawczuk. He assumed that the crack occurring in the plate was nonpropagating, open, and that the crack only changes the stiffness of the plate, while the mass is unchanged. The effect of the position and length of the crack on the

natural frequencies of the simply supported and cantilever plates was analysed and he concluded that the decreasing natural frequencies are a function of the length and location of the crack, the mode shape, and the boundary conditions of the plate. In 1994, Krawczuk and Ostachowicz used a similar method in order to create the stiffness matrix of a plate finite element having a single, nonpropagating, internal, open crack, with an additional example to study the influence of the length and position of the crack upon the transverse forced vibration amplitude. Similar results for natural frequency were obtained by Krawczuk and Ostachowicz (1994) as for previous work, but in terms of the influence of the transverse forced vibration amplitude of the cracked plate, the results showed that increasing amplitudes are a function of the location and length of the crack.

Krawczuk *et al.* (2001) declared that all the research completed by them assumed that the material around the crack tip behaved in a purely elastic manner. However, in reality a plastic zone appears at the vicinity of the crack tip and affects more the flexibility of the structure compared to a purely elastic material. A model of a plate finite element having a single, nonpropagating, open through crack was presented by Krawczuk *et al.* (2001) in which the influence of the plastic zone ahead of the crack tip on the flexibility of the element was taken into account. This was done by considering the effect of flexural bending deformation within the stiffness matrix. Their study showed that for plate structures the influence of crack tip plasticity on changes in natural frequencies can be neglected because the differences between the elastic and elasto-plastic crack model were rather small. Fujimoto *et al.* (2003) analysed the vibration characteristics of centrally cracked plates subjected to uniaxial tension using a hybrid of the finite element method (FEM) and body force method (BFM). In that study a central crack perpendicular to the direction of the tensile load was investigated. The loading edges were clamped to constrain out-of-plane deformations while the others were left free. The FEM was performed for the purpose of eigenvalue analysis in order to study the dependencies of the vibration characteristics on the crack length and the in-plane force intensity, whereas the BFM was used to study local crack buckling caused by the compressive in-plane stress around the crack that affects the vibration characteristics. In particular these authors considered the effect of local buckling and ignored the effect of post buckling due to the assumption that the in-plane stresses are linearly proportional to the applied tensile load. They concluded from their results that the crack length and the range of applied tensile load would affect the natural frequency and mode shapes differently, and found that crack buckling occurred at a small tensile load, as the crack length increases. In 2009, Saito *et al.* investigated the linear and nonlinear vibration response of a cantilevered rectangular plate with a transverse

crack using a finite element model. Bachene *et al.* in 2009 adopted the extended finite element method (XFEM) to analyse the vibrations of rectangular and square plates containing through edge and central cracks for different boundary conditions. In this study, the effects of shear deformation and rotary inertia were taken into account based on Mindlin's plate theory. The results obtained showed that the XFEM was an efficient method for the dynamic analysis of plates containing discontinuities.

2.4.3 Vibration Analysis of a Plate with a Variably Orientated Crack

Based on the literature which has been reviewed for the vibration analysis of a cracked plate it is seen that most of the published papers have analysed vibrations in plates with part-through surface cracks, part-through finite length cracks, all over part-through cracks and internal cracks. All of these cracks have tended to be located at the side or edge of the plate, or have been centrally located cracks parallel to one side of the plate. Only a few papers have investigated the vibration analysis of a plate with a crack which is not horizontally or vertically aligned along one side of the plate. In 1989, Maruyama and Ichinomiya experimentally investigated the effect of the lengths, positions, and inclination angles of slits on the natural frequencies and corresponding mode shapes of clamped rectangular plates with straight narrow slits, using free vibration analysis by applying the real-time technique of time-averaged holographic interferometry. A slit has a long, narrow cut or opening. One of the main differences between actual cracks and slits is the crack tip diameter. Some cracks which are fully opened at the tip, have a crack tip diameter close to that of slits and others have much smaller diameters than slits (Date *et al.*, 1982). In terms of crack orientation angle effects, they concluded from their experimental results that most of the natural frequencies of the plates with a slit length of 40% of that of a longer side monotonously increased up to an angle of 60° and then decreased when the angle exceeded this. The natural frequencies of the mode λ_{21} decrease monotonously with an increase of crack orientation angle because the slit gradually approaches a vertical nodal line. Wu and Law (2004) presented an anisotropic damage model for a thick plate with a non-propagating, open and inclined crack. The crack was assumed to be a narrow through-depth crack, such that it did not change the mass of the plate. An effective anisotropic stiffness model of the cracked element was proposed, and the sensitivity for its detection was studied.

Huang and Leissa (2009) applied the Ritz method with a special displacement function to investigate the effects of location, length, and orientation of side cracks on the free vibration frequencies and mode shapes of simply supported and completely free square plates with side cracks, including cracks which are not along a symmetric axis. A set of functions was proposed which more appropriately describes the behaviour of stress singularities at the crack tip, and which are able to meet the discontinuities of displacement and slope crossing the crack. More recently, Huang *et al.* (2011) extended their work from side cracks to internal cracks. They claimed the first published vibration data for cracks oriented at various angular positions by applying the Ritz method to analyse the free vibration of a simply supported and completely free square plate with an internal through crack having an arbitrary location and angular orientation. Analyses were carried out for crack orientation angles varying from 0° to 45° , in 15° steps, and they found that for simply supported square plates the first four frequencies decreased when the orientation angle of the crack increased. However, in the case of completely free square plates the trend was different, and an increase in the crack orientation angle caused a decrease in the first and third frequencies, but an increase in the second, fourth and fifth frequencies. In the papers of Huang and Leissa (2009) and Huang *et al.* (2011) the Ritz method was applied based on classical thin plate theory. Later a vibration study of a thick cracked rectangular plate using the Ritz method with Mindlin plate theory was presented by Huang *et al.* (2011). In this study rectangular plates having a side crack and an internal crack were considered for simply supported and cantilevered rectangular plate boundary conditions, and the obtained results showed that the proposed new sets of functions appropriately represented the stress singularity behaviour around the crack tip and elucidated the discontinuities of transverse displacement and bending rotations across the crack.

2.4.4 Line-Spring Model (LSM)

Generally cracks that exist in a structure take the form of surface or internal cracks. At present several techniques are available to study surface crack problems including the finite element method, the boundary integral method, and the body force method, particularly for evaluating fracture parameters in surface cracked plates and shells (Miyoshi *et al.*, 1985). All these methods are regarded as reliable but have a disadvantage because a large amount of computer time is needed. To overcome this difficulty a new method based on the line-spring model has been developed. The line-spring model has been used widely for fracture mechanics analysis of plate and shell structures containing

surface or internal cracks. According to Yang (1988), it has been demonstrated in the literature that the line-spring model can effectively produce very useful approximate solutions for highly complicated three dimensional crack problems in plates and shells. This approach is computationally inexpensive compared to treating full three dimensional models, and, within certain restrictions, can provide acceptable accuracy. Most importantly the line-spring model is also versatile, adapting to a variety of crack geometries and loading cases. For instance, the model has been successfully applied to the mixed mode case, elastic-plastic fracture problems, crack contact problems, and to the case of arbitrary loading due to residual stresses (Cordes and Joseph, 1995).

The line-spring model was first developed by Rice and Levy (1972) to give an approximate treatment for the three dimensional problem of a surface crack penetrating partly through the thickness of an elastic plate. The idea behind this concept was to reduce the problem of a three dimensional surface crack to a quasi-two-dimensional problem in which the constraint effects of net ligaments from the three dimensional problem were incorporated in the form of a membrane load and bending moment imposed on the through crack. This transition was accomplished using compliance relations from the plane strain, edge-cracked strip solutions. In their study, they employed two dimensional generalised plane stresses, and used Kirchhoff's plate bending theories with a continuously distributed line spring to represent a part-through crack, and also chose compliance coefficients to match those of an edge-cracked strip in plane strain. The line of discontinuity was of length $2a$ and the plate was subjected to remote uniform stretching and bending loads along the far sides of the plate. These authors computed the force and moment across the cracked section to determine the stress intensity factor, and the solution to the problem was characterised in terms of the Airy stress function.

In the literature, the line-spring model has been incorporated with singular integral equation formulations of an isotropic elastic plate or shell theory, it has been combined with the finite element method, and has also been coupled with the boundary element method (LSBEM) in order to study surface crack problems, due to the effectiveness of the line-spring model as a tool for evaluating fracture parameters in surface cracked plates and shells. In 1981, Delale and Erdogan reformulated the line spring model in the context of Reissner plate bending theory to include transverse shear effects. New expressions for the stress intensity factor of the plane strain problem of a strip containing an edge crack and subjected to tension and bending were used with a valid ratio of depth to thickness value of up to 0.8. Then, in 1983, King presented a simplified line-spring model in which some

simplifications were made by reducing the line-spring model to a purely analytical one in which the actual crack front was replaced with a crack of constant depth, and displacement compatibility between the ligament spring and the crack was enforced only at the centre of the crack. Despite the simplicity of this, the model also gave reasonably accurate predictions for calculating the fracture parameters such as the J -integral or crack opening displacement (COD) at the root of a surface crack. Joseph and Erdogan (1987) extended the line-spring model for the analysis of mixed mode crack problems. Miyazaki (1989) presented a transient analysis of the dynamic stress intensity factor by use of the combination of the finite element method with a static line-spring model. Considering the advantage of the line-spring model, Zeng and Dai in 1993 developed a line-spring boundary element method (LSBEM) in which the line-spring model was combined with the boundary element method, based on the theory of Reissner's plate problem, and the elastic plane problem, and then the model was used to analyse the stress intensity factor of general part through cracks in a finite plate.

The problem of a mode I surface or internal crack in a plate with a residual stresses was examined by Cordes and Joseph in 1995 with an emphasis on the crack surface contact. Residual stresses are usually caused by unintentional activities during manufacturing and installation, and need to be determined to ensure that the material responds in a safe, predictable manner during its lifetime. In the study of Cordes and Joseph (1995), the line-spring model was used iteratively to determine the border of the closed portion of the crack and the stress intensity factors along the open portion. These authors presented a series of results for different crack lengths and depths, and compared their results with the LSM classical theory (the Irwin model of 1962) and the finite element model, which showed that their model results ranged from 0.6-0.8% higher, whereas the average percentage difference was found to be 4.2%. The discrepancy increased slightly as the order of the loading increased. It demonstrated that the model could be versatile in solving contact problems.

The basis of the simplified line-spring model proposed by King (1983) was used by Zeng and Dai (1994) to derive a closed-form solution for the stress intensity factors at the deepest point for an inclined surface crack under the biaxial stress state. This model reduced the three dimensional problem of an inclined surface crack into two quasi two dimensional problems of a horizontally orientated through crack. Analytical solutions for the mode I and mode III stress intensity factors at the maximum depth point of a surface crack were derived, and the effects of the biaxial load ratio and the crack inclination angle

on these values of stress intensity factors (SIFs) were discussed. The study showed that the mode I normalised SIF increases and the mode III normalised SIF decreases as the biaxial load ratio increases with fixed values of crack inclination angle, while if the ratio of biaxial load is fixed, the mode I normalised SIF decreases and the mode III normalised SIF increases as the angle of crack inclination increases. The formulation of a representative model for a horizontal part-through crack located at the centre of a plate in a Duffing equation was first proposed by Israr (2008) and Israr *et al.* (2009). Initially this model was motivated by results from Rice and Levy (1972) in which a part-through crack formulation was initiated using the concept of a line-spring model. After some further developments based on this model these authors obtained a set of equations for the relationships between the nominal tensile and bending stresses at the crack location and the nominal tensile and bending stresses at the far sides of the plate.

2.5 Perturbation Methods

Solutions for differential equations for plates, as well as for beams, have been examined very extensively in the literature. Such solutions are substantially more complicated in the nonlinear case, specifically for geometrically nonlinearity as covered in this thesis, than those discussed for linear problems. Some of the same solution techniques can be applied in nonlinear cases as are applied for linear problems after some modifications have been made. Solutions can be classified into two solution groups, the first being exact analytical solutions and the second being approximate solutions. Exact solutions to the nonlinear plate are obviously difficult to obtain, particularly for the study of the dynamic behaviour of nonlinearly deflecting rectangular plates. However, approximate solution techniques exist for some general nonlinear plate problems in which these solutions either use approximating functions, or assume certain terms to be negligible, or use some form of finite discretisation method (Israr, 2008). Such approximation solutions are purely numerical, purely analytical, or a combination of both. Useful information on nonlinear plates with a variety of methods offered to approach different plate problems can be found in detail in the book by Chia (1980).

In the literature solutions for the vibration analysis of damaged plates have also been investigated using various approaches. These including Rayleigh's method, the finite displacement method, the finite Fourier transform, the Rayleigh-Ritz method, the finite element method, the Galerkin method, the harmonic balance method, and the

decomposition method. Each solution technique is of special relevance, and treatment involves some particular type of approximation. The method applied in this thesis is the perturbation method of multiple scales, as first used by Israr in 2008 and Israr *et al.* in 2009 for the vibration analysis of a plate containing a crack in the form of a continuous line with its centre located at the centre of the plate and parallel to one edge of the plate. Thus it is intended to be major enhancement of this previous work on cracked plates for which the orientation of the angle was not included.

Perturbation methods are well established and have been used for over a century to determine approximate analytical solutions for nonlinear mathematical models. Such mathematical models take many forms including differential equations, difference equations and integro-differential equations, and can be solved approximately with perturbation methods. Perturbation methods work by applying small nonlinear perturbations to known linearised solutions. Their correct application is restricted to weakly nonlinear systems, so the nonlinear terms are small compared to the linear terms. This is usually the case when the motions are finite but not very large. The correctness of perturbation analysis decreases with growing amplitude of motion. Many different perturbation methods such as the Lindstedt-Poincaré technique (LP), the Renormalisation method, the Incremental Harmonic Balance (IHB), Averaging methods, Krylov-Bogoliubov (KB), Krylov-Bogoliubov-Mitropolski (KBM) and the Method of multiple scales (MMS), have all been developed.

The development of basic perturbation theory for differential equations was fairly complete by the middle of the 19th century. Laplace firstly used perturbation methods to solve the problem of equilibrium of a large weightless drop on a plane (1749–1827) and Delaunay (1816–1872) discovered the so-called problem of small denominators in a study of the perturbative expansion of the three body problem. There are books which introduce and discuss several perturbation methods that can be used to develop approximate solutions to nonlinear problems, such as Nayfeh (1973) and (1981), also Kevorkian and Cole (1981). Nayfeh used the perturbation method of multiple scales to solve the differential equations for symmetrically excited circular and rectangular plates, and documented this in Nayfeh and Mook (1979). According to Israr (2008), Chu and Herrmann in 1956 investigated a perturbation solution of the dynamic w (deflection)- F (stress function) formulation using a double series and double cosine series, for the first mode shape only. Lynn and Kumbasar (1967) solved the integral equation for the vibration analysis of cracked rectangular plates by use of the Krylov and Bogoliubov method. In

1973 Hamilton's principle, with a combination of a perturbation procedure, was applied by Rehfield in order to study the nonlinear free vibrations of beams and plates. Niyogi and Meyers (1981) presented the nonlinear dynamic response of orthotropic plates using a perturbation technique. Wang (1990) employed the Lindstedt-Poincaré perturbation technique to solve a form of the Duffing equation with an additional quadratic spring term that was derived in a vibration analysis of imperfect rectangular plates. The effects of random initial geometric imperfections on the vibration behaviour of simply supported rectangular plates were studied by Wang (1990). In 1991, Cheung *et al.* presented a modified Lindstedt-Poincaré method for a certain strongly nonlinear oscillator with a single-degree-of-freedom. In that study a new parameter was defined, which enables a strongly nonlinear oscillation corresponding to the original parameter to be transformed into a small parameter system with the new parameter.

Wang *et al.* (2009) studied the nonlinear thickness-shear vibrations of an infinite and isotropic elastic plate. In this procedure, a perturbation method was used in order to solve the nonlinear ordinary differential equation that was obtained by use of the Galerkin method. The amplitude-frequency relation showed that the nonlinear frequency of the thickness-shear vibrations depended on amplitude and on the thickness of the plate. Hao *et al.* (2011) presented a nonlinear dynamic analysis of a rectangular cantilever plate made of functionally graded materials and based on Reddy's third order plate theory and the asymptotic perturbation method. This perturbation method was employed to obtain four nonlinear averaged equations which were then solved by the Runge-Kutta method in order to find the nonlinear dynamic response of the plate.

2.5.1 Method of Multiple Scales

The classical perturbation methods, including the method of multiple scales, are really restricted to solving weakly nonlinear problems. The restriction of these methods is that the perturbation parameter ε must definitionally be very small. Since the nonlinear vibration characteristics of basic structural components such as cables, beams, plates and shells can often be modelled as a weakly nonlinear system, the method of multiple scales has been widely used in many analyses. The main idea of the method of multiple scales is to split the single independent variable up into several new independent variables. This method allows the construction of a set of perturbation equations that can be solved under the condition of removal of secular terms. Cartmell *et al.* (2003) reviewed the comprehensive

literature dealing with the analyses of weakly nonlinear mechanical systems by the method of multiple scales. In that paper the role of term ordering, the integration of the small perturbation parameter within system constants, non-dimensionalisation and time-scaling, series truncation, inclusion and exclusion of higher order nonlinearities and typical problems in the handling of secular terms were all examined. These authors showed in a comparative example that the form of the adopted power series and the ordering terms can have a major bearing on the structure of the solution, with clear suggestion for accuracy and physical relevance. Ideas were suggested for how one might deal with ordering by basing it on some sort of physical appreciation of the problem in terms of hard and soft or strong and weak quantities within the equation of motion such as damping mechanisms, excitation amplitudes, and the coefficients of nonlinear terms.

Some useful theories were highlighted by Israr (2008) regarding the application of the method of multiple scales to dynamical systems. Firstly, reduced-order discretisation models may be inadequate to describe the dynamics of the original continuous system in the presence of quadratic nonlinearities. Studies by Pakdemirli, Nayfeh, and Nayfeh (1995), Nayfeh and Lacarbonara (1997), Alhazza and Nayfeh (2001), Emam and Nayfeh (2002), and Nayfeh and Arafat (2002) found that the application of the method of multiple scales, or any other perturbation method to the reduced-order model, obtained by the Galerkin, or other discretisation procedures, of a weakly nonlinear continuous system with quadratic nonlinearities can lead to both quantitative and qualitative erroneous results. Lacarbonara, in 1999, showed that quadratic nonlinearities produce a second-order contribution from all of the modes to the system response in the case of a primary resonance. Secondly, the application of the method of multiple scales to dynamical systems expressed in second-order form can lead to modulation equations that can be derived from a Lagrangian in the absence of dissipation and external excitation, but cannot necessarily be shown to lead to closed form or even to numerical steady-state solutions. This is potentially contrary to the conservative character of these dynamical systems. More specifically, this problem is encountered while determining approximate solutions of nonlinear systems possessing internal resonances to orders higher than the order at which the influence of the internal resonance first appears, as associated with the work of Rega *et al.*, (1999). Interestingly, transforming the second-order governing equations into a system of first-order equations and then treating them with the method of multiple scales yields modulation equations derivable from a Lagrangian, and is presented in Nayfeh (2000) and Nayfeh and Chin (1999), and Malatkar (2003).

Abe (2006) investigated primary and subharmonic resonances on a hinged-hinged Euler-Bernoulli beam resting on a nonlinear elastic foundation with distributed quadratic and cubic nonlinearities. Steady-state responses were found by using the method of multiple scales and Galerkin's procedure. A multiple scales solution for the nonlinear vibration of isotropic rectangular plates was presented by Shooshtari and Khadem (2007). In their study invariant manifold theory was applied to the plate problem and it was confirmed that the nonlinearities were of stiffness and inertia types. The multiple scale method was applied to the equations of motion, and closed-form relations for the nonlinear natural frequencies and mode shapes of the plate were derived. Using the obtained relation, the effects of initial displacement, thickness and dimensions of the plate on the nonlinear natural frequencies and displacements were investigated. The results showed that by increasing the ratio of thickness to the dimensions of the plate the nonlinear frequencies of the plate will increase. Hegazy (2010) studied the dynamic behaviour of a rectangular thin plate under parametric and external excitations modelled by coupled second-order nonlinear ordinary differential equations, and their approximate solutions were sought by applying the method of multiple scales. The steady-state response, and the stability of the solutions for various parameters, were both studied numerically using the frequency-response function and phase-plane methods. Hegazy found that the system parameters generated different effects on the nonlinear response of the thin plate.

The literature does not appear to contain any substantial references to using the method of multiple scales for nonlinear vibration analysis of a cracked or damaged plate except by Israr *et al.* (2006, 2008 and 2009). Starting in 2006, Israr *et al.* developed an approximate analytical solution for the free vibration of cracked isotropic plates using the multiple scales method. An elliptical crack and the local stress field with loading conditions were incorporated into the partial differential equation (PDE) for an edge loaded plate with various types of boundary conditions. Berger's formulation was used to generate the nonlinear term within the model. The plate PDE was converted into a nonlinear Duffing-type ODE in the time domain by use of the Galerkin procedure, and then an arbitrarily small perturbation parameter was introduced in order to apply the method of multiple scales. In 2008, these authors extended their work by considering the application of periodic loading for forced vibration analysis of cracked plates with different boundary conditions. The results were obtained by the use of the method of multiple scales and showed the influence of crack length and boundary conditions on the vibration characteristics of the plate. It showed that depending on increased crack length, the vibration frequency decreases and the amplitude increases. A comparison between the

method of multiple scales with direct integration, finite element analysis, and experimental work was undertaken and reported. In this study it was shown conclusively, by using a first order multiple scales approximation, that the nonlinear characteristics of the steady-state responses are encoded within the non-autonomous modulation equations. An extremely close agreement between the differently obtained results was noted. However, these studies were limited to a crack located parallel to one side of the plate only.

2.6 Routes to Chaos in Nonlinear Systems

In practice, most models are nonlinear, so a study of dynamic stability, bifurcations, and routes from order to chaos in nonlinear systems is usually very important. Such a study serves not only to promote further understanding of the complex dynamics under different combination of system parameters, but also to capture essential mechanisms that generate chaos. Additionally, this sort of study is essential to developing controls of bifurcation and chaos. Period-doubling bifurcations, the coexistence of attractors with complicated basin structures, strange attractors with the fundamental property of a sensitive dependence on initial conditions, and the existence of positive or negative Lyapunov exponents are some of the most important features of dynamical behaviour. Chaos theory is the study of highly adjustable nonlinear systems i.e. nonlinear systems that are sensitive to initial conditions. A system is characterised as chaotic if it meets certain criteria, such as exhibiting an exponential rate of period doubling in its return map, or possessing a positive Lyapunov exponent.

In recent years, there has been a lot of literature dealing with bifurcation sequences, the stability analysis of Lyapunov, and transitions to chaos. Exhaustive information on this subject is presented in the monographs of Thompson and Stewart (2002), Moon (1987), Hilborn (2000) and Solari *et al.* (1996). According to Thompson and Stewart (2002), the founder of geometric dynamics is universally acknowledged to be Poincaré (1854–1912), who, alone among his contemporaries, saw the usefulness of studying topological structures in the phase space of dynamical trajectories. The theoretical foundations laid by Poincaré were strengthened by Birkhoff (1844–1944), but, apart from a few instances such as the stability analysis of Lyapunov, Poincaré's ideas had little impact on applied dynamics for almost half a century. Subsequently, in 1927, Van der Pol and Van der Mark reported irregular noise in experiments with an electronic oscillator. It has been frequently mentioned that chaotic vibrations occur when some strong nonlinearity exists. Some

examples of nonlinearities that can be observed in many physical systems are; nonlinear elastic or spring elements, damping, boundary conditions etc. In mechanical continua nonlinear effects arise from a number of different sources which includes kinematics, constitutive relations, boundary conditions, nonlinear body forces, and geometric nonlinearities associated with large deformations in structural solids.

In 1985, Parlitz and Lauterborn presented resonance curves, bifurcation diagrams, and phase diagrams for the Duffing equation. This was intended to improve their understanding of this type of equation by emphasising the important role of nonlinear resonance. They showed a periodic recurrence of a specific and fine structure in the bifurcation set, which was closely connected with the nonlinear resonances of the system. They also found evidence for a superstructure in the bifurcation set related to nonlinear resonances in a model of acoustic turbulence by Lauterborn and Cramer (1981), in the Toda oscillator (Meyer-Ilse, 1984), in a nonlinear bubble oscillator (Lauterborn, 1976) and in a nonlinear electronic oscillator (Klinker *et al.*, 1984 and Brorson *et al.*, 1983). At the same time, Wolf *et al.* presented a technique that allows the estimation of non-negative Lyapunov exponents from experimental time series data. Lyapunov exponents provide a qualitative and quantitative characterisation of dynamical behaviour and are related to the average exponential rates of divergence or convergence of nearby orbits in phase space. They are positive for chaos, zero for a marginally stable orbit, and negative for a periodic orbit. It means that an attractor for a dissipative system with one or more positive Lyapunov exponents is said to be strange or chaotic. Wolf *et al.* claimed that their algorithm can detect and quantify chaos in experimental data by accurately estimating the first few non-negative Lyapunov exponents, and they tested this method on famous model systems such as those of Hénon (1976), Rössler (1976), Lorenz (1989), and the Rössler-hyperchaos problem (1979) with known Lyapunov spectra. They also found that chaos can be distinguished in some cases from external noise and topological complexity.

Numerical and experimental works to study the nonlinear vibration and nonlinear acoustic radiation of a typical aircraft fuselage panel forced by plane acoustic waves at normal incidence were demonstrated by Maestrello *et al.* (1992). In this study, they found that the motion normally starts periodically, and eventually becomes chaotic with time with the increase of the pressure level. A good agreement between the experimental and numerical results were obtained, which showed that when a panel is excited at a resonant frequency by plane acoustic waves, linear, nonlinear and chaotic responses can be obtained by changing the intensity of the loading. Lu and Evan-Iwanowski in 1994, initiated a

computational analysis in order to explore the effects of stationary and nonstationary excitations on the response of a softening Duffing oscillator in the region of the parameter space where the period doubling sequence occurs. They found significant differences between these two types of excitation. *Mathematica*TM packages for analysing and controlling discrete and continuous nonlinear systems, and for estimating the Lyapunov exponents of continuous and discrete differentiable dynamical systems were devised by Guitiérrez and Iglesias (1998), and Sandri (1996), respectively. A program by Guitiérrez and Iglesias (1998) was shown to be capable of obtaining the periodic points and the stability regions of nonlinear systems, as well as bifurcatory analysis and Lyapunov exponents, while a program by Sandri (1996) can compute the Lyapunov spectrum of continuous and discrete differentiable dynamical systems. The Lyapunov spectrum can be calculated until it shows convergence, or until a maximum iteration count is reached.

Tan and Kang (2000) studied the forced response of a Mathieu-Duffing oscillator subjected to combined parametric and quasiperiodic excitation in the context of a large ratio between the excitation frequencies. The response characteristics were examined in terms of the time histories, frequency responses, Poincaré sections, and Lyapunov exponents. Numerical results were obtained by the use of the spectral balance method, and the Lyapunov exponents were computed based on the algorithm proposed by Wolf *et al.* (1995). They observed that routes to chaotic motions were different for a frequency range near the natural frequency of the linear system, and also near to the parametric resonance frequency. In 2008, Shen *et al.* investigated the bifurcations and routes to chaos of the Mathieu-Duffing oscillator using the incremental harmonic balance (IHB) procedure, together with a developed new scheme that can be used for selecting the initial value conditions. A series of periodic-doubling bifurcation points and threshold values of the control parameters at the onset of chaos of the Mathieu-Duffing oscillator were calculated, and they showed that this sequence of periodic doubling bifurcations observed the universal rule approximately.

Chapter 3

A Plate with a Surface Crack of Variable Angular Orientation

3.1 Introduction

In this chapter, an analytical approach is presented for the forced vibration analysis of a plate containing an arbitrarily orientated surface crack, based on three different boundary conditions. The method is based on classical plate theory. Firstly, the equation of motion is derived for the plate containing the angled surface crack (angled with respect to one side of the plate) and subjected to transverse harmonic excitation. The crack formulation representing the surface crack of variable angular orientation is based on a simplified line-spring model. Then, by employing the Berger formulation, the derived governing equation of motion of the cracked plate model is transformed into a cubic nonlinear system which is shown to take the form of a specialised Duffing equation.

3.2 Cracked Plate Modelling

It is necessary still to develop an understanding of the derivation of the model of a cracked plate, especially for the nonlinear case. Much research work has been undertaken on the linear model, and there are restricted nonlinear models available for vibration problems in cracked plates. A detailed derivation of the nonlinear differential equation based on classical plate theory for modelling the vibration of a cracked plate was initiated by Israr (2008) and Israr *et al.* (2009). In these works, the concept of a line-spring model based on Kirchhoff's plate bending theories, as first introduced by Rice and Levy (1972), was used for the crack formulation. The idea behind this concept was to reduce the problem of a three-dimensional surface crack to a quasi-two-dimensional problem. The type of crack considered by these authors was a part-through crack located at the centre and parallel to one side of the plate.

King (1983) simplified this line-spring model for surface flaws in a plate in order to predict the fracture parameters, for instance, the J -integral or crack opening displacement at the root of a surface crack. In his simplification the crack front was replaced with a crack of constant depth which reduced the coupled integral equations in the paper by Rice and Levy (1972) to a pair of linear algebraic equations, and which was more convenient to

implement computationally. Then the basis of this simplified line-spring model was used by Zheng and Dai (1994) to propose an analytical model for an angled surface crack under biaxial stresses for investigating the effect of the biaxial load ratio and the crack orientation angle on the values of stress intensity factors for this type of crack. Hence, the aim of this section is to extend the vibration analysis of the cracked plate discussed in the work of Israr (2008) and Israr *et al.* (2009) by considering an alternative geometry whereby the crack orientation is variable. The model and methods of Israr (2008), Israr *et al.* (2009), and Zheng and Dai (1994) are used as references and are modified to accommodate a nonlinear model for a plate with an arbitrarily orientated surface crack.

3.3 The Classical Dynamic Equation of a Plate with Variably Orientated Crack

In this section, the governing equation of motion for a plate with an arbitrarily orientated surface crack of length $2a$ is developed. The crack is assumed to be located at the centre of the top surface of the plate in the x - y plane, and oriented at an angle β with respect to the x axis of the plate, and the plate is subjected to a tension σ_o and bending moment m_o , as shown in Figure 3-1. The following assumptions are made during the derivation:

1. The plate is made of thin elastic, homogeneous, and isotropic material, and has a uniform thickness which is much smaller than the other dimensions,
2. The stress normal to the mid-plane σ_z , is considered to be small when compared with the other stress components, and is therefore neglected,
3. Plane sections initially normal to the middle surface remain plane and normal to that surface after bending, so that shear deformation can be neglected,
4. The effects of rotary inertia and shear forces are also neglected,
5. The effect of the in-plane forces on the deflection of the plate only acts in the x direction, so that the in-plane forces in the y and x - y directions can be discounted (Timoshenko and Woinowsky-Krieger, 1959, and Israr *et al.*, 2009).

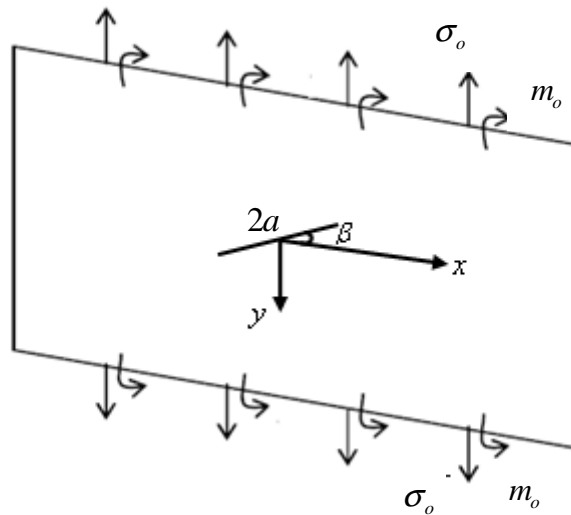


Figure 3-1 : A rectangular plate with a surface crack of length $2a$ orientated at an angle β to the horizontal x -axis and showing the bending and tensile stresses

To derive the equilibrium equation, an element of the plate of sides dx and dy , aligned with the $\{x, y\}$ axis, and of thickness h is considered, as illustrated in Figure 3-2, with Q_x and Q_y defining the forces per unit length projected parallel to the z axis, M_x and M_y are the bending moments per unit length, M_{xy} is the twisting moment per unit length, \bar{M}_y and \bar{M}_x are the bending moments per unit length due to the variably orientated crack situated at the centre of the plate, ρ is the density of the plate material, and q_z is the lateral load per unit area applied normal to the surface of the plate.

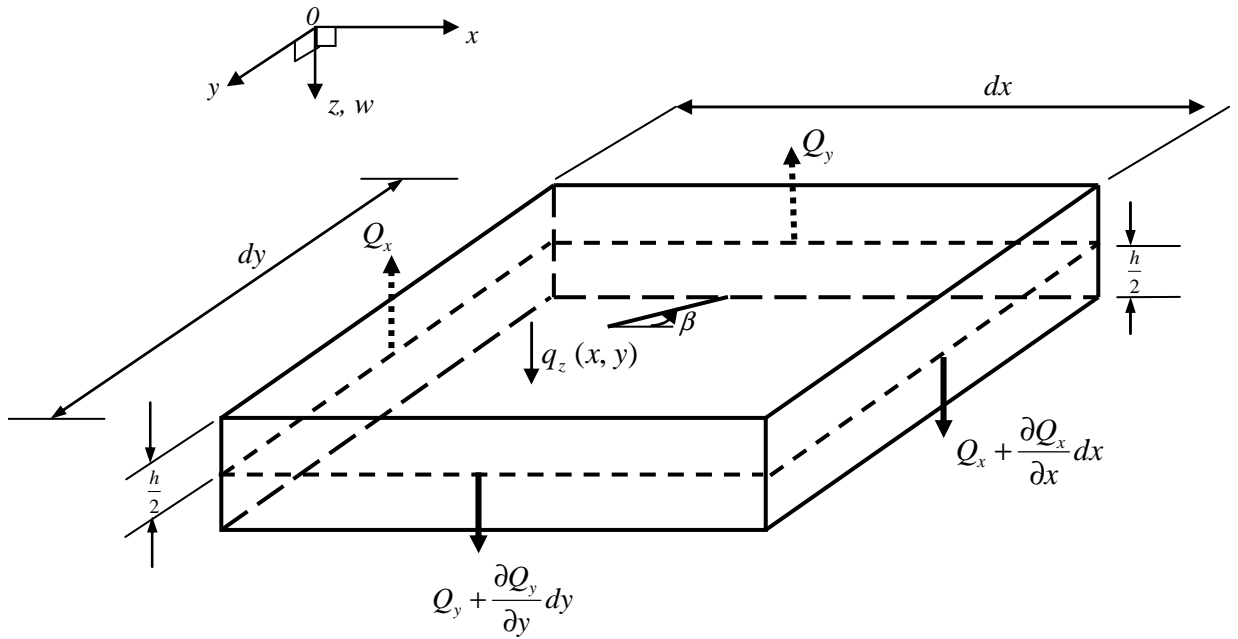
By summing all the forces in the z direction and applying Newton's Second Law, we obtain,

$$\begin{aligned}
 + \downarrow \Sigma F_z &= ma \\
 - Q_x dy + \left(Q_x + \frac{\partial Q_x}{\partial x} dx \right) dy - Q_y dx + \left(Q_y + \frac{\partial Q_y}{\partial y} dy \right) dx + q_z dx dy &= \rho h \frac{\partial^2 w}{dt^2} dx dy
 \end{aligned} \tag{3.1}$$

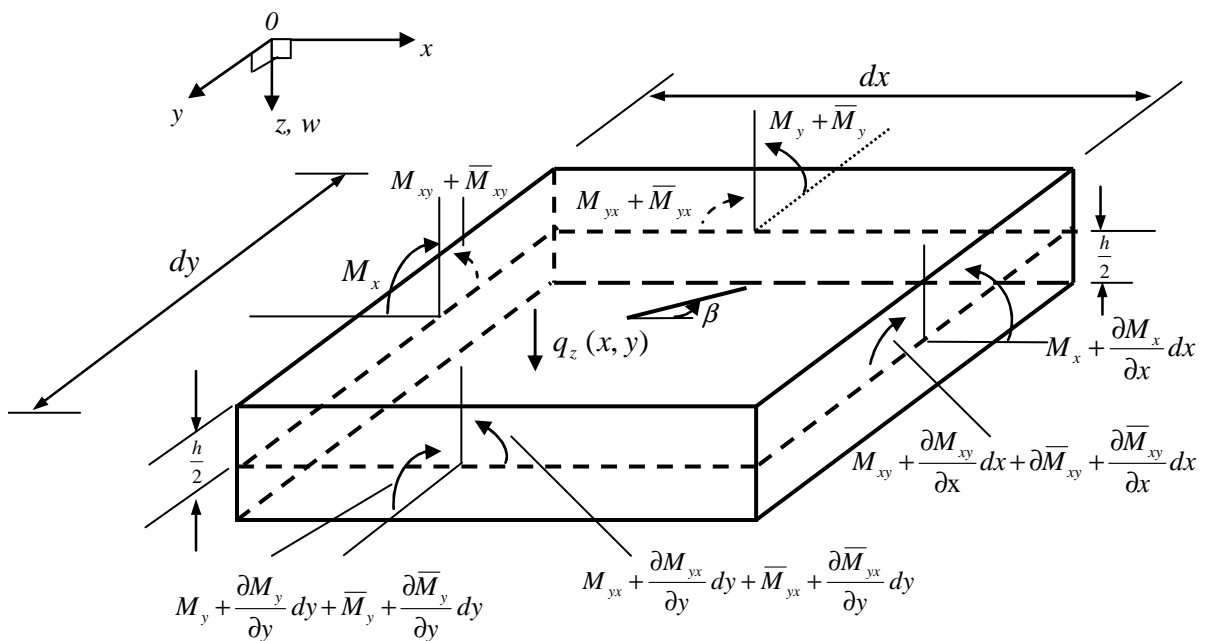
where $\rho h \frac{\partial^2 w}{dt^2}$ is the inertia force, which is assumed to be acting downwards.

Therefore,

$$\frac{\partial Q_x}{\partial x} + \frac{\partial Q_y}{\partial y} = \rho h \frac{\partial^2 w}{dt^2} - q_z \tag{3.2}$$



(a) A plate element containing a variably orientated crack, and with forces shown



(b) A plate element containing a variably orientated crack, with applied moments

Figure 3-2 : A plate structure loaded by uniform pressure with a variably orientated crack located at the centre of the plate

Summing the moments about the x and y axes and then equating them individually to zero leads to moment equilibrium about the y axis,

$$\begin{aligned} \Sigma M_y &= 0 \\ -M_x dy + \left(M_x + \frac{\partial M_x}{\partial x} dx \right) dy - (M_{yx} + \bar{M}_{yx}) dx + \left(M_{yx} + \frac{\partial M_{yx}}{\partial y} dy + \bar{M}_{yx} + \frac{\partial \bar{M}_{yx}}{\partial y} dy \right) dx \\ -Q_x dy \cdot \frac{dx}{2} - \left(Q_x + \frac{\partial Q_x}{\partial x} dx \right) dy \frac{dx}{2} &= 0 \end{aligned} \quad (3.3)$$

After simplification, and the term containing $\frac{1}{2} \frac{\partial Q_x}{\partial x} (dx)^2 dy$ is neglected in equation (3.3)

since it is small quantity of a higher order than those retained, gives the following equation,

$$\frac{\partial M_x}{\partial x} + \frac{\partial M_{yx}}{\partial y} + \frac{\partial \bar{M}_{yx}}{\partial y} = Q_x \quad (3.4)$$

Differentiating with respect to x , equation (3.4) becomes,

$$\frac{\partial^2 M_x}{\partial x^2} + \frac{\partial^2 M_{yx}}{\partial x \partial y} + \frac{\partial^2 \bar{M}_{yx}}{\partial x \partial y} = \frac{\partial Q_x}{\partial x} \quad (3.5)$$

Similarly, by summing for moment equilibrium about the x axis the moment equation can be obtained as,

$$\begin{aligned} \Sigma M_x &= 0 \\ (M_y + \bar{M}_y) dx - \left(M_y + \frac{\partial M_y}{\partial y} dy + \bar{M}_y + \frac{\partial \bar{M}_y}{\partial y} dy \right) dx - (M_{xy} + \bar{M}_{xy}) dy \\ + \left(M_{xy} + \frac{\partial M_{xy}}{\partial x} dx + \bar{M}_{xy} + \frac{\partial \bar{M}_{xy}}{\partial x} dx \right) dy + Q_y dx \cdot \frac{dy}{2} + \left(Q_y + \frac{\partial Q_y}{\partial y} dy \right) dx \frac{dy}{2} &= 0 \end{aligned} \quad (3.6)$$

Simplifying and also neglecting the term containing $\frac{1}{2} \frac{\partial Q_y}{\partial y} (dy)^2 dx$, leads to,

$$-\frac{\partial M_y}{\partial y} - \frac{\partial \bar{M}_y}{\partial y} + \frac{\partial M_{xy}}{\partial x} + \frac{\partial \bar{M}_{xy}}{\partial x} = -Q_y \quad (3.7)$$

Differentiating equation (3.7) with respect to y , leads to,

$$-\frac{\partial^2 M_y}{\partial y^2} - \frac{\partial^2 \bar{M}_y}{\partial y^2} + \frac{\partial^2 M_{xy}}{\partial x \partial y} + \frac{\partial^2 \bar{M}_{xy}}{\partial x \partial y} = -\frac{\partial Q_y}{\partial y} \quad (3.8)$$

Then, by substituting equations (3.5) and (3.8) into equation (3.2), the following equilibrium equation can be derived,

$$\frac{\partial^2 M_x}{\partial x^2} - 2 \frac{\partial^2 M_{xy}}{\partial x \partial y} - 2 \frac{\partial^2 \bar{M}_{xy}}{\partial x \partial y} + \frac{\partial^2 M_y}{\partial y^2} + \frac{\partial^2 \bar{M}_y}{\partial y^2} = \rho h \frac{\partial^2 w}{\partial t^2} - q_z \quad (3.9)$$

Where M_x , M_y and M_{xy} are the bending moments per unit length along the x and y directions, whereas \bar{M}_y and \bar{M}_{xy} are the bending moments per unit length due to the variably orientated crack situated at the centre of the plate.

From Timoshenko and Krieger (1959), and Szilard (2004), M_x , M_y and M_{xy} can be written in the following forms,

$$M_x = \int_{-h/2}^{+h/2} \sigma_x z dz \quad (3.10)$$

$$M_y = \int_{-h/2}^{+h/2} \sigma_y z dz \quad (3.11)$$

$$M_{xy} = -M_{yx} = \int_{-h/2}^{+h/2} \tau_{xy} z dz \quad (3.12)$$

with σ_x , σ_y and τ_{xy} representing the stresses along the x and y directions of the plate and all these stresses components can be expressed by deflection w of the plate, defined as,

$$\sigma_x = -\frac{E z}{1-\nu^2} \left(\frac{\partial^2 w}{\partial x^2} + \nu \frac{\partial^2 w}{\partial y^2} \right) \quad (3.13)$$

$$\sigma_y = -\frac{E z}{1-\nu^2} \left(\frac{\partial^2 w}{\partial y^2} + \nu \frac{\partial^2 w}{\partial x^2} \right) \quad (3.14)$$

$$\tau_{xy} = \frac{E z}{1-\nu^2} (1-\nu) \frac{\partial^2 w}{\partial x \partial y} \quad (3.15)$$

Deflection w is a function of the two coordinates in the plane of the plate. Substitution of equations (3.13) to (3.15) into equations (3.10) to (3.12), respectively, generates expressions for M_x , M_y and M_{xy} as follows,

$$M_x = -D \left(\frac{\partial^2 w}{\partial x^2} + \nu \frac{\partial^2 w}{\partial y^2} \right) \quad (3.16)$$

$$M_y = -D \left(\frac{\partial^2 w}{\partial y^2} + \nu \frac{\partial^2 w}{\partial x^2} \right) \quad (3.17)$$

$$M_{xy} = -M_{yx} = D(1-\nu) \frac{\partial^2 w}{\partial x \partial y} \quad (3.18)$$

$$D \text{ is the flexural rigidity of the plate in the conventional form of } D = \frac{Eh^3}{12(1-\nu^2)} \quad (3.19)$$

where E is the modulus of elasticity and ν is the Poisson's ratio. Therefore, equations (3.16), (3.17) and (3.18) can now be substituted into equation (3.9). When there is no lateral load acting on the plate, the partial differential equation of motion for the plate with an arbitrarily oriented surface crack is of this form,

$$D \left(\frac{\partial^4 w}{\partial x^4} + 2 \frac{\partial^4 w}{\partial x^2 \partial y^2} + \frac{\partial^4 w}{\partial y^4} \right) = -\rho h \frac{\partial^2 w}{\partial t^2} - 2 \frac{\partial^2 \bar{M}_{xy}}{\partial x \partial y} + \frac{\partial^2 \bar{M}_y}{\partial y^2} \quad (3.20)$$

For plates subjected to a lateral load per unit area q_z applied normal to the surface of the plate, the equation extends to,

$$D \left(\frac{\partial^4 w}{\partial x^4} + 2 \frac{\partial^4 w}{\partial x^2 \partial y^2} + \frac{\partial^4 w}{\partial y^4} \right) = -\rho h \frac{\partial^2 w}{\partial t^2} + q_z - 2 \frac{\partial^2 \bar{M}_{xy}}{\partial x \partial y} + \frac{\partial^2 \bar{M}_y}{\partial y^2} \quad (3.21)$$

3.4 The equation of motion of a cracked plate including relevant forces in the middle plane of the plate

Figure 3-3 shows a plate element of thickness h and dimensions dx and dy subjected to in-plane forces per unit length. These in-plane forces per unit length are denoted by n_x , n_y , $n_{xy} = n_{yx}$, \bar{n}_y and $\bar{n}_{xy} = \bar{n}_{yx}$. The in-plane forces \bar{n}_y and $\bar{n}_{xy} = \bar{n}_{yx}$ are the in-plane forces per unit length due to the existence of a variably orientated crack located at the centre of the plate. The in-plane force \bar{n}_x is not needed due to the transformation of the variably orientated surface crack into two basic problems namely a horizontal surface crack parallel to the x -axis and subjected to normal tensile stress and bending moment, and a horizontal surface crack parallel to the x -axis and subjected to a tangential tensile stress and a twisting moment.

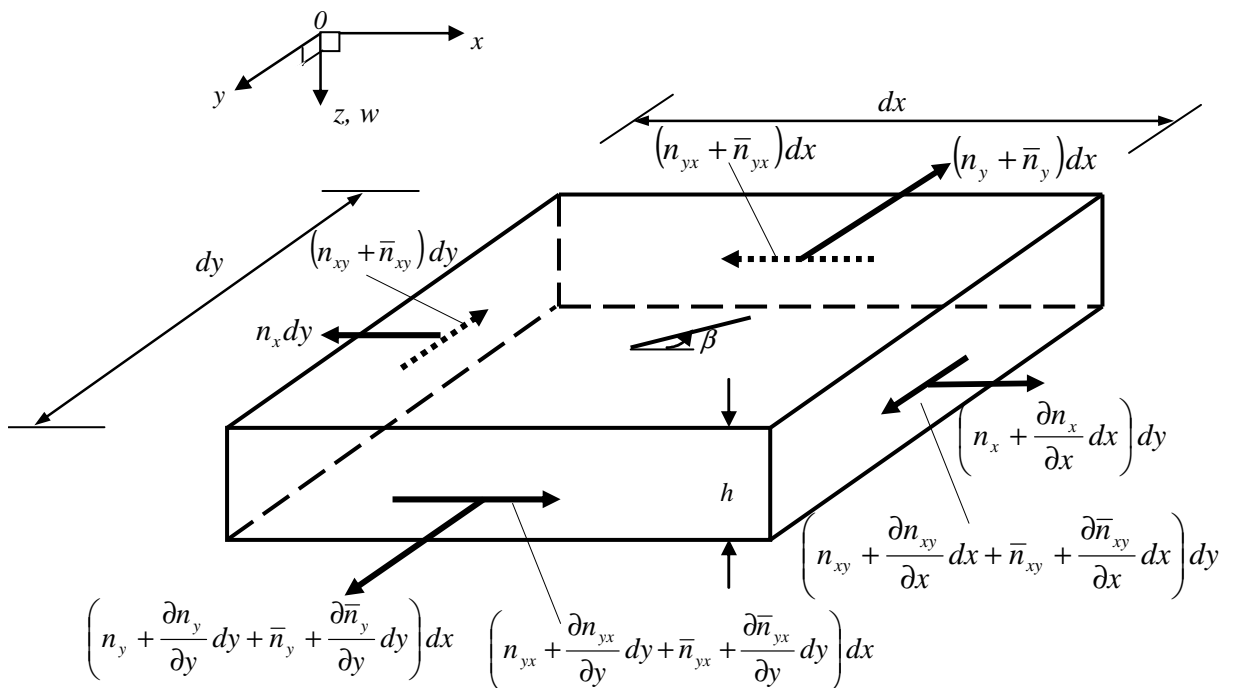


Figure 3-3 : In-plane forces acting on a plate with an arbitrarily orientated crack of length $2a$ located at the centre of the plate

In order to develop the equation of motion of the system shown in Figure 3-3 an equilibrium principle is applied to the plate element, and this is assuming that there are no body forces acting in the x and y directions of the plate. Thus, the equilibrium equation of the in-plane forces along the x axis gives,

$$\begin{aligned}
& + \rightarrow \Sigma F_x = 0 \\
& - n_x dy + \left(n_x + \frac{\partial n_x}{\partial x} dx \right) dy - (n_{yx} + \bar{n}_{yx}) dx + \left(n_{yx} + \frac{\partial n_{yx}}{\partial y} dy + \bar{n}_{yx} + \frac{\partial \bar{n}_{yx}}{\partial y} dy \right) dx = 0 \quad (3.22)
\end{aligned}$$

and hence,

$$\frac{\partial n_x}{\partial x} + \frac{\partial n_{yx}}{\partial y} + \frac{\partial \bar{n}_{yx}}{\partial y} = 0 \quad (3.23)$$

By summing the in-plane forces in the direction of the y axis we obtain the following equation of equilibrium,

$$\begin{aligned}
& + \swarrow \Sigma F_y = 0 \\
& - (n_y + \bar{n}_y) dx + \left(n_y + \frac{\partial n_y}{\partial y} dy + \bar{n}_y + \frac{\partial \bar{n}_y}{\partial y} dy \right) dx - (n_{xy} + \bar{n}_{xy}) dy \\
& + \left(n_{xy} + \frac{\partial n_{xy}}{\partial x} dx + \bar{n}_{xy} + \frac{\partial \bar{n}_{xy}}{\partial x} dx \right) dy = 0 \quad (3.24)
\end{aligned}$$

Therefore,

$$\frac{\partial n_y}{\partial y} + \frac{\partial \bar{n}_y}{\partial y} + \frac{\partial n_{xy}}{\partial x} + \frac{\partial \bar{n}_{xy}}{\partial x} = 0 \quad (3.25)$$

However, to consider the equilibrium of forces along the direction of the z axis we must take into account the bending of the plate and the resulting small angles between the forces n_x and n_y that act on the opposite sides of the element (Timoshenko and Krieger, 1959). In this case an arbitrary choice of boundary condition of the Fixed-Fixed-Free-Free boundary condition as applied by Israr (2008) as shown in Figure 3-4 is considered here. However other boundary conditions are equally possible. As a result of this selection the equilibrium equation of the in-plane forces along the z axis can be written as,

$$\begin{aligned}
\sum F_z(x, y) = & \left(n_x + \frac{\partial n_x}{\partial x} dx \right) dy \left(\frac{\partial^2 w}{\partial x^2} dx \right) + \left(n_y + \frac{\partial n_y}{\partial y} dy + \bar{n}_y + \frac{\partial \bar{n}_y}{\partial y} dy \right) dx \left(\frac{\partial^2 w}{\partial y^2} dy \right) \\
& + \left(n_{xy} + \frac{\partial n_{xy}}{\partial x} dx + \bar{n}_{xy} + \frac{\partial \bar{n}_{xy}}{\partial x} dx \right) dy \left(\frac{\partial^2 w}{\partial x \partial y} dx \right) \\
& + \left(n_{yx} + \frac{\partial n_{yx}}{\partial y} dy + \bar{n}_{yx} + \frac{\partial \bar{n}_{yx}}{\partial y} dy \right) dx \left(\frac{\partial^2 w}{\partial x \partial y} dy \right)
\end{aligned} \tag{3.26}$$

Simplification and subsequent neglect of terms of higher than second order, leading to the following form, where the terms on the right hand side are all loads per unit area,

$$\begin{aligned}
\sum F_z(x, y) = & n_x \frac{\partial^2 w}{\partial x^2} dx dy + n_y \frac{\partial^2 w}{\partial y^2} dx dy + \bar{n}_y \frac{\partial^2 w}{\partial y^2} dx dy + n_{xy} \frac{\partial^2 w}{\partial x \partial y} dx dy \\
& + \bar{n}_{xy} \frac{\partial^2 w}{\partial x \partial y} dx dy + n_{yx} \frac{\partial^2 w}{\partial x \partial y} dx dy + \bar{n}_{yx} \frac{\partial^2 w}{\partial x \partial y} dx dy
\end{aligned} \tag{3.27}$$

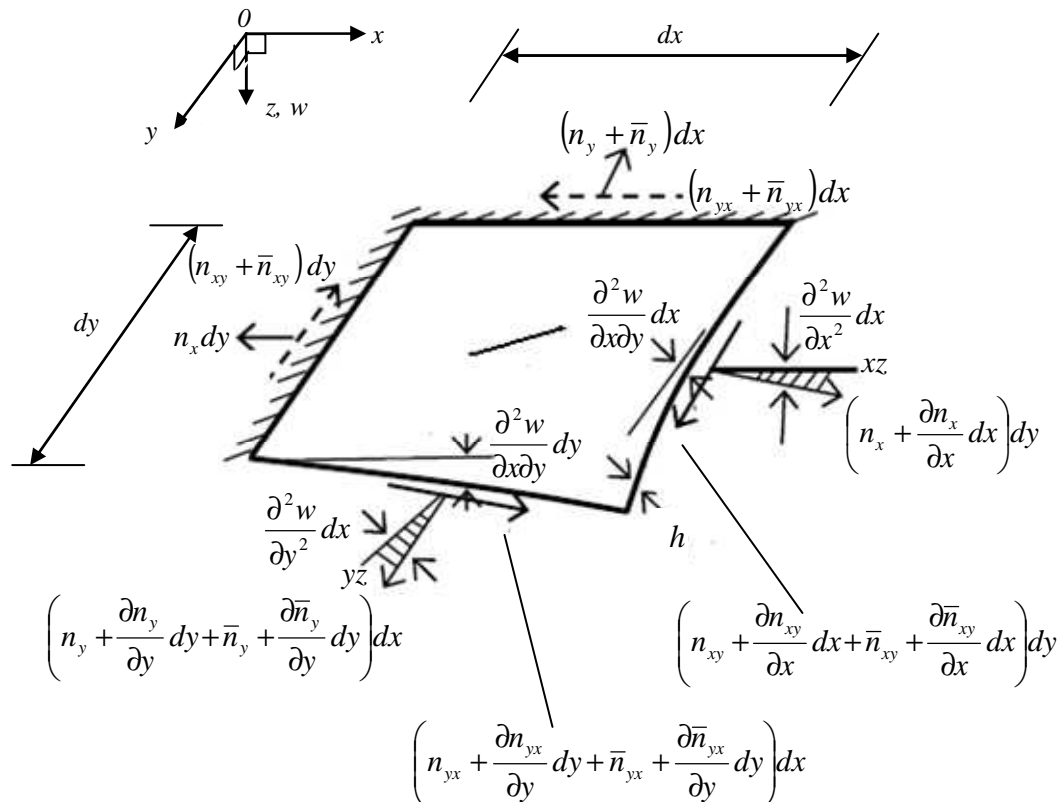


Figure 3-4 : Boundary condition with two edges fixed and two edges free and subsequent deformation of the plate having an arbitrarily orientated crack at the centre of the plate (after Israr, 2008)

Dividing equation (3.27) by $dxdy$ leads to,

$$\sum F_z(x, y) = n_x \frac{\partial^2 w}{\partial x^2} + n_y \frac{\partial^2 w}{\partial y^2} + \bar{n}_y \frac{\partial^2 w}{\partial y^2} + 2n_{xy} \frac{\partial^2 w}{\partial x \partial y} + 2\bar{n}_{xy} \frac{\partial^2 w}{\partial x \partial y} \quad (3.28)$$

In equation (3.21) the lateral load q_z is acting on the plate element in the z direction which is normal to the surface of the plate, thus by adding equation (3.28) to the lateral load per unit area q_z , we obtain the following equation of equilibrium for the cracked plate,

$$D \left(\frac{\partial^4 w}{\partial x^4} + 2 \frac{\partial^4 w}{\partial x^2 \partial y^2} + \frac{\partial^4 w}{\partial y^4} \right) = -\rho h \frac{\partial^2 w}{\partial t^2} + n_x \frac{\partial^2 w}{\partial x^2} + n_y \frac{\partial^2 w}{\partial y^2} + \bar{n}_y \frac{\partial^2 w}{\partial y^2} + 2n_{xy} \frac{\partial^2 w}{\partial x \partial y} + 2\bar{n}_{xy} \frac{\partial^2 w}{\partial x \partial y} + \frac{\partial^2 \bar{M}_y}{\partial y^2} - 2 \frac{\partial^2 \bar{M}_{xy}}{\partial x \partial y} + q_z \quad (3.29)$$

At this stage the effect of the in-plane forces on the deflection of the plate is assumed to act just in the x -direction, so the in-plane forces in the y and xy directions can justifiably be neglected. After neglecting the two terms $n_y \frac{\partial^2 w}{\partial y^2}$ and $2n_{xy} \frac{\partial^2 w}{\partial x \partial y}$, the equation of motion for the forced vibration of a thin plate with an arbitrarily orientated surface crack becomes,

$$D \left(\frac{\partial^4 w}{\partial x^4} + 2 \frac{\partial^4 w}{\partial x^2 \partial y^2} + \frac{\partial^4 w}{\partial y^4} \right) = -\rho h \frac{\partial^2 w}{\partial t^2} + n_x \frac{\partial^2 w}{\partial x^2} + \frac{\partial^2 \bar{M}_y}{\partial y^2} + \bar{n}_y \frac{\partial^2 w}{\partial y^2} - 2 \frac{\partial^2 \bar{M}_{xy}}{\partial x \partial y} + 2\bar{n}_{xy} \frac{\partial^2 w}{\partial x \partial y} + q_z \quad (3.30)$$

This equation (3.30) differs from Israr's equation (2008) because two new terms, \bar{M}_{xy} , and \bar{n}_{xy} caused by the crack of variable angular orientation are introduced.

3.5 The Variably Orientated Crack Term Formulations

The formulation of a representative model for a horizontal part-through crack located at the centre of an isotropic plate was proposed by Israr (2008) and Israr *et al.* (2009). Initially this model was motivated by results from Rice and Levy (1972) in which a part-through crack formulation was initiated using the concept of a line-spring model based on

Kirchoff's bending theory for thin plates and shells. In their research, an approximate relationship between nominal tensile and bending stresses at the crack location has been obtained. After some further work, Israr (2008) and Israr *et al.* (2009) obtained a set of equations for the relationships between the nominal tensile and bending stresses at the crack location and the nominal tensile and bending stresses at the far sides of the plate. Thus, in order to use these methods to get more accurate relationships for a thin, elastic, isotropic plate containing a variably orientated surface crack of length $2a$, it was found to be necessary to obtain new relationships for the tension and bending stress fields for this problem as shown in Figure 3-1.

The formulation of the variably orientated surface crack terms is developed by using a proposal made by Zheng and Dai (1994). These authors presented a simplified analytical model for a variably orientated surface-cracked plate using the concept of the simplified line-spring model given by King (1983). The main objective of Zheng and Dai (1994) was to develop closed-form solutions for Mode I and Mode III stress intensity factors at the maximum depth point of a variably orientated surface crack. These solutions were used to investigate the effect of the biaxial load ratio and the crack orientation angle on the values of the stress intensity factors for this type of crack. In this research, the model proposed by Zheng and Dai (1994) is used with some modification, i.e. by considering the cracked plate model loaded in uniaxial tension σ_o and edge bending m_o , as depicted in Figure 3-5.

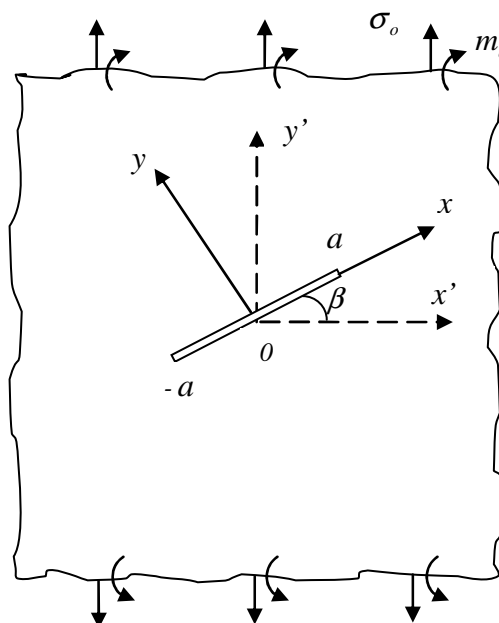


Figure 3-5 : A plate with an arbitrarily orientated surface crack loaded in tension and with a bending moment

In this particular system the boundary conditions of the cracked plate relative to the x' - y' coordinate system are assumed at infinity to become,

$$\sigma_{x'} = 0, \sigma_{y'} = \sigma_o \text{ and } \tau_{x'y'} = 0 \quad \text{at} \quad y' \rightarrow \infty \quad (3.31)$$

$$M_{x'x'} = 0, M_{y'y'} = m_o \text{ and } M_{x'y'} = 0 \quad \text{at} \quad y' \rightarrow \infty \quad (3.32)$$

where the stress σ_o acts along the $0y'$ axis. The boundary conditions relative to the x - y coordinate system (Timoshenko and Krieger, 1959, and Zheng and Dai, 1994) become,

$$\begin{aligned} \sigma_{xx} &= \frac{1}{2}\sigma_o - \frac{1}{2}\sigma_o \cos 2\beta \\ \sigma_{yy} &= \frac{1}{2}\sigma_o + \frac{1}{2}\sigma_o \cos 2\beta \\ \tau_{xy} &= \frac{1}{2}\sigma_o \sin 2\beta \end{aligned} \quad (3.33)$$

$$\begin{aligned} M_{xx} &= \frac{1}{2}m_o - \frac{1}{2}m_o \cos 2\beta \\ M_{yy} &= \frac{1}{2}m_o + \frac{1}{2}m_o \cos 2\beta \\ M_{xy} &= \frac{1}{2}m_o \sin 2\beta \end{aligned} \quad (3.34)$$

The system illustrated in Figure 3-5 can be transformed into two basic problems. The first of these is that the plate is assumed to have a horizontal surface crack parallel to the x -axis and subjected to normal tensile stress and bending moment. The second problem is where the plate has a horizontal surface crack parallel to the x -axis and is subjected to a tangential tensile stress and a twisting moment. Zheng and Dai (1994) developed appropriate expressions involving the tensile and bending stresses at the crack location and tensile stresses at the far sides of the plate. These expressions are employed here but are modified by considering the fact that the cracked plate is also subjected to bending moment, m_o as well as σ_o . These expressions are classified into four types, and are re-arranged by

applying the relationship between tensile and bending stresses at the far side of the plate (Israr, 2008), as follows,

$$\sigma_{12} = \frac{n_{12}}{h} = \frac{1}{h} \int_{-h/2}^{+h/2} \tau_{12}(x, y, z) dz \quad (3.35)$$

$$m_{12} = \frac{6}{h^2} M_{12} = \frac{6}{h^2} \int_{-h/2}^{+h/2} z \tau_{12}(x, y, z) dz. \quad (3.36)$$

In this case, the subscripts 1, 2 are represented by m, n for the first problem and p, q for the second problem. These are intermediate variables required for algebraic simplification. Thus, the relationship between the normal tensile stress, $\bar{\sigma}_{mn}$ at the crack location and the normal tensile stress, σ_{yy} at the far side of the plate becomes,

$$\bar{\sigma}_{mn} = \frac{2a}{(6\alpha_{tb} + \alpha_{tt})(1 - \nu^2)h + 2a} \sigma_{yy} \quad (3.37)$$

The relationship between the bending stress, \bar{m}_{mn} at the crack location and the bending moment, M_{yy} at the far side of the plate is given by,

$$\bar{m}_{mn} = \frac{2a}{3 \left(\frac{\alpha_{bt}}{6} + \alpha_{bb} \right) (3 + \nu)(1 - \nu)h + 2a} M_{yy} \quad (3.38)$$

In the tangential direction the relationship between the tangential tensile stress, $\bar{\sigma}_{pq}$ at the crack location and the tangential tensile stress, τ_{xy} at the far side of the plate is found to be,

$$\bar{\sigma}_{pq} = \frac{2a}{(6C_{tb} + C_{tt})(1 + \nu)h + 2a} \tau_{xy} \quad (3.39)$$

The last expression relating the bending stress, \bar{m}_{pq} at the crack location and the twisting moment, M_{xy} at the far side of the plate is found to be of the form,

$$\bar{m}_{pq} = \frac{2a}{3 \left(\frac{C_{bt}}{6} + C_{bb} \right) (1 + \nu)h + 2a} M_{xy} \quad (3.40)$$

This relationship is newly presented here because the twisting moment M_{xy} is specifically encountered in this equation. Later, the boundary conditions in equations (3.33) and (3.34) are applied to these expressions (3.37)-(3.40), and then the stress relationships for Figure 3-5 can be represented as,

$$\bar{\sigma}_{mn} = \frac{a(1 + \cos 2\beta)}{(6\alpha_{tb} + \alpha_{tt})(1 - \nu^2)h + 2a} \sigma_o \quad (3.41)$$

$$\bar{m}_{mn} = \frac{a(1 + \cos 2\beta)}{3\left(\frac{\alpha_{bt}}{6} + \alpha_{bb}\right)(3 + \nu)(1 - \nu)h + 2a} m_o \quad (3.42)$$

$$\bar{\sigma}_{pq} = \frac{a \sin 2\beta}{(6C_{tb} + C_{tt})(1 + \nu)h + 2a} \sigma_o \quad (3.43)$$

$$\bar{m}_{pq} = \frac{a \sin 2\beta}{3\left(\frac{C_{bt}}{6} + C_{bb}\right)(1 + \nu)h + 2a} m_o \quad (3.44)$$

At the crack location, $\bar{\sigma}_{mn}$ and \bar{m}_{mn} are acting in the y -direction, whereas $\bar{\sigma}_{pq}$ and \bar{m}_{pq} are acting in the x - y directions. At the far sides of the plate, σ_{yy} and M_{yy} act in the y -direction, whereas in the x - y directions, τ_{xy} and M_{xy} apply. h is the thickness of the plate, a is the half crack length, α_{tt} and C_{tt} are the non-dimensional stretching compliances, α_{bb} and C_{bb} are the non-dimensional bending or twisting compliances, and $\alpha_{bt} = \alpha_{tb}$ and $C_{bt} = C_{tb}$ represent the non-dimensional stretching-bending or non-dimensional stretching-twisting compliance coefficients at the crack centre, respectively. The compliance coefficients α_{tt} , α_{bb} and $\alpha_{bt} = \alpha_{tb}$ can be found in the paper by Rice and Levy (1972), and the compliance coefficients C_{tt} , C_{bb} , and $C_{bt} = C_{tb}$ can be seen in the papers of Joseph and Erdogan (1991) and Lu and Xu (1986).

According to Israr (2008), these tensile and bending stresses can be expressed in terms of the tensile and bending force effects. Therefore, equations (3.41)-(3.44) can be stated in the form of forces and moments by replacing the tensile and bending stress terms at the crack location and at the far sides of the plate (Rice and Levy, 1972). These equations therefore become,

$$\bar{n}_{mn} = \frac{a(1 + \cos 2\beta)}{(6\alpha_{tb} + \alpha_{tt})(1 - \nu^2)h + 2a} n_o \quad (3.45)$$

$$\bar{M}_{mn} = \frac{a(1 + \cos 2\beta)}{3\left(\frac{\alpha_{bt}}{6} + \alpha_{bb}\right)(3 + \nu)(1 - \nu)h + 2a} M_o \quad (3.46)$$

$$\bar{n}_{pq} = \frac{a \sin 2\beta}{(6C_{tb} + C_{tt})(1 + \nu)h + 2a} n_o \quad (3.47)$$

$$\bar{M}_{pq} = \frac{a \sin 2\beta}{3\left(\frac{C_{bt}}{6} + C_{bb}\right)(1 + \nu)h + 2a} M_o \quad (3.48)$$

The force and moment equations thus obtained give the desired terms, and these are then added into the equation of motion of the plate for a variably orientated surface crack, and with a negative sign introduced because in reality damage can cause a reduction in the overall stiffness, as discussed by Israr (2008) and Israr *et al.* (2009). Therefore they can be written as follows,

$$\bar{n}_y = -\bar{n}_{mn} = -\frac{a(1 + \cos 2\beta)}{(6\alpha_{tb} + \alpha_{tt})(1 - \nu^2)h + 2a} n_o \quad (3.49)$$

$$\bar{M}_y = -\bar{M}_{mn} = -\frac{a(1 + \cos 2\beta)}{3\left(\frac{\alpha_{bt}}{6} + \alpha_{bb}\right)(3 + \nu)(1 - \nu)h + 2a} M_o \quad (3.50)$$

$$\bar{n}_{xy} = -\bar{n}_{pq} = -\frac{a \sin 2\beta}{(6C_{tb} + C_{tt})(1 + \nu)h + 2a} n_o \quad (3.51)$$

$$\bar{M}_{xy} = -\bar{M}_{pq} = -\frac{a \sin 2\beta}{3\left(\frac{C_{bt}}{6} + C_{bb}\right)(1 + \nu)h + 2a} M_o \quad (3.52)$$

where \bar{n}_{mn} and \bar{M}_{mn} are the force and moment per unit length, respectively, in the y direction, and \bar{n}_{pq} and \bar{M}_{pq} are the force and moment per unit length in the x - y directions. Both the forces and moments are acting at the crack location of the plate. Substituting the expressions for \bar{n}_y , \bar{M}_y , \bar{n}_{xy} , and \bar{M}_{xy} from equations (3.49)-(3.52) into the equation of motion for the cracked plate model, equation (3.30), results in the following equation form,

$$\begin{aligned}
D \left(\frac{\partial^4 w}{\partial x^4} + 2 \frac{\partial^4 w}{\partial x^2 \partial y^2} + \frac{\partial^4 w}{\partial y^4} \right) &= -\rho h \frac{\partial^2 w}{\partial t^2} + n_x \frac{\partial^2 w}{\partial x^2} + q_z \\
- \frac{a(1 + \cos 2\beta)}{3 \left(\frac{\alpha_{bt}}{6} + \alpha_{bb} \right) (3 + \nu)(1 - \nu)h + 2a} \frac{\partial^2 M_o}{\partial y^2} - \frac{a(1 + \cos 2\beta)}{(6\alpha_{tb} + \alpha_{tt})(1 - \nu^2)h + 2a} n_o \frac{\partial^2 w}{\partial y^2} \\
+ \frac{2a \sin 2\beta}{3 \left(\frac{C_{bt}}{6} + C_{bb} \right) (1 + \nu)h + 2a} \frac{\partial^2 M_o}{\partial x \partial y} - \frac{2a \sin 2\beta}{(6C_{tb} + C_{tt})(1 + \nu)h + 2a} n_o \frac{\partial^2 w}{\partial x \partial y}
\end{aligned} \quad (3.53)$$

We note that the bending stresses at the far side of the plate are defined by Timoshenko and Krieger (1959) as follows,

$$M_y = M_{mn} = -D \left(\frac{\partial^2 w}{\partial y^2} + \nu \frac{\partial^2 w}{\partial x^2} \right) \quad (3.54)$$

$$M_{xy} = M_{pq} = -D(1 - \nu) \frac{\partial^2 w}{\partial x \partial y} \quad (3.55)$$

Therefore, by substituting equations (3.54) and (3.55) into equation (3.53), the final form of the equation of motion for the forced vibration of a thin plate with an arbitrarily oriented surface crack emerges, as follows,

$$\begin{aligned}
D \left(\frac{\partial^4 w}{\partial x^4} + 2 \frac{\partial^4 w}{\partial x^2 \partial y^2} + \frac{\partial^4 w}{\partial y^4} \right) &= -\rho h \frac{\partial^2 w}{\partial t^2} + n_x \frac{\partial^2 w}{\partial x^2} + q_z \\
+ \frac{aD(1 + \cos 2\beta) \left(\frac{\partial^4 w}{\partial y^4} + \nu \frac{\partial^4 w}{\partial x^2 \partial y^2} \right)}{3 \left(\frac{\alpha_{bt}}{6} + \alpha_{bb} \right) (3 + \nu)(1 - \nu)h + 2a} - \frac{a(1 + \cos 2\beta)}{(6\alpha_{tb} + \alpha_{tt})(1 - \nu^2)h + 2a} n_o \frac{\partial^2 w}{\partial y^2} \\
- \frac{2aD \sin 2\beta \left(\frac{\partial^4 w}{\partial x \partial y^3} + \nu \frac{\partial^4 w}{\partial x^3 \partial y} \right)}{3 \left(\frac{C_{bt}}{6} + C_{bb} \right) (1 + \nu)h + 2a} - \frac{2a \sin 2\beta}{(6C_{tb} + C_{tt})(1 + \nu)h + 2a} n_o \frac{\partial^2 w}{\partial x \partial y}
\end{aligned} \quad (3.56)$$

3.6 Application of Galerkin's Method

The transverse deflection $w(x, y, t)$ is a function of the two coordinates in the plane of the plate and time. It can be separated in the usual manner by recourse to Galerkin's method. Galerkin's method can be used to obtain global approximations for the solution of

differential equations. It is a weighted residual method and has a wider applicability than the Rayleigh-Ritz method because in general it is applicable to differential and integral equations whereas the Rayleigh-Ritz method is applicable only to variational formulations (Vendhan and Das, 1975). Kopmaz and Telli (2002) used Galerkin's method to reduce the equation of motion of a simply supported rectangular plate carrying a uniformly distributed mass for free vibration analysis. Zhou and Ji (2006) also studied the free vibration of rectangular plates with a continuously distributed spring-mass in which they represented the free vibration of a human-structure system. They used a combination of the Ritz-Galerkin method to derive an approximation for this model with three edges simply supported and one edge in the free boundary condition. Israr *et al.* (2009) used the Galerkin method to investigate the forced vibration of a cracked plate with the crack located at the centre, and parallel to one edge of the plate.

In this section Galerkin's method is applied in the usual manner to discretise the partial differential equation and transform the transverse deflection coordinate $w(x, y, t)$ into time dependent modal coordinates. The three different types of boundary conditions specified in Israr *et al.* (2009) are re-applied here. In order to use the method, a physical system comprising a rectangular plate of length l_1 in the x direction and l_2 in the y direction, as shown in Figure 3.6 is considered. This Figure is modified from Israr (2008) by considering the crack orientated at angle β with respect to the x -axis. A point load q_z is applied normal to the surface of the plate at an arbitrary location of (x_o, y_o) , and is based on the application of the appropriate delta function. $w(x, y, t)$ is a set of functions dependent on time and stated in the generalised form of the transverse deflection of the plate as follows,

$$w(x, y, t) = \sum_{i=1}^{\infty} \sum_{j=1}^{\infty} A_{ij} X_i Y_j \psi_{ij}(t) \quad (3.57)$$

This equation describes the important behaviour of the plate, where X_i and Y_j represent the characteristic or modal functions in the x and y directions of the cracked rectangular plate, respectively. A_{ij} and ψ_{ij} are the arbitrary amplitude and the time dependent modal coordinate for the system, respectively, with i, j being the plate mode designators.

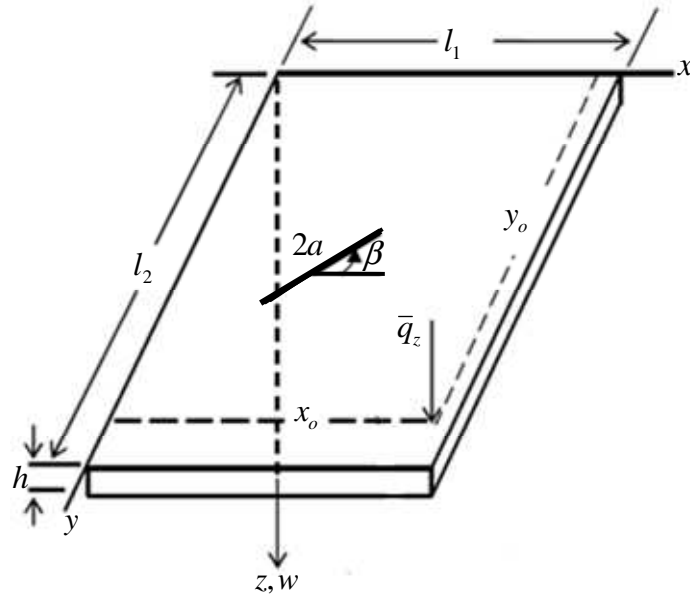


Figure 3-6 : A cracked plate subjected to an arbitrarily located load, \bar{q}_z (Israr, 2008)

The lateral load \bar{q}_z at position (x_o, y_o) , as illustrated in Figure 3-6, can be expressed as follows (Israr *et al.*, 2009),

$$\bar{q}_z = q_o(t)\delta(x - x_o)\delta(y - y_o) \quad (3.58)$$

By substituting equations (3.57) and (3.58) into (3.56), the following equation results,

$$\begin{aligned} & \frac{\partial^4 X_i}{\partial x^4} Y_j A_{ij} \psi_{ij}(t) + 2 \frac{\partial^4 X_i Y_j}{\partial x^2 \partial y^2} A_{ij} \psi_{ij}(t) + \frac{\partial^4 Y_j}{\partial y^4} X_i A_{ij} \psi_{ij}(t) - \frac{n_x}{D} \frac{\partial^2 X_i}{\partial x^2} Y_j A_{ij} \psi_{ij}(t) \\ & + \frac{a(1 + \cos 2\beta)}{(6\alpha_{tb} + \alpha_{tt})(1 - \nu^2)h + 2a} \frac{n_o}{D} \frac{\partial^2 Y_j}{\partial y^2} X_i A_{ij} \psi_{ij}(t) \\ & - \frac{a(1 + \cos 2\beta)}{3\left(\frac{\alpha_{bt}}{6} + \alpha_{bb}\right)(3 + \nu)(1 - \nu)h + 2a} \left(\frac{\partial^4 Y_j}{\partial y^4} X_i + \nu \frac{\partial^4 X_i Y_j}{\partial x^2 \partial y^2} \right) A_{ij} \psi_{ij}(t) \\ & + \frac{2a \sin 2\beta}{(6C_{tb} + C_{tt})(1 + \nu)h + 2a} \frac{n_o}{D} \frac{\partial^2 X_i Y_j}{\partial x \partial y} A_{ij} \psi_{ij}(t) \\ & + \frac{2a \sin 2\beta}{3\left(\frac{C_{bt}}{6} + C_{bb}\right)(1 + \nu)h + 2a} \left(\frac{\partial^4 X_i Y_j}{\partial x \partial y^3} + \nu \frac{\partial^4 X_i Y_j}{\partial x^3 \partial y} \right) A_{ij} \psi_{ij}(t) \\ & = - \frac{\rho h}{D} \frac{\partial^2 \psi_{ij}(t)}{\partial t^2} A_{ij} X_i Y_j + \frac{q_o(t)}{D} \delta(x - x_o) \delta(y - y_o) \end{aligned} \quad (3.59)$$

In this work, three types of boundary condition which were applied by Israr *et al.*, 2009 are re-used, namely all edges simply supported (SSSS), two adjacent edges of the plate clamped and the other two freely supported (CCSS), and two edges of the plate clamped and the other two free (CCFF). The appropriate expressions for the characteristics or modal functions that satisfy the stated boundary conditions of the plate are given below,

(a) With all edges simply supported (SSSS)

$$X_i = \sum_{i=1}^{\infty} \sin\left(\frac{i\pi x}{l_1}\right)$$

$$Y_j = \sum_{j=1}^{\infty} \sin\left(\frac{j\pi y}{l_2}\right) \quad (3.60)$$

(b) With two adjacent edges of the plate clamped and the other two freely supported (CCSS)

$$X_i = \sum_{i=1}^{\infty} \sin\frac{i\pi x}{l_1} \sin\frac{i\pi x}{2l_1}$$

$$Y_j = \sum_{j=1}^{\infty} \sin\frac{j\pi y}{l_2} \sin\frac{j\pi y}{2l_2} \quad (3.61)$$

(c) With two edges of the plate clamped and the other two free (CCFF)

$$X_i = \cos\left(\frac{\lambda_i x}{l_1}\right) - \cosh\left(\frac{\lambda_i x}{l_1}\right) - \gamma_i \left[\sin\left(\frac{\lambda_i x}{l_1}\right) - \sinh\left(\frac{\lambda_i x}{l_1}\right) \right]$$

$$Y_j = \cos\left(\frac{\lambda_j y}{l_2}\right) - \cosh\left(\frac{\lambda_j y}{l_2}\right) - \gamma_j \left[\sin\left(\frac{\lambda_j y}{l_2}\right) - \sinh\left(\frac{\lambda_j y}{l_2}\right) \right] \quad (3.62)$$

3.7 Application of the Berger Formulation

The Berger formulation can be used to investigate nonlinear vibrations when the strain energy due to the second invariant of the strains in the middle surface of the plate can justifiably be ignored. This condition is applied in order to determine the deflection of plates when that deflection is of the order of magnitude of the thickness of the plate. The applicability and simplicity of this approximation to the nonlinear vibration analysis of plates makes it a useful approach. Wah (1963) introduced the simplified Berger equation by imposing the condition that the in-plane displacements u and v can be assumed to disappear at the external boundaries, and therefore applied this equation for the vibration analysis of rectangular plates with large amplitudes, and with various boundary conditions. Vendhan (1975) considered the Berger equation for the nonlinear vibration analysis of elastic plates. In this research the Berger formulation is used to convert the derived governing equation of motion of the plate with a variably orientated surface crack into a nonlinear ordinary differential equation model. Initially an equation is developed for the in-plane forces in terms of the transverse deflection, w . This can be done by taking the components of the additional strain in the middle plane of the plate, due to small deflections in the x and y directions, as given by Timoshenko and Krieger (1959). The strain in the x direction taken in the middle of the plate is,

$$\varepsilon_x = \frac{\partial u}{\partial x} + \frac{1}{2} \left(\frac{\partial w}{\partial x} \right)^2 \quad (3.63)$$

Similarly the strain in the y direction is,

$$\varepsilon_y = \frac{\partial v}{\partial y} + \frac{1}{2} \left(\frac{\partial w}{\partial y} \right)^2 \quad (3.64)$$

Based on Kirchoff's assumptions the plane stress equations that relate in-plane stresses to in-plane strains for an isotropic material can be represented as (Timoshenko and Krieger, 1956),

$$n_x = \frac{Eh}{1-\nu^2} (\varepsilon_x + \nu\varepsilon_y) \quad (3.65)$$

$$n_o = \frac{Eh}{1-\nu^2} (\varepsilon_y + \nu\varepsilon_x) \quad (3.66)$$

Substitution of (3.63) and (3.64) into equations (3.65) and (3.66) give,

$$n_x = \frac{Eh}{1-\nu^2} \left[\frac{\partial u}{\partial x} + \frac{1}{2} \left(\frac{\partial w}{\partial x} \right)^2 + \nu \frac{\partial v}{\partial y} + \frac{1}{2} \nu \left(\frac{\partial w}{\partial y} \right)^2 \right] \quad (3.67)$$

$$n_o = \frac{Eh}{1-\nu^2} \left[\frac{\partial v}{\partial y} + \frac{1}{2} \left(\frac{\partial w}{\partial y} \right)^2 + \nu \frac{\partial u}{\partial x} + \frac{1}{2} \nu \left(\frac{\partial w}{\partial x} \right)^2 \right] \quad (3.68)$$

Given that $D = \frac{Eh^3}{12(1-\nu^2)}$ then equations (3.67) and (3.68) become,

$$\frac{n_x h^2}{12D} = \frac{\partial u}{\partial x} + \nu \frac{\partial v}{\partial y} + \frac{1}{2} \left(\frac{\partial w}{\partial x} \right)^2 + \frac{1}{2} \nu \left(\frac{\partial w}{\partial y} \right)^2 \quad (3.69)$$

$$\frac{n_o h^2}{12D} = \frac{\partial v}{\partial y} + \nu \frac{\partial u}{\partial x} + \frac{1}{2} \left(\frac{\partial w}{\partial y} \right)^2 + \frac{1}{2} \nu \left(\frac{\partial w}{\partial x} \right)^2 \quad (3.70)$$

Multiplying equations (3.69) and (3.70) by $dxdy$, and after integrating them over the plate area, leads to,

$$\frac{n_x h^2 l_1 l_2}{12D} = \int_0^{l_1} \int_0^{l_2} \left(\frac{\partial u}{\partial x} + \nu \frac{\partial v}{\partial y} + \frac{1}{2} \left(\frac{\partial w}{\partial x} \right)^2 + \frac{1}{2} \nu \left(\frac{\partial w}{\partial y} \right)^2 \right) dxdy \quad (3.71)$$

$$\frac{n_o h^2 l_1 l_2}{12D} = \int_0^{l_1} \int_0^{l_2} \left(\frac{\partial v}{\partial y} + \nu \frac{\partial u}{\partial x} + \frac{1}{2} \left(\frac{\partial w}{\partial y} \right)^2 + \frac{1}{2} \nu \left(\frac{\partial w}{\partial x} \right)^2 \right) dxdy \quad (3.72)$$

By imposing the condition that u and v can disappear at the external boundaries and around the crack because it is symmetrical, the equations reduce to,

$$\frac{n_x h^2 l_1 l_2}{12D} = \frac{1}{2} \int_0^{l_1} \int_0^{l_2} \left[\left(\frac{\partial w}{\partial x} \right)^2 + \nu \left(\frac{\partial w}{\partial y} \right)^2 \right] dxdy \quad (3.73)$$

$$\frac{n_o h^2 l_1 l_2}{12D} = \frac{1}{2} \int_0^{l_1} \int_0^{l_2} \left[\left(\frac{\partial w}{\partial y} \right)^2 + \nu \left(\frac{\partial w}{\partial x} \right)^2 \right] dxdy \quad (3.74)$$

Substituting then the expression for the transverse deflection $w(x, y, t)$ from equation (3.57) into equation (3.73) and (3.74), leads to, the resulting in-plane force equations in the x and y directions, in terms of the transverse deflection, which become,

$$n_x = \frac{6D}{h^2 l_1 l_2} A_{ij}^2 \psi_{ij}^2(t) \int_0^{l_1} \int_0^{l_2} \left[\left(\frac{\partial X_i}{\partial x} \right)^2 Y_j^2 + \nu \left(\frac{\partial Y_j}{\partial y} \right)^2 X_i^2 \right] dx dy \quad (3.75)$$

$$n_o = \frac{6D}{h^2 l_1 l_2} A_{ij}^2 \psi_{ij}^2(t) \int_0^{l_1} \int_0^{l_2} \left[\left(\frac{\partial Y_j}{\partial y} \right)^2 X_i^2 + \nu \left(\frac{\partial X_i}{\partial x} \right)^2 Y_j^2 \right] dx dy \quad (3.76)$$

These two in-plane force equations for n_x and n_o can be conveniently re-written as,

$$n_x = DP_{1ij} A_{ij}^2 \psi_{ij}^2(t) \quad (3.77)$$

where

$$P_{1ij} = \frac{6}{h^2 l_1 l_2} \sum_{i=1}^{\infty} \sum_{j=1}^{\infty} \int_0^{l_1} \int_0^{l_2} \left[\left(\frac{\partial X_i}{\partial x} \right)^2 Y_j^2 + \nu \left(\frac{\partial Y_j}{\partial y} \right)^2 X_i^2 \right] dx dy \quad (3.78)$$

and,

$$n_o = DP_{2ij} A_{ij}^2 \psi_{ij}^2(t) \quad (3.79)$$

with

$$P_{2ij} = \frac{6}{h^2 l_1 l_2} \sum_{i=1}^{\infty} \sum_{j=1}^{\infty} \int_0^{l_1} \int_0^{l_2} \left[\left(\frac{\partial Y_j}{\partial y} \right)^2 X_i^2 + \nu \left(\frac{\partial X_i}{\partial x} \right)^2 Y_j^2 \right] dx dy \quad (3.80)$$

Following on from this by substitution of the in-plane force expressions into equation (3.59), then by multiplying each term of this equation by the modal functions X_i and Y_j for one of the three types of boundary condition stated above, and then by integrating over the plate area, it can be seen that the following equation may be obtained,

$$\begin{aligned}
& \int_0^{l_1} \int_0^{l_2} \frac{\rho h}{D} A_{ij} X_i^2 Y_j^2 \ddot{\psi}_{ij}(t) \, dx dy + \\
& \int_0^{l_1} \int_0^{l_2} \left[X_i^{iv} Y_j + 2X_i'' Y_j'' + Y_j^{iv} X_i - \frac{a(1 + \cos 2\beta)}{3 \left(\frac{\alpha_{bt}}{6} + \alpha_{bb} \right) (3 + \nu)(1 - \nu)h + 2a} (Y_j^{iv} X_i + \nu X_i'' Y_j'') \right. \\
& \left. + \frac{2a \sin 2\beta}{3 \left(\frac{C_{bt}}{6} + C_{bb} \right) (1 + \nu)h + 2a} (X_i' Y_j''' + \nu X_i''' Y_j') \right] A_{ij} X_i Y_j \psi_{ij}(t) \, dx dy + \\
& \int_0^{l_1} \int_0^{l_2} \left[-P_{1ij} X_i'' Y_j + \frac{a(1 + \cos 2\beta)}{(6\alpha_{tb} + \alpha_{tt})(1 - \nu^2)h + 2a} P_{2ij} X_i Y_j'' \right. \\
& \left. + \frac{2a \sin 2\beta}{(6C_{tb} + C_{tt})(1 + \nu)h + 2a} P_{2ij} X_i' Y_j' \right] A_{ij}^3 X_i Y_j \psi_{ij}^3(t) \, dx dy \\
& = \int_0^{l_1} \int_0^{l_2} \frac{q_o(t) \delta(x - x_o) \delta(y - y_o)}{D} X_i Y_j \, dx dy
\end{aligned} \tag{3.81}$$

where X_i' , X_i'' , X_i''' , and X_i^{iv} are the first, second, third, and fourth derivatives of X_i with respect to x , and Y_j' , Y_j'' , Y_j''' , and Y_j^{iv} denote the first, second, third, and fourth derivatives of Y_j with respect to y . Equation (3.81) can be re-stated in the form of a nonlinear ordinary differential equation in terms of modal coordinates, as follows,

$$M_{ij} \ddot{\psi}_{ij}(t) + K_{ij} \psi_{ij}(t) + G_{ij} \psi_{ij}^3(t) = q_{ij} \tag{3.82}$$

Where

$$M_{ij} = \frac{\rho h}{D} \sum_{i=1}^{\infty} \sum_{j=1}^{\infty} A_{ij} \int_0^{l_1} \int_0^{l_2} X_i^2 Y_j^2 \, dx dy \tag{3.83}$$

$$\begin{aligned}
K_{ij} = \sum_{i=1}^{\infty} \sum_{j=1}^{\infty} A_{ij} \int_0^{l_1} \int_0^{l_2} & \left[X_i^{iv} Y_j + 2X_i'' Y_j'' + Y_j^{iv} X_i \right. \\
& - \frac{a(1 + \cos 2\beta)}{3 \left(\frac{\alpha_{bt}}{6} + \alpha_{bb} \right) (3 + \nu)(1 - \nu)h + 2a} (Y_j^{iv} X_i + \nu X_i'' Y_j'') \\
& \left. + \frac{2a \sin 2\beta}{3 \left(\frac{C_{bt}}{6} + C_{bb} \right) (1 + \nu)h + 2a} (X_i' Y_j''' + \nu X_i''' Y_j') \right] X_i Y_j \, dx dy
\end{aligned} \tag{3.84}$$

$$G_{ij} = \sum_{i=1}^{\infty} \sum_{j=1}^{\infty} A_{ij}^3 \int_0^{l_1} \int_0^{l_2} \left[-P_{1ij} X_i'' Y_j + \frac{a(1 + \cos 2\beta)}{(6\alpha_{tb} + \alpha_{tt})(1 - \nu^2)h + 2a} P_{2ij} X_i Y_j'' \right. \\ \left. + \frac{2a \sin 2\beta}{(6C_{tb} + C_{tt})(1 + \nu)h + 2a} P_{2ij} X_i Y_j' \right] X_i Y_j \, dx dy \quad (3.85)$$

and,

$$q_{ij} = \frac{q_o(t)}{D} Q_{ij} \quad (3.86)$$

where $Q_{ij} = X_i(x_o)Y_j(y_o)$ is the integral of the delta function given by Israr *et al.* (2009) in the form,

$$\int_{-\infty}^{\infty} X_i(x)\delta(x - x_o)dx = X_i(x_o) \quad (3.87)$$

By considering the system to be under the influence of weak classical linear viscous damping μ , and the load to be harmonic, then dividing through by the modal mass in equation (3.82) leads to the form of a specialised Duffing equation,

$$\ddot{\psi}_{ij}(t) + 2\mu\dot{\psi}_{ij}(t) + \omega_{ij}^2\psi_{ij}(t) + \gamma_{ij}\psi_{ij}^3(t) = \frac{\eta_{ij}}{D}q \cos \Omega_{ij}t \quad (3.88)$$

where

$$\omega_{ij}^2 = \frac{K_{ij}}{M_{ij}}, \quad (3.89)$$

$$\gamma_{ij} = \frac{G_{ij}}{M_{ij}}, \quad (3.90)$$

$$\eta_{ij} = \frac{Q_{ij}}{M_{ij}}, \quad (3.91)$$

also noting that q is the applied load acting on the surface of the plate and Ω_{ij} is the excitation frequency. This equation is also containing a cubic nonlinear term, damping term and the excitation term. ω_{ij} is the natural frequency of the plate with a variably

orientated crack and γ_{ij} is the nonlinear cubic term that can be positive or negative. It is positive valued when representing a hard spring and negative valued when representing a soft spring.

3.8 Enhanced Cracked Plate Simulation

In this section, simulation results are presented for the intact plate and the enhanced cracked plate model with three arbitrarily chosen types of boundary condition, namely SSSS, CCSS and CCFE. The type of material used in this investigation is an aluminium alloy of 5083 grade, with the following material properties: Modulus of elasticity $E = 7.03 \times 10^{10} \text{ N/m}^2$, plate density $\rho = 2660 \text{ kg/m}^3$, Poisson's ratio $\nu = 0.33$, and a measured damping ratio of $\mu = 0.08$. Results are presented for an investigation into the natural frequency of the first mode of the intact plate and the enhanced cracked plate model for various aspect ratios. These results are divided into three parts. A convergence study is firstly carried out for the cracked plate model of Israr *et al.* (2009) with a centrally located crack which is parallel to one side of the plate, in order to verify the correctness of the enhanced crack model within an analytical model of the plate. Secondly, studies are presented for a plate model with a variably oriented surface crack, and in this case onwards the cracked plate model with scaled geometry is used for comparison with the experimental results, as discussed later. The natural frequency for this model can be calculated using the definition from equation (3.88). The effects of the boundary conditions, geometry of the plate, the crack orientation angle, and crack length on the natural frequency value are all demonstrated in both sections. Thirdly, factors that influence changes in the trend of the natural frequency for the CCFE type of boundary condition are discussed in section 3.8.3.

3.8.1 A plate with a horizontally located centre crack, $\beta = 0^\circ$

The geometry of the plate used in this section is similar to that of Israr (2008) defined as $l_1 = 0.5 \text{ m}$, $l_2 = 1.0 \text{ m}$, and with plate thickness, $h = 0.01 \text{ m}$. The magnitude of the load chosen acting on the surface of the plate is, $q = 10 \text{ N}$ at some arbitrarily specified point located at $x_o = 0.375 \text{ m}$ and $y_o = 0.75 \text{ m}$ measured from the origin of the plate. Table 1 shows the results obtained for an intact and cracked plate with a horizontal centre crack, and where the middle point of the crack coincides with the centre of the plate. The half

crack lengths a chosen are 0.01m and 0.025m. The percentage differences between this model and that of Israr (2008) are presented here for the three boundary conditions. The results of the comparison of Table 3-1 show a very close agreement for all three boundary conditions. The values of the differences in the first mode natural frequencies of these two models are small with a maximum percentage error of approximately 0.012. Additionally, for all three cases, the results show generally that the natural frequency reduces with an increase in half-crack length and it is also influenced when the boundary condition and geometry of the plate is changed.

First mode natural Frequency, ω_j (rad/s)											
BCs.	Length of the plate (m)		Intact Plate		Error (%)	Cracked Plate $a = 0.01$ (m)		Error (%)	Cracked Plate $a = 0.025$ (m)		Error (%)
	l_1	l_2	This thesis	Israr (2008)		This thesis	Israr (2008)		This thesis	Israr (2008)	
SSSS	1.0	1.0	77.58	77.58	0	75.54	75.54	0	73.39	73.39	0
	0.5	1.0	193.95	193.95	0	192.54	192.54	0	191.09	191.09	0
	1.0	0.5	193.95	193.95	0	183.18	183.18	0	171.42	171.42	0
	0.5	0.5	310.32	310.32	0	302.17	302.17	0	293.57	293.57	0
CCSS	1.0	1.0	445.67	445.67	0	432.51	432.51	0	418.58	418.58	0
	0.5	1.0	1161.77	1161.77	0	1154.27	1154.27	0	1146.53	1146.53	0
	1.0	0.5	1161.77	1161.77	0	1089.99	1089.98	0.001	1011.06	1011.04	0.002
	0.5	0.5	1782.66	1782.66	0	1730.05	1730.04	0.001	1674.33	1674.31	0.001
CCFF	1.0	1.0	80.47	80.46	0.012	77.39	77.39	0	74.10	74.10	0
	0.5	1.0	231.08	231.06	0.009	229.97	229.95	0.009	228.82	228.80	0.009
	1.0	0.5	231.08	231.06	0.009	213.87	213.85	0.009	194.63	194.61	0.010
	0.5	0.5	321.87	321.85	0.006	309.56	309.54	0.006	296.40	296.38	0.007

Table 3-1 : Natural frequencies of the intact and cracked plate models with a horizontal crack located at the centre of the plate for various types of boundary condition and different aspect ratios

3.8.2 A plate with a variably orientated surface crack

In this section scaled geometric values of the plate model are used to make it compatible with experimental work specimens. The dimensions are $l_1 = 0.15$ m, $l_2 = 0.3$ m, plate thickness $h = 0.003$ m, and the load acting on the surface of the plate, q is assumed to be the same as previously used, which is 10 N. Tables 3-2, 3-3 and 3-4 show the results for the first mode natural frequency ω_{ij} for different boundary conditions, different lengths of half-crack and for different values of crack orientation angle, β . The orientation angle is chosen from 0° to 80° , in 20° steps and finishes at 90° . The crack is also located at the centre of the plate having 0.003 m and 0.0075 m half-crack lengths, respectively.

Crack angle, β (deg)	First Mode Natural Frequency, ω_{ij} (rad/s)					
	Intact Plate	Cracked Plate, $a = 0.003$ (m)	Cracked Plate, $a = 0.0075$ (m)	Intact Plate	Cracked Plate, $a = 0.003$ (m)	Cracked Plate, $a = 0.0075$ (m)
	Length of the square plate $l_1 = 0.3$ $l_2 = 0.3$			Length of the square plate $l_1 = 0.15$ $l_2 = 0.15$		
	258.60	-	-	1034.41	-	-
0°		251.81	244.65		1007.24	978.58
20°		252.61	246.32		1010.46	985.28
40°		254.64	250.51		1018.55	1002.02
60°		256.92	255.18		1027.68	1020.74
80°		258.40	258.19		1033.60	1032.77
90°		258.60	258.60		1034.41	1034.41
	Length of the rectangular plate $l_1 = 0.15$ $l_2 = 0.3$			Length of the rectangular plate $l_1 = 0.3$ $l_2 = 0.15$		
	646.50	-	-	646.50	-	-
0°		641.81	636.96		610.60	571.41
20°		642.36	638.08		614.91	580.69
40°		643.75	640.92		625.68	603.57
60°		645.33	644.13		637.72	628.57
80°		646.36	646.22		645.45	644.37
90°		646.50	646.50		646.50	646.50

Table 3-2 : Natural frequencies of the intact and cracked plate models with a variably orientated surface crack for the simply supported (SSSS) boundary condition, at various orientation angles.

As before, the results show that the natural frequency reduces with an increase in half-crack length, and this phenomenon is illustrated in Figure 3-7, as an example for a plate aspect ratio of 0.15/0.3. This ratio is also chosen for the experimental specimen in the next chapter since it has an exact rectangular geometry. From Figure 3-7 it can be seen that the derived cracked plate model predicts the natural frequency very well for cases with SSSS and CCSS boundary conditions compared to the case with CCFF boundary condition for which the prediction is rather inaccurate, especially for a half-crack length a of less than 0.001 m, as shown in Figure 3-7 for the CCFF case.

Crack angle, β (deg)	First Mode Natural Frequency, ω_{ij} (rad/s)					
	Intact Plate	Cracked Plate, $a = 0.003$ (m)	Cracked Plate, $a = 0.0075$ (m)	Intact Plate	Cracked Plate, $a = 0.003$ (m)	Cracked Plate, $a = 0.0075$ (m)
	Length of the square plate $l_1 = 0.3$ $l_2 = 0.3$			Length of the square plate $l_1 = 0.15$ $l_2 = 0.15$		
	1485.55	-	-	5942.22	-	-
0°		1441.70	1395.27		5766.82	5581.10
20°		1446.84	1406.06		5787.35	5624.25
40°		1459.88	1433.16		5839.53	5732.63
60°		1474.63	1463.41		5898.51	5853.66
80°		1484.22	1482.88		5936.87	5931.50
90°		1485.55	1485.55		5942.22	5942.22
	Length of the rectangular plate $l_1 = 0.15$ $l_2 = 0.3$			Length of the rectangular plate $l_1 = 0.3$ $l_2 = 0.15$		
	3872.56	-	-	3872.56	-	-
0°		3847.57	3821.77		3633.32	3370.19
20°		3850.31	3827.53		3662.06	3432.70
40°		3857.62	3842.51		3733.95	3586.21
60°		3866.06	3859.64		3814.09	3753.20
80°		3871.70	3870.92		3865.53	3858.34
90°		3872.56	3872.56		3872.56	3872.56

Table 3-3 : Natural frequencies of the intact and cracked plate models with a variably orientated surface crack for the clamped-clamped simply supported (CCSS) boundary condition, at various orientation angles

Crack angle, β (deg)	First Mode Natural Frequency, ω_{ij} (rad/s)					
	Intact Plate	Cracked Plate, $a = 0.003$ (m)	Cracked Plate, $a = 0.0075$ (m)	Intact Plate	Cracked Plate, $a = 0.003$ (m)	Cracked Plate, $a = 0.0075$ (m)
	Length of the square plate $l_1 = 0.3$ $l_2 = 0.3$			Length of the square plate $l_1 = 0.15$ $l_2 = 0.15$		
	268.22	-	-	1072.89	-	-
0°		247.29	223.78		989.15	895.10
20°		265.40	247.30		1061.58	989.21
40°		279.11	268.65		1116.42	1074.59
60°		282.94	279.22		1131.74	1116.86
80°		275.47	275.35		1101.90	1101.42
90°		268.22	268.22		1072.89	1072.89
	Length of the rectangular plate $l_1 = 0.15$ $l_2 = 0.3$			Length of the rectangular plate $l_1 = 0.3$ $l_2 = 0.15$		
	770.27	-	-	770.27	-	-
0°		743.88	715.78		650.48	498.48
20°		765.52	742.67		703.75	586.80
40°		782.78	769.00		757.28	689.93
60°		788.05	783.03		788.12	762.82
80°		779.10	778.91		784.84	782.59
90°		770.27	770.27		770.27	770.27

Table 3-4 : Natural frequencies of the intact and cracked plate models with a variably orientated surface crack for the clamped-clamped free-free (CCFF) boundary condition, at various orientation angles

Furthermore, in terms of the crack orientation angle effect for the boundary conditions SSSS and CCSS, as shown in Figure 3-8, it can clearly be seen that the natural frequency increases with the increase in the crack angle, up to 90°. But it is different for the case of the CCFF boundary condition, where the frequency increases up to 60°, and then decreases when β exceeds 60°. This similar trend in the crack orientation effect was also studied by Maruyama and Ichinomiya (1989) who did experiments on clamped rectangular plates with a crack at various orientation angles. Wu and Law (2004) also investigated experimentally a thick plate with an oriented crack for the free boundary condition case, where the frequency was found to increase with an increase in the crack angle of up to 60°, but which reduced for crack angles exceeding 60°.

The results show overall that the cracked plate model is very sensitive to the crack length and crack orientation angle and that it is able to predict natural frequency values for the crack very well for the cases tested using the SSSS and CCSS boundary conditions. However, for a cracked plate with the CCFE boundary condition the prediction showed some disagreement between the intact plate and the cracked plate for a crack orientation angle of 40° and above. In this case the natural frequency value for the cracked plate is higher than for the intact plate, and this does not fulfil the general expectation that cracks lower the natural frequencies due to their reductions in the overall stiffness of the plate.

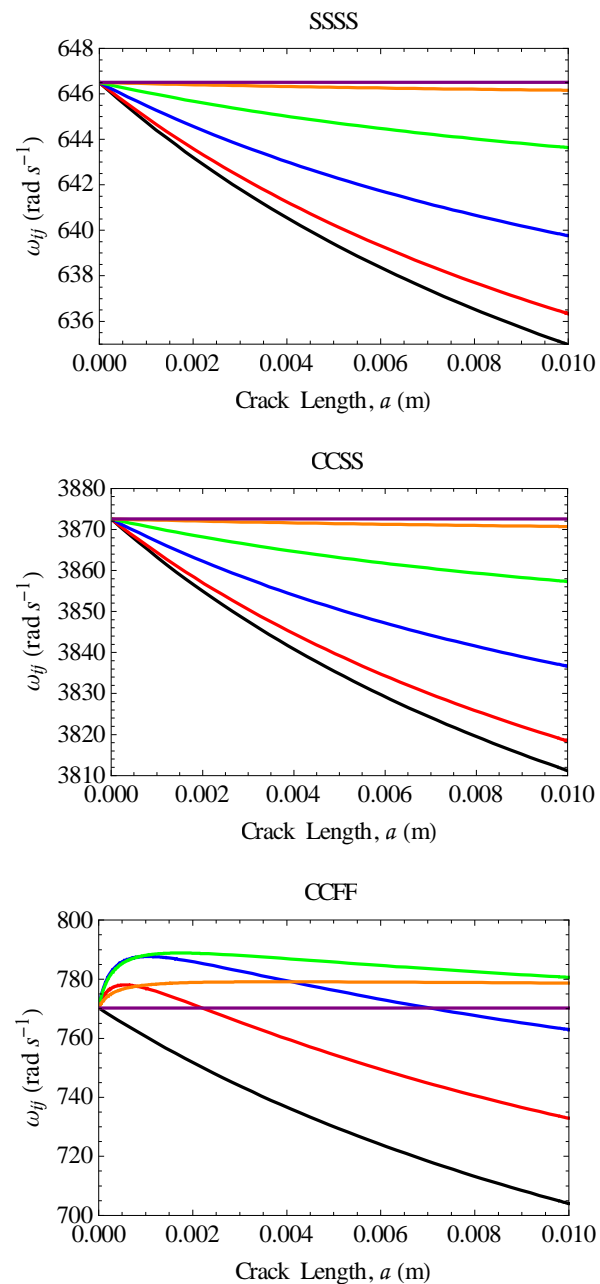


Figure 3-7: First mode natural frequency as a function of half-crack length for the cracked plate model with an aspect ratio of 0.15/0.3, at different values of crack orientation angle from 0° to 90° for the SSSS, CCSS, and CCFE boundary conditions (Black, 0° ; Red, 20° ; Blue, 40° ; Green, 60° ; Orange, 80° ; Purple, 90°)

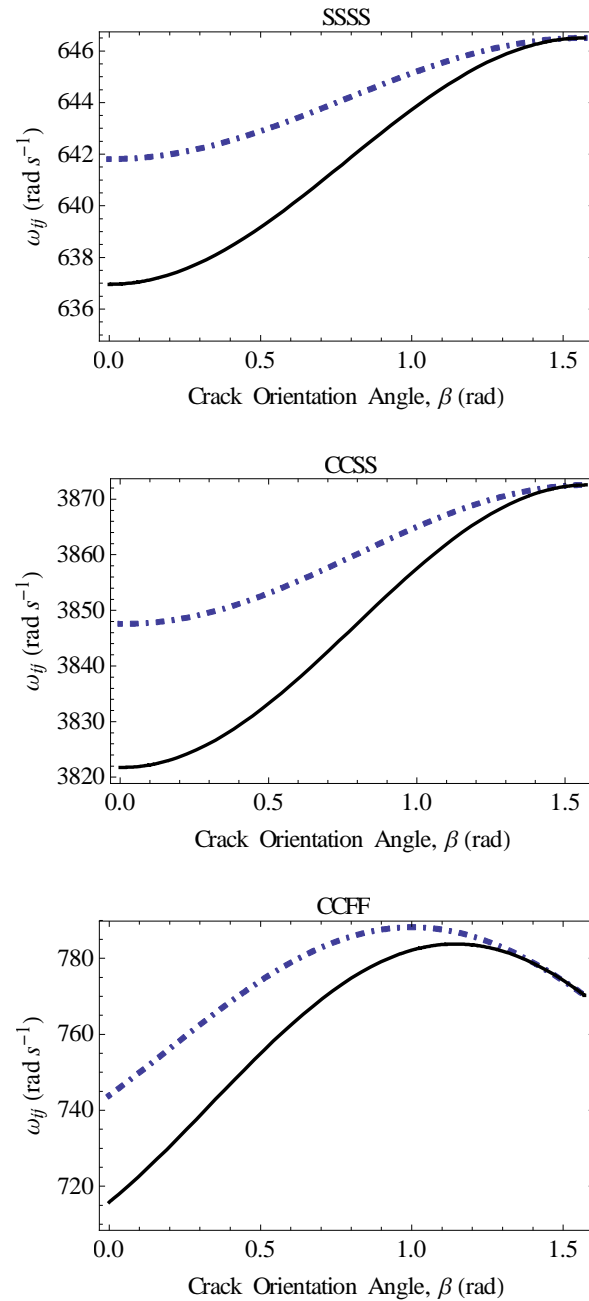


Figure 3-8: First mode natural frequency as a function of crack orientation angle for the cracked plate model with an aspect ratio of 0.15/0.3, for SSSS, CCSS, and CCF boundary conditions (Dotted line, half-crack length of 3.0 mm; Black line, half-crack length of 7.5 mm)

3.8.3 Factors which influence changes in the natural frequency

Besides the effect of crack length it is also found that the vibrational characteristics i.e. the natural frequency of the cracked plate structure, can be affected significantly by the orientation of the crack in the surface of the plate depending on the type of boundary condition applied. In this section a parametric study is performed on the natural frequency equation of the cracked plate for the case of the CCF boundary condition. This type of boundary condition is selected because the results showed changes in the trend of the

natural frequency values at an angle of 60° and where this trend is seen to be different to that of the SSSS and CCSS boundary conditions. Therefore, the objective of this study is to examine cracked plate model configurations in order to determine the physical parameters that influence the changeover of the maximum value of crack orientation angle. Here, *maximum* means that value of crack orientation angle for which the natural frequency reaches a maximum value before it then decreases. In this simulation the natural frequency of the cracked plate model is calculated by using equation (3.89). The series of natural frequency equations in term of crack orientation angle is obtained and this is then used to calculate the natural frequency value for a range of β values from 0° to 90° . From here, the maximum natural frequency can be found. However there are competing effects within the analysis at this stage and only a lengthy parametric study could uncover the numerical mechanisms causing this effect.

3.8.3.1 Crack Length

In this simulation half-crack lengths are chosen from the range of 0.1 mm to 30 mm. Results of the crack orientation angle for maximum natural frequency as a function of half-crack length a , is plotted and shown in Figure 3-9. It is found that the crack length influences the crack orientation angle for maximum natural frequency, for example when the half-crack length is 1 mm the natural frequency increases for the crack angle β , up to 50.77° and reduces when β exceeds 50.77° . When the half-crack length increases to 30 mm, the natural frequency increases up to $\beta = 75.06^\circ$ and then decreases when β exceeds 75.06° . The results given in Figure 3-9 shows that the crack orientation angle for which the natural frequency is maximum increases with the crack length.

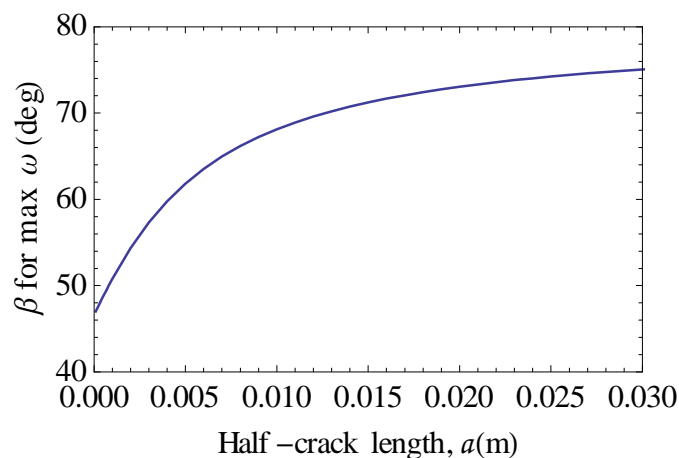


Figure 3-9 : β for maximum natural frequency as a function of half-crack length for the cracked plate model with an aspect ratio of 0.15/0.3

3.8.3.2 Plate Thickness, h

Figure 3-10 shows the crack orientation angle, β , for maximum natural frequency as a function of the plate thickness h , from the range of 0.1 mm to 30 mm. The result shows that the orientation of the crack for maximum natural frequency is also affected by the thickness of the plate, in which the value of β for maximum natural frequency decreases with an increase in the plate thickness.

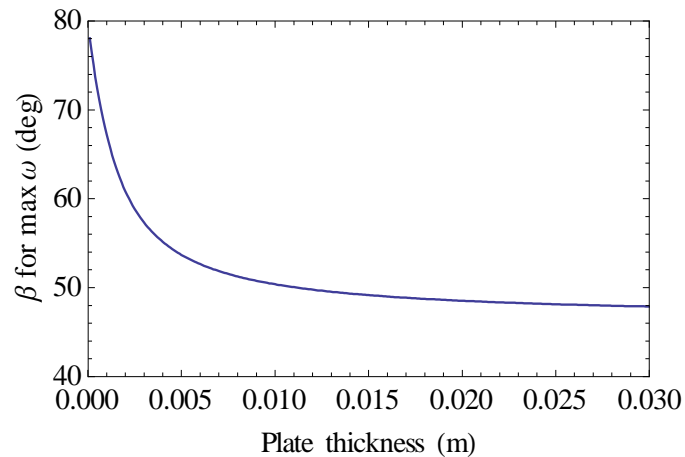


Figure 3-10 : β for maximum natural frequency as a function of plate thickness for the cracked plate model with an aspect ratio of 0.15/0.3

3.8.3.3 Plate Aspect Ratio (l_1/l_2), R_p

Plate aspect ratio is defined here as the length ratio of the side on the x -direction to the side on the y -direction. In this simulation the plate aspect ratio is studied for the range 0.1 to 1.0. Plate aspect ratio effects on the crack angle for the maximum natural frequency can be observed in Figure 3-11. The result shows that the crack orientation angle for maximum natural frequency increases with the plate aspect ratio.

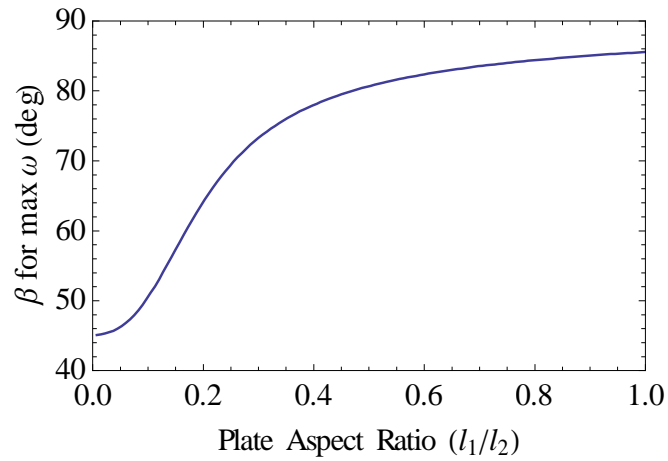


Figure 3-11 : β for maximum natural frequency as a function of plate aspect ratio for the cracked plate model

3.8.3.4 Poisson Ratio

The crack orientation angle for maximum natural frequency as a function of Poisson ratio is illustrated in Figure 3-12. It can be seen that the crack angle for which the natural frequency is maximum decreases up to 0.42, and then increases when the ratio exceeds 0.42.

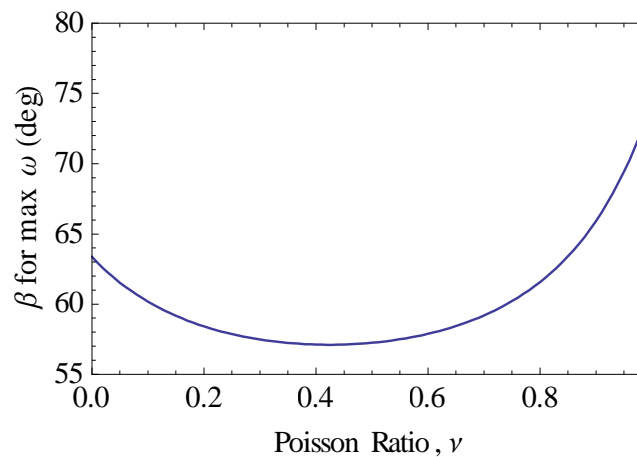


Figure 3-12 : β for maximum natural frequency as a function of Poisson Ratio for the cracked plate model

3.8.3.5 Density, ρ and Modulus of Elasticity, E

In this simulation density and modulus of elasticity of the cracked plate are varied from the range of 1500 kgm^{-3} to 3000 kgm^{-3} and $1.0 \times 10^{10} \text{ Nm}^{-2}$ to $10 \times 10^{10} \text{ Nm}^{-2}$, respectively. However, both of the results only show a very slight difference in the crack orientation angle for a maximum natural frequency value, and no significant changes can be observed from Figure 3-13.

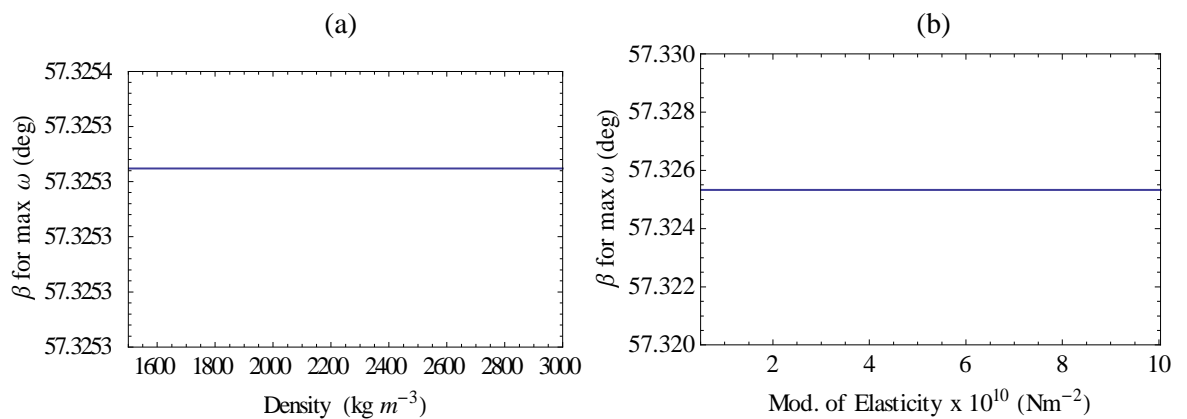


Figure 3-13 : β for maximum natural frequency as a function of (a) Density and (b) Modulus of Elasticity

3.9 Chapter Conclusions

The equation of motion for a plate containing a surface crack of variable angular orientation in the form of a specialised Duffing equation has been derived. This proposed mathematical model is capable of detecting and predicting the vibration behaviour of the cracked plate, and showing the trend of the natural frequency values for the SSSS, CCSS and CCFE boundary conditions. Besides the boundary conditions, crack length, and location of the point load, it is also found that the vibrational characteristics of the plate structure can be affected significantly by the orientation of the crack. In addition, the physical parameters such as crack length, plate thickness, plate aspect ratio, Poisson ratio, plate density and modulus of elasticity also contribute to the changes in the orientation angles for which the natural frequency is maximum.

Chapter 4

Approximate Solution Methods

4.1 Introduction

This chapter presents approximate solutions for the nonlinear problem of a plate with a surface crack of variable angular orientation. The solutions obtained are used in order to study and interpret the physical behaviour of this cracked plate model. An approximate analytical method based on the perturbation method of multiple scales and an appropriate numerical solution technique i.e. the Finite Element Method, within the Abaqus/CAE environment, are applied here to solve this problem. In addition, for purposes of comparison, the numerical results are also calculated by directly integrating the nonlinear ordinary differential equation for the model and the results from this are compared with the results obtained from the multiple scales method.

4.2 Approximate Analytical Method: First Order Multiple Scales Method

One of the most widely used perturbation methods is the method of multiple scales. This is an approximate analytical technique and is frequently used for obtaining close-form solutions for nonlinear problems. The multiple scales method was successfully applied by Israr (2008) and Israr *et al.* (2009) for the horizontal centrally located crack problem. In the case of primary resonance analysis the excitation frequency is usually assumed to be close to the linear natural frequency of the system, and the detailed derivation of the appropriate amplitude frequency-response equations are described in those references. Here this method is re-applied in order to investigate the nonlinear behaviour of a plate with a variably orientated surface crack.

The basic idea behind this approach is that the single independent variable, T is uniformly split up into several new independent variables $T_1, T_2, T_3, \dots, T_n$ and these independent variables define successively slower dependencies for the dependent variables when expressed in term of a uniformly valid expansion equation. The dependent variables are typically expressed by the following (Cartmell *et al.*, 2010):

$$x(t, \varepsilon) = \sum_{n=0}^{m-1} \varepsilon^n x_n(T_0, T_1, \dots, T_m) + o(\varepsilon T_m) \quad (4.1)$$

where $T_n = \varepsilon^n t$ and the parameter, ε , is known as a (small) perturbation parameter with $\varepsilon \ll 1$. $x(t, \varepsilon)$ is a vector and its expansion in equation (4.1) is considered to be uniformly valid for times up to $O(\varepsilon^{-m})$. The aim of this section is to find an approximate analytical solution to the forced nonlinear vibration problem for a plate with a variably orientated crack by using a first order multiple scales expansion. So, for the co-ordinate that we are using here, ψ_{ij} , the dependent variables would typically have this form,

$$\psi_{ij}(t, \varepsilon) = \psi_{0ij}(T_0, T_1) + \varepsilon \psi_{1ij}(T_0, T_1) + o(\varepsilon^2) \quad (4.2)$$

where ψ_{0ij} and ψ_{1ij} are solution functions yet to be determined and T_0 and T_1 are successively slower time scales. The multiple independent variables T_n are generated with respect to real (clock) time t given by,

$$T_n = \varepsilon^n t \quad \text{for } n = 0, 1, 2, \dots \quad (4.3)$$

So, when $n = 0$;

$$T_0 = t, \quad (4.4)$$

And when $n = 1$;

$$T_1 = \varepsilon^1 t \quad (4.5)$$

On this basis the first and second time derivatives can be perturbed as follows,

$$\frac{d}{dt} = \frac{dT_0}{dt} \frac{\partial}{\partial T_0} + \frac{dT_1}{dt} \frac{\partial}{\partial T_1} + \frac{dT_2}{dt} \frac{\partial}{\partial T_2} + \dots \quad (4.6)$$

$$\text{or } \frac{d}{dt} = \frac{\partial}{\partial T_0} + \varepsilon \frac{\partial}{\partial T_1} + \varepsilon^2 \frac{\partial}{\partial T_2} + \dots \quad (4.7)$$

Re-stating equation (4.6) by using the D -operator to represent the term $\frac{\partial}{\partial T_n}$ gives,

$$\frac{d}{dt} = D_0 + \varepsilon D_1 + \varepsilon^2 D_2 + \dots + \varepsilon^n D_n \quad (4.8)$$

The second time derivative is,

$$\begin{aligned} \frac{d^2}{dt^2} = & \frac{\partial(D_0 + \varepsilon D_1 + \varepsilon^2 D_2 + \dots)}{\partial T_0} + \varepsilon \frac{\partial(D_0 + \varepsilon D_1 + \varepsilon^2 D_2 + \dots)}{\partial T_1} \\ & + \varepsilon^2 \frac{\partial(D_0 + \varepsilon D_1 + \varepsilon^2 D_2 + \dots)}{\partial T_2} + \dots \end{aligned} \quad (4.9)$$

thus,

$$\frac{d^2}{dt^2} = D_0^2 + 2\varepsilon D_0 D_1 + \varepsilon^2 (D_1^2 + 2D_0 D_2) + 2\varepsilon^3 D_1 D_2 + \varepsilon^4 D_2^2 + \dots \quad (4.10)$$

Before applying the method of multiple scales to obtain an approximate solution to this problem it is necessary to *order* the cubic term, the damping, and the excitation term. These terms are ordered by means of the small parameter ε according to their perceived relative numerical strength. To accomplish this we assume that the cubic term is a definitionally weak term, thus it is assumed to become,

$$\gamma = \varepsilon \hat{\gamma} \quad (4.11)$$

We also choose to impose a condition of weak damping which gives,

$$\mu = \varepsilon \hat{\mu} \quad (4.12)$$

and we decide to classify the excitation term as a soft excitation, so,

$$q = \varepsilon \hat{q} \quad (4.13)$$

Clearly, all terms are ordered to $O(\varepsilon)^1$ so that they will appear at the first order of approximation. By substitution of (4.11), (4.12) and (4.13) into equation (3.88) it becomes as follows,

$$\ddot{\psi}_{ij}(t) + 2\varepsilon \hat{\mu} \dot{\psi}_{ij}(t) + \omega_{ij}^2 \psi_{ij}(t) + \varepsilon \hat{\gamma}_{ij} \psi_{ij}^3(t) = \varepsilon \frac{\eta_{ij}}{D} \hat{q} \cos \Omega_{ij} t \quad (4.14)$$

From this, substituting the uniformly valid expansion of equation (4.2) and the time derivative equations (4.8) and (4.10) into the ordinary differential equation (ODE) of the equation (4.14), we obtain,

$$\begin{aligned} & (D_0^2 + 2\varepsilon D_0 D_1 + 2\varepsilon^2 D_0 D_2 + \varepsilon D_1^2) (\psi_{0ij} + \varepsilon \psi_{1ij}) \\ & + 2\varepsilon \hat{\mu} (D_0 + \varepsilon D_1 + \varepsilon^2 D_2) (\psi_{0ij} + \varepsilon \psi_{1ij}) + \omega_{ij}^2 (\psi_{0ij} + \varepsilon \psi_{1ij}) \\ & + \varepsilon \hat{\gamma} (\psi_{0ij} + \varepsilon \psi_{1ij})^3 = \varepsilon \frac{\eta_{ij}}{D} \hat{q} \cos \Omega_{ij} t \end{aligned} \quad (4.15)$$

Expanding equation (4.15) leads to the following form,

$$\begin{aligned} & D_0^2 \psi_{0ij} + 2\varepsilon D_0 D_1 \psi_{0ij} + 2\varepsilon^2 D_0 D_2 \psi_{0ij} + \varepsilon^2 D_1^2 \psi_{0ij} + \varepsilon D_0^2 \psi_{1ij} + 2\varepsilon^2 D_0 D_1 \psi_{1ij} \\ & + 2\varepsilon^3 D_0 D_2 \psi_{1ij} + \varepsilon^3 D_1^2 \psi_{1ij} + 2\varepsilon \hat{\mu} D_0 \psi_{0ij} + 2\varepsilon^2 \hat{\mu} D_1 \psi_{0ij} + 2\varepsilon^3 \hat{\mu} D_2 \psi_{0ij} \\ & + 2\varepsilon^2 \hat{\mu} D_0 \psi_{1ij} + 2\varepsilon^3 \hat{\mu} D_1 \psi_{1ij} + 2\varepsilon^4 \hat{\mu} D_2 \psi_{1ij} + \omega_{ij}^2 \psi_{0ij} + \omega_{ij}^2 \varepsilon \psi_{1ij} \\ & + \varepsilon \hat{\gamma} \psi_{0ij}^3 + 3\varepsilon^2 \hat{\gamma} \psi_{0ij}^2 \psi_{1ij} + 3\varepsilon^3 \hat{\gamma} \psi_{0ij} \psi_{1ij}^2 + \varepsilon^4 \hat{\gamma} \psi_{1ij}^3 = \varepsilon \frac{\eta_{ij}}{D} \hat{q} \cos \Omega_{ij} t \end{aligned} \quad (4.16)$$

By equating the coefficients of like powers of ε , and neglecting terms of order greater than ε^1 in equation (4.16) leads to a definition of the zeroth order perturbation equation,

$$\varepsilon^0 : D_0^2 \psi_{0ij} + \omega_{ij}^2 \psi_{0ij} = 0, \quad (4.17)$$

and also the first order perturbation equation,

$$\varepsilon^1 : D_0^2 \psi_{1ij} + \omega_{ij}^2 \psi_{1ij} = -2D_0 D_1 \psi_{0ij} - 2\hat{\mu} D_0 \psi_{0ij} - \hat{\gamma}_{ij} \psi_{0ij}^3 + \frac{\eta_{ij}}{D} \hat{q} \cos \Omega_{ij} t \quad (4.18)$$

The general solution of the zeroth order perturbation equation can be written in pure function form or in complex exponential form. In this case we choose the complex

exponential form as a general solution for equation (4.17) because this solution is ultimately more algebraically convenient,

$$\psi_{0ij} = B e^{i\omega_j T_0} + \bar{B} e^{-i\omega_j T_0} \quad (4.19)$$

B is an as yet unknown complex amplitude and a function of the slower time scale T_1 and \bar{B} is the complex conjugate of B . Next, by substituting this solution appropriately into the right hand side of equation (4.18), we get

$$\begin{aligned} D_0^2 \psi_{1ij} + \omega_{ij}^2 \psi_{1ij} = & -2D_0 D_1 (B e^{i\omega_j T_0} + \bar{B} e^{-i\omega_j T_0}) - 2\hat{\mu} D_0 (B e^{i\omega_j T_0} + \bar{B} e^{-i\omega_j T_0}) \\ & - \hat{\gamma}_{ij} (B e^{i\omega_j T_0} + \bar{B} e^{-i\omega_j T_0})^3 + \frac{\eta_{ij}}{D} \hat{q} \cos \Omega_{ij} t \end{aligned} \quad (4.20)$$

Expanding, and after differentiating as necessary with respect to T_0 , gives the following equation,

$$\begin{aligned} D_0^2 \psi_{1ij} + \omega_{ij}^2 \psi_{1ij} = & -2i\omega_{ij} D_1 B e^{i\omega_j T_0} + 2i\omega_{ij} D_1 \bar{B} e^{-i\omega_j T_0} - 2i\hat{\mu}\omega_{ij} B e^{i\omega_j T_0} + 2i\hat{\mu}\omega_{ij} \bar{B} e^{-i\omega_j T_0} \\ & - \hat{\gamma}_{ij} B^3 e^{3i\omega_j T_0} - 3\hat{\gamma}_{ij} B^2 \bar{B} e^{i\omega_j T_0} - 3\hat{\gamma}_{ij} B \bar{B}^2 e^{-i\omega_j T_0} - \hat{\gamma}_{ij} \bar{B}^3 e^{-3i\omega_j T_0} \\ & + \frac{\eta_{ij}}{D} \left(\frac{\hat{q}}{2} e^{i\Omega_{ij} t} + \frac{\hat{q}}{2} e^{-i\Omega_{ij} t} \right) \end{aligned} \quad (4.21)$$

It can be seen that equation (4.21) contains secular terms that will lead to non-uniform contributions from ψ_{1ij} . Accordingly, to identify secular terms easily, for removal, we have in this case to take a common factor of $e^{i\omega_j T_0}$ out from the right hand side of equation (4.21),

$$\begin{aligned} D_0^2 \psi_{1ij} + \omega_{ij}^2 \psi_{1ij} = & e^{i\omega_j T_0} \left(-2i\omega_{ij} D_1 B + 2i\omega_{ij} D_1 \bar{B} e^{-i2\omega_j T_0} - 2i\hat{\mu}\omega_{ij} B + 2i\hat{\mu}\omega_{ij} \bar{B} e^{-i2\omega_j T_0} \right. \\ & - \hat{\gamma}_{ij} B^3 e^{i2\omega_j T_0} - 3\hat{\gamma}_{ij} B^2 \bar{B} - 3\hat{\gamma}_{ij} B \bar{B}^2 e^{-i2\omega_j T_0} \\ & \left. - \hat{\gamma}_{ij} \bar{B}^3 e^{-i4\omega_j T_0} + \frac{\eta_{ij}}{D} \frac{\hat{q}}{2} e^{i(\Omega_{ij} - \omega_j) T_0} + \frac{\eta_{ij}}{D} \frac{\hat{q}}{2} e^{-i(\Omega_{ij} + \omega_j) T_0} \right) \end{aligned} \quad (4.22)$$

In equation (4.22), if Ω_{ij} is close to ω_{ij} which means that $\Omega_{ij} \approx \omega_{ij}$ then the second last term inside the large brackets becomes almost secular, and if $\Omega_{ij} = \omega_{ij}$ then this term is

secular. So we take the well known form of the detuning parameter, as given by Nayfeh and Mook (1979),

$$\Omega_{ij} = \omega_{ij} + \varepsilon \sigma_{ij} \quad (4.23)$$

In general this is called the primary resonance condition with σ_{ij} as the detuning parameter. The detuning parameter is introduced to signify the closeness of the excitation frequency, Ω_{ij} to a natural frequency, ω_{ij} of this system. Subsequently, substitution of (4.23) into (4.22) leads to the following equation,

$$\begin{aligned} D_0^2 \psi_{1ij} + \omega_{ij}^2 \psi_{1ij} = e^{i\omega_{ij}T_0} & \left(-2i\omega_{ij} D_1 B + 2i\omega_{ij} D_1 \bar{B} e^{-i2\omega_{ij}T_0} - 2i\hat{\mu}\omega_{ij} B + 2i\hat{\mu}\omega_{ij} \bar{B} e^{-i2\omega_{ij}T_0} \right. \\ & - \hat{\gamma}_{ij} B^3 e^{i2\omega_{ij}T_0} - 3\hat{\gamma}_{ij} B^2 \bar{B} - 3\hat{\gamma}_{ij} B \bar{B}^2 e^{-i2\omega_{ij}T_0} - \hat{\gamma}_{ij} \bar{B}^3 e^{-i4\omega_{ij}T_0} \\ & \left. + \frac{\eta_{ij}}{D} \frac{\hat{q}}{2} e^{i\varepsilon\sigma_{ij}T_0} + \frac{\eta_{ij}}{D} \frac{\hat{q}}{2} e^{-i(2\omega_{ij} + \varepsilon\sigma_{ij})T_0} \right) \end{aligned} \quad (4.24)$$

Eliminating the secular terms by setting these terms to zero gives,

$$-i2\omega_{ij} D_1 B - i2\hat{\mu}\omega_{ij} B - 3\hat{\gamma}_{ij} B^2 \bar{B} + \frac{\eta_{ij}}{D} \frac{\hat{q}}{2} e^{i\varepsilon\sigma_{ij}T_0} = 0 \quad (4.25)$$

Imposing the conditions that $B = B(T_1)$ for the amplitude to be steady-state or nearly so, thus the steady-state value of the complex amplitude, B , is given in the usual form of,

$$B = \frac{1}{2} b e^{i\alpha} \quad (4.26)$$

This allows us to introduce real valued amplitude and phase information ($b = b(T_1)$ and $\alpha = \alpha(T_1)$). By differentiating this equation (4.26) with respect to slow time T_1 we obtain,

$$\frac{dB}{dT_1} = D_1 B = \frac{1}{2} b' e^{i\alpha} + i \frac{b}{2} \alpha' e^{i\alpha} \quad (4.27)$$

Substituting equations (4.26) and (4.27) into equation (4.25) yields,

$$\begin{aligned}
 & -i2\omega_{ij}\left(\frac{1}{2}b'e^{i\alpha} + i\frac{b}{2}\alpha'e^{i\alpha}\right) - i2\hat{\mu}\omega_{ij}\left(\frac{1}{2}be^{i\alpha}\right) - 3\hat{\gamma}_{ij}\left(\frac{1}{2}be^{i\alpha}\right)^2\left(\frac{1}{2}be^{-i\alpha}\right) \\
 & + \frac{\eta_{ij}}{D}\frac{\hat{q}}{2}e^{i\sigma_{ij}T_1} = 0
 \end{aligned} \tag{4.28}$$

Expanding equation (4.28) and dividing through by $e^{i\alpha}$ gives,

$$\omega_{ij}b\alpha' - i\omega_{ij}b' - i\hat{\mu}\omega_{ij}b - \frac{3}{8}\hat{\gamma}_{ij}b^3 + \frac{\eta_{ij}}{D}\frac{\hat{q}}{2}e^{i(\sigma_{ij}T_1 - \alpha)} = 0 \tag{4.29}$$

Converting the excitation term into real and imaginary parts means that equation (4.29) becomes,

$$\omega_{ij}b\alpha' - i\omega_{ij}b' - i\hat{\mu}\omega_{ij}b - \frac{3}{8}\hat{\gamma}_{ij}b^3 + \frac{\eta_{ij}}{D}\frac{\hat{q}}{2}[\cos(\sigma_{ij}T_1 - \alpha) + i\sin(\sigma_{ij}T_1 - \alpha)] = 0 \tag{4.30}$$

Separating this out into its real and imaginary parts leads to the following equations,

$$\text{Re: } b\alpha' = \frac{3\hat{\gamma}_{ij}b^3}{8\omega_{ij}} - \frac{\eta_{ij}}{2D\omega_{ij}}\hat{q}\cos(\sigma_{ij}T_1 - \alpha) \tag{4.31}$$

$$\text{Im: } b' = -\mu b + \frac{\eta_{ij}}{2D\omega_{ij}}\hat{q}\sin(\sigma_{ij}T_1 - \alpha) \tag{4.32}$$

Equation (4.31) contains the slowly varying phase angle α' in one term. Equation (4.32) contains the slowly varying amplitude b' . Both of these equations also contain explicit references to time through the time scale T_1 . This can conveniently be removed for subsequent ease of solution by introducing a transformed phase angle, ϕ ,

$$\phi = \sigma_{ij}T_1 - \alpha \tag{4.33}$$

Thus the slow-time phase and amplitude modulation equations become,

$$b\phi' = b\sigma_{ij} - \frac{3\hat{\gamma}_{ij}b^3}{8\omega_{ij}} + \frac{\eta_{ij}}{2D\omega_{ij}}\hat{q}\cos\phi \quad (4.34)$$

$$b' = -\mu b + \frac{\eta_{ij}}{2D\omega_{ij}}\hat{q}\sin\phi \quad (4.35)$$

For steady state conditions b' and ϕ' are taken to be zero, so we obtain,

$$\sigma_{ij}b - \frac{3\hat{\gamma}_{ij}b^3}{8\omega_{ij}} = -\frac{\eta_{ij}}{2D\omega_{ij}}\hat{q}\cos\phi, \quad (4.36)$$

and equation (4.35) becomes,

$$\mu b = \frac{\eta_{ij}}{2D\omega_{ij}}\hat{q}\sin\phi \quad (4.37)$$

Substituting equation (4.37) into equation (4.36) and applying a basic trigonometrical identity, leads to the frequency-response equation,

$$\sigma_{ij} = \frac{3\hat{\gamma}_{ij}b^2}{8\omega_{ij}} \pm \sqrt{\frac{\eta_{ij}^2}{4D^2\omega_{ij}^2b^2}\hat{q}^2 - \hat{\mu}^2} \quad (4.38)$$

This can readily be re-structured,

$$\hat{\mu}^2b^2 + \left(\sigma_{ij} - \frac{3\hat{\gamma}_{ij}b^2}{8\omega_{ij}}\right)^2 = \frac{\eta_{ij}^2}{4D^2\omega_{ij}^2}\hat{q}^2 \quad (4.39)$$

Next, the first order perturbation solution can be obtained by considering the right hand side of equation (4.24) with the secular terms removed,

$$D_0^2\psi_{ij} + \omega_{ij}^2\psi_{ij} = e^{i\omega_j T_0} \left(-\hat{\gamma}_{ij}B^3 e^{i2\omega_j T_0} - \hat{\gamma}_{ij}\bar{B}^3 e^{-i4\omega_j T_0} \right) \quad (4.40)$$

Multiplying out the right hand side,

$$D_0^2 \psi_{1ij} + \omega_{ij}^2 \psi_{1ij} = -\hat{\gamma}_{ij} B^3 e^{i3\omega_{ij}T_0} - \hat{\gamma}_{ij} \bar{B}^3 e^{-i3\omega_{ij}T_0} \quad (4.41)$$

Equation (4.41) can also be written as,

$$D_0^2 \psi_{1ij} + \omega_{ij}^2 \psi_{1ij} = -\hat{\gamma}_{ij} B^3 e^{i3\omega_{ij}T_0} + cc \quad (4.42)$$

where cc denotes the complex conjugate of the first right hand side term of equation (4.42).

The particular solution of ψ_{1ij} can be obtained by taking a trial solution for this equation, and its first and second time derivatives, in the form of,

$$\psi_{1ij} = A e^{i3\omega_{ij}T_0} + C e^{-i3\omega_{ij}T_0} \quad (4.43)$$

$$\dot{\psi}_{1ij} = i3\omega_{ij} A e^{i3\omega_{ij}T_0} - i3\omega_{ij} C e^{-i3\omega_{ij}T_0} \quad (4.44)$$

$$\ddot{\psi}_{1ij} = -9\omega_{ij}^2 A e^{i3\omega_{ij}T_0} - 9\omega_{ij}^2 C e^{-i3\omega_{ij}T_0} \quad (4.45)$$

Substituting equations (4.43) and (4.45) into equation (4.42) and grouping terms together with the same exponent, we then get the constants A and C,

$$A = \frac{\hat{\gamma}_{ij} B^3}{8\omega_{ij}^2} \quad \text{and} \quad C = \frac{\hat{\gamma}_{ij} \bar{B}^3}{8\omega_{ij}^2} \quad (4.46)$$

By substituting these quantities back into equation (4.43), gives the particular solution for ψ_{1ij} , as,

$$\psi_{1ij} = \left(\frac{\hat{\gamma}_{ij} B^3}{8\omega_{ij}^2} \right) e^{i3\omega_{ij}T_0} + \left(\frac{\hat{\gamma}_{ij} \bar{B}^3}{8\omega_{ij}^2} \right) e^{-i3\omega_{ij}T_0} \quad (4.47)$$

It should be noted that this equation can also be obtained directly by using the DSolve function in *Mathematica*TM. Finally, the uniformly valid expansion for the first order approximate solution can be obtained by substituting equations (4.19) and (4.47) into

equation (4.2), and after converting the exponent terms into trigonometric forms the full solution to first order ε becomes,

$$\psi_{ij}(t, \varepsilon) = b \cos(\Omega t - \phi) + \frac{\hat{\gamma}_{ij} b^3}{32\omega_{ij}^2} \cos(3\Omega t - 3\phi) + o(\varepsilon^2) \quad (4.48)$$

Into which numerically calculated values for b can be obtained from equation (4.39).

4.2.1 Linear and Nonlinear frequency response curves

The analytical results for the solution based on the approximate method of multiple scales are shown in Figures 4.1 and 4.2. These Figures show curves for the nonlinear response which represent the behaviour of square and rectangular plates containing the orientated surface crack for the three different types of boundary conditions. Equation (4.39) is used to plot these curves, in which the nonlinear coefficient, γ_{ij} is initially set to zero to generate the linear response curve. The aspect ratio chosen for the rectangular plate is 1:2 and similar mechanical and geometric properties as used in the previous section are re-used here. For $\gamma_{ij} \neq 0$ the system displays typical nonlinear characteristics, as evident in the Figures, with characteristic hardening and softening phenomena for a 0.003 m half-crack length. In these Figures, for the cracked plate model with the SSSS and CCSS boundary conditions, the nonlinearity bends the curves to the right, as for a hardening system. In this case the nonlinear hardening effect is clearly much stronger for the SSSS boundary condition. However, for the CCFB boundary condition the nonlinearity bends the curves to the left as for a softening system. It is evident that for all types of boundary condition, the cracked rectangular plate model with an aspect ratio of 1:2 displays a much stronger general nonlinearity than that for a square plate model.

4.2.2 Factors that influence nonlinearity

4.2.2.1 Crack orientation angle, β

The influence of the crack orientation angle on the frequency response is observed. The results are shown in Figures 4-1 and 4-2. Cases tested for the SSSS and CCSS boundary conditions show no obvious hardening effects for rectangular plates. However for square

plates, with an increase in the crack orientation angle, the nonlinear hardening increases. For the CCFF boundary condition it can clearly be seen that the nonlinear hardening effect increases up to 60° and then reduces when the crack orientation angles starts to exceed 60° . It should be noted that the amplitude decreases with the increase in frequency.

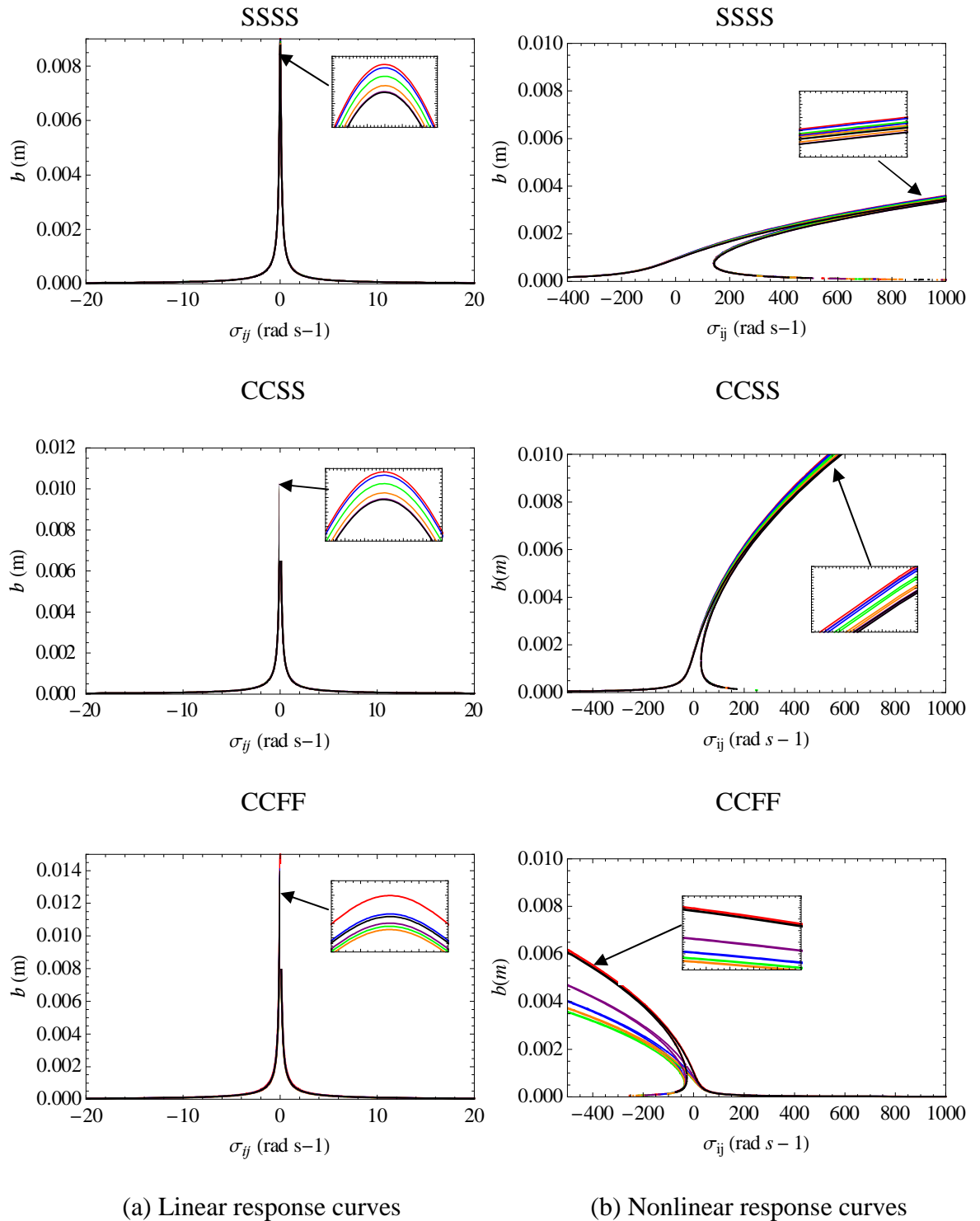


Figure 4-1 : Linear and nonlinear response curves for the cracked square plate model, for three types of boundary conditions (0° : Red line, 20° : Blue line, 40° : Green line, 60° : Orange line, 80° : Purple line, 90° : Black line)

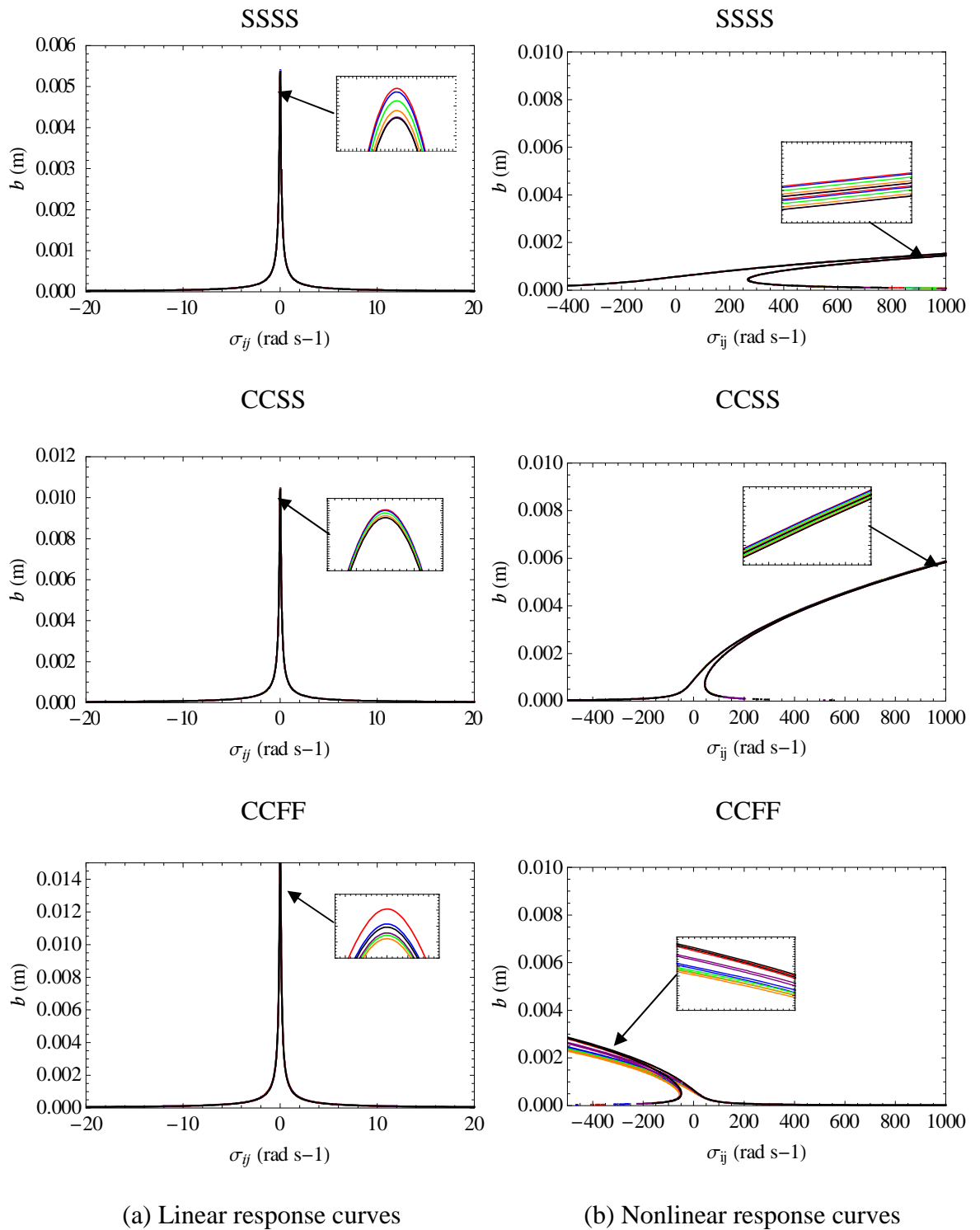


Figure 4-2 : Linear and nonlinear response curves for the cracked rectangular plate model with an aspect ratio of 1:2, for three types of boundary conditions (0° : Red line, 20° : Blue line, 40° : Green line, 60° : Orange line, 80° : Purple line, 90° : Black line)

4.2.2.2 Location of the applied load

Next, the effect of the location of the applied load (x_o, y_o) on the plate surface for a cracked rectangular plate where $l_1 = 0.15$ m and $l_2 = 0.3$ m, with the CCFB boundary condition and 3 mm half-crack length is investigated, as shown in Figure 4-3. The Figure shows the responses for the cracked plate with 0° , 40° , 60° and 90° crack orientation angles. For instance, p1 in the caption represents the location of an applied load at point (0.1125, 0.1125), p2 at point (0.1125, 0.15) and p3 at point (0.1125, 0.225). The point (x_o, y_o) is measured from the fixed end of the plate. As shown in this Figure, it is found that the widths of the nonlinear region become narrower as the excitation location moves closer to the constrained area.

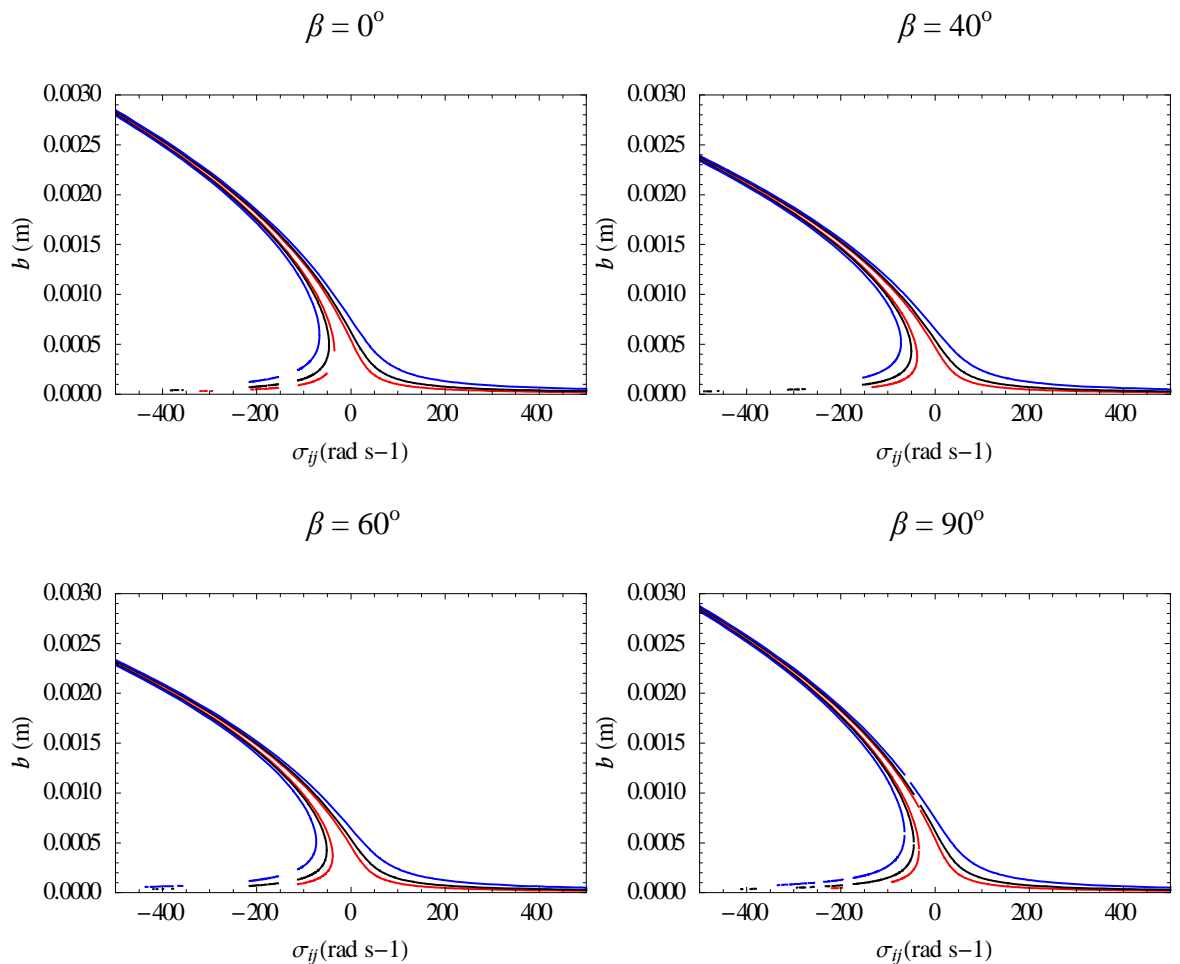


Figure 4-3 : Frequency response curves for a rectangular plate with a variably orientated surface crack for different locations of the applied load (p1: Red line, p2: Black line, p3: Blue line.

4.2.2.3 Excitation amplitude

Subsequently, as shown in Figure 4-4, the influence of the excitation amplitude on the frequency response curves is shown. A similar plate as investigated to that of the previous section is used, with an excitation amplitude value which is varied, i.e. to 5 N, 10 N, 15 N and 20 N. The results show that the amplitudes increase when the excitation amplitude increases.

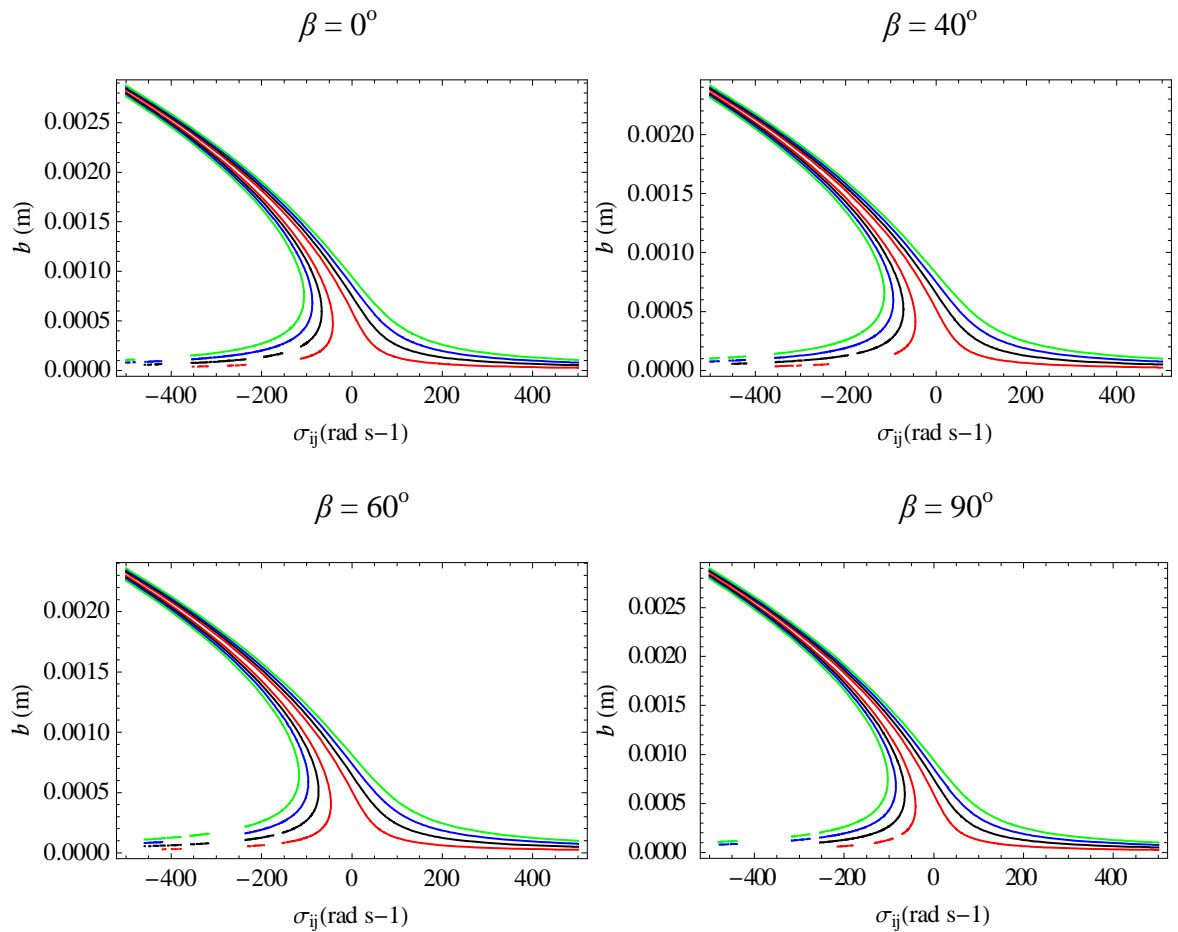


Figure 4-4 : The influence of the excitation amplitude on the nonlinearity of the rectangular plate with a surface crack of variable orientation (5N: Red line, 10N: Black line, 15N: Blue line, 20N: Green line)

4.2.2.4 Damping coefficient

In general the damping coefficient will influence the response curves. As the damping coefficient becomes larger the peaks of each harmonic gradually reduce, and then finally disappear. For the undamped situation i.e. when $\mu = 0$, the predicted peak amplitude is infinite.

4.3 Direct Integration Method

In order to make meaningful conclusions some appropriate bench-marking is needed. The numerical results are therefore calculated by directly integrating the nonlinear ordinary differential equation (3.88). For this numerical computation the NDSolve function is used by imposing the initial conditions $\psi_{ij}(0) = 0$ and $\dot{\psi}_{ij}(0) = 0$. In this simulation the frequency detuning values are chosen from the range of -400 rad/s to 400 rad/s. The simulation is run for 0° , 20° , 40° , 60° , 80° and 90° crack orientation angles. The solution can be used to construct plots in the time and frequency domains and then a list of amplitude values can be obtained from these graphs. The amplitude values are selected for steady state condition. Figure 4-6 shows the responses of the cracked plate for each crack orientation angle, and a comparison is made with the approximate analytical solutions obtained in section 4.1. In this figure, NI represents the numerical integration result and MMS represents the result obtained from the method of multiple scales. The numerical integration results qualitatively and quantitatively produce a similarly decreasing response in the frequency and an increasing response in the amplitude. It can be seen in all figures that there is an apparent changeover from upper to lower branches at around frequency detuning value of -150 rad/s in which the jump phenomena can be observed. The NI solution captures the amplitude response of the MMS very well for the range of the excitation frequencies. However, the overhanging part of the curve represents an unstable solution, and this over-prediction of the softening overhang by the multiple scales solution is undoubtedly due to an over-correction to the solution from the first order perturbation contribution.

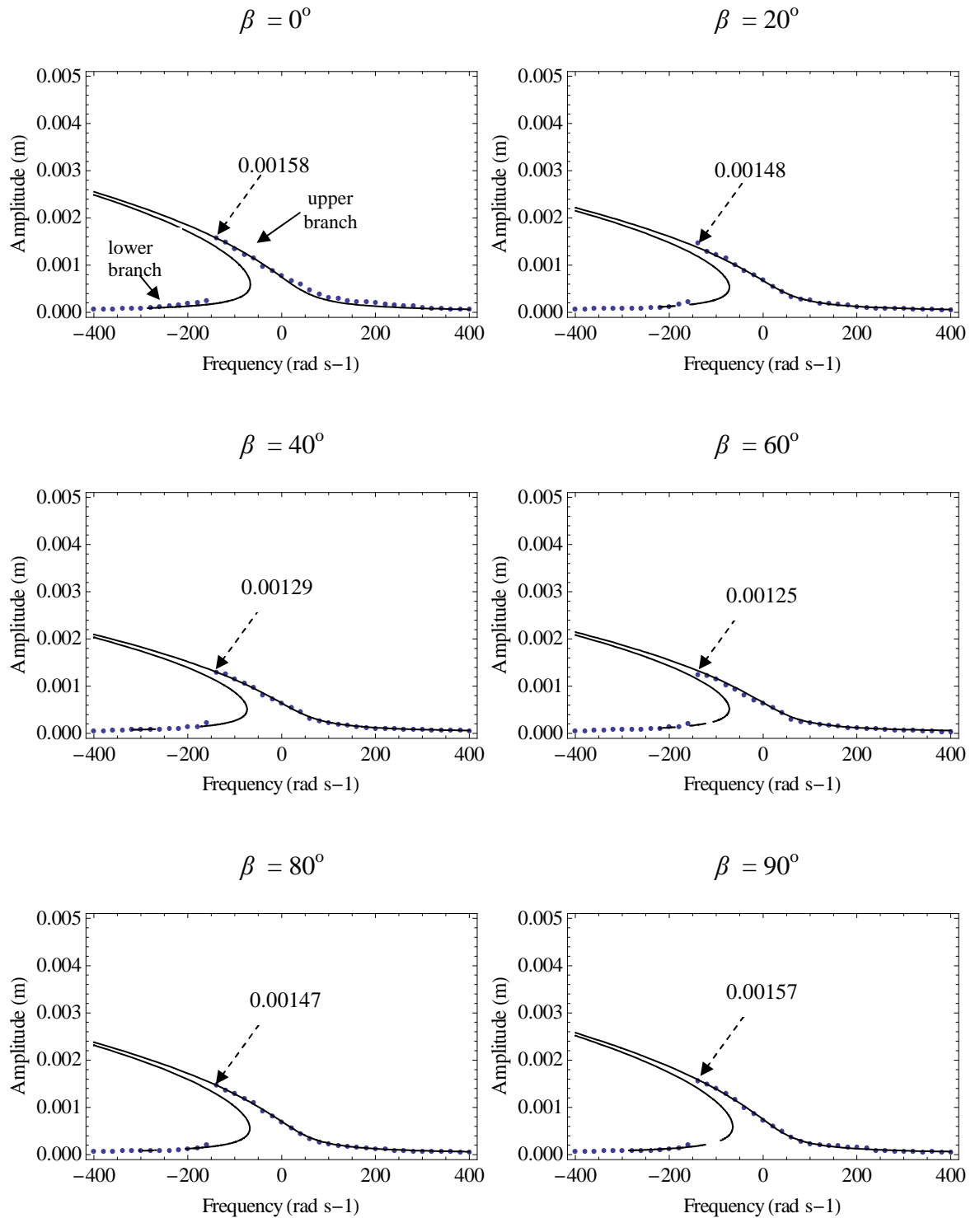


Figure 4-5 : Comparison of nonlinear response curves for the cracked rectangular plate model with an aspect ratio of 1:2 between numerical integration and the method of multiple scales, for different crack orientation angles (Dotted line: NI, Solid line: MMS).

4.4 Numerical Solution Technique: FE Method (ABAQUS/CAE 6.9.1)

Various numerical solution techniques have been developed and applied to solve numerous vibration problems in order to find their approximate solutions. The finite element method is one of the major numerical solution techniques and is the most widely applied computer simulation method in engineering. The main advantage of the finite element method is that a general purpose computer program can be easily modified in order to analyse specific problem types. This is very useful for the study of structures of irregular geometry subjected to various types of loading and boundary conditions. The finite element procedure involves three basic steps for the computation carried out, which may be termed as; i) Pre-processing (building the finite element model, loading and imposition of constraints), ii) FEA solver (assembly and solution of the system of equations), and iii) Post-processing (sorting and displaying the results).

There are many available commercial FEM software packages, good examples being ANSYS, NASTRAN, PATRAN, Dyna-3D, and ABAQUS. In this study, finite element analysis using ABAQUS/CAE 6.9.1 is undertaken to model and analyse the vibration of the intact and cracked plate problem. ABAQUS can solve problems of relatively simple structural analysis to the most complicated linear and nonlinear analyses. In ABAQUS, there are several intrinsic methods that can be used to perform dynamic analysis. However, for the study and analysis of a nonlinear dynamics problem expressed in ODE form, as here, then direct integration of the system must be used. There are two basic types of direct integration methods offered in ABAQUS, namely, i) Implicit Direct Integration which is provided in ABAQUS/Standard and ii) Explicit Direct Integration provided in ABAQUS/Explicit.

The direct integration method provided in ABAQUS/Standard uses an implicit Hilber-Hughes-Taylor operator in order to integrate the equations of motion. The integration operator matrix is inverted and a set of nonlinear equilibrium equations are solved at each time increment. This offers the use of all elements in ABAQUS, however it can be slower than the explicit, approach. ABAQUS/Explicit uses a central-difference integration operator as the method of solution. In nonlinear dynamic analysis ABAQUS/CAE automatically selects appropriate load increments and convergence tolerances and continually adjusts them during the analysis to make sure that an accurate solution is achieved. For reasons of validation and comparison of the theoretical model a finite

element model is used for a further modal analysis in order to corroborate the effect of crack length and crack orientation angle on the modal parameters i.e. natural frequency and also the vibrational amplitude as predicted by the theoretically-calculated results.

4.4.1 The sequence of steps required to perform the FE Analysis

The model used is a 150 x 300 x 3 mm aluminium alloy plate. Table 4-2 shows the material and element properties of the model. The material used in this investigation is Aluminium type 5083 which was used in the previous section and commonly found in many industrial applications. The steps taken to perform the elastic finite element analysis using ABAQUS/CAE are as follows:

1. Creation of the part

- Initially, the rectangular plate is modelled in three-dimensions, giving a deformable solid model by sketching the two dimensional profile of the rectangular plate and extruding it. Thirteen plate models are created. One represents the intact plate and another twelve plates representing the plates with various crack orientation angles, specifically at 0° , 20° , 40° , 60° , 80° , and 90° with respect to the x direction of the plate, for a half-crack length of 3 mm and 7.5 mm, respectively. A crack with a depth of 1.8 mm is created on each plate by the use of the cut feature under the shape entry in the main menu.

2. Creation of the material definition

- This defines the material properties in the Property module, including the modulus of elasticity, Poisson's ratio and density of the plate, as listed in Table 4-2.

3. Definition and assignation of the section properties

- Here one creates a homogeneous solid section, and performs section assignment of the part in the same module.

4. Assembly of the model

- In the Assembly module one creates a new part instance by double clicking the entry instances shown in the model tree.

Property name		Details
Material	Name	Aluminium 5083
	Density	2 660 kg/m ³
	Young's Modulus	7.03 × 10 ¹⁰ N/m ²
	Poisson's ratio	0.33
Element	Type	C3D8R- Linear solid element
	Geometric order	Linear

Table 4-1 : Properties of the aluminium rectangular plate model for FE analysis

5. Configuration of the analysis

- Creation of the steps for the analysis using the step module.
 - Step - Linear Perturbation – Frequency

A frequency extraction analysis is performed to determine the vibration modes of the plate. The standard Lanczos method (ABAQUS, 2011) has been applied to extract the natural frequencies and mode shapes for the intact and cracked plates. The frequency range allows for 10 vibration modes to be identified.

- Step – General – Dynamic, Implicit

An implicit analysis is used to analyse the intact and cracked plates. This procedure is used to compute the amplitude response of the plate models. This step specifies the initial increment size and the number of increments which is allowed. NLGEOM is a geometrically nonlinear switch. The problem is under a geometrically linear analysis when the switch is off. When the switch is on geometrically nonlinear analysis is performed.

6. Application of Boundary Conditions and a Load

- The boundary conditions and loading are applied in the load module. The Boundary condition chosen is CCFF, and a concentrated force of 10 N is applied at a distance of 225 mm from the fixed edge parallel to the x -axis and 115 mm from the fixed edge parallel to the y -axis.

7. Meshing the model

- The Mesh Module is used to generate the finite element mesh. The mesh of the part is created using the element shape and analysis with the standard, 3D stress, C3D8R -8 node linear brick using reduced integration. The C3D8R is an 8-node 3D hexahedral element and a good mesh with this type of element usually provides a solution of equivalent accuracy at less cost (ABAQUS, 2011).

8. Creating and submitting an analysis job

- When the definition of the plate model is complete, an analysis is created and submitted to analyse the model. The job is submitted in the job module and analysis is performed.

9. Viewing the analysis results

- The results of the analysis are viewed in the visualisation module

4.4.2 Numerical Results

The finite element analysis is undertaken on thirteen rectangular plate models, comprising one for the plate without a crack and twelve for the plate with a crack located at the centre. The crack lengths chosen are 3 mm and 7.5 mm, while the orientation angle, β of the crack with respect to the x -axis is varied from 0° to 80° in 20° steps, and for an inclination angle of 90° as well. The arbitrary boundary condition for all the plate models is CCFF and the lengths of the sides of the plate are taken as $l_1 = 150$ mm in the x -direction and $l_2 = 300$ mm in the y -direction, which means the aspect ratio of the plate is 0.5/1. A concentrated force of 10 N is applied at a distance of 225 mm from the fixed edge on the x -axis and 115 mm from the fixed edge on the y -axis. The plates are discretised using from 22 043 up to

24 817 linear solid (C3D8R) elements. The number of elements for each plate differs depending on the length and the orientation angle of the crack. Initially, a frequency extraction analysis is performed using the Lanczos method to extract the natural frequencies and mode shapes of the intact and cracked plate models. The frequency range allowed for 10 vibration modes to be identified.

Subsequently an implicit dynamic nonlinear analysis is employed in order to obtain the amplitude responses of this model. In implicit dynamic analysis the integration operator matrix is inverted and a set of nonlinear equilibrium equations is solved at each time increment (ABAQUS, 2011). In the step module of this analysis a specific value of the initial increment size and the number of increments is required. Thus, to perform the implicit dynamic analysis for this model, the Step module is edited as follows:

Basic tab time period: 20

Incrementation tab type: Fixed

Maximum number of increments: 2000

Increment size: 0.01

Check: Suppress half-step residual calculation.

NLGEOM: On

The periodic load is applied with a magnitude of 10 N under the resonant frequency. The steps taken in order to define this load are:

Tools --- amplitude --- create --- periodic.

In the Edit Amplitude dialog box, one enters a value of frequency for each plate model in the circular frequency field.

4.4.2.1 Frequency Extraction Analysis

In Table 4-3 the frequency values taken from the frequency extraction analysis for the three first modes of the cracked plate, for orientation angle β , are shown, together with the results for an intact plate. It can be seen that the large crack shifts the frequency values of the 1st, 2nd and 3rd modes downwards, as expected and due to reduced plate stiffness. In terms of the crack orientation angle effects for both crack lengths of 3 mm and 7.5 mm, the frequency values increase monotonously from 0° up to 60° ($0^\circ < \beta \leq 60^\circ$), and then decrease when β is more than 60° ($\beta > 60^\circ$).

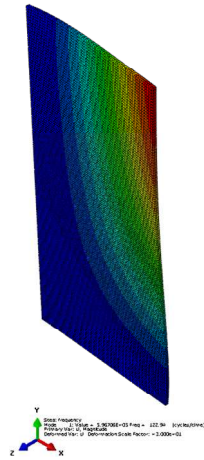
FEA Results					
		Crack Orientation angle, β	Frequency (Hz)		
			First vibration mode	Second vibration mode	Third vibration mode
Intact Plate		-	122.94	259.80	525.16
Cracked Plate	3 mm	0°	122.73	259.32	524.18
		20°	122.77	259.49	524.37
		40°	122.84	259.82	525.00
		60°	123.05	260.79	527.47
		80°	122.82	259.54	524.38
		90°	122.73	259.36	524.22
	7.5mm	0°	122.69	259.13	524.00
		20°	122.75	259.37	524.18
		40°	122.81	259.74	524.79
		60°	123.04	260.72	527.34
		80°	122.81	259.57	524.29
		90°	122.69	259.33	524.12

Table 4-2 : Frequency extraction analysis for 1st, 2nd, and 3rd modes of vibration

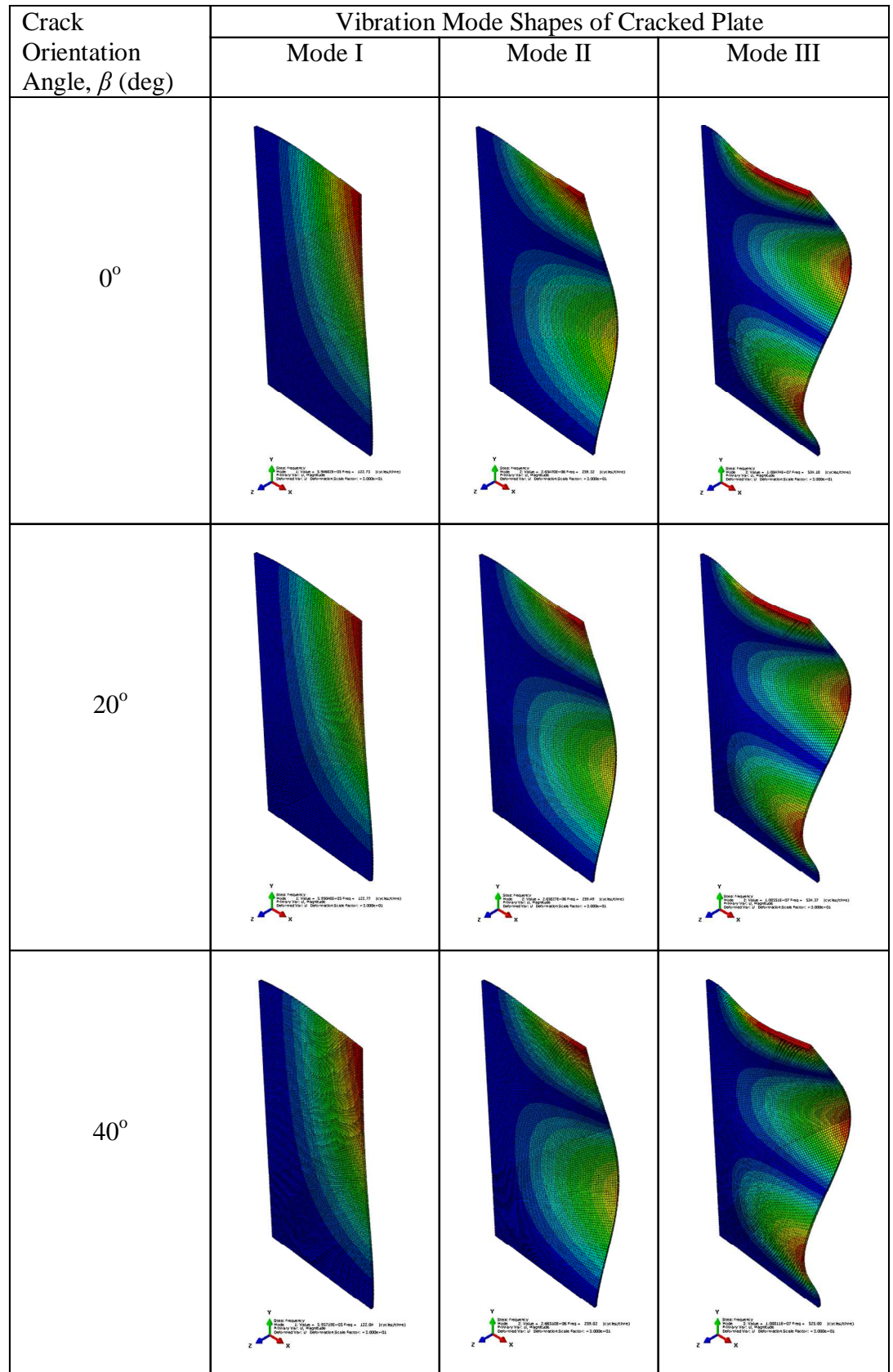
Figure 4-7 shows the first three modes of vibration for the intact plate. Figures 4-8 to 4-19 illustrate the first three mode shapes of the plates for a surface crack with an orientation angle from 0° to 90°. The dark blue areas in these Figures indicate nodal displacements for the first three modes of vibration, representing the areas where the displacement is close to zero.

4.4.2.1.1 The first three vibration mode shapes of the intact plate

(a) Mode I



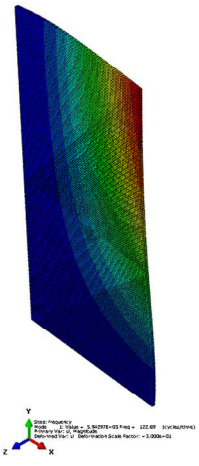
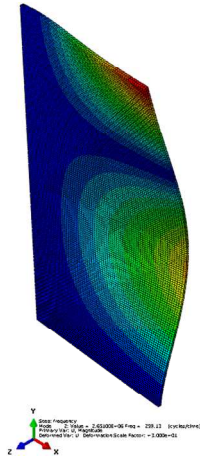
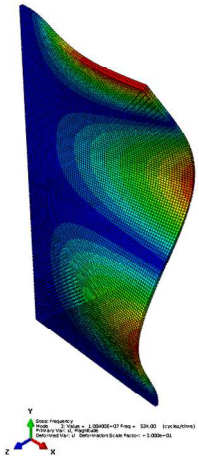
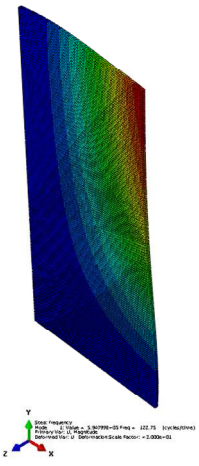
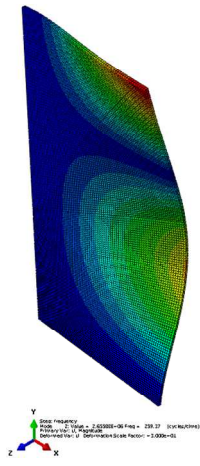
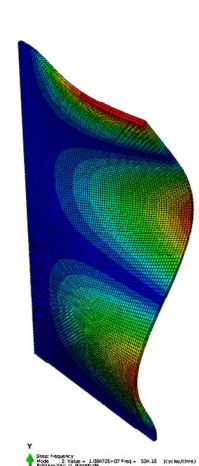
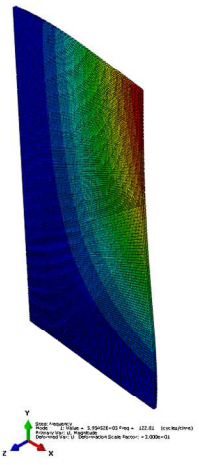
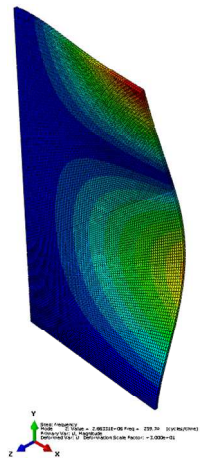
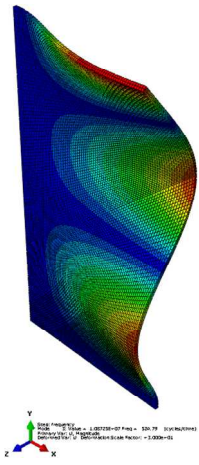
4.4.2.1.2 The first three vibration mode shapes of the plate with a crack of variable orientation for a half-crack length of 3 mm



Crack Orientation Angle, β (deg)	Vibration Mode Shapes of Cracked Plate		
	Mode I	Mode II	Mode III
60°			
80°			
90°			

Table 4-3 : Vibration mode shapes of cracked plates for half-crack length of 3 mm

4.4.2.1.3 The first three vibration mode shapes of the plate having a crack of variable orientation for a half-crack length of 7.5 mm

Crack Orientation Angle, β (deg)	Vibration Mode Shapes of Cracked Plate		
	Mode I	Mode II	Mode III
0°			
20°			
40°			

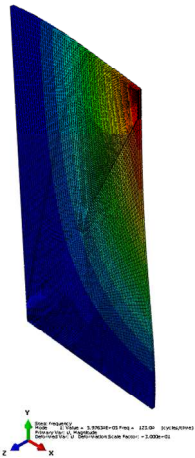
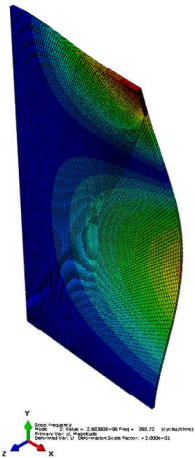
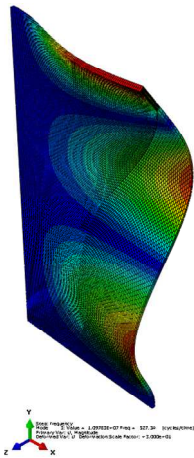
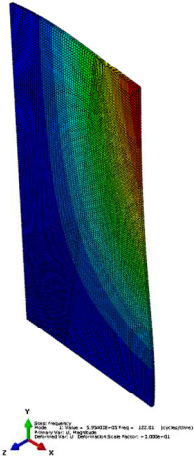
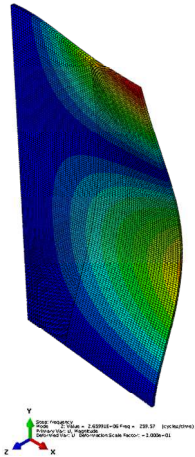
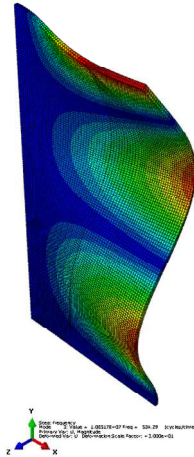
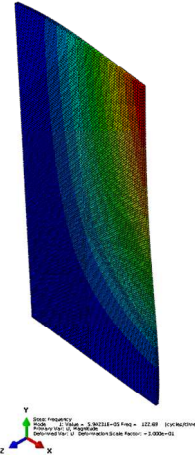
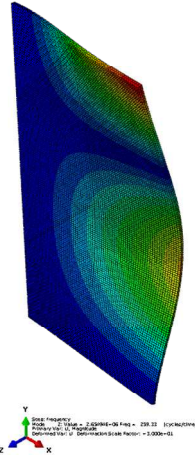
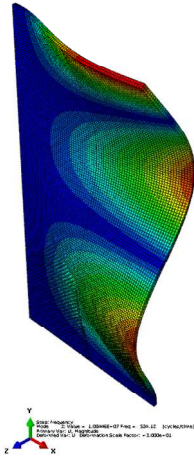
Crack Orientation Angle, β (deg)	Vibration Mode Shapes of Cracked Plate		
	Mode I	Mode II	Mode III
60°			
80°			
90°			

Table 4-4 : Vibration mode shapes of cracked plates for half-crack length of 7.5 mm

4.4.2.2 Dynamic Implicit Analysis

Table 4-5 shows the results of the amplitude response for simulations that are carried out for an intact and cracked plate with the following crack orientation angles, β are 0° , 20° , 40° , 60° , 80° and 90° by applying an implicit dynamic nonlinear analysis within the ABAQUS/CAE environment, and, as expected, the amplitude values increase due to the small crack in the plate. These amplitude responses are also affected by the crack orientation angle where the amplitude decreases from 0° up to 60° by increasing the frequency value, and then the amplitude increases again when the frequency value decreases.

		Crack Orientation angle	FEA Results	
			Frequency (Hz)	Amplitude (mm)
			First vibration mode	
Intact Plate		-	122.94	7.372
Cracked plate	3 mm	0°	122.73	7.483
		20°	122.77	7.379
		40°	122.84	7.263
		60°	123.05	7.200
		80°	122.82	7.727
		90°	122.73	7.739
	7.5 mm	0°	122.69	7.564
		20°	122.75	7.227
		40°	122.81	6.969
		60°	123.04	6.796
		80°	122.81	7.309
		90°	122.69	7.614

Table 4-5 : Amplitude responses from the FE analysis

A comparison of the frequency values and the amplitude responses is made between the theoretical model and the FEA results and discussed in chapter 7.

4.5 Chapter Conclusions

An approximate analytical method based on the perturbation methods of multiple scales and numerical solution techniques using the Finite Element Method within the ABAQUS/CAE environment have been applied. The nonlinear behaviour of the cracked plate model has been investigated from the amplitude-frequency equation and this has showed that the inclusion of a crack within the plate produces a global effect on the nonlinear response of the overall system. In this study it has been found that the SSSS and CCSS boundary conditions showed a hardening spring behaviour while a softening spring phenomenon was found for the CCFE boundary condition. The influence of the crack orientation angle on the frequency response has been observed. For the SSSS and CCSS boundary conditions no obvious hardening effects emerged for rectangular plates. However for square plates with an increase in the crack orientation angle, the nonlinear hardening phenomenon clearly increases. In addition changing the location of the applied load on the plate surface slightly affects the nonlinear behaviour of the plate whereby the width of the nonlinear region becomes narrower as the excitation location moves closer to the constrained area.

The solution obtained by the multiple scales method has been compared with numerical integration for a cracked plate with the CCFE boundary condition. The NI solution captures the amplitude response of the MMS very well for the range of excitation frequencies chosen. However, the overhanging part of the curve was obtained during the amplitude transitions. This situation was not found in the multiple scales solution because of inevitable over-correction to the solution during the first-order perturbation expansion. Results from the finite element analysis have also shown that the large crack shifts the frequency values of the 1st, 2nd and 3rd modes downwards, and, as expected, the amplitude values increase due to the small crack in the plates. As a conclusion, it can be said that the vibration characteristics and nonlinear characteristics of the plate structure are affected by the orientation of the crack in the plate.

Chapter 5

Dynamical Systems Analysis

5.1 Introduction

In investigating the nonlinear behaviour of the plate it is necessary to study the numerical dynamics of the system in order to understand its stability, the relevant bifurcatory phenomena, and therefore possible routes from order to chaos. This study is not only intended to lead to an understanding of the complex dynamics under different combination of system parameters, but also to capture the essential mechanism that generate chaos in this system. In this chapter, an analysis of the nonlinear behaviour of a cracked plate that contains a surface crack of variable angular orientation and which takes the form of a specialised Duffing equation, has been conducted using dynamical system tools within the MathematicaTM environment for the calculation of bifurcations, stability of the phase states, and the Poincaré map.

5.2 Equation of Motions for Dynamical System Analysis

In investigating the behaviour of the dynamics of this cracked plate model from nonlinear transition to chaos, a nonlinear ordinary differential equation of the system which takes the form of a specialised Duffing equation (3.88) is used. The equation is rewritten to make it easier to use, as follows,

$$\ddot{x} + C_1 \dot{x} + C_2 x + C_3 x^3 = A \cos(\Omega t) \quad (5.1)$$

$$\text{where} \quad C_1 = 2\mu \quad (5.2)$$

$$C_2 = \omega_{ij}^2 \quad (5.3)$$

$$C_3 = \gamma_{ij} \quad (5.4)$$

$$A = \frac{q_{ij}}{M_{ij}} = \frac{\eta_{ij}}{D} q \quad (5.5)$$

This equation contains dimensional parameters and Ω is the frequency of excitation. In order to make the form of the equation better for numerical simulation and reduced computational time scaling needs to be performed first. Nondimensionalisation of the timescale in equation (5.1) is introduced as a basis for nondimensionalisation (Israr (2008), Atepor (2008), and Lim (2003)), given by,

$$\tau = \sqrt{\omega} t \quad (5.6)$$

$$\ddot{x} = \omega \frac{d^2 x}{d\tau^2} \quad \therefore \ddot{x}(t) = \omega x''(\tau) \quad (5.7)$$

$$\dot{x} = \sqrt{\omega} \frac{dx}{d\tau} \quad \therefore \dot{x}(t) = \sqrt{\omega} x'(\tau) \quad (5.8)$$

where ω is the natural frequency of the first mode of the cracked plate model. Therefore for the dimensionless timescale, τ , equation (5.1) becomes,

$$\omega x'' + \sqrt{\omega} C_1 x' + C_2 x + C_3 x^3 = A \cos\left(\frac{\Omega}{\sqrt{\omega}} \tau\right) \quad (5.9)$$

The prime (') denotes differentiation with respect to the dimensionless time τ . Then, dividing through by ω in equation (5.9) leads to,

$$x'' + \frac{1}{\sqrt{\omega}} C_1 x' + \frac{1}{\omega} C_2 x + \frac{1}{\omega} C_3 x^3 = \frac{A}{\omega} \cos\left(\frac{\Omega}{\sqrt{\omega}} \tau\right) \quad (5.10)$$

Assuming that the frequency of excitation, Ω is equal to the natural frequency of the fundamental plate mode, ω , then $\Omega = \omega$ giving,

$$x'' + \frac{1}{\sqrt{\omega}} C_1 x' + \frac{1}{\omega} C_2 x + \frac{1}{\omega} C_3 x^3 = \frac{A}{\omega} \cos(\sqrt{\omega} \tau) \quad (5.11)$$

For these types of analyses the second order differential equation (5.11) is split into the more compact first order ordinary differential equation form as,

$$x' = y \quad (5.12)$$

$$y' = -\frac{1}{\sqrt{\omega}} C_1 y - \frac{1}{\omega} C_2 x - \frac{1}{\omega} C_3 x^3 + \frac{A}{\omega} \cos\left(\frac{\Omega}{\sqrt{\omega}} \tau\right) \quad (5.13)$$

5.3 Numerical Methods: Mathematica™ code

Dynamic analysis of the cracked plate is carried out using special integration code written in Mathematica™. The first order equations (5.12) and (5.13) are used to calculate time domain responses and phase plane trajectories, also Poincaré maps and predictions of bifurcations, by using the program code developed by the author within this software. The route to chaos is observed with the above mentioned feature properties. In this work the *NDSolve* integrator, Mathematica's differential equation package is employed to perform the integration and to enable prediction of the dynamics of the cracked plate for a given initial conditions. The parameter values for the program code are calculated using the similar mechanical properties of the aluminium alloy described in Chapters 3 and 4 with a point load of 10N applied at some arbitrarily specified point chosen here, to be located at $x_o = 0.375\text{m}$ and $y_o = 0.75\text{m}$. These values are tabulated in Tables 5-1, 5-2, and 5-3 for a cracked plate with the following crack orientation angles, β are 0° , 20° , 40° , 60° , 80° and 90° .

System Parameters (SSSS)						
Crack Angle β (deg)	Half-crack length (m)	Damping C_1 (s^{-1})	Linear Stiffness C_2 (s^{-2})	Cubic Nonlinearity C_3 ($m^{-2}s^{-2}$)	Excitation amplitude A (ms^{-2})	Natural frequency ω ($rads^{-1}$)
Intact	-	0.16	417968.00	7.72182×10^{11}	102.91	646.50
0	0.003		411921.00	7.60673×10^{11}		641.81
	0.0075		405716.00	7.47524×10^{11}		636.96
20	0.003		412629.00	7.62019×10^{11}		642.36
	0.0075		407150.00	7.50409×10^{11}		638.08
40	0.003		414420.00	7.65428×10^{11}		643.75
	0.0075		410779.00	7.57712×10^{11}		640.92
60	0.003		416456.00	7.69305×10^{11}		645.33
	0.0075		414905.00	7.66018×10^{11}		644.13
80	0.003		417786.00	7.71835×10^{11}		646.36
	0.0075		417599.00	7.71438×10^{11}		646.22
90	0.003		417968.00	7.72182×10^{11}		646.50
	0.0075		417968.00	7.72182×10^{11}		646.50

Table 5-1 : Data used for numerical simulations for the SSSS boundary condition

System Parameters (CCSS)						
Crack Angle β (deg)	Half-crack length (m)	Damping C_1 (s^{-1})	Linear Stiffness C_2 (s^{-2})	Cubic Nonlinearity C_3 ($m^{-2}s^{-2}$)	Excitation amplitude A (ms^{-2})	Natural frequency ω ($rads^{-1}$)
Intact	-	0.16	1.49967×10^7	3.01634×10^{11}	161.71	3872.56
0	0.003		1.48038×10^7	2.97138×10^{11}		3847.57
	0.0075		1.46059×10^7	2.92002×10^{11}		3821.77
20	0.003		1.48249×10^7	2.97664×10^{11}		3850.31
	0.0075		1.46500×10^7	2.93128×10^{11}		3827.53
40	0.003		1.48812×10^7	2.98995×10^{11}		3857.62
	0.0075		1.47649×10^7	2.95981×10^{11}		3842.51
60	0.003		1.49464×10^7	3.00510×10^{11}		3866.06
	0.0075		1.48968×10^7	2.99226×10^{11}		3859.64
80	0.003		1.49901×10^7	3.01498×10^{11}		3871.70
	0.0075		1.49841×10^7	3.01343×10^{11}		3870.92
90	0.003		1.49967×10^7	3.01634×10^{11}		3872.56
	0.0075		1.49967×10^7	3.01634×10^{11}		3872.56

Table 5-2 : Data used for numerical simulations for the CCSS boundary condition

System Parameters (CCFF)						
Crack Angle β (deg)	Half-crack length (m)	Damping C_1 (s ⁻¹)	Linear Stiffness C_2 (s ⁻²)	Cubic Nonlinearity C_3 (m ⁻² s ⁻²)	Excitation amplitude A (ms ⁻²)	Natural frequency ω (rads ⁻¹)
Intact	-	0.16	593312.00	-1.26484×10^{11}	39.36	770.27
0	0.003		553353.00	-1.24599×10^{11}		743.88
	0.0075		512347.00	-1.22445×10^{11}		715.78
20	0.003		586013.00	-1.70743×10^{11}		765.52
	0.0075		551558.00	-1.91314×10^{11}		742.67
40	0.003		612740.00	-1.95737×10^{11}		782.78
	0.0075		591365.00	-2.28903×10^{11}		769.00
60	0.003		621027.00	-1.87886×10^{11}		788.05
	0.0075		613140.00	-2.17624×10^{11}		783.03
80	0.003		606998.00	-1.50863×10^{11}		779.10
	0.0075		606696.00	-1.62755×10^{11}		778.91
90	0.003		593312.00	-1.26484×10^{11}		770.27
	0.0075		593312.00	-1.26484×10^{11}		770.27

Table 5-3 : Data used for numerical simulations for the CCFF boundary condition

5.4 Bifurcation Analysis

Bifurcation theory is the mathematical study of changes in the qualitative behaviour of a system. These qualitative changes may occur when the parameter values of a system are varied and they can be shown by a bifurcation diagram. In the study of dynamical systems, the bifurcation diagram is useful in order to see a possible route from order to chaos. The location at which bifurcations occur in this diagram are called bifurcation points. In addition bifurcation diagrams can also be used to indicate nonperiodic motion. In this study a period doubling bifurcation can readily be observed and analysed. A period doubling bifurcation is a bifurcation in which the behaviour of the system changes at integer multiples of the periodicity of the original response. The motion may then become chaotic if the control parameter is further varied (Moon, 1992).

In this study the MathematicaTM software environment is used for numerically integrating the governing equations of motion to produce a bifurcation diagram in order to understand the dynamics within the cracked plate models, as discussed in Chapter 3. The bifurcation behaviour of the amplitude responses as a function of normalised excitation acceleration is

plotted for three types of boundary conditions with variable crack orientation angles, using nondimensionalised parameters as tabulated in Table 5-1, 5-2, and 5-3. All the cases are illustrated in Figures 5-2 to 5-10.

5.5 Lyapunov Exponents

Lyapunov exponents offer a means to study numerically whether a system has a sensitive dependence on initial conditions. They measure the average rate of convergence or divergence of nearby trajectories in the phase space. A positive exponent means divergence and a negative represents convergence. Figure 5.1 provides a visual example of divergent trajectories by considering two points in space, X_0 and $X_0 + \Delta x_0$. A trajectory in that space is assumed to be generated by using some equation or system of equations. These trajectories can be thought of as parametric functions of a variable such as time. If one of the trajectories is used as a reference trajectory then the separation between the two trajectories will also be a function of time.

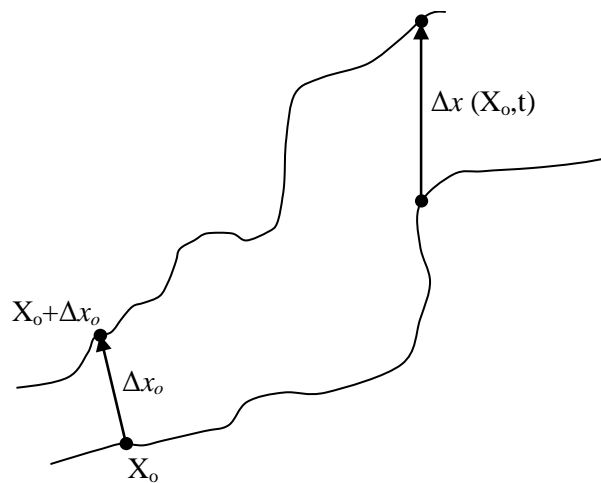


Figure 5-1 : An illustration of the divergence of trajectories (after Israr, 2008)

A system with all negative Lyapunov exponents will have an attracting fixed point or periodic points, thus $\Delta x(X_0, t)$ diminishes asymptotically with time and will not present chaotic behaviour. For chaotic points, the function $\Delta x(X_0, t)$ will behave erratically. The Lyapunov exponent, λ can be defined by the natural logarithm of the Lyapunov number as,

$$\lambda = \lim_{\substack{t \rightarrow \infty \\ |\Delta x_0|}} \frac{1}{t} \ln \frac{|\Delta x(X_0, t)|}{|\Delta x_0|} \quad (5.13)$$

For systems with negative exponents ($\lambda < 0$), the trajectories move together and attract to a stable fixed point. These systems exhibit asymptotic stability in which the more negative the exponent the greater the stability. For system with zero Lyapunov exponents ($\lambda = 0$) the trajectory is a neutral fixed point or an eventually fixed point. Such systems are indicated to be in some sort of steady-state mode and are physically conservative, and thus exhibit Lyapunov stability. Subsequently, for systems with positive exponents ($\lambda > 0$) the trajectory is unstable and also chaotic. Two initially close trajectories in a system with positive Lyapunov exponent will separate very quickly. A positive Lyapunov exponent will cause this separation to increase over further iterations, and the more positive the exponent the faster they move apart. After separation the two numerical solutions grow more dissimilar until they are completely different. Any system containing at least one positive Lyapunov exponent indicates chaotic motion (Wolf *et al.*, 1985).

5.6 Bifurcations as Functions of Normalised Excitation Acceleration

The chaotic motion of both the intact plate and the cracked plate models is investigated here. In this study the first mode is examined in detail around the resonant region. The excitation frequency is set equal to the first mode resonance frequency from Tables 5-1, 5-2, and 5-3 for the SSSS, CCSS, and CCFF boundary conditions, respectively. Figures 5-2 to 5-10 show the bifurcation diagrams for the amplitude response, x , of the intact and cracked plate models, for the cases of half-crack lengths of 0.003 m and 0.0075 m, and as controlled by the normalised excitation acceleration. Periodic doubling bifurcation can be observed in all the Figures with an increase in the normalised excitation acceleration, and when the normalised excitation acceleration value is increased to a high level this periodic response bifurcates to chaos. There are five types of system motion which exist over the range of normalised excitation acceleration, namely stable single period motion, stable period-2 motion, stable period-4 motion, stable multiperiod motion, and finally what appears to be chaotic motion. ρ , ρ is the normalised acceleration amplitude of the system.

In the case of the SSSS boundary condition for the intact plate model, as shown in Figure 5-2, period-2 and period-4 motion can be found in regions of normalised excitation acceleration of 11.78 to 11.98 and 11.98 to 12.02, respectively. For the cracked plate model with a half-crack length of 0.03 m (Figure 5-3(a)), these regimes can be found in the regions of 11.69 to 11.89 and 11.89 to 11.92, respectively, whereas for a half-crack length

of 0.0075 m, period-2 motion in the regions of normalised excitation acceleration of 11.61 to 11.82 and 11.82 to 11.85 for period-4 as shown in Figure 5-4(a). It can be observed from these figures that as the periodic response become chaotic less excitation acceleration is required in each case. This is due to the decrease in the normalised excitation frequency and the effect of the cubic nonlinear coefficient.

Figures 5-2(a-f) and 5-3(a-f) show the bifurcation diagram for the cracked plate model with crack orientation angles of 0° , 20° , 40° , 60° , 80° and 90° and with a half-crack length of 0.003 m and 0.0075 m, respectively. The region of normalised excitation acceleration for period-2 and period-4 motion is summarised in Table 5-4 as an example. It can be clearly seen that by increasing the crack orientation angles the periodic response bifurcates to period doubling, and finally leads to chaos, and more excitation acceleration is required for each case for the periodic response to become chaotic due to the increase in the normalised excitation frequency and the cubic nonlinear coefficient. The same phenomenon also exists for the CCSS boundary condition, as shown in Figures 5-5 to 5-7.

SSSS

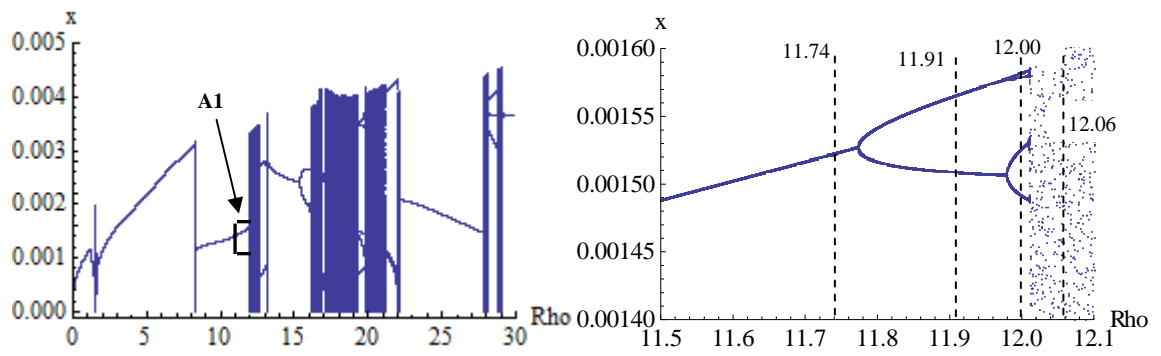
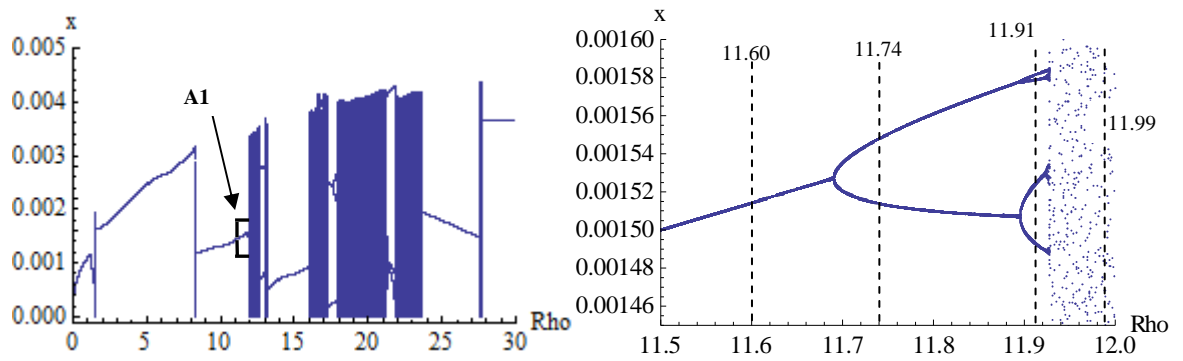
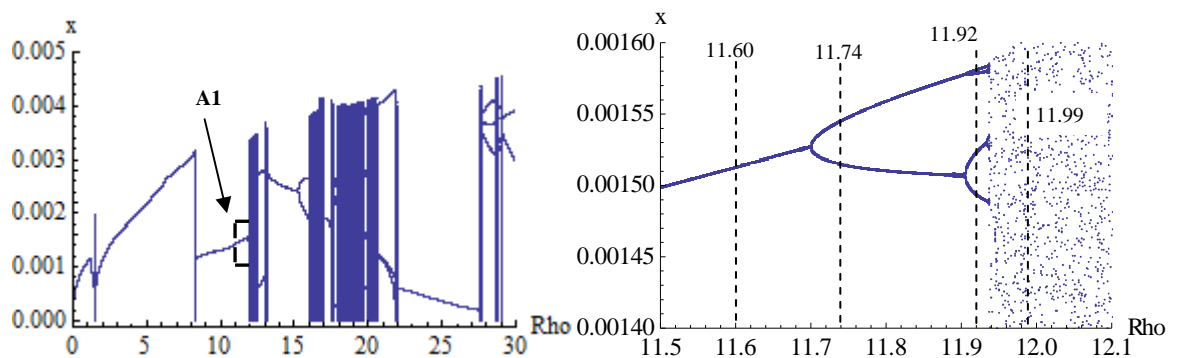


Figure 5-2 : Intact plate and the enlarged view of A1

SSSS

(a) Cracked plate with $\beta = 0^\circ$ and the enlarged view of A1(b) Cracked plate with $\beta = 20^\circ$ and the enlarged view of A1

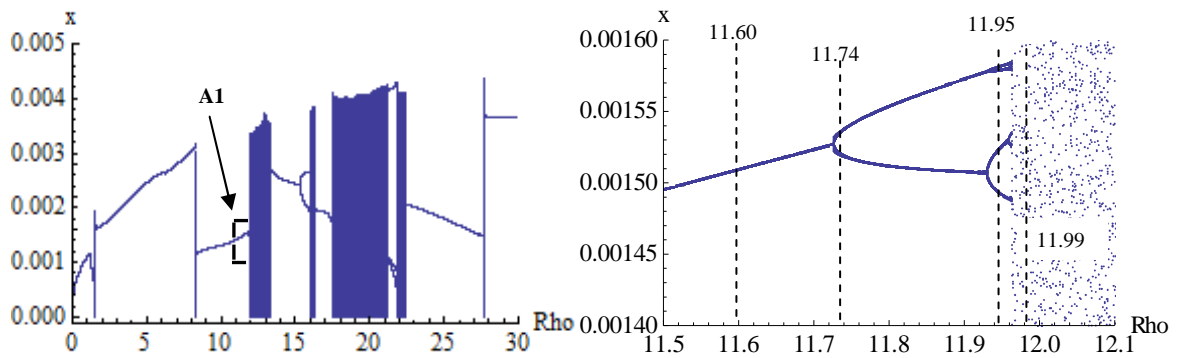
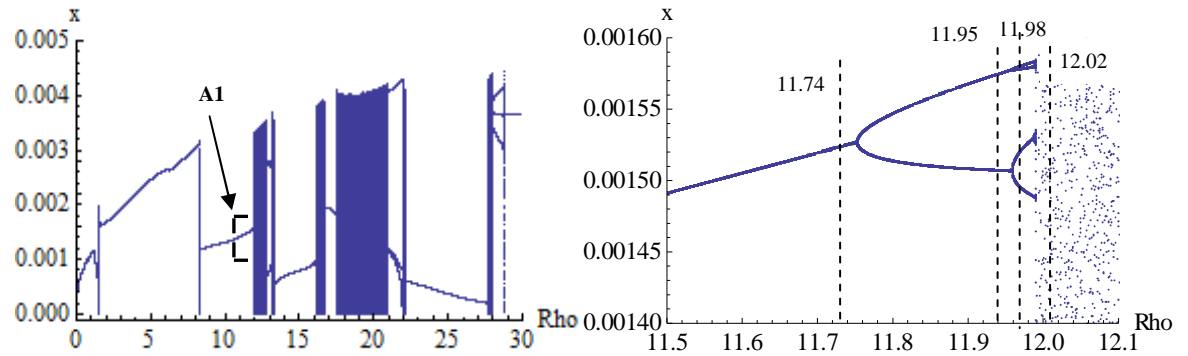
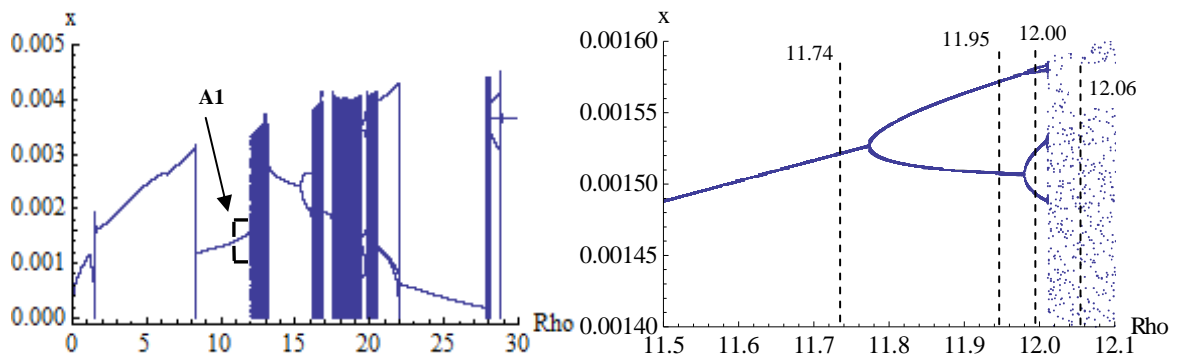
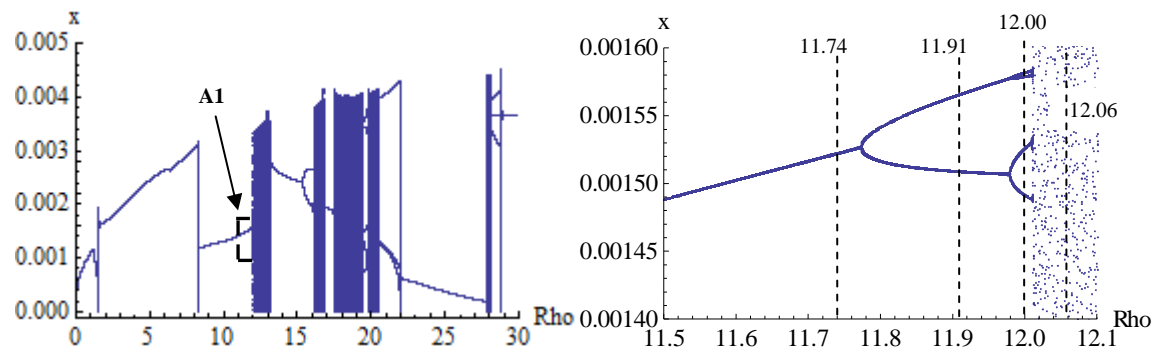
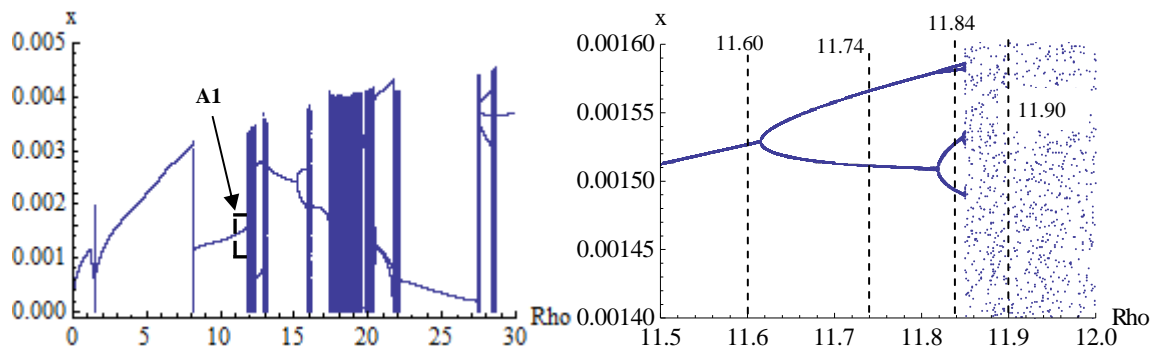
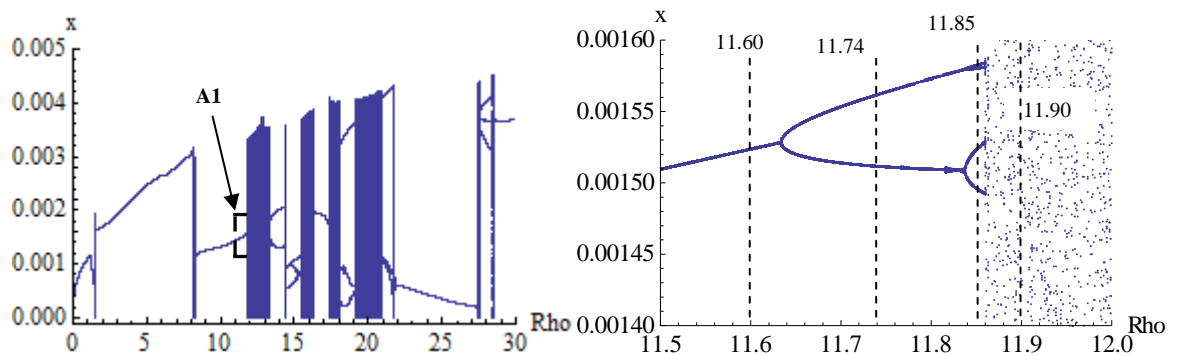
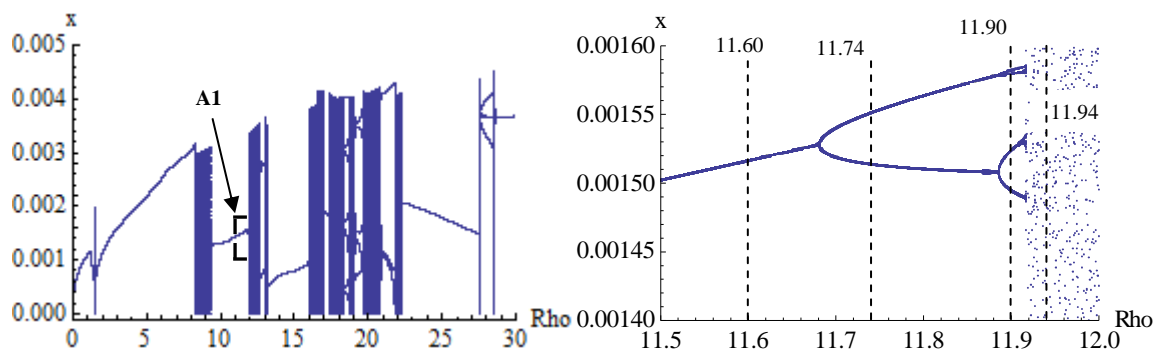
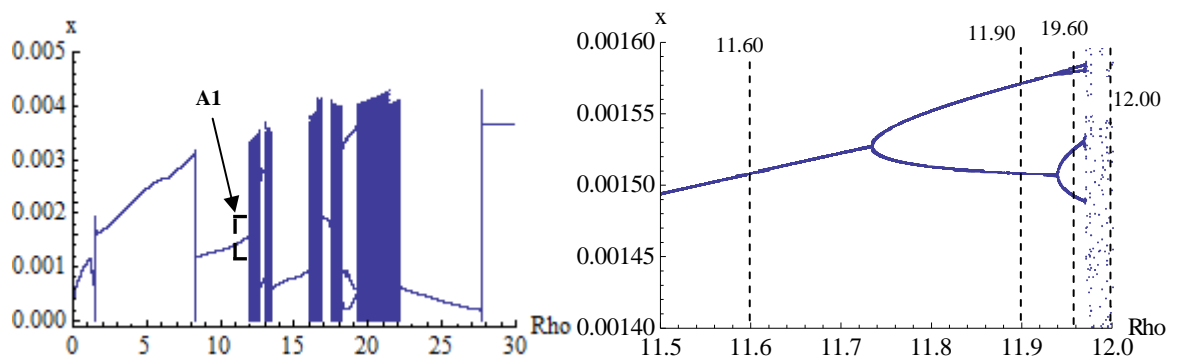
(c) Cracked plate with $\beta = 40^\circ$ and the enlarged view of A1(d) Cracked plate with $\beta = 60^\circ$ and the enlarged view of A1(e) Cracked plate with $\beta = 80^\circ$ and the enlarged view of A1(f) Cracked plate with $\beta = 90^\circ$ and the enlarged view of A1

Figure 5-3 : Bifurcation diagrams for SSSS boundary condition and a half-crack length of 0.003 m for amplitude as a function of the normalised excitation acceleration in the x -direction

SSSS

(a) Cracked plate with $\beta = 0^\circ$ and the enlarged view of A1(b) Cracked plate with $\beta = 20^\circ$ and the enlarged view of A1(c) Cracked plate with $\beta = 40^\circ$ and the enlarged view of A1(d) Cracked plate with $\beta = 60^\circ$ and the enlarged view of A1

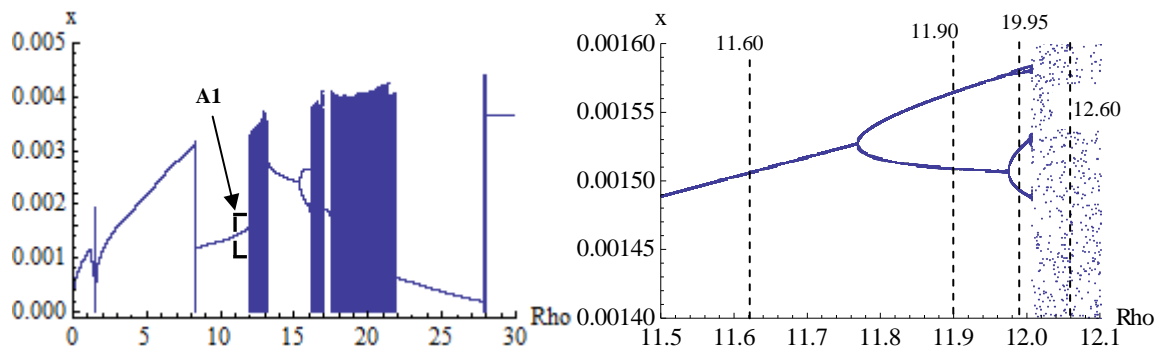
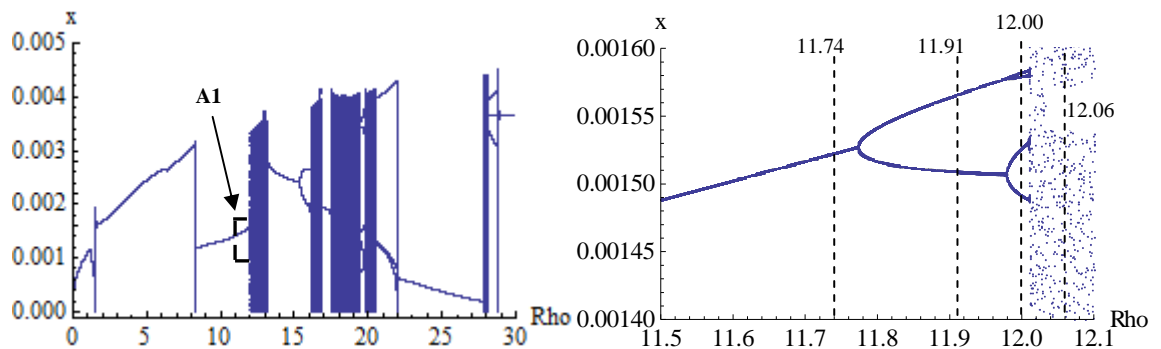
(e) Cracked plate with $\beta = 80^\circ$ and the enlarged view of A1(f) Cracked plate with $\beta = 90^\circ$ and the enlarged view of A1

Figure 5-4 : Bifurcation diagrams for SSSS boundary condition and a half-crack length of 0.0075 m for amplitude as a function of the normalised excitation acceleration in the x -direction

Crack orientation angle, β (deg)	Region of normalised excitation acceleration, Rho			
	Period-2 motion		Period-4 motion	
0°	11.69	11.89	11.89	11.93
20°	11.70	11.90	11.90	11.94
40°	11.72	11.93	11.93	11.96
60°	11.75	11.96	11.96	11.98
80°	11.77	11.97	11.97	12.01
90°	11.78	11.98	11.98	12.02

Table 5-4 : Period doubling bifurcation of cracked plate for the SSSS boundary condition and 0.003 m half-crack length.

CCSS

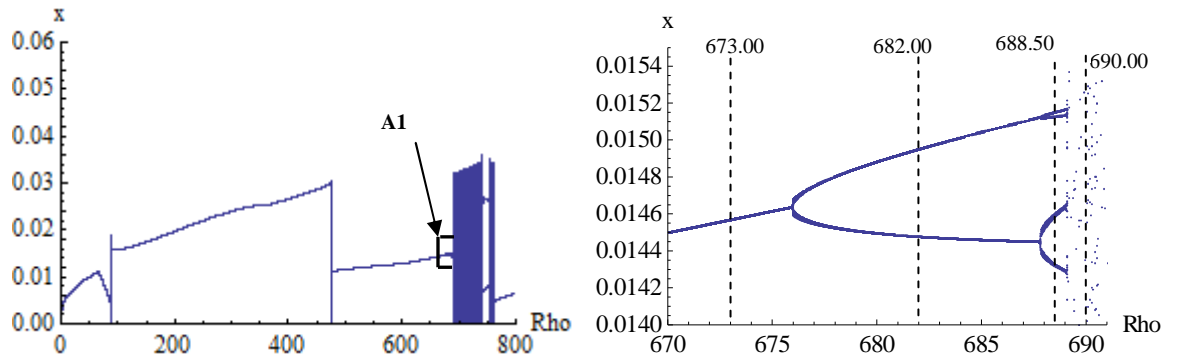
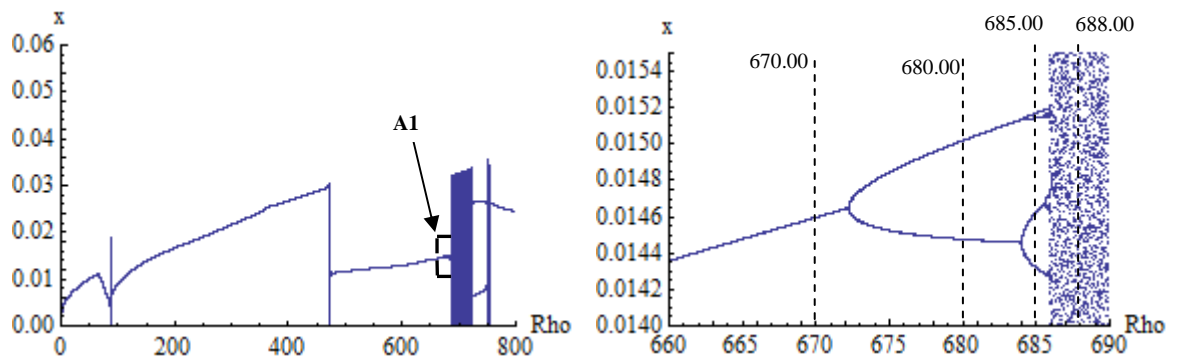
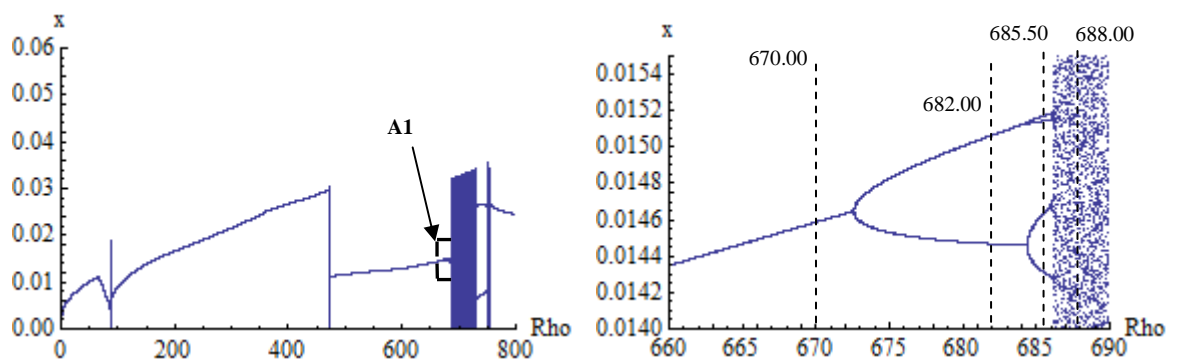


Figure 5-5 : Intact plate and the enlarged view of A1

CCSS

(a) Cracked plate with $\beta = 0^\circ$ and the enlarged view of A1(b) Cracked plate with $\beta = 20^\circ$ and the enlarged view of A1

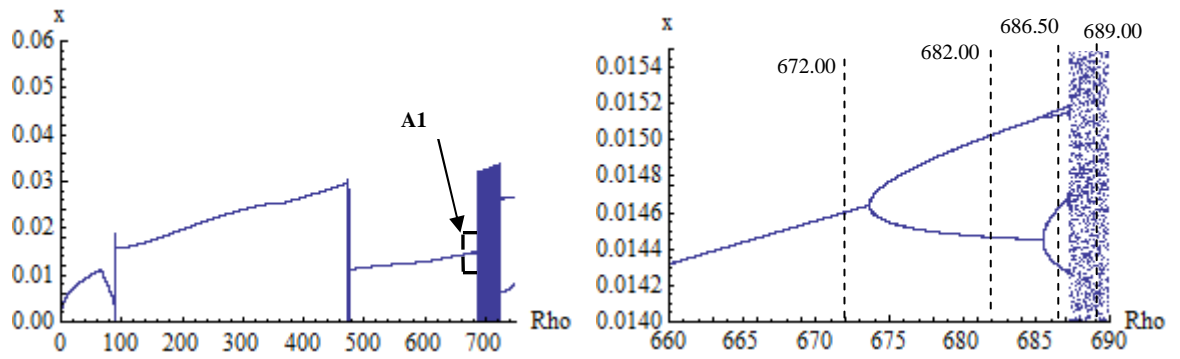
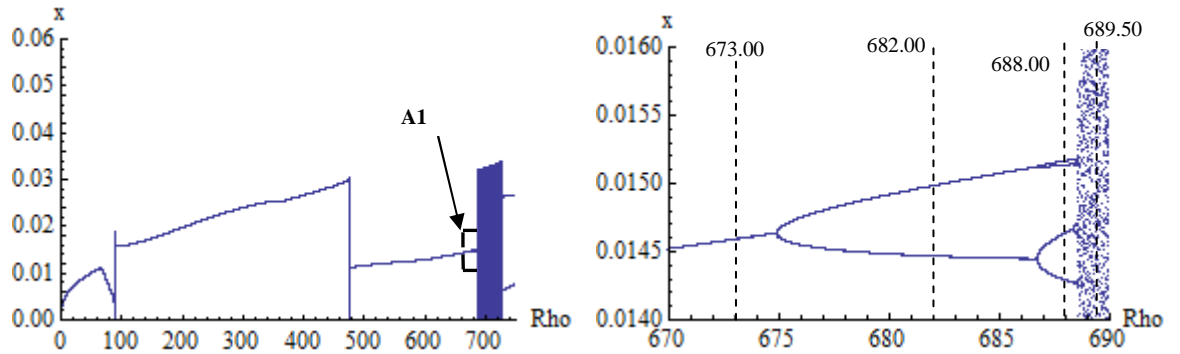
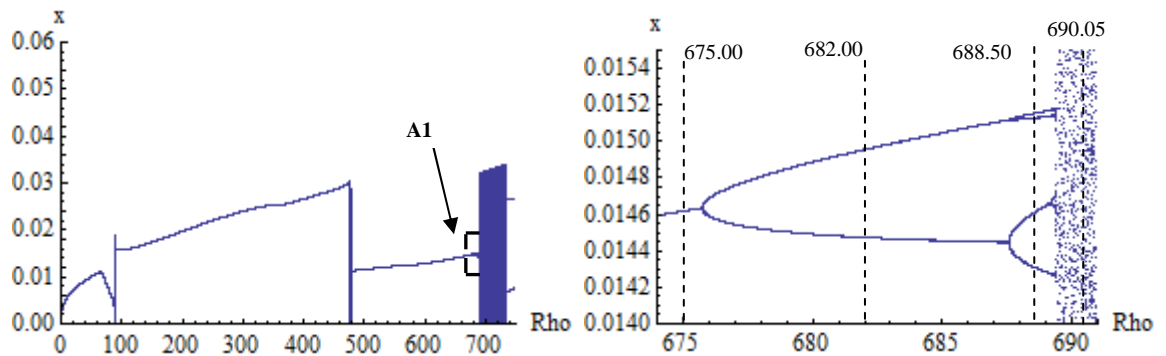
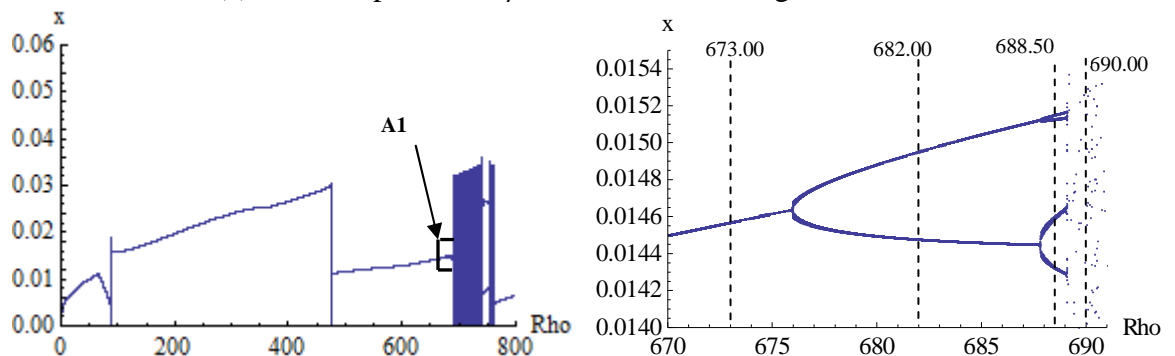
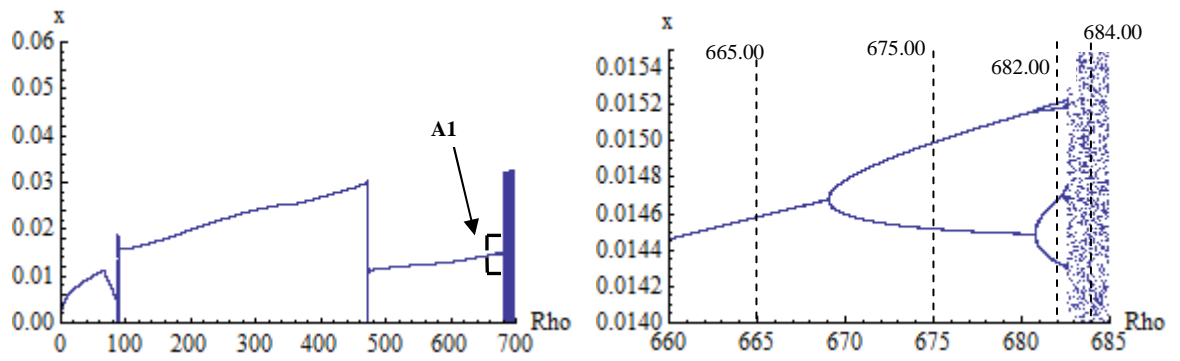
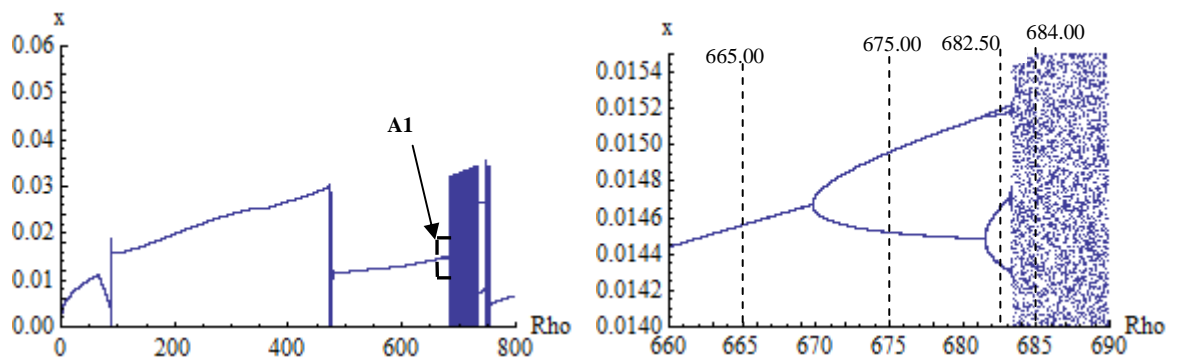
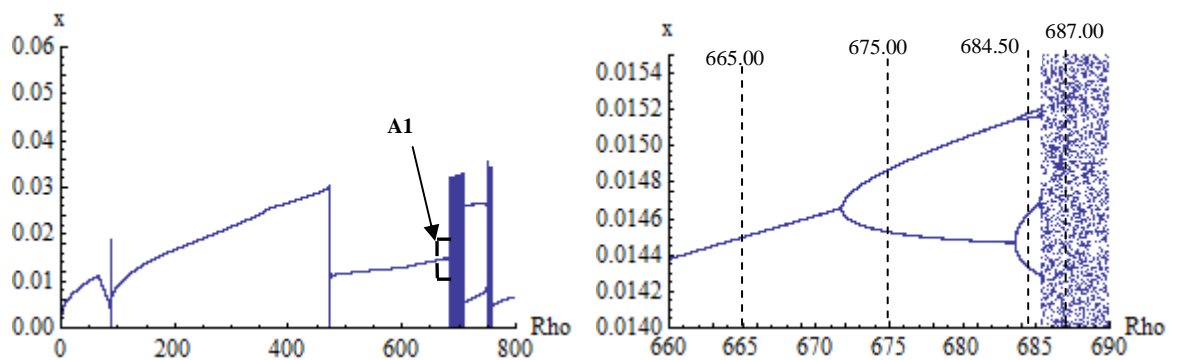
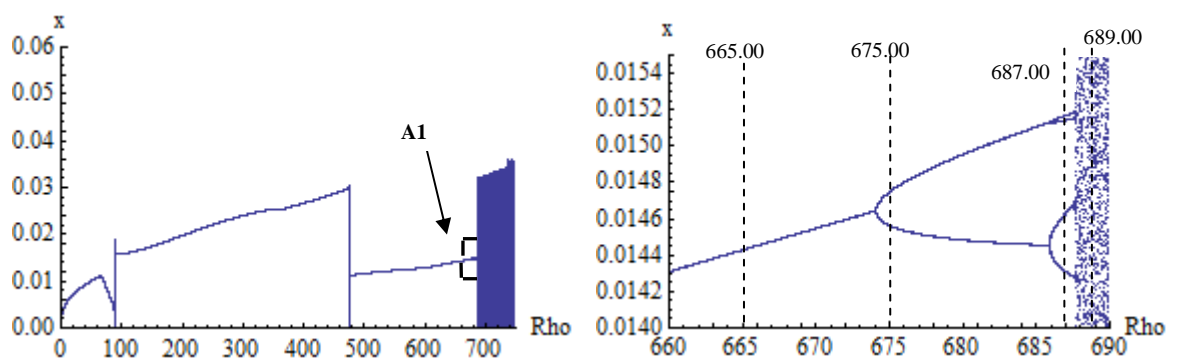
(c) Cracked plate with $\beta = 40^\circ$ and the enlarged view of A1(d) Cracked plate with $\beta = 60^\circ$ and the enlarged view of A1(e) Cracked plate with $\beta = 80^\circ$ and the enlarged view of A1(f) Cracked plate with $\beta = 90^\circ$ and the enlarged view of A1

Figure 5-6 : Bifurcation diagrams for CCSS boundary condition and a half-crack length of 0.003 m for amplitude as a function of the normalised excitation acceleration in the x -direction

CCSS

(a) Cracked plate with $\beta = 0^\circ$ and the enlarged view of A1(b) Cracked plate with $\beta = 20^\circ$ and the enlarged view of A1(c) Cracked plate with $\beta = 40^\circ$ and the enlarged view of A1(d) Cracked plate with $\beta = 60^\circ$ and the enlarged view of A1

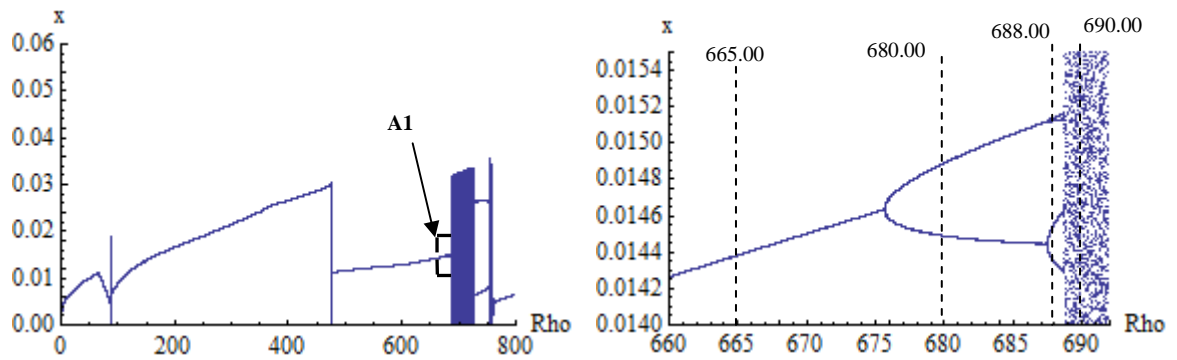
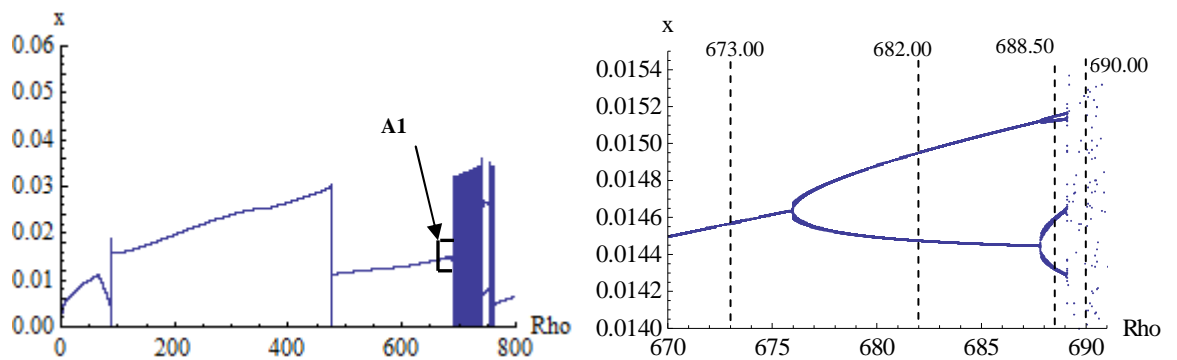
(e) Cracked plate with $\beta = 80^\circ$ and the enlarged view of A1(f) Cracked plate with $\beta = 90^\circ$ and the enlarged view of A1

Figure 5-7 : Bifurcation diagrams for CCSS boundary condition and a half-crack length of 0.0075 m for amplitude as a function of the normalised excitation acceleration in the x -direction

The bifurcation diagrams in Figure 5-8, 5-9 and 5-10 show the intact plate, a cracked plate with an 0.003 m half-crack length, and a cracked plate with an 0.0075 m half-crack length, respectively, for the CCFF boundary condition. The region of normalised excitation acceleration for period-2 and period-4 motion is listed in Table 5-5. Period doubling is a classical transition route to chaos. It can be observed from these figures that as the increase in half-crack length goes from 0.003 m to 0.0075 m the system also bifurcates to period-2, period-4, and multiperiod motions or stable quasi-periodic motions, and finally transitions to chaos, due to the decrease in normalised excitation frequency and the effect of the cubic nonlinear coefficient. However by increasing the orientation angle of the crack less excitation acceleration is required from 0° to 40° for the response of the system to become chaotic. After 40° more excitation acceleration is needed to get into this regime. In the next section, discrete excitation acceleration points, as depicted in Figures 5-2 to 5-10, are

selected for the plotting of trajectories on the phase plane, Poincaré maps, and time plots for each boundary condition in order to get more understanding of the system behaviour.

CCFF

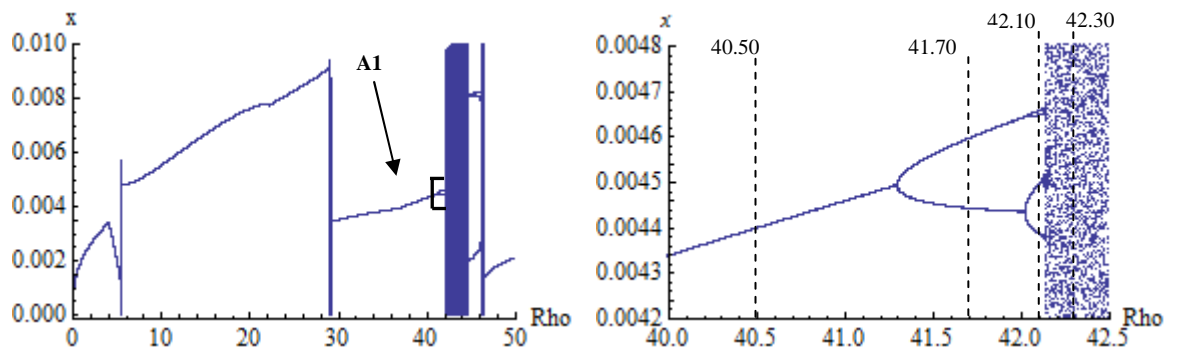
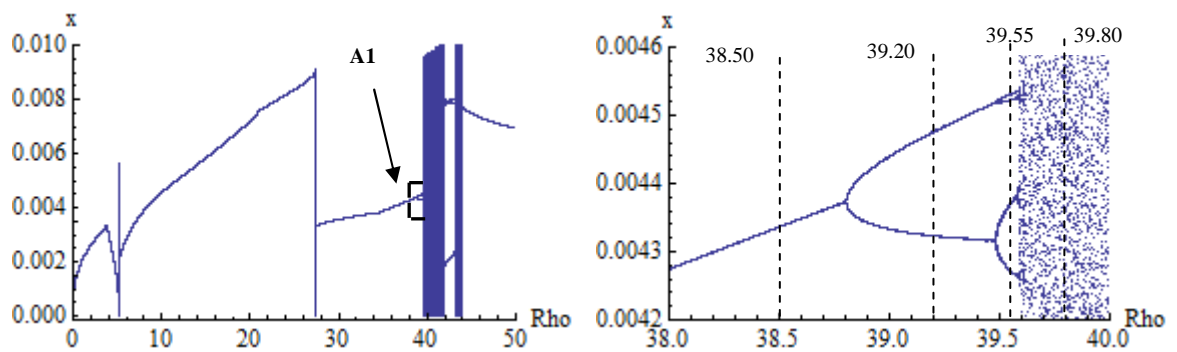
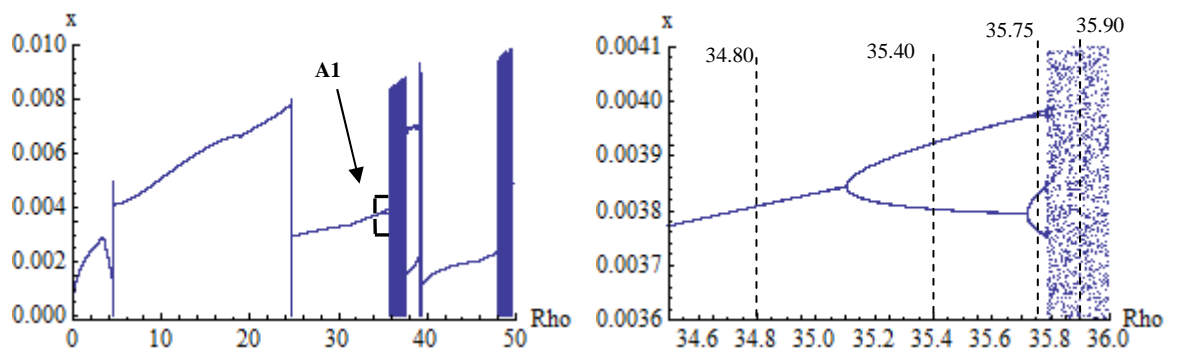


Figure 5-8 : Intact plate and the enlarged view of A1

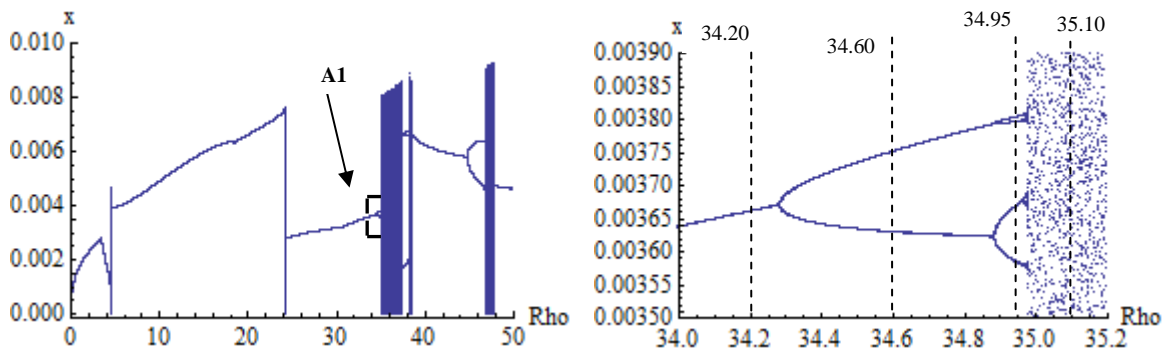
CCFF



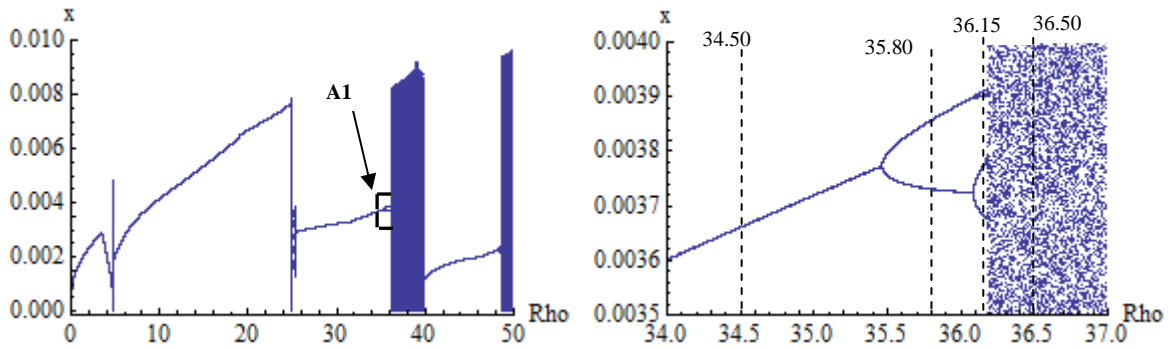
(a) Cracked plate with $\beta = 0^\circ$ and the enlarged view of A1



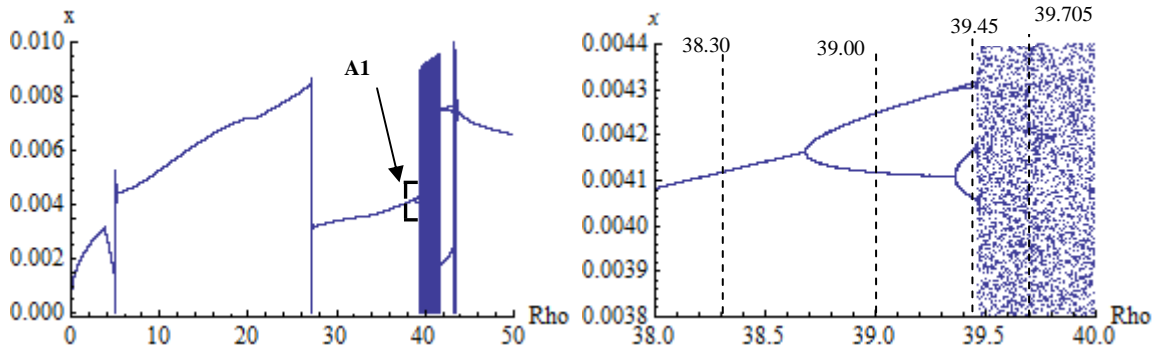
(b) Cracked plate with $\beta = 20^\circ$ and the enlarged view of A1



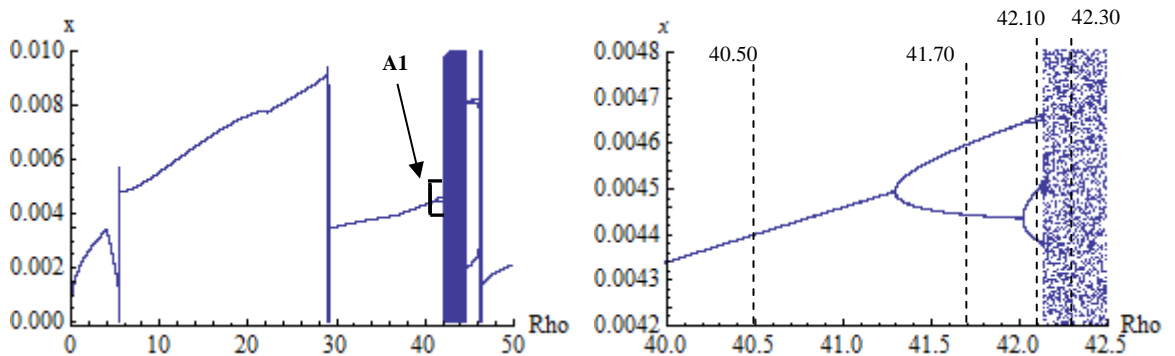
(c) Cracked plate with $\beta = 40^\circ$ and the enlarged view of A1



(d) Cracked plate with $\beta = 60^\circ$ and the enlarged view of A1



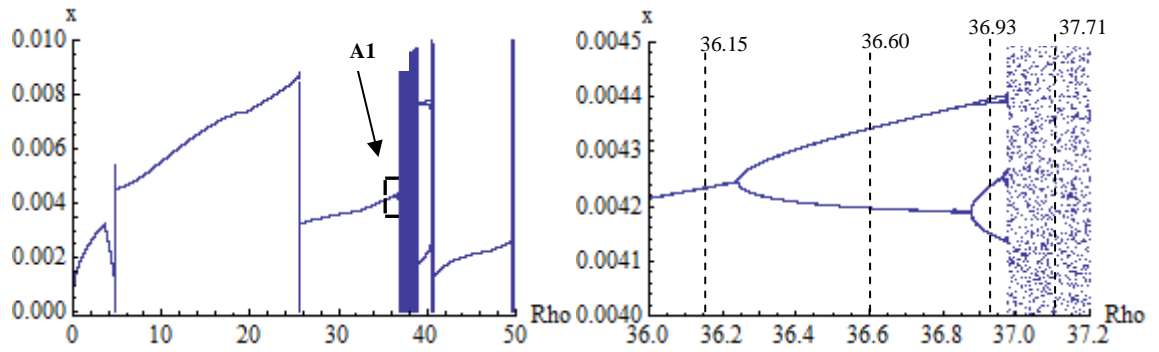
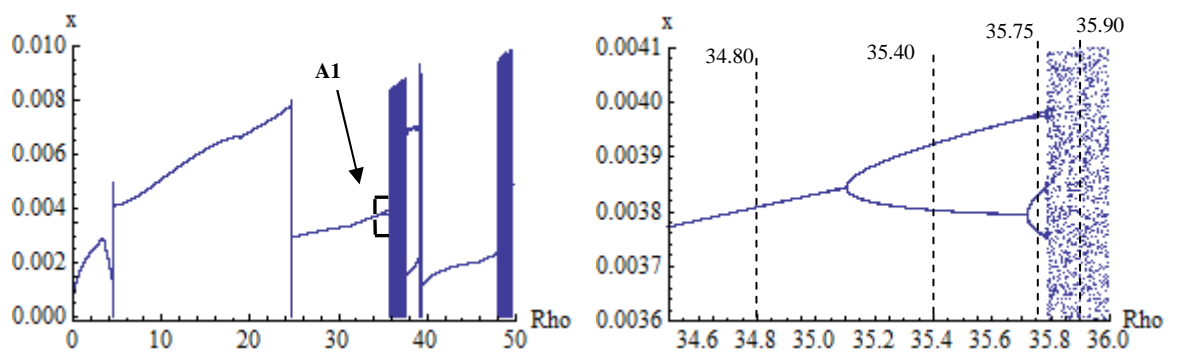
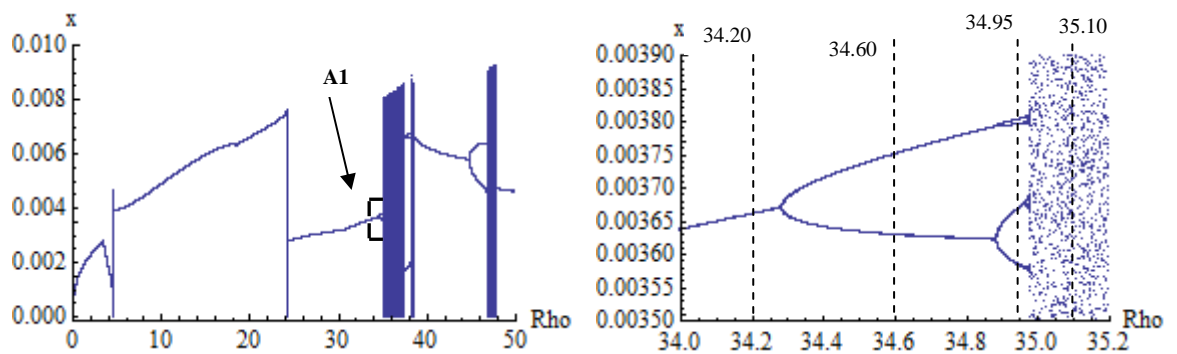
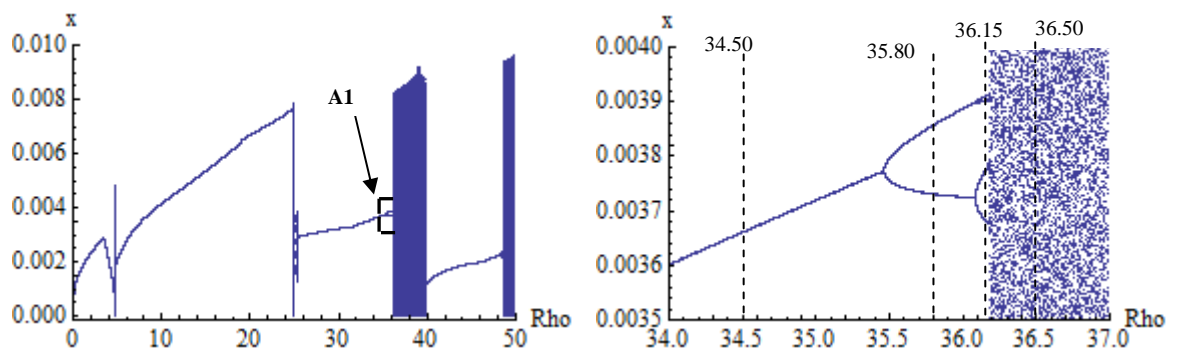
(e) Cracked plate with $\beta = 80^\circ$ and the enlarged view of A1



(f) Cracked plate with $\beta = 90^\circ$ and the enlarged view of A1

Figure 5-9 : Bifurcation diagrams for CCFF boundary condition and a half-crack length of 0.003 m for amplitude as a function of the normalised excitation acceleration in the x -direction

CCFF

(a) Cracked plate with $\beta = 0^\circ$ and the enlarged view of A1(b) Cracked plate with $\beta = 20^\circ$ and the enlarged view of A1(c) Cracked plate with $\beta = 40^\circ$ and the enlarged view of A1(d) Cracked plate with $\beta = 60^\circ$ and the enlarged view of A1

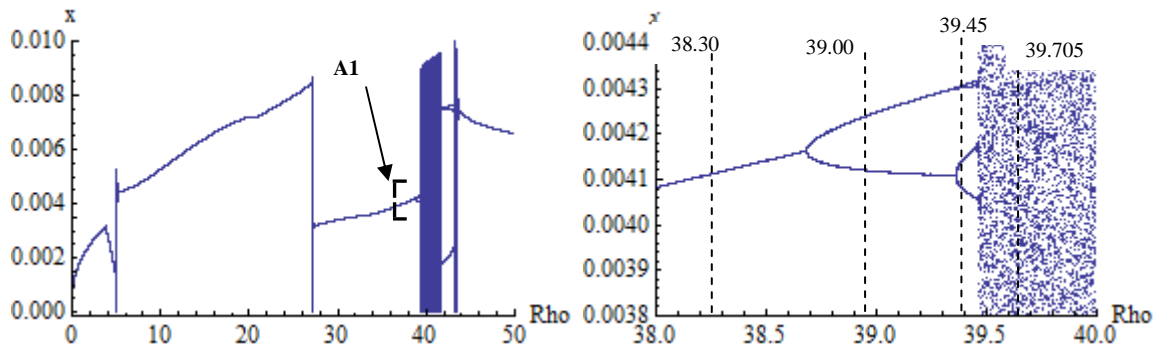
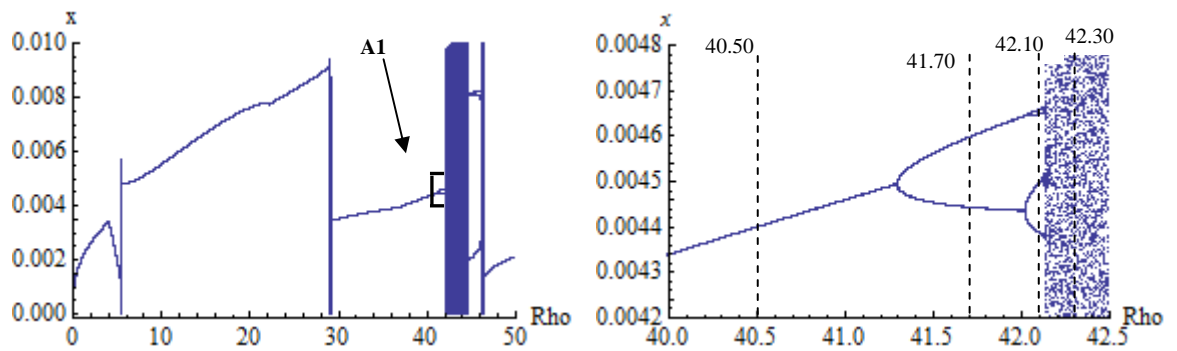
(e) Cracked plate with $\beta = 80^\circ$ and the enlarged view of A1(f) Cracked plate with $\beta = 90^\circ$ and the enlarged view of A1

Figure 5-10 : Bifurcation diagrams for CCFF boundary condition and a half-crack length of 0.0075 m for amplitude as a function of the normalised excitation acceleration in the x -direction

Plate structure	Half-crack length (m)	Crack orientation angle, β (deg)	Normalised excitation acceleration, Rho			
			Period-2 motion		Period-4 motion	
Intact plate	-		41.30	42.00	42.00	42.15
Cracked plate	0.003	0°	38.80	39.50	39.50	39.60
		20°	35.10	35.70	35.70	35.80
		40°	34.30	34.90	34.90	34.97
		60°	35.40	36.50	36.50	36.20
		80°	38.70	39.35	39.35	39.50
		90°	41.30	42.00	42.00	42.15
Cracked plate	0.0075	0°	36.25	36.87	36.87	36.98
		20°	35.10	35.73	35.73	35.78
		40°	34.28	34.87	34.87	34.96
		60°	35.45	36.10	36.10	36.18
		80°	38.69	39.38	39.38	39.48
		90°	41.30	42.00	42.00	42.15

Table 5-5 : Period doubling bifurcation of cracked plate for the CCFB boundary condition.

5.7 Time Plots, Phase Planes, and Poincaré Maps

Generally the response of a dynamic system can be in the form of a fixed point, a periodic solution, or a non-periodic solution. Poincaré maps can easily differentiate between periodic and non-periodic motions, and therefore can assist in the definition of chaotic motion. In this section, the definition of the term period(s) for a periodic motion as being the number of period(s) for a response function to repeat itself is applied. Taking the period as $T = 2\pi/\omega$ means that the Poincaré maps sample the displacements and the velocity of the cracked plate model every $2\pi/\omega$. If the system repeats itself after every T sec, and periodically returns to the same point in the phase space, this is called period-1 motion, and in a Poincaré map this will be as a single point. For two points it is indicating period-2 motion, for four points period-4 motion, and therefore period- n motion generally shows up as n points in the Poincaré map. Subsequently chaotic motion reveals itself as an infinite number of orderly distributed points as the chaotic orbits visit all parts of the phase space (Thomsen, 2003).

In this study, the phase planes, Poincaré maps and time plots are produced at discrete excitation acceleration points in order to investigate in more detail the qualitative changes in system behaviour of Figures 5-2 to 5-10. The phase plane and time plots are plotted at assumed steady-state conditions with the interval of time taken from 495.50 to 500 seconds, whereas the Poincaré maps are plotted after the transient time of 0 to 500 seconds. This transient time for plotting Poincaré maps is selected because most of them converged to a periodic motion with just a point, therefore as richer diagrams are preferred, and so as these maps converge to a point, then the times are sufficient. This is usually called a point attractor. The analyses are made for intact and cracked plate models with different normalised excitation acceleration values. As an example the results for the plate with a crack at an orientation angle of 0° and 60° , with 0.003m and 0.0075m half-crack lengths are shown in Figures 5-11 to 5-25. The routes to chaotic motion are investigated by observing the dynamic transitions of the plate models between the range of normalised excitation acceleration, $Rho = 11.60$ to $Rho = 12.06$ for the SSSS boundary condition, $Rho = 665.00$ to $Rho = 690.05$ for CCSS, and $Rho = 34.20$ to $Rho = 42.30$ for the CCFF boundary condition. This range of normalised excitation acceleration consists of motion from steady-state motion through to chaos. The observations are obtained as in the following sub-sections:

5.7.1 Figures 5-11(a) to 5-25(a), showing Period-1 motion

All the bifurcation diagrams for the three different types of boundary conditions with the two cases of the half-crack length and different values of crack orientation angle show periodic and stable motion, as depicted in Figures 5-2 to 5-10. Figures 5-11(a) to 5-25(a) show the plate motion in five different normalised excitation accelerations for each type of boundary condition, namely SSSS, CCSS, and CCFF. In the case of the SSSS condition, the normalised excitation accelerations chosen are $Rho = 11.74$, 11.60 , 11.74 , 11.60 , and 11.60 for the intact plate, cracked plate for an 0.003m half-crack length with 0° and 60° crack orientation angle, and for the cracked plate for an 0.0075m half-crack length with 0° and 60° crack orientation angle, respectively. For the CCSS case, the normalised excitation accelerations chosen are $Rho = 673.00$, 670.00 , 673.00 , 665.00 , and 665.00 while $Rho = 40.50$, 38.50 , 34.50 , 36.15 , and 34.50 for the CCFF boundary condition. From these Figures it can be observed that:

- The time plots for the SSS, CCSS and CCFF cases show clear evidence of a periodic response. The oscillations repeat every one period.

- The phase planes show periodic orbits corresponding to the bifurcation diagrams, and these phase plane plots show only stationary and post-transient motion by the elimination of the initial part of the solutions.
- All the Poincaré maps converge into a single point. The maps consist of one single point, which implies periodic motion, and indicates a period-1 motion with a stable attractor.

5.7.2 Figures 5-11(b) to 5-25(b), showing Period-2 motion

In these cases all the bifurcation diagrams for the three different types of boundary conditions, with the two cases of the half-crack length and different values of crack orientation angle, show periodic and stable motion of period-2. The normalised excitation accelerations chosen for the SSSS boundary condition, as shown in Figures 5-11(b) to 5-15(b), are $\text{Rho} = 11.91, 11.74, 11.74, 11.74,$ and 11.90 for the intact plate, the cracked plate for an 0.003m half-crack length with 0° and 60° crack orientation angle, and the cracked plate for an 0.0075m half-crack length with 0° and 60° crack orientation angle, respectively. For the CCSS case, the normalised excitation accelerations chosen are $\text{Rho} = 682.00, 680.00, 682.00, 675.00,$ and 675.00 in Figures 5-16(b) to 5-20(b), whereas $\text{Rho} = 41.70, 39.20, 35.80, 36.60,$ and 35.80 for the CCFF boundary condition is used, as depicted in Figures 5-21(b) to 5-25(b). From these Figures it can be observed that:

- All the time plots show evidence of periodic motions.
- All the phase plane trajectories indicate period doubling behaviour which correspond with the bifurcation diagrams, as illustrated in Figure 5-2 to 5-10. All these phase plane results depict a period-2 motion.
- The Poincaré maps converge to two points which indicate period-2 motion.

5.7.3 Figures 5-11 (c) to 5-25(c), showing Period-4 motion

The bifurcation diagrams in Figure 5-2 to 5-10 show a period-4 motion for all boundary conditions, and this period is explored through Figures 5-11(c) to 5-25(c) for the normalised excitation accelerations, $\text{Rho} = 12.00, 11.91, 11.98, 11.84,$ and $11.96,$ $\text{Rho} = 688.50, 685.00, 688.00, 682.00,$ and $687.00,$ and $\text{Rho} = 42.10, 39.55, 36.15, 36.93,$ and

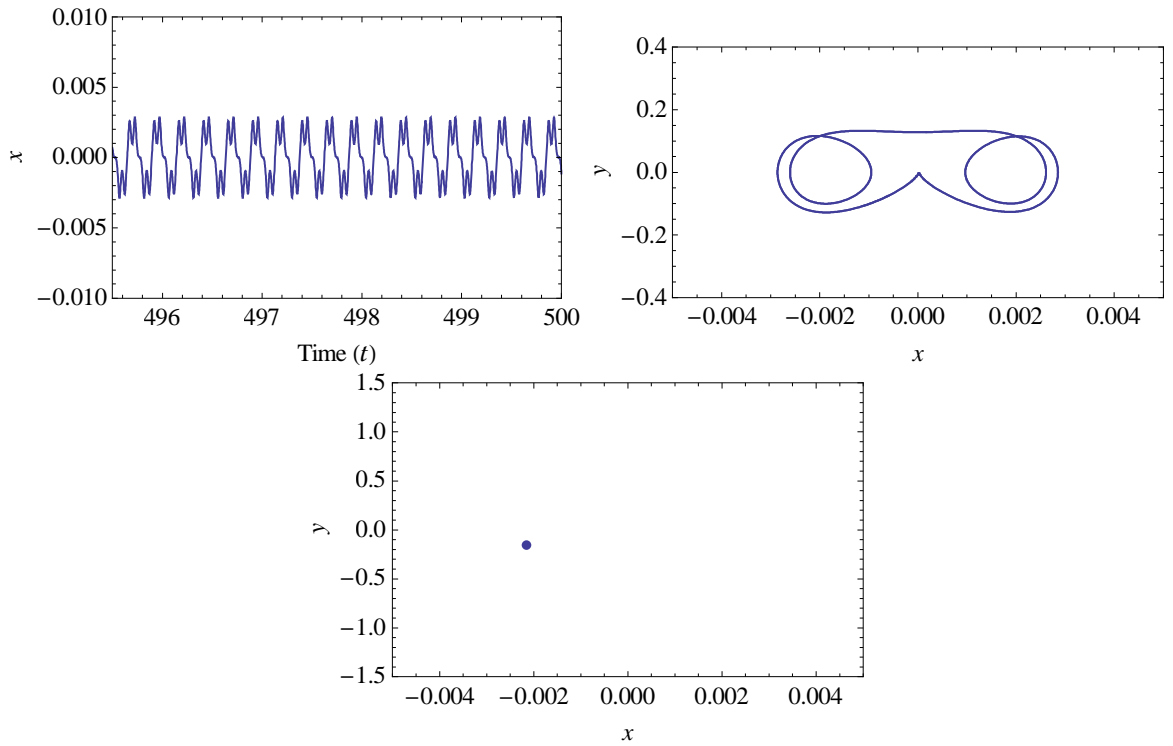
36.15 for the SSSS, CCSS and CCFF boundary conditions, respectively. The results obtained show that:

- All the time plots appear to be periodic, in which the oscillations do repeat after every 4 periods.
- Their corresponding phase plane plots also indicate period-4 motion as suggested in their bifurcation diagrams.
- The Poincaré maps consist of four points. The maps converge to four distinct points indicating period-4 motions.

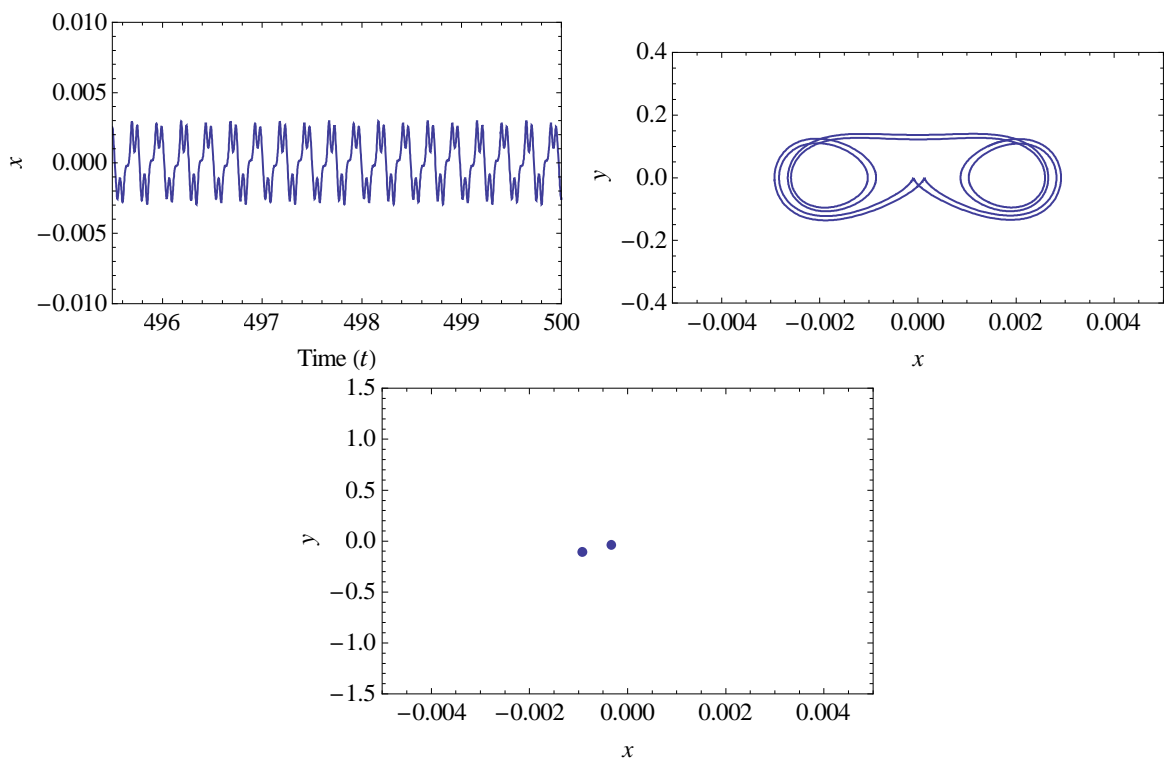
5.7.4 Figures 5-11(d) to 5-25(d), showing Chaotic motion

All the bifurcation diagrams for these cases show chaotic motion, and the results from the time plots, phase plane plots, and Poincaré maps are explored further through Figures 5-11(d) to 5-25(d) for the normalised excitation accelerations, $Rho = 12.06, 11.99, 12.02, 11.90, \text{ and } 12.00$, $Rho = 690.00, 688.00, 689.50, 684.00, \text{ and } 689.00$, and $Rho = 42.30, 39.80, 36.50, 37.71, \text{ and } 36.50$ for the SSSS, CCSS and CCFF boundary conditions, respectively. Observations for Figures 5-11(d) to 5-25(d) are as follows:

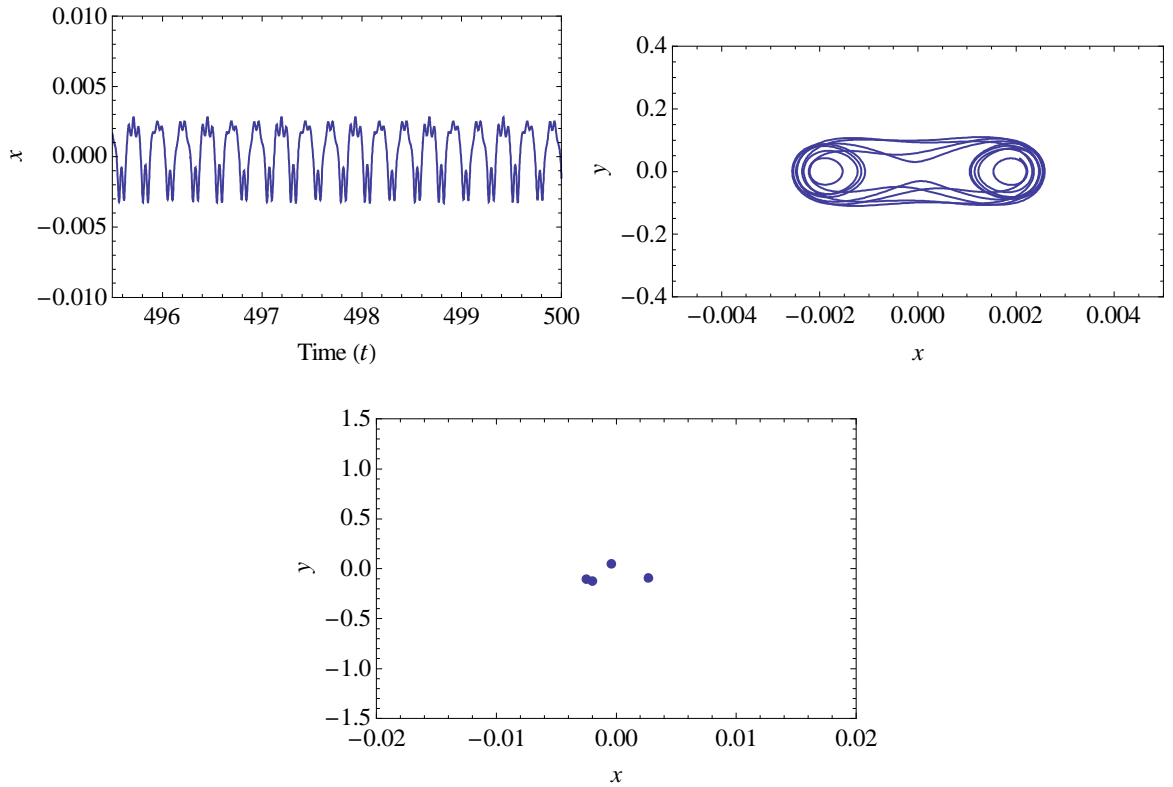
- All the time plots show non-periodic motion in which the oscillations do not repeat. In these cases this could be a qualitative visual indicator of chaotic motion.
- In the phase plane plots a densely filled phase plane is obtained. In particular, a densely filled phase plane in a diagram is usually taken as a signature of chaotic motion. It also can be seen that the plots are very complicated, and overlaid by repeated orbit cross-overs.
- The Poincaré maps show a large number of points and an irregular shape. This represents highly nonlinear behaviour and is an indicator of chaotic motion.



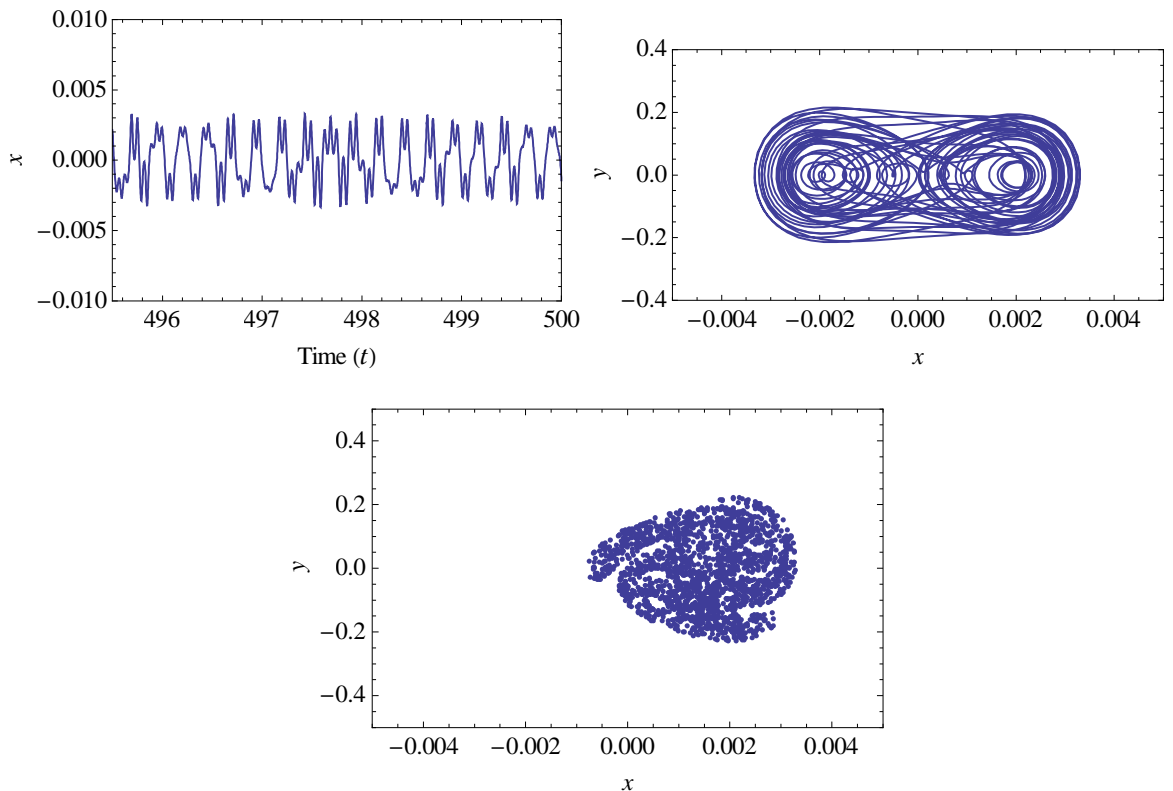
(a) Time plot, phase plane, and Poincaré map for normalised excitation acceleration of 11.74 (Period-1 motion)



(b) Time plot, phase plane, and Poincaré map for normalised excitation acceleration of 11.91 (Period-2 motion)

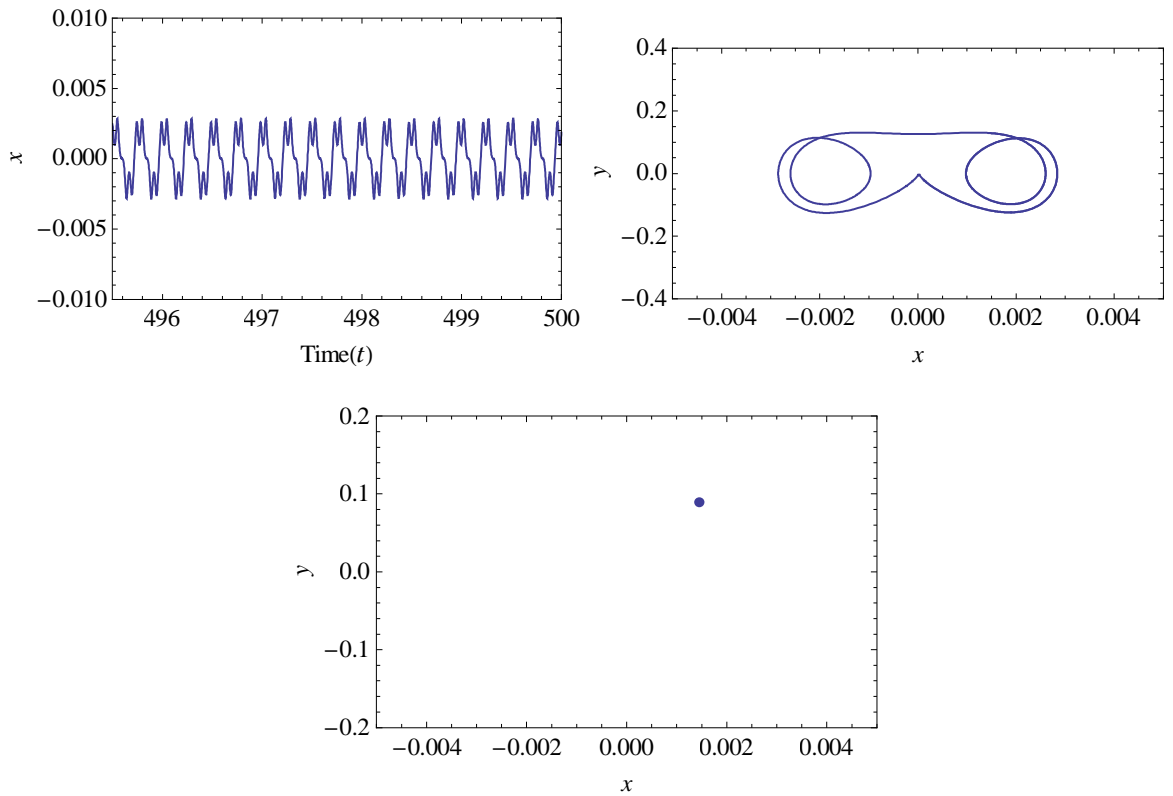


(c) Time plot, phase plane, and Poincaré map for normalised excitation acceleration of 12.00 (Period-4 motion)

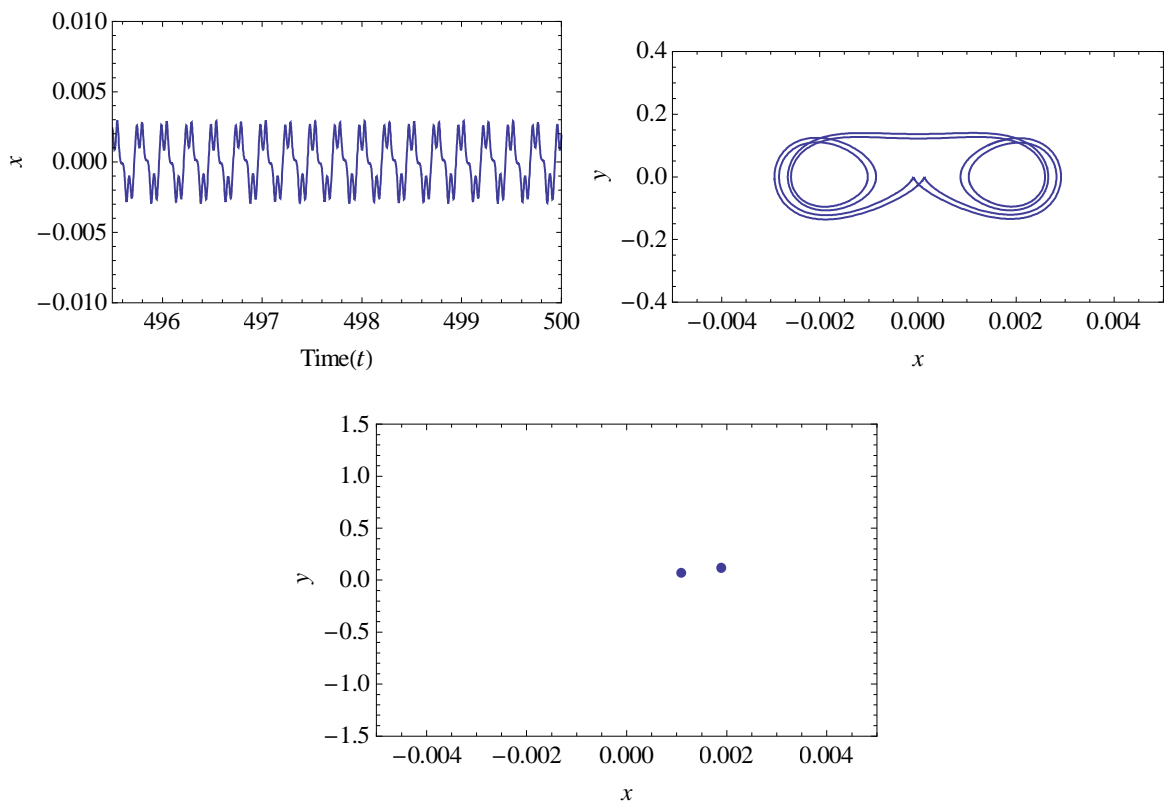


(d) Time plot, phase plane, and Poincaré map for normalised excitation acceleration of 12.06 (Chaotic motion)

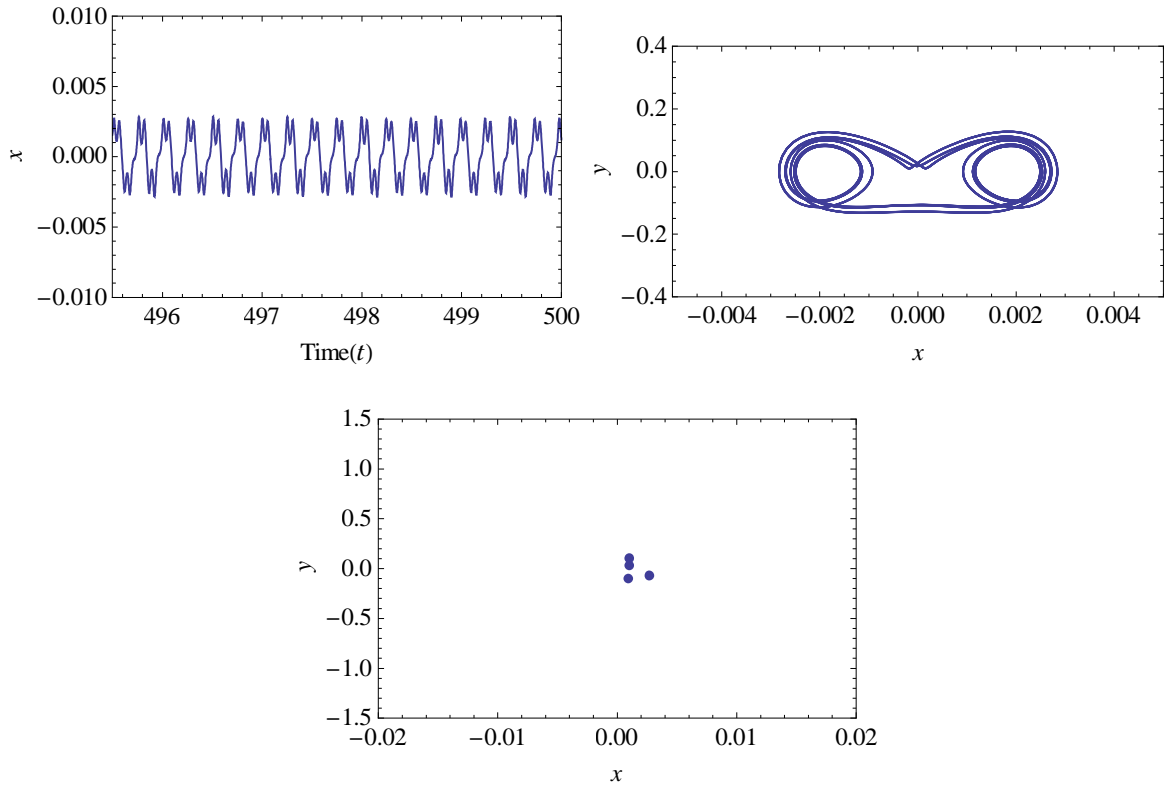
Figure 5-11 : Dynamical systems analysis for an intact plate with SSSS boundary condition



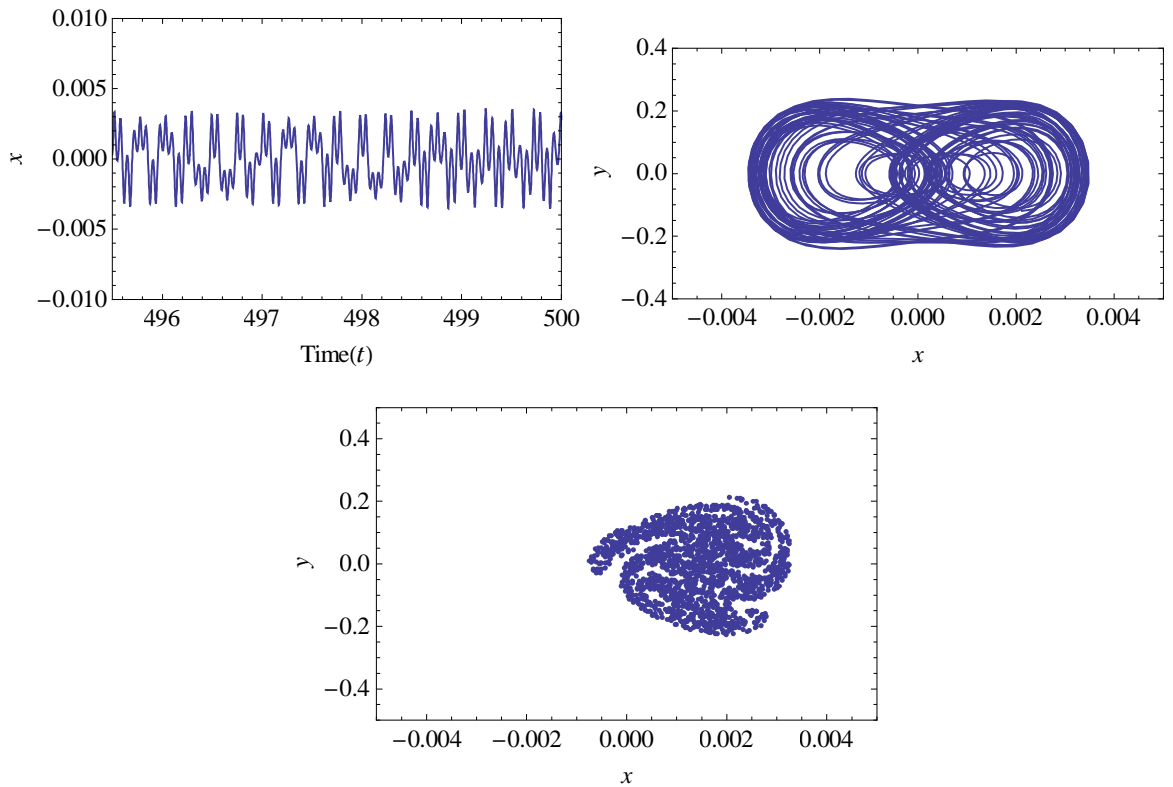
(a) Time plot, phase plane, and Poincaré map for normalised excitation acceleration of 11.60 (Period-1 motion)



(b) Time plot, phase plane, and Poincaré map for normalised excitation acceleration of 11.74 (Period-2 motion)

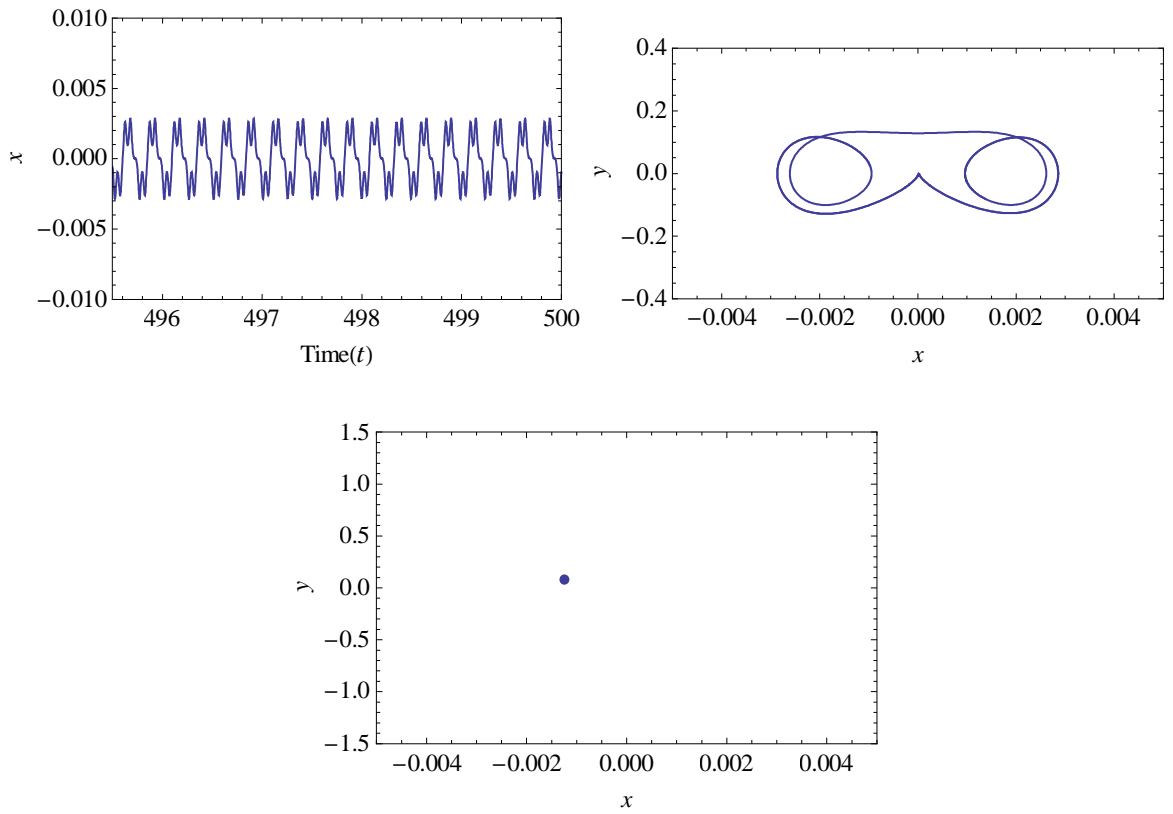


(c) Time plot, phase plane, and Poincaré map for normalised excitation acceleration of 11.91 (Period-4 motion)

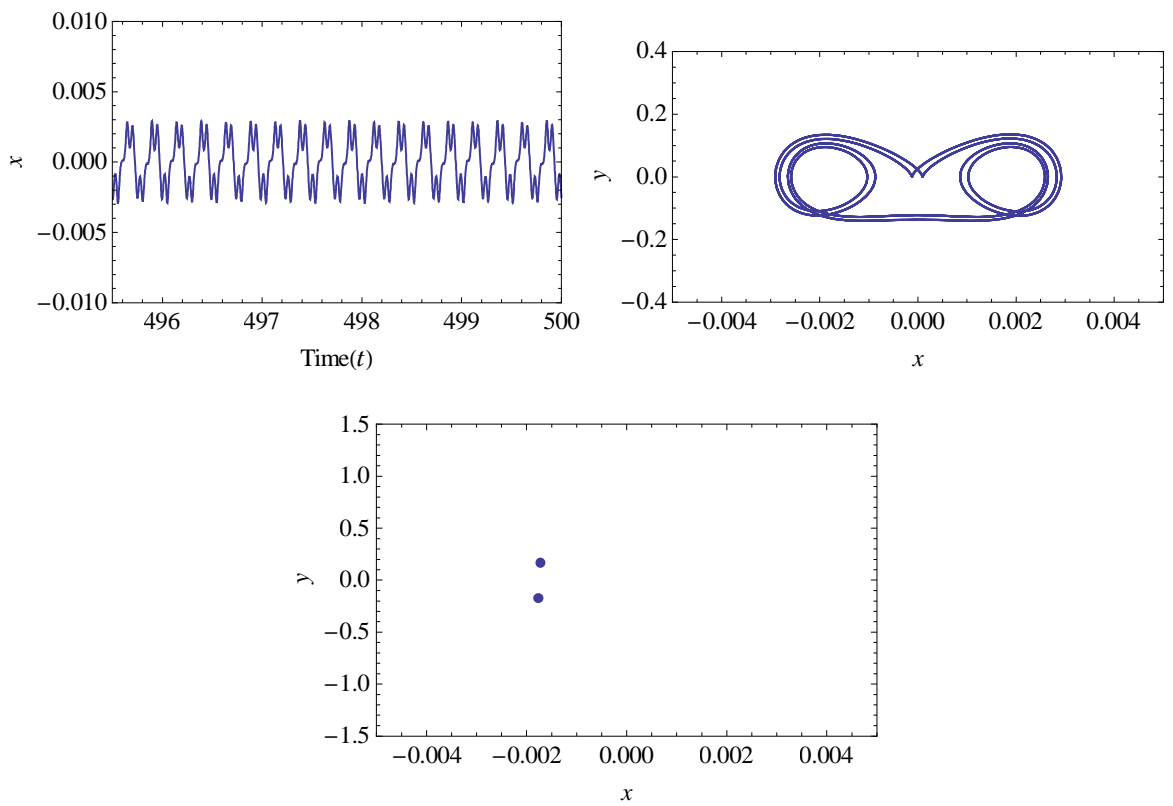


(d) Time plot, phase plane, and Poincaré map for normalised excitation acceleration of 11.99 (Chaotic motion)

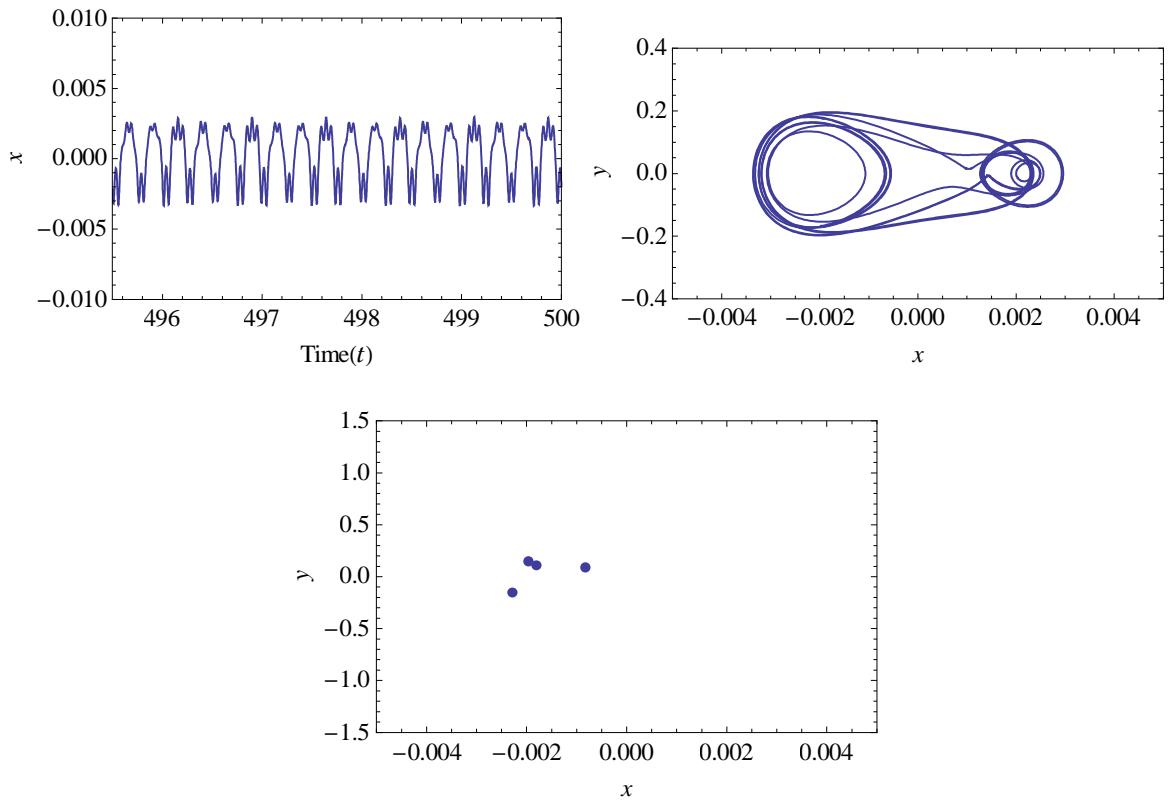
Figure 5-12 : Dynamical systems analysis for a cracked plate with half-crack length of 0.003 m and $\beta = 0^\circ$ m with SSSS boundary condition



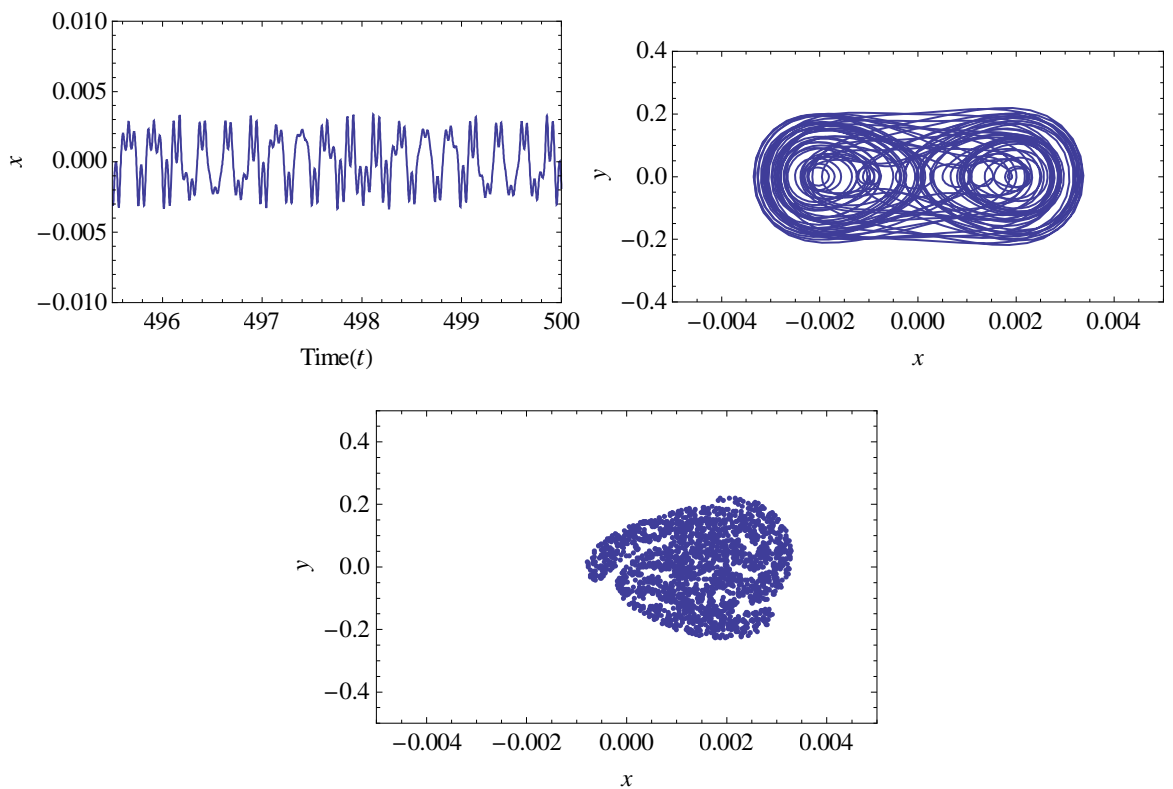
(a) Time plot, phase plane, and Poincaré map for normalised excitation acceleration of 11.74 (Period-1 motion)



(b) Time plot, phase plane, and Poincaré map for normalised excitation acceleration of 11.95 (Period-2 motion)

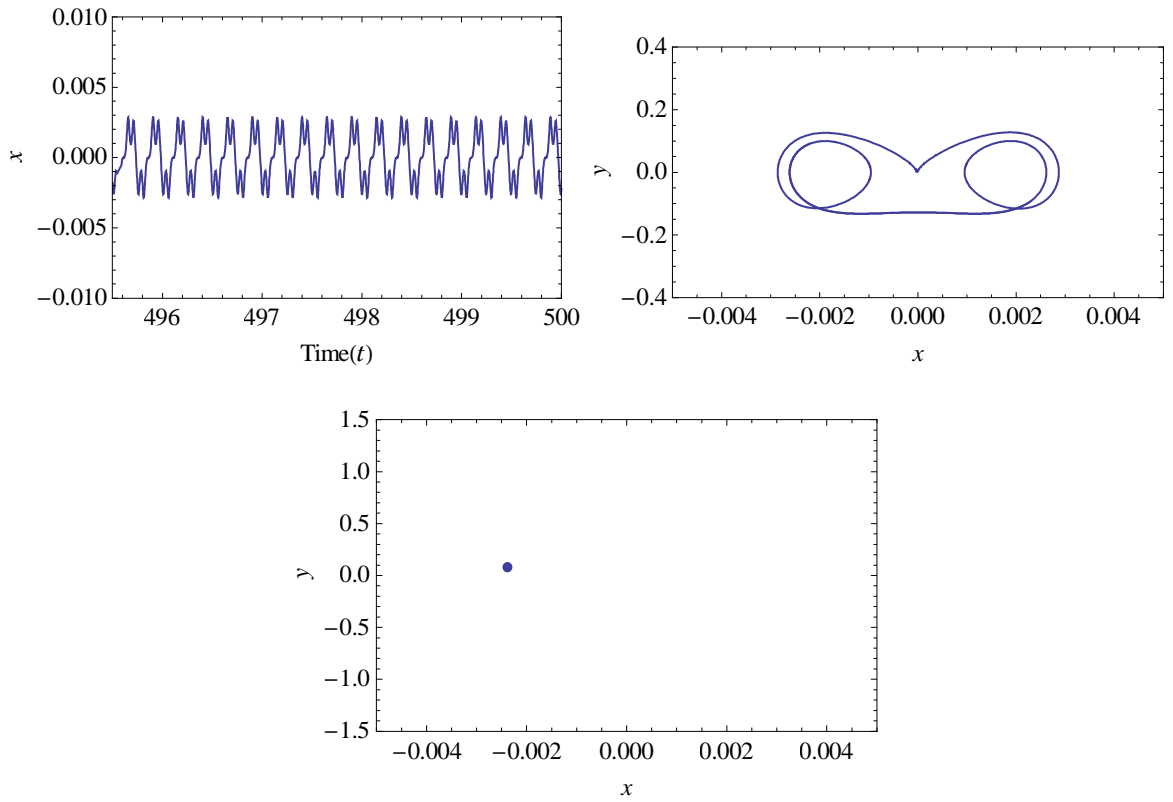


(c) Time plot, phase plane, and Poincaré map for normalised excitation acceleration of 11.98 (Period-4 motion)

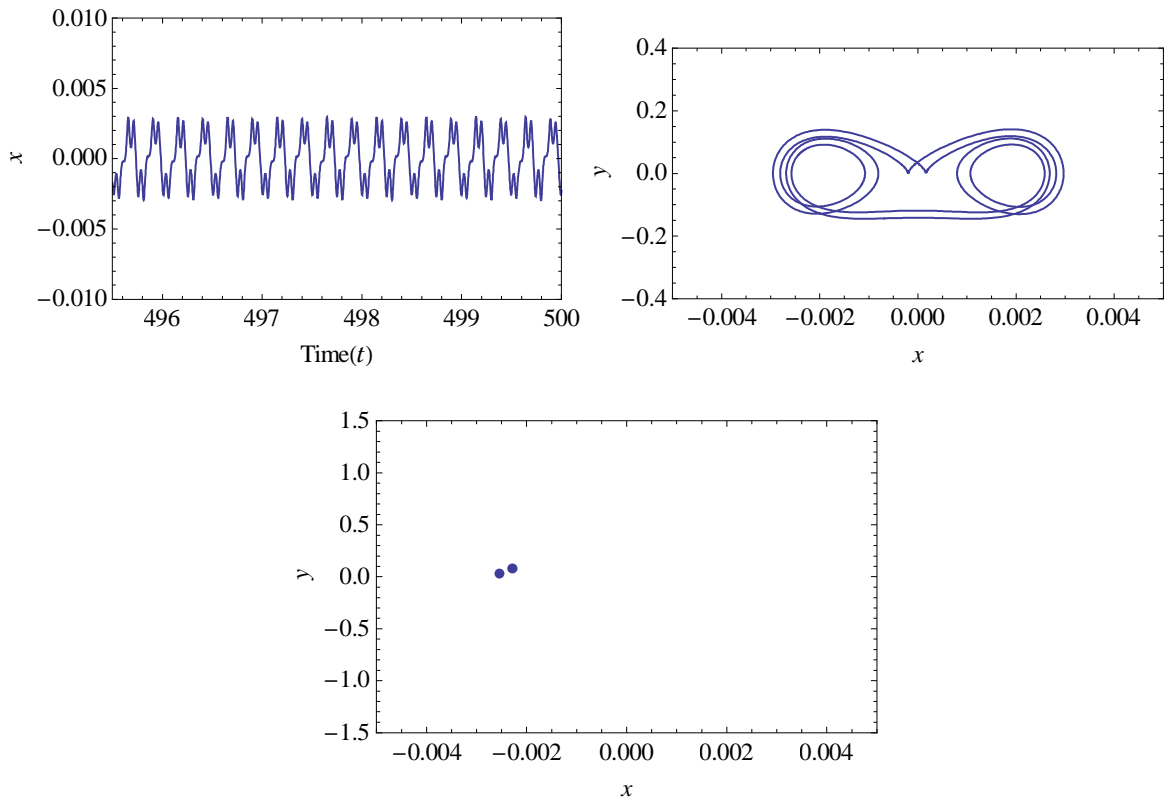


(d) Time plot, phase plane, and Poincaré map for normalised excitation acceleration of 12.02 (Chaotic motion)

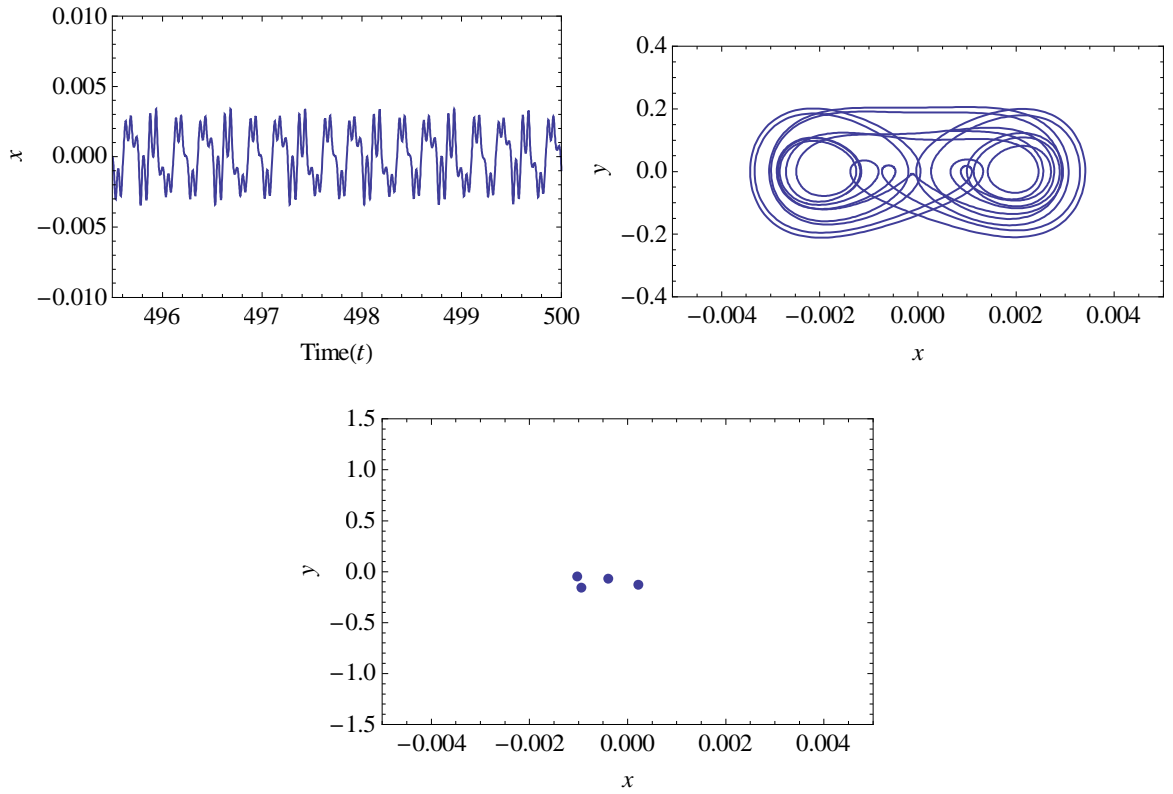
Figure 5-13 : Dynamical systems analysis for a cracked plate with half-crack length of 0.003 m and $\beta = 60^\circ$ m with SSSS boundary condition



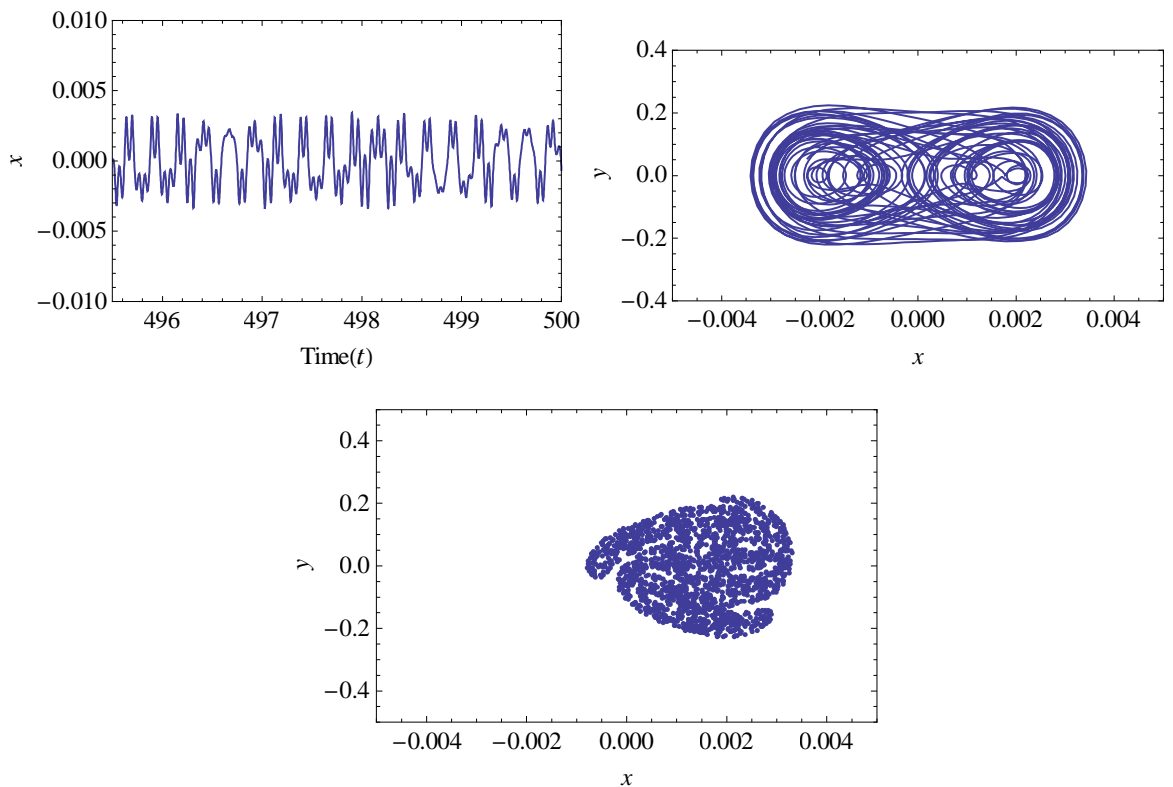
(a) Time plot, phase plane, and Poincaré map for normalised excitation acceleration of 11.60 (Period-1 motion)



(b) Time plot, phase plane, and Poincaré map for normalised excitation acceleration of 11.74 (Period-2 motion)

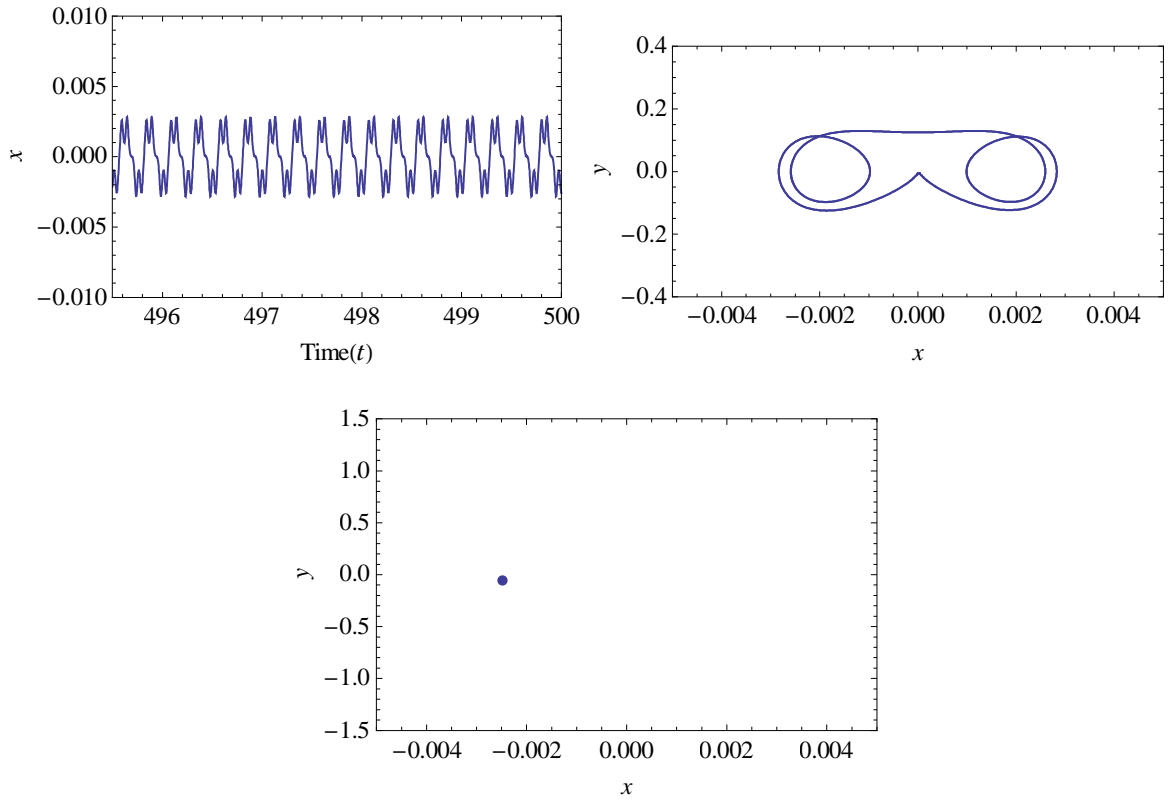


(c) Time plot, phase plane, and Poincaré map for normalised excitation acceleration of 11.84 (Period-4 motion)

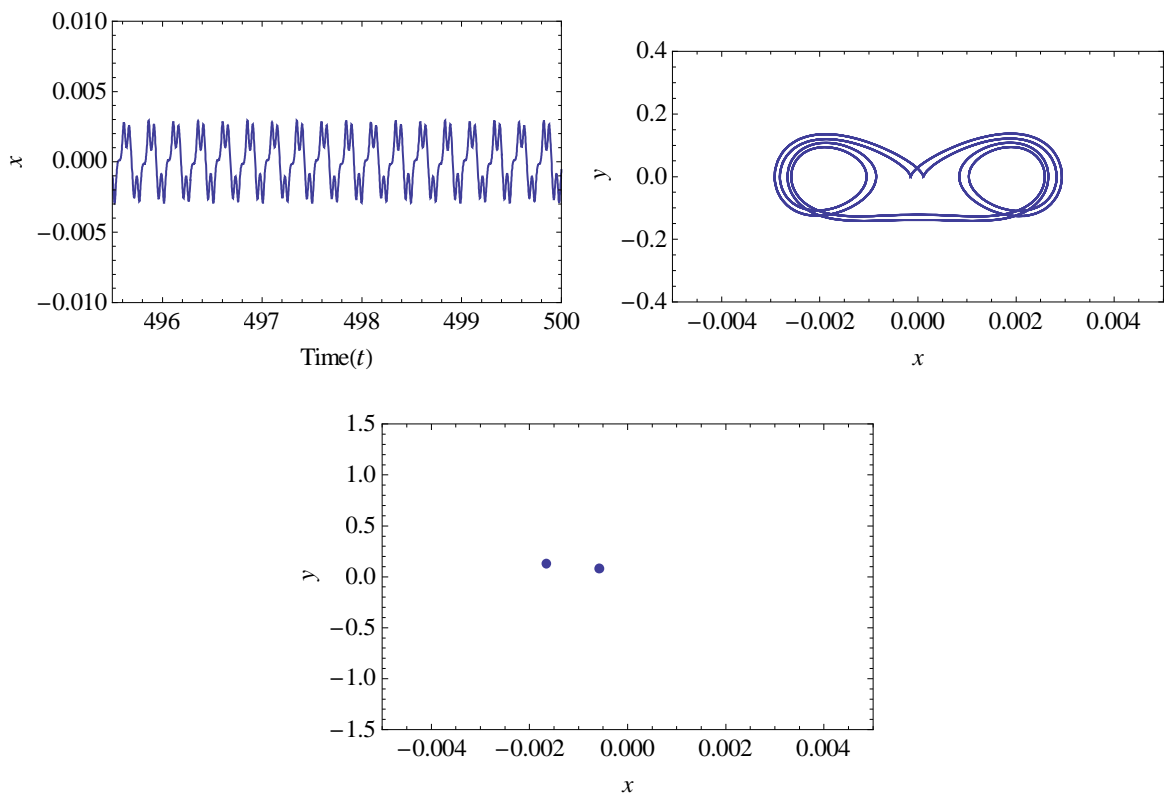


(d) Time plot, phase plane, and Poincaré map for normalised excitation acceleration of 11.90 (Chaotic motion)

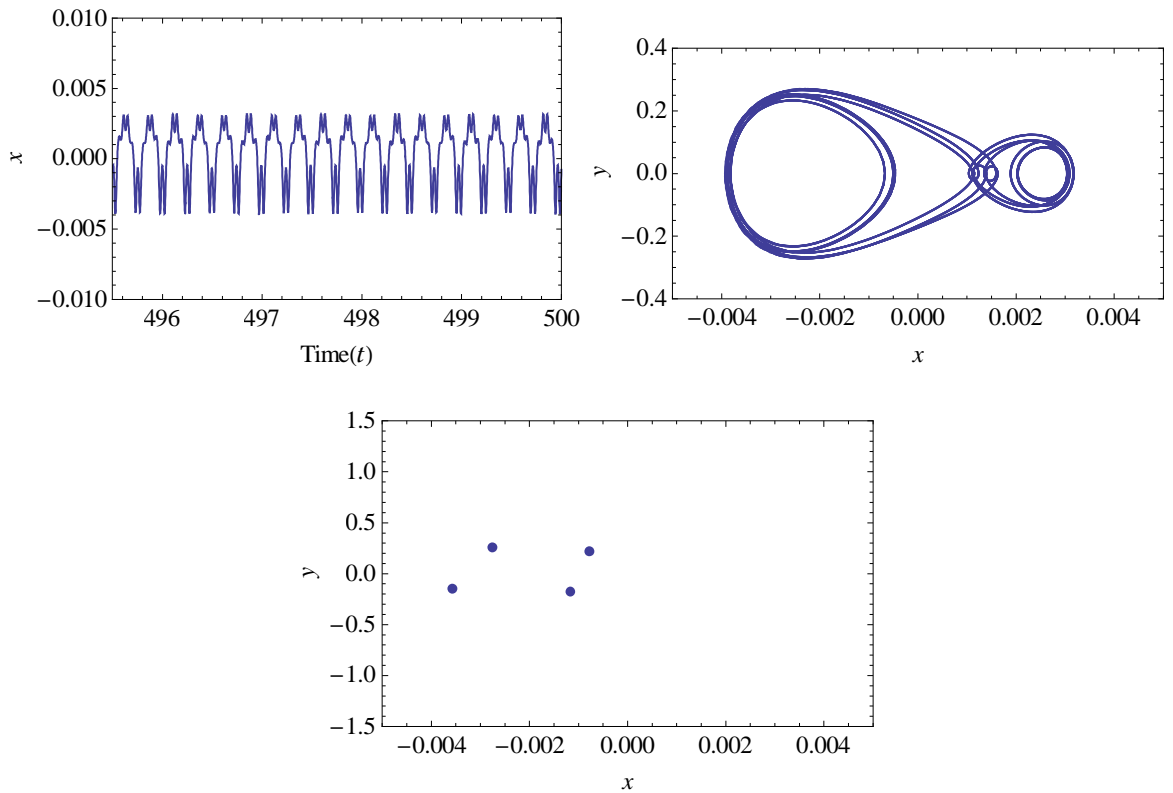
Figure 5-14 : Dynamical systems analysis for a cracked plate with half-crack length of 0.0075 m and $\beta = 0^\circ$ m with SSSS boundary condition



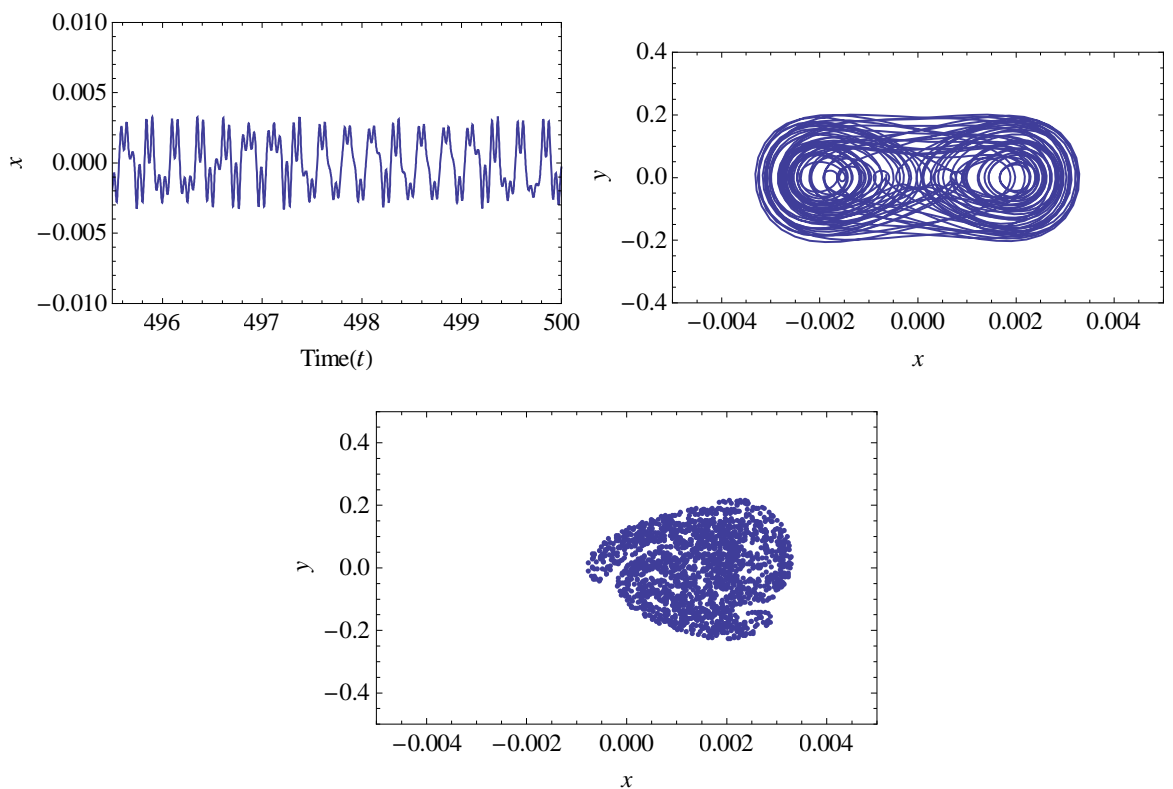
(a) Time plot, phase plane, and Poincaré map for normalised excitation acceleration of 11.60 (Period-1 motion)



(b) Time plot, phase plane, and Poincaré map for normalised excitation acceleration of 11.90 (Period-2 motion)

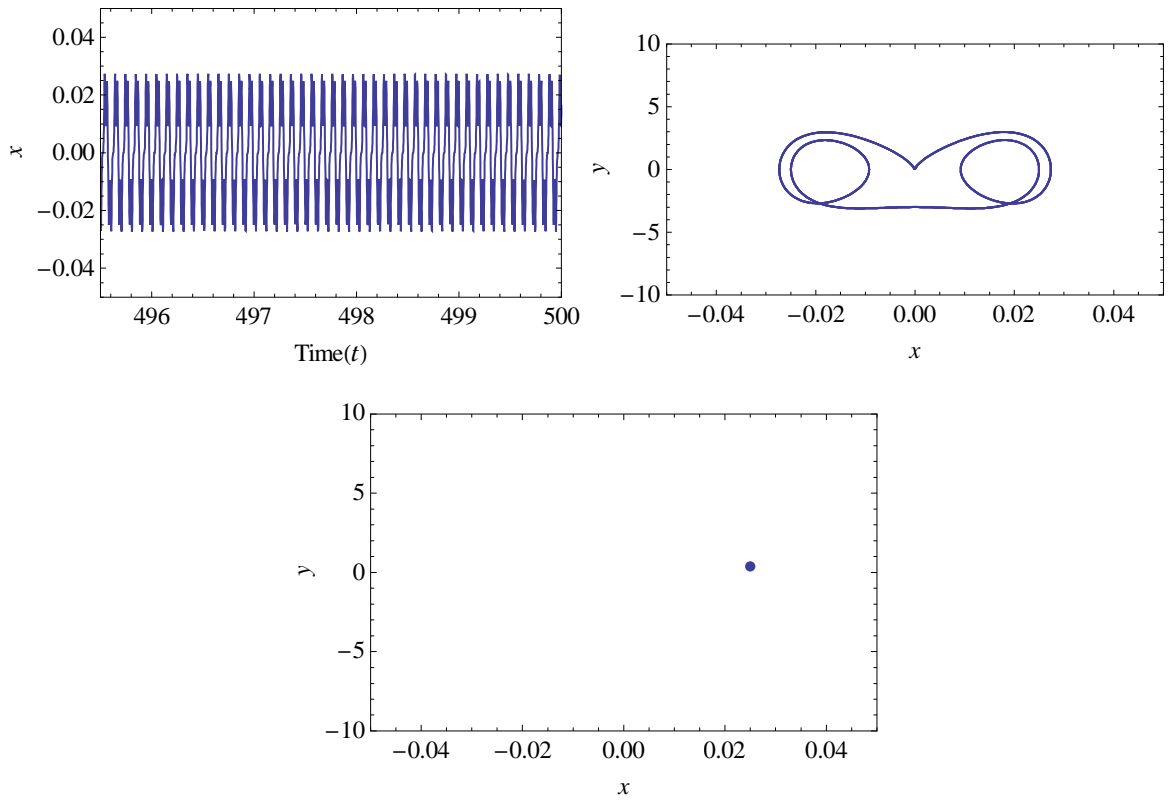


(c) Time plot, phase plane, and Poincaré map for normalised excitation acceleration of 11.96 (Period-4 motion)

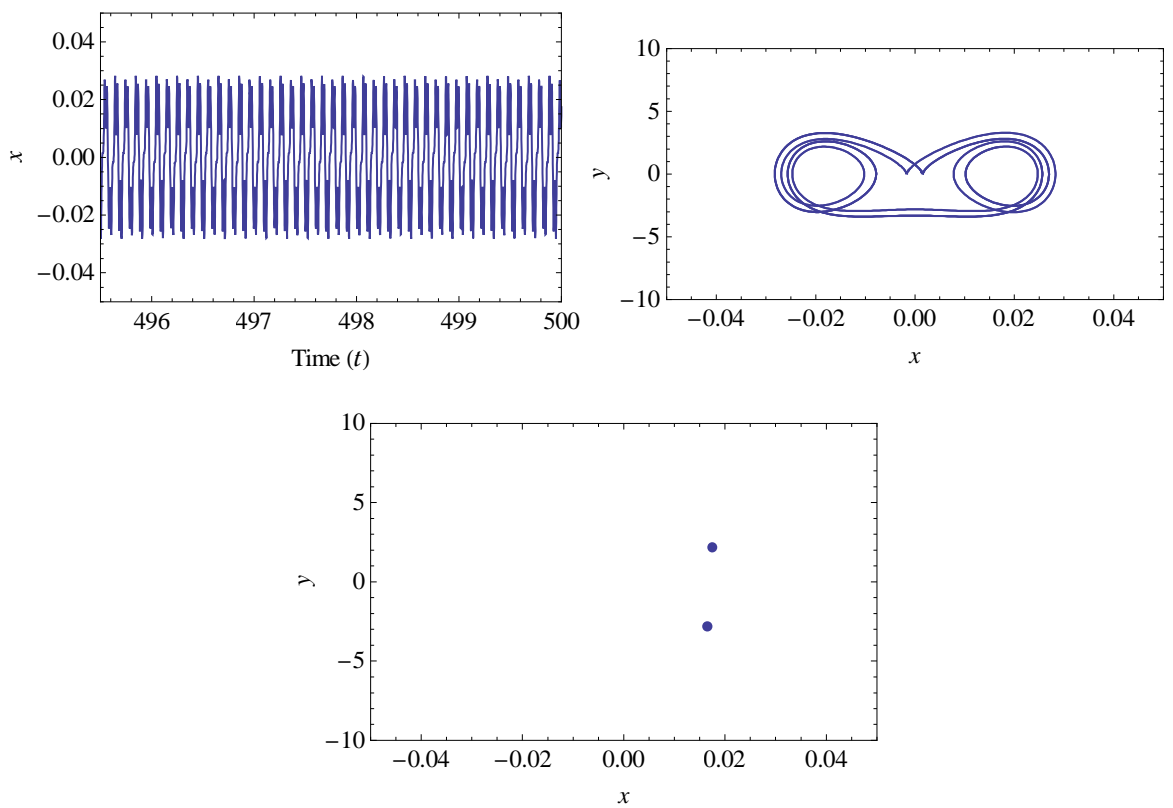


(d) Time plot, phase plane, and Poincaré map for normalised excitation acceleration of 12.00 (Chaotic motion)

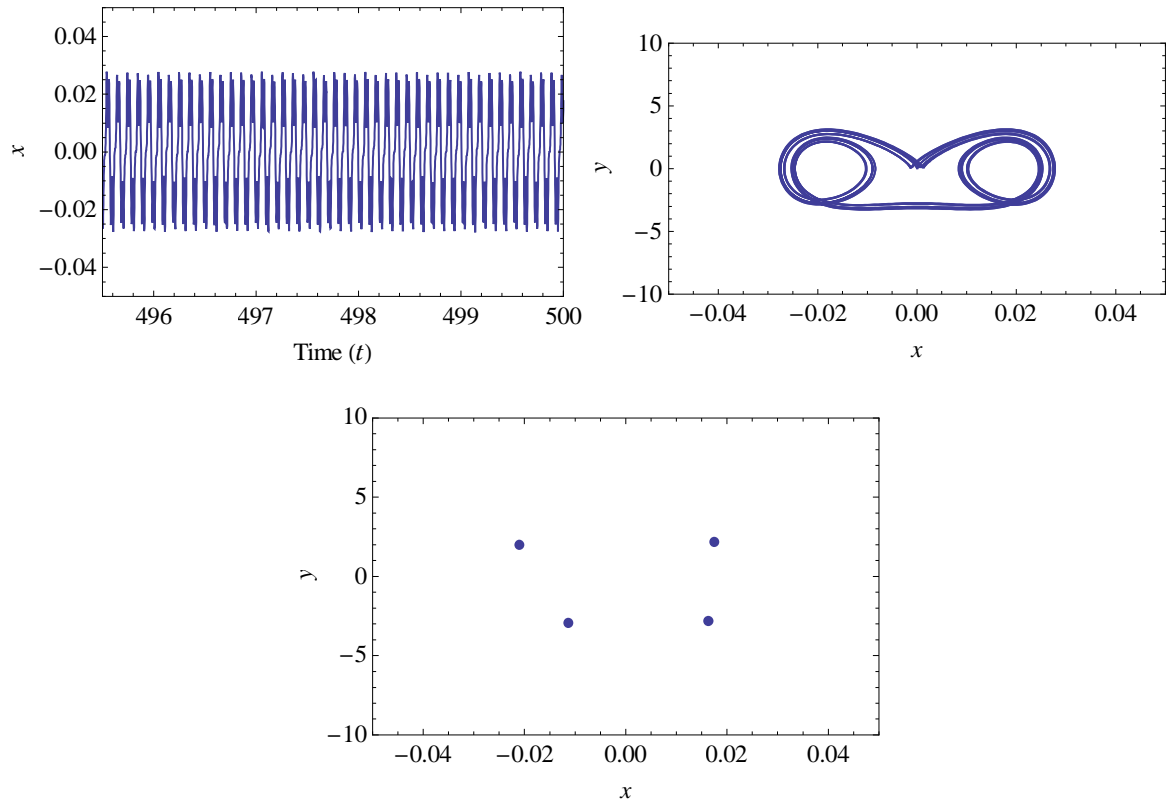
Figure 5-15 : Dynamical systems analysis for a cracked plate with half-crack length of 0.0075 m and $\beta = 60^\circ$ m with SSSS boundary condition



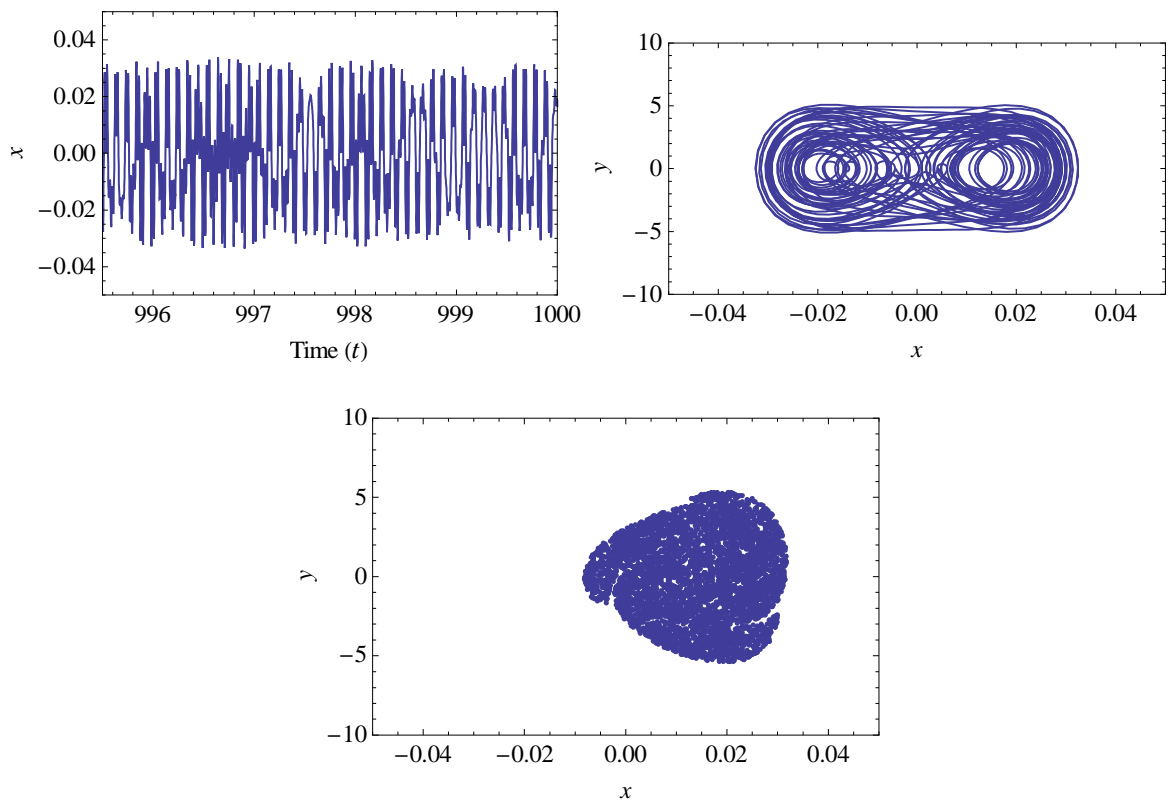
(a) Time plot, phase plane, and Poincaré map for normalised excitation acceleration of 673.00 (Period-1 motion)



(b) Time plot, phase plane, and Poincaré map for normalised excitation acceleration of 682.00 (Period-2 motion)

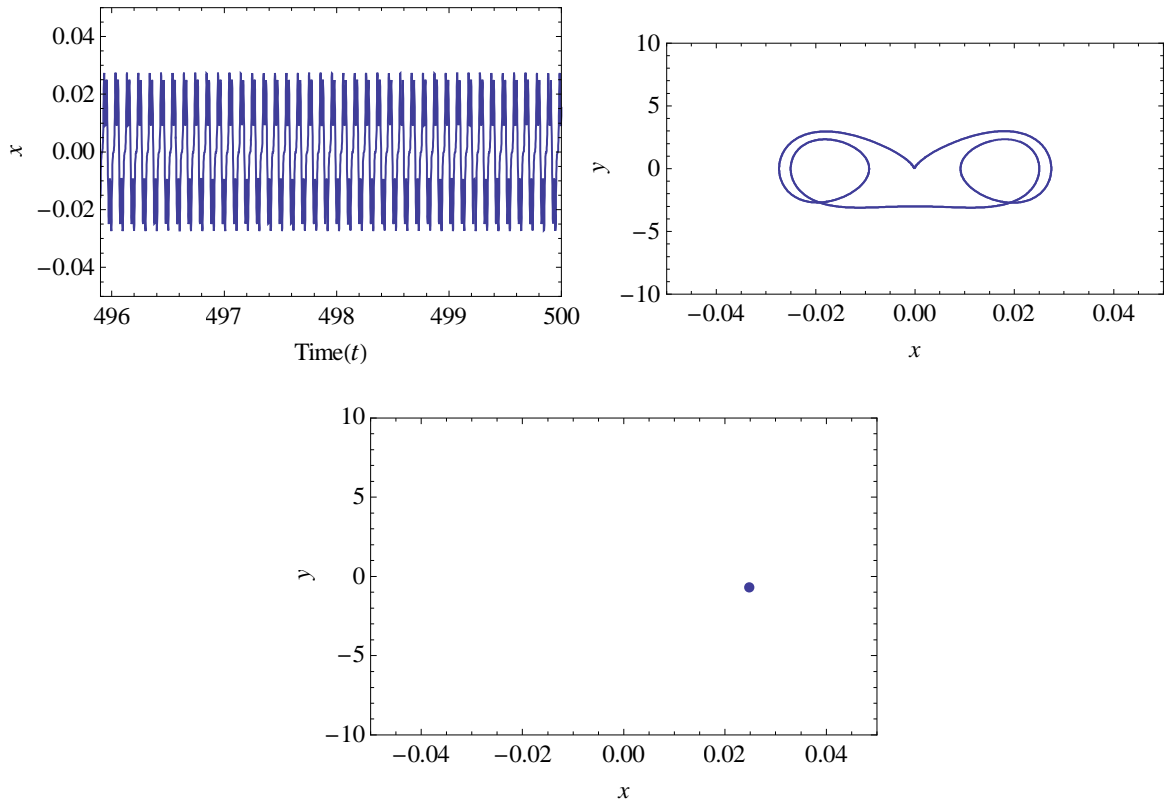


(c) Time plot, phase plane, and Poincaré map for normalised excitation acceleration of 688.50 (Period-4 motion)

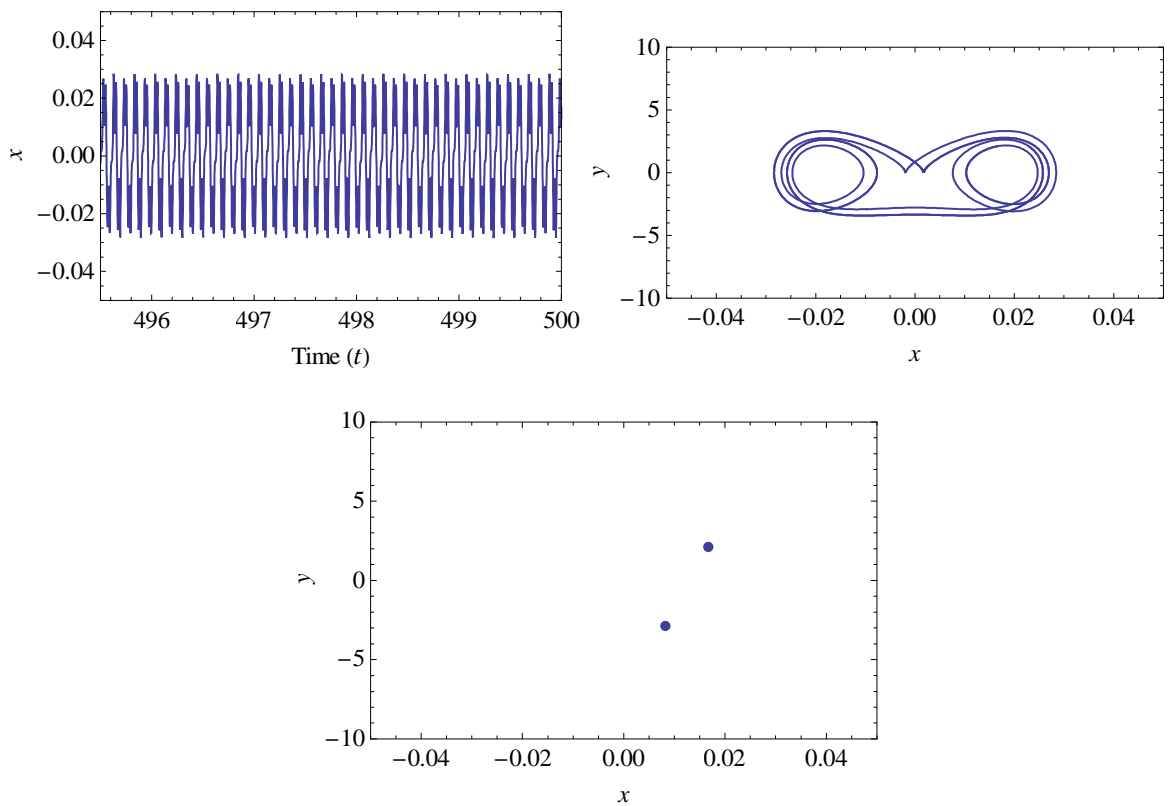


(d) Time plot, phase plane, and Poincaré map for normalised excitation acceleration of 690.00 (Chaotic motion)

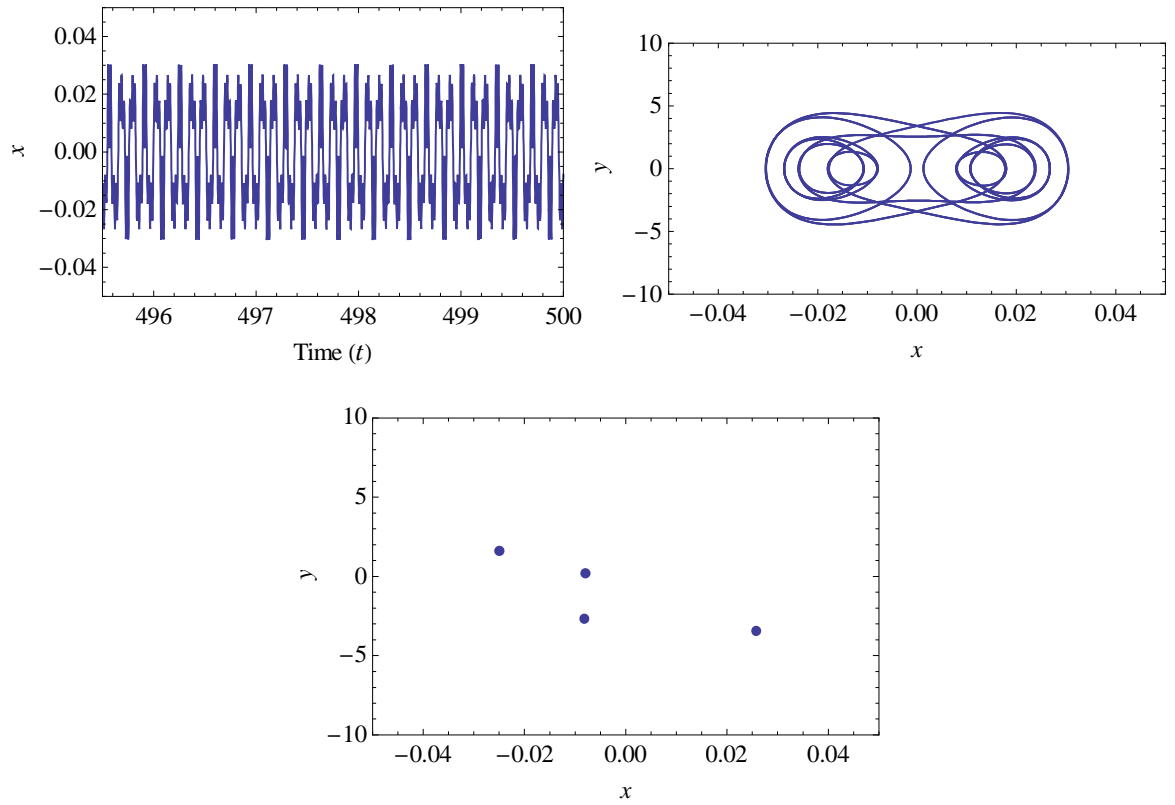
Figure 5-16 : Dynamical systems analysis for an intact plate with CCSS boundary condition



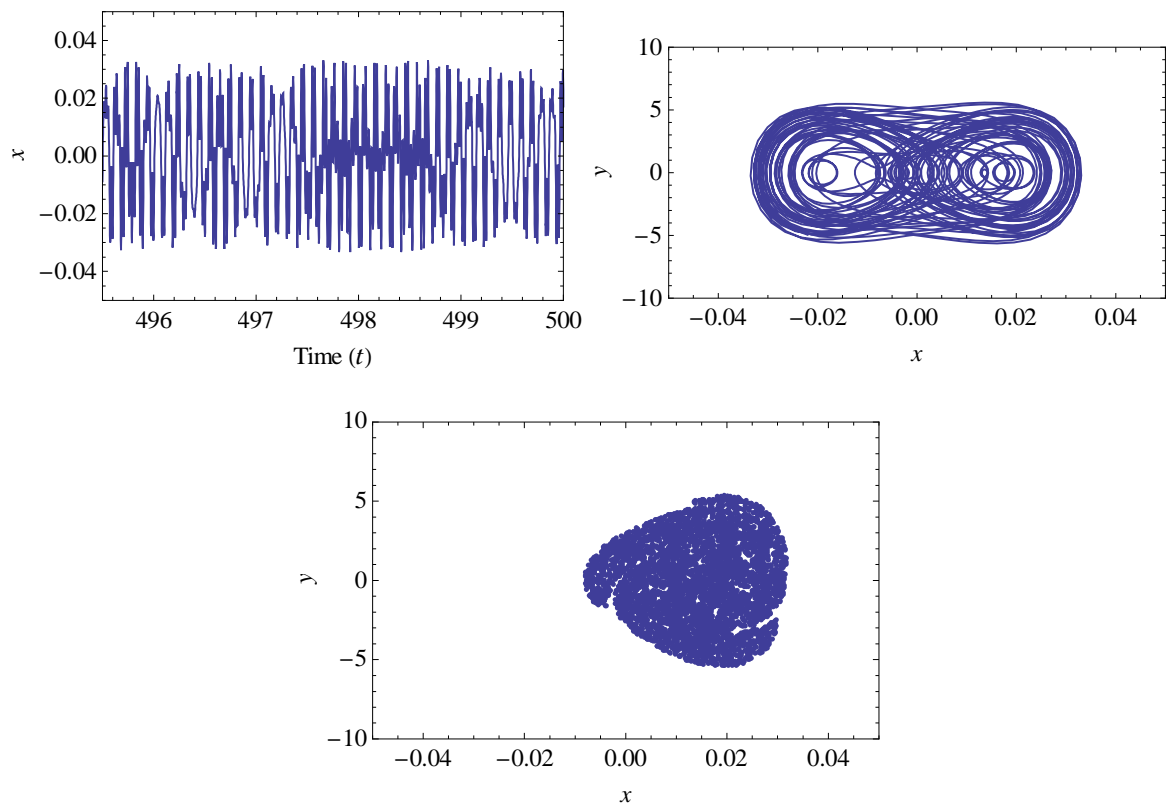
(a) Time plot, phase plane, and Poincaré map for normalised excitation acceleration of 670.00 (Period-1 motion)



(b) Time plot, phase plane, and Poincaré map for normalised excitation acceleration of 680.00 (Period-2 motion)

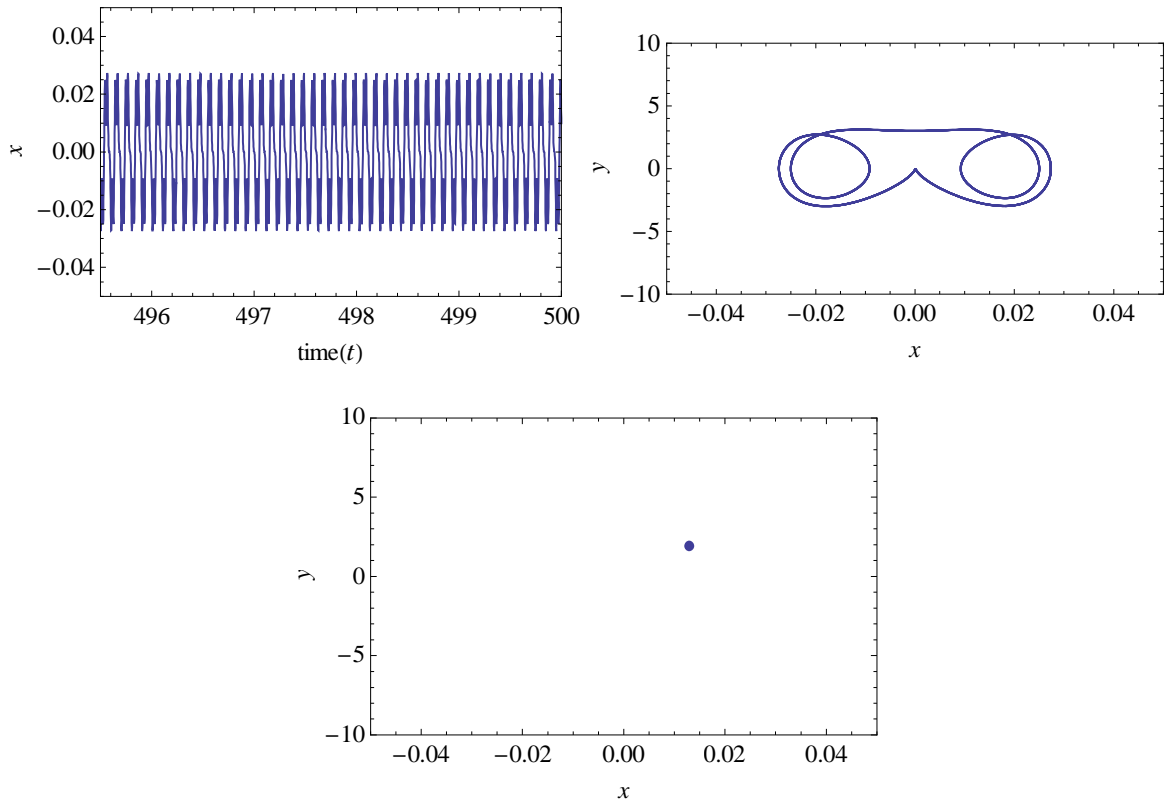


(c) Time plot, phase plane, and Poincaré map for normalised excitation acceleration of 685.00 (Period-4 motion)

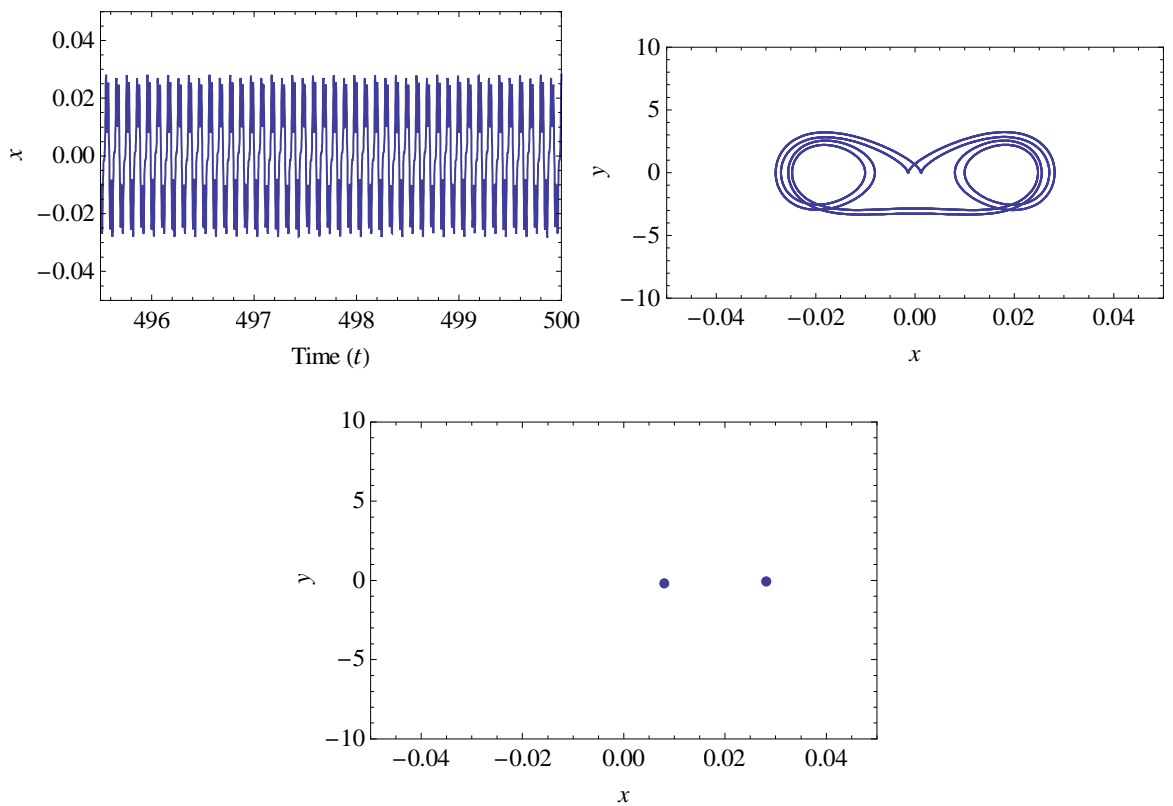


(d) Time plot, phase plane, and Poincaré map for normalised excitation acceleration of 688.00 (Chaotic motion)

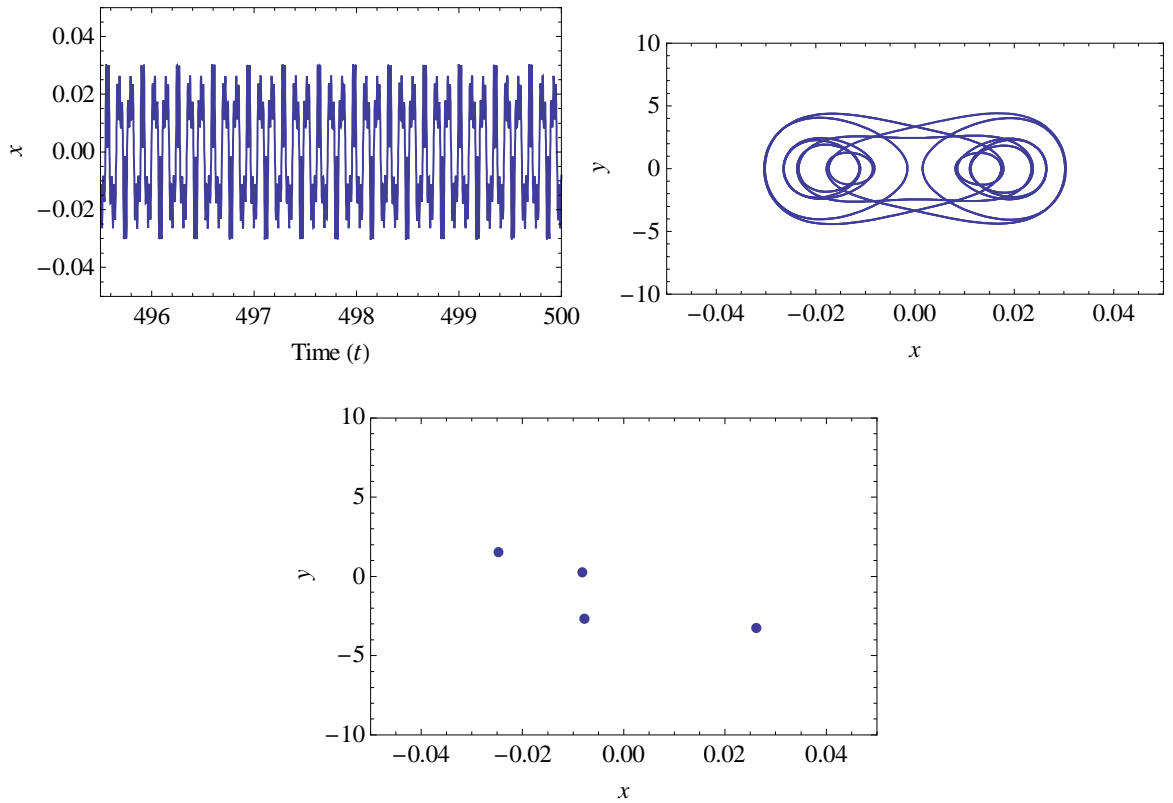
Figure 5-17 : Dynamical systems analysis for a cracked plate with half-crack length of 0.003 m and $\beta = 0^\circ$ with CCSS boundary condition



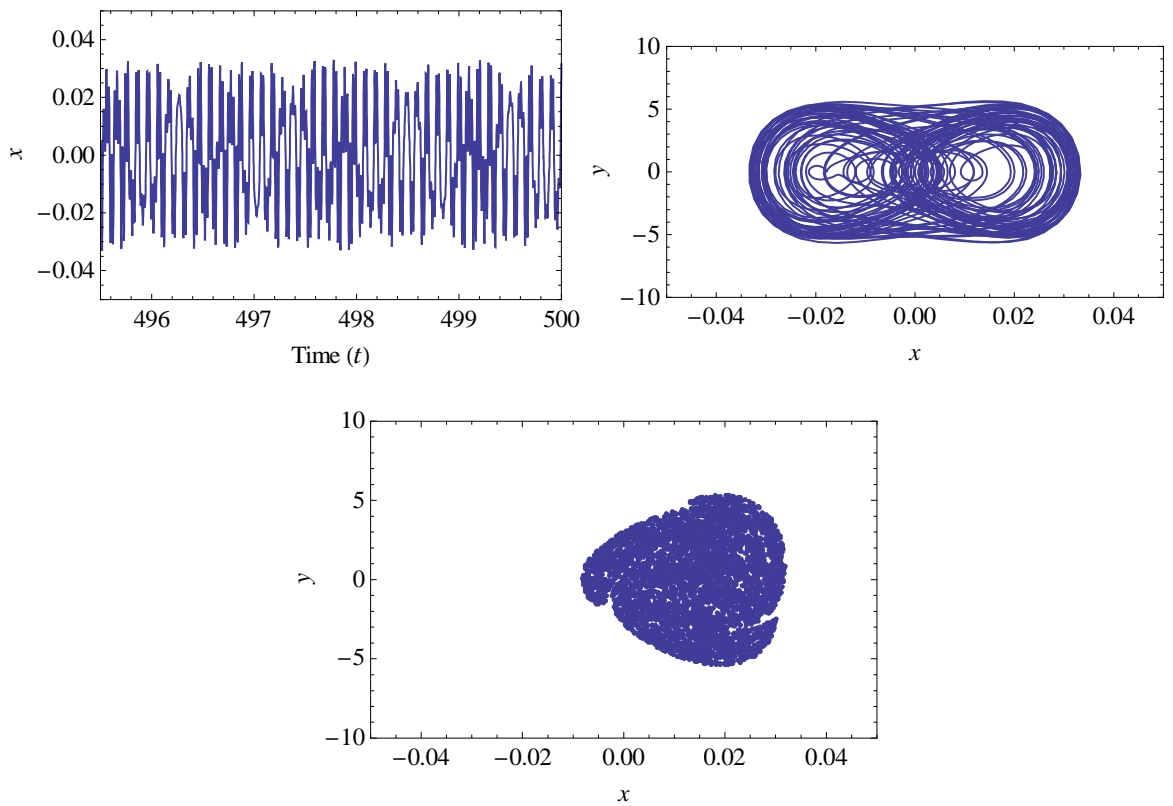
(a) Time plot, phase plane, and Poincaré map for normalised excitation acceleration of 673.00 (Period-1 motion)



(b) Time plot, phase plane, and Poincaré map for normalised excitation acceleration of 682.00 (Period-2 motion)

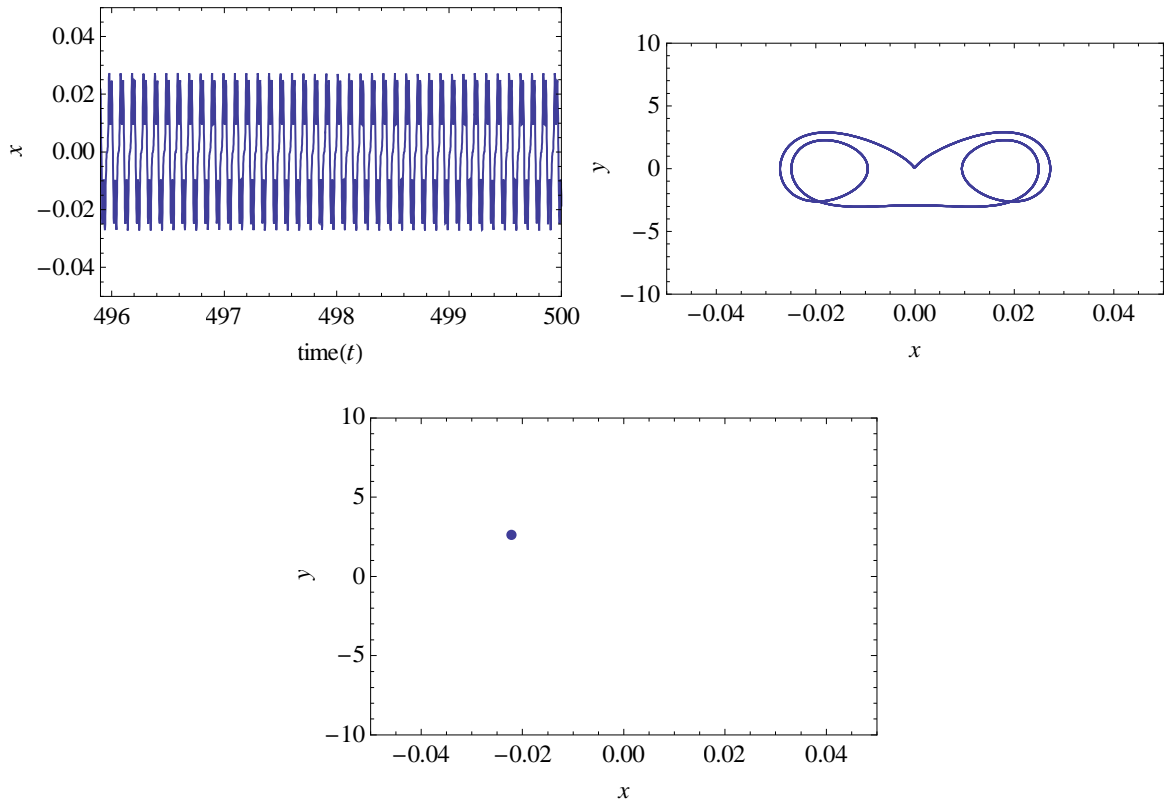


(c) Time plot, phase plane, and Poincaré map for normalised excitation acceleration of 688.00 (Period-4 motion)

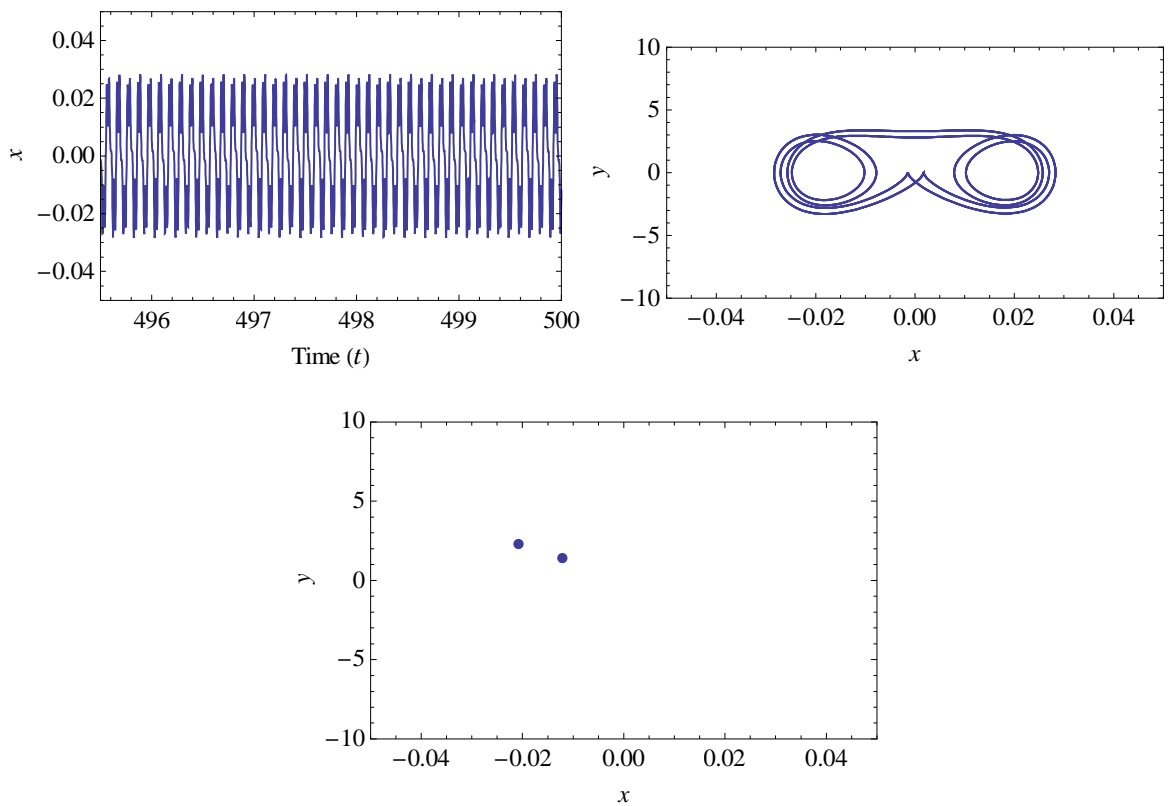


(d) Time plot, phase plane, and Poincaré map for normalised excitation acceleration of 689.50 (Chaotic motion)

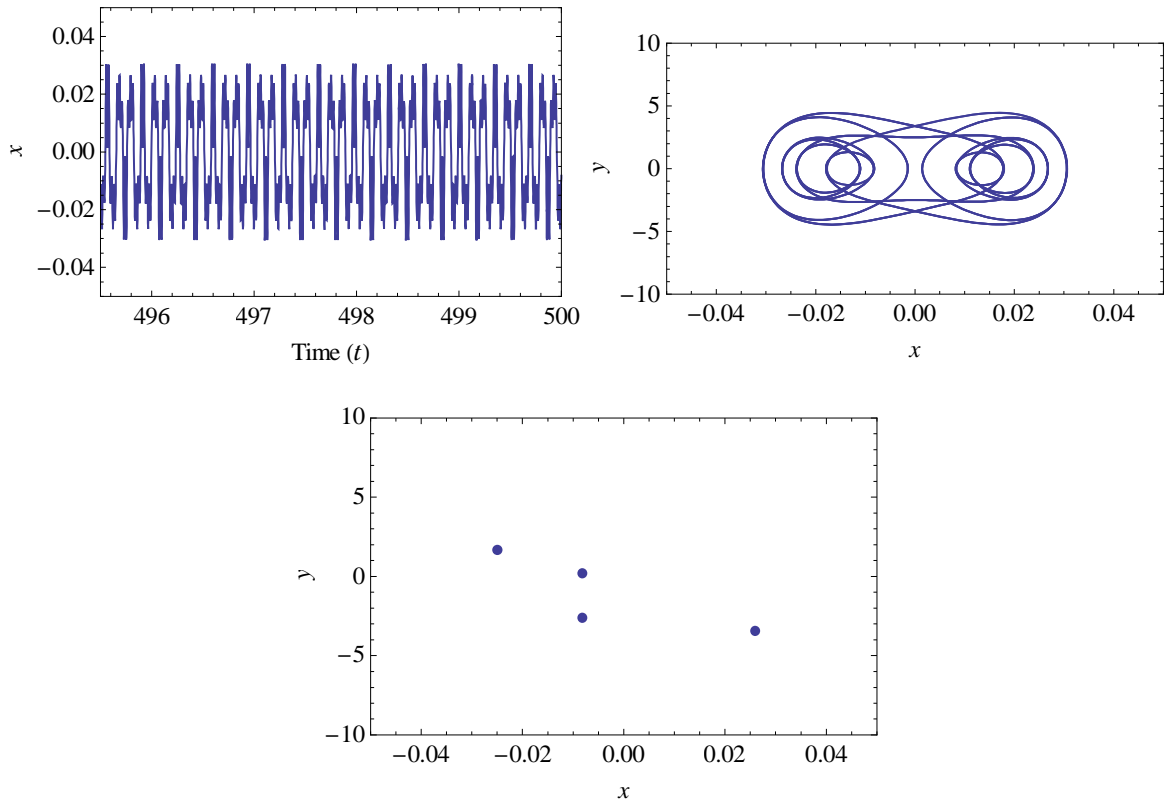
Figure 5-18 : Dynamical systems analysis for a cracked plate with half-crack length of 0.003 m and $\beta = 60^\circ$ with CCSS boundary condition



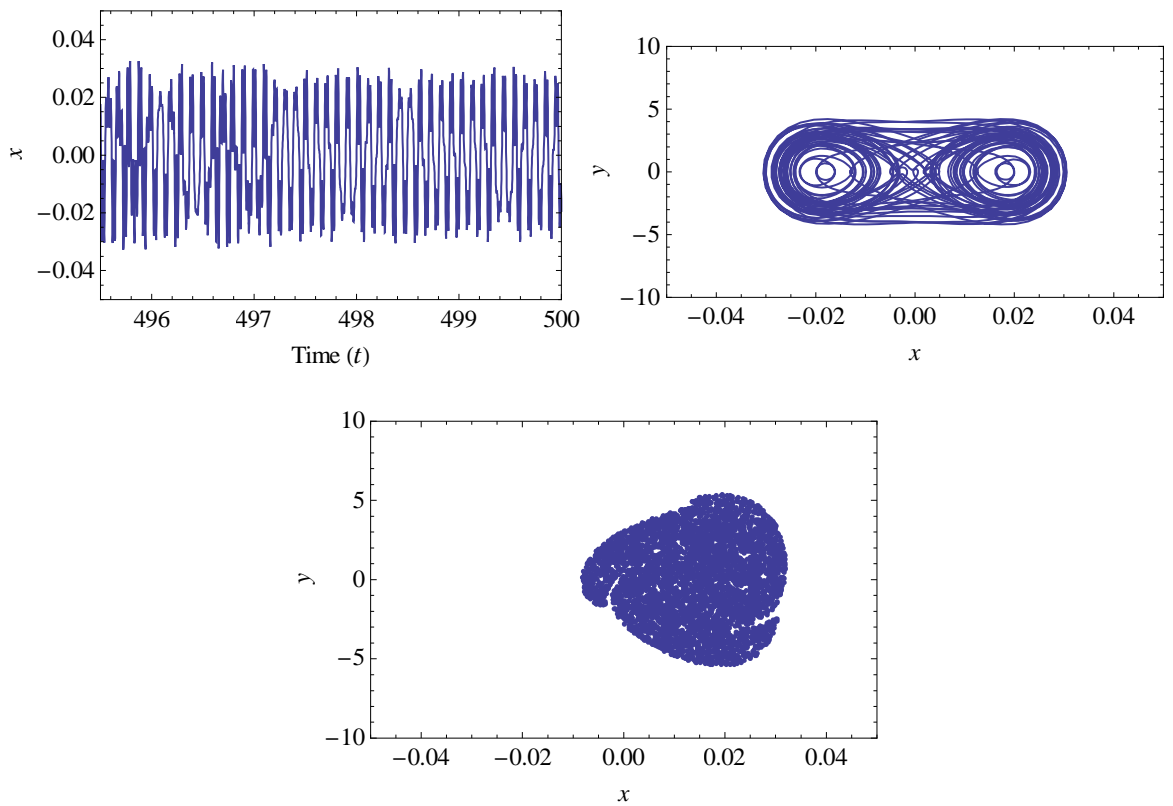
(a) Time plot, phase plane, and Poincaré map for normalised excitation acceleration of 665.00 (Period-1 motion)



(b) Time plot, phase plane, and Poincaré map for normalised excitation acceleration of 675.00 (Period-2 motion)

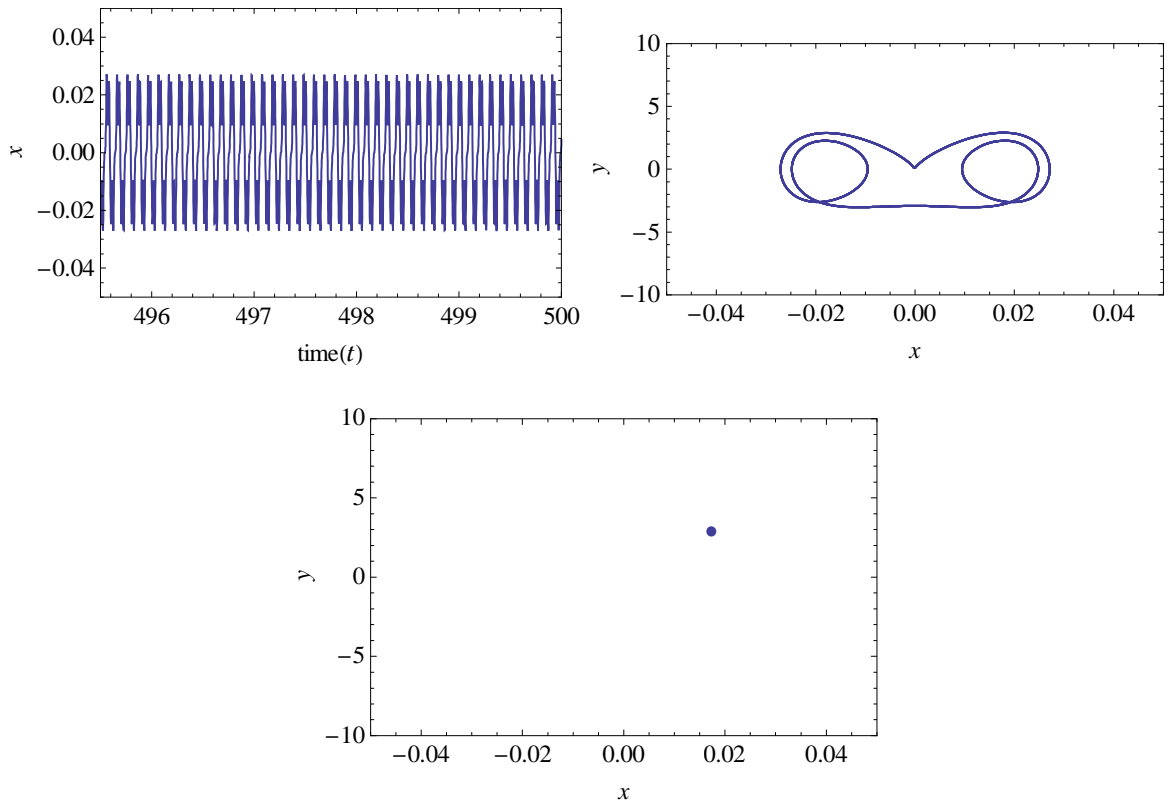


(c) Time plot, phase plane, and Poincaré map for normalised excitation acceleration of 682.00 (Period-4 motion)

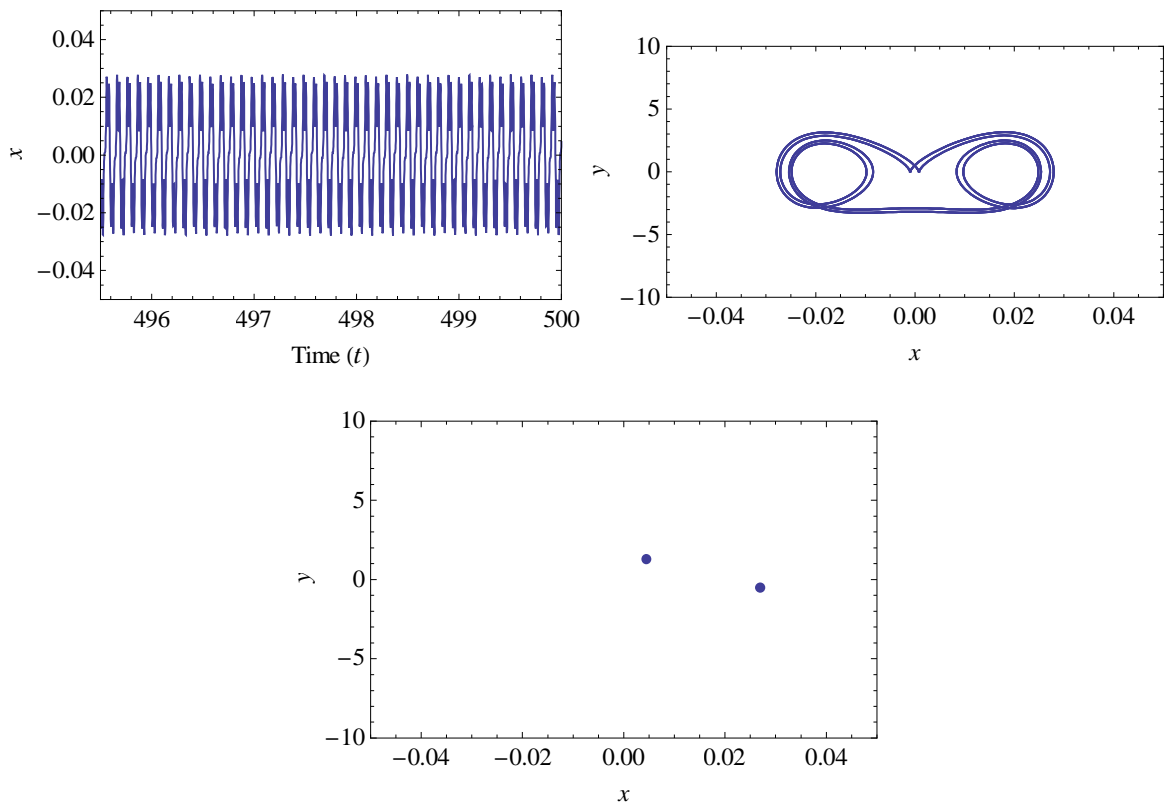


(d) Time plot, phase plane, and Poincaré map for normalised excitation acceleration of 684.00 (Chaotic motion)

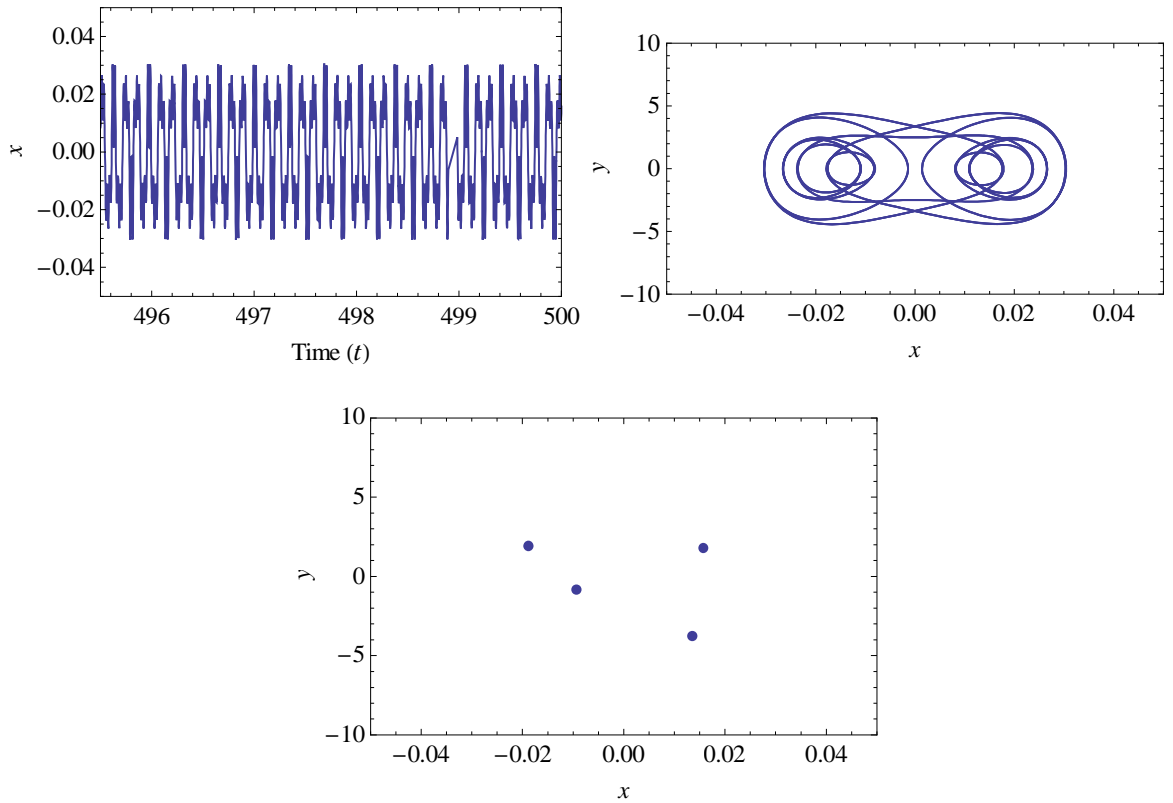
Figure 5-19 : Dynamical systems analysis for a cracked plate with half-crack length of 0.0075 m and $\beta = 0^\circ$ with CCSS boundary condition



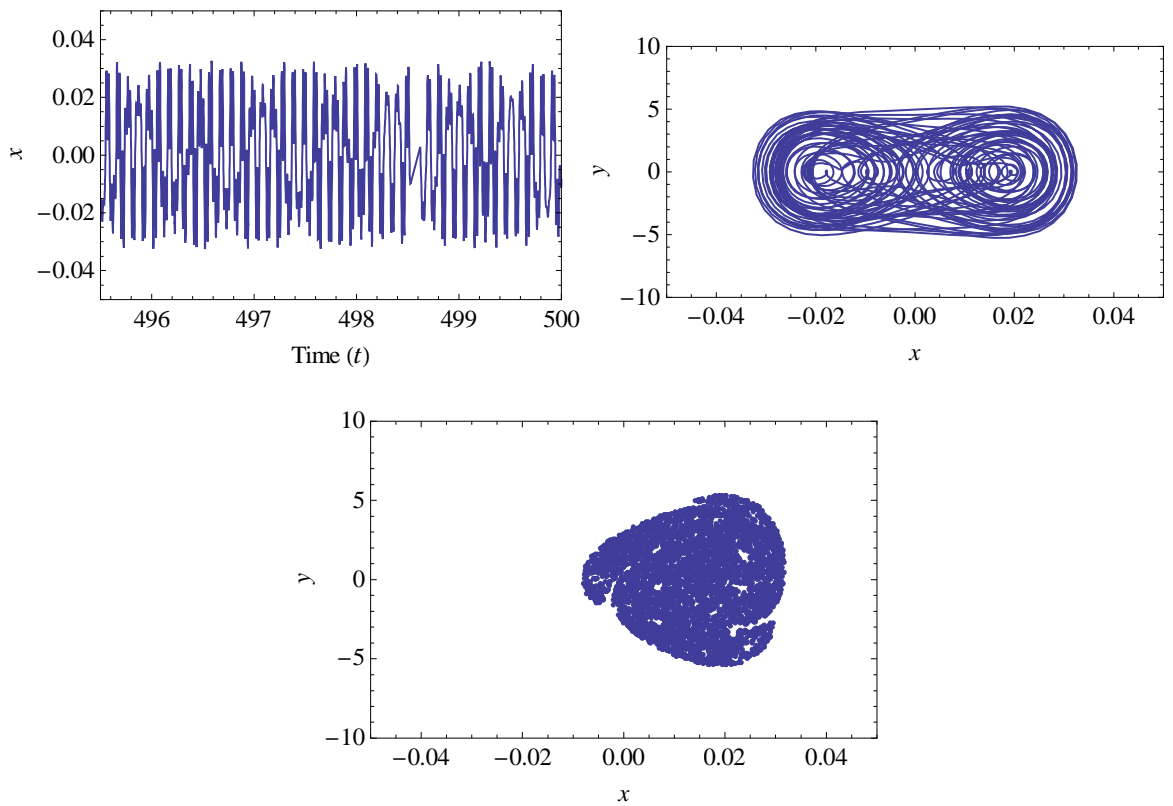
(a) Time plot, phase plane, and Poincaré map for normalised excitation acceleration of 665.00 (Period-1 motion)



(b) Time plot, phase plane, and Poincaré map for normalised excitation acceleration of 675.00 (Period-2 motion)

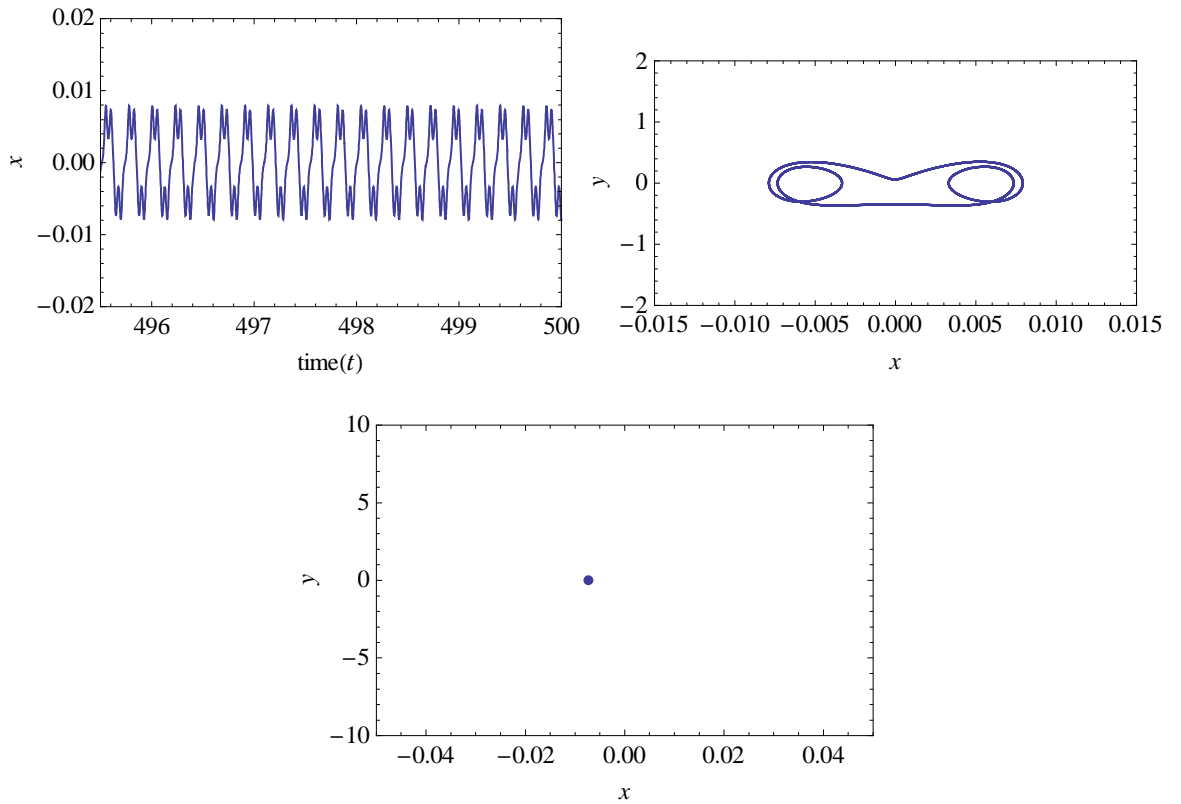


(c) Time plot, phase plane, and Poincaré map for normalised excitation acceleration of 687.00 (Period-4 motion)

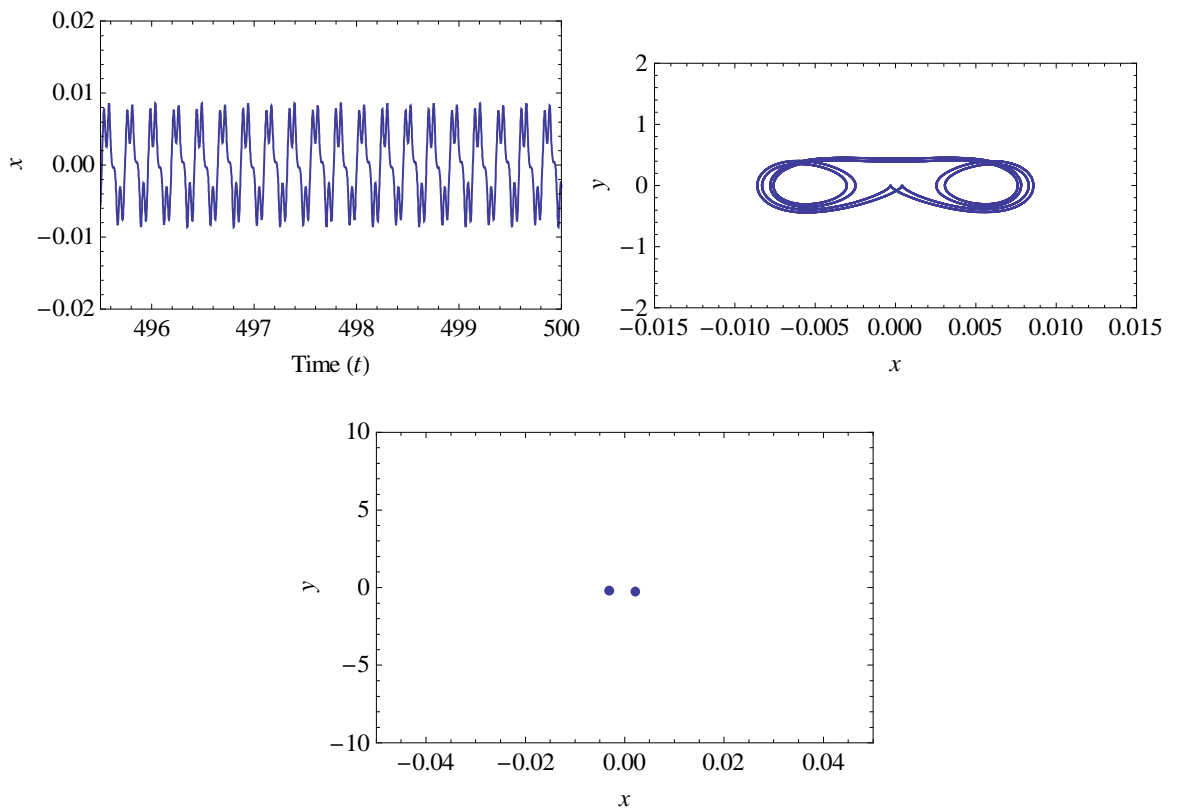


(d) Time plot, phase plane, and Poincaré map for normalised excitation acceleration of 689.00 (Chaotic motion)

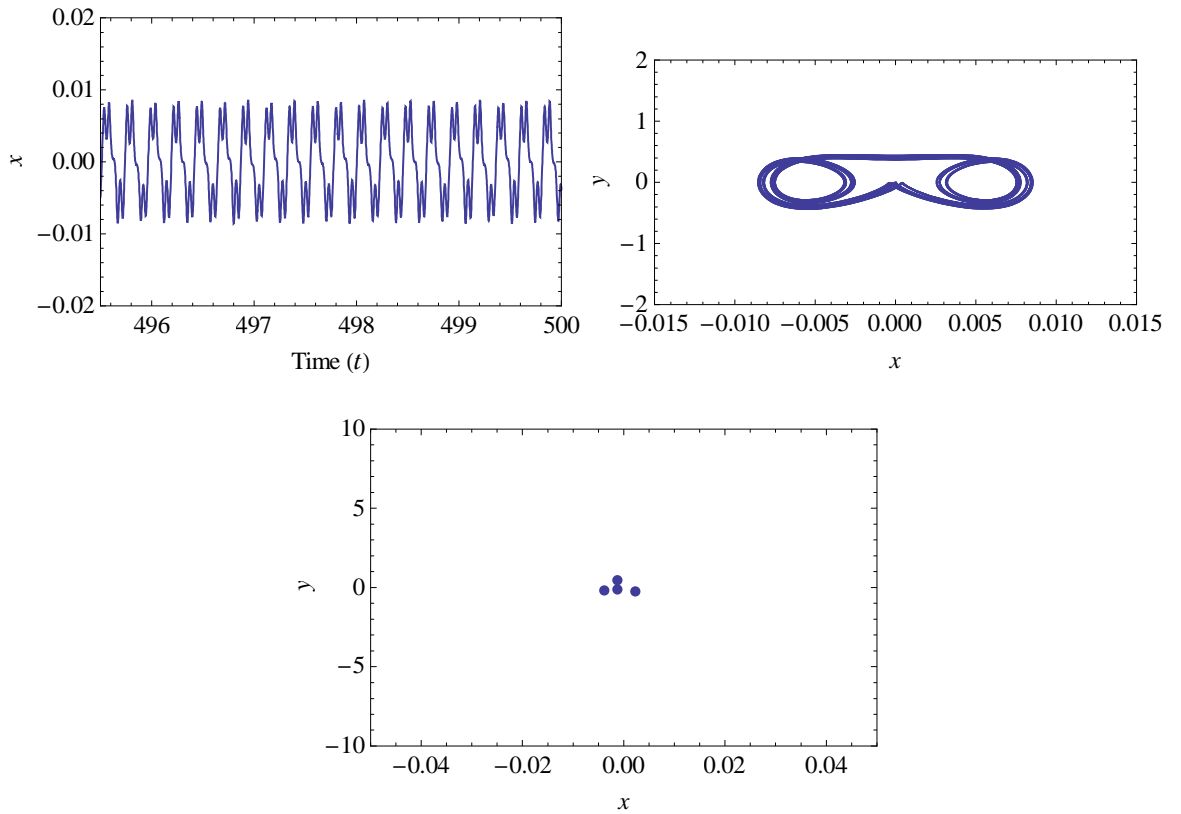
Figure 5-20 : Dynamical systems analysis for a cracked plate with half-crack length of 0.0075 m and $\beta = 60^\circ$ with CCSS boundary condition



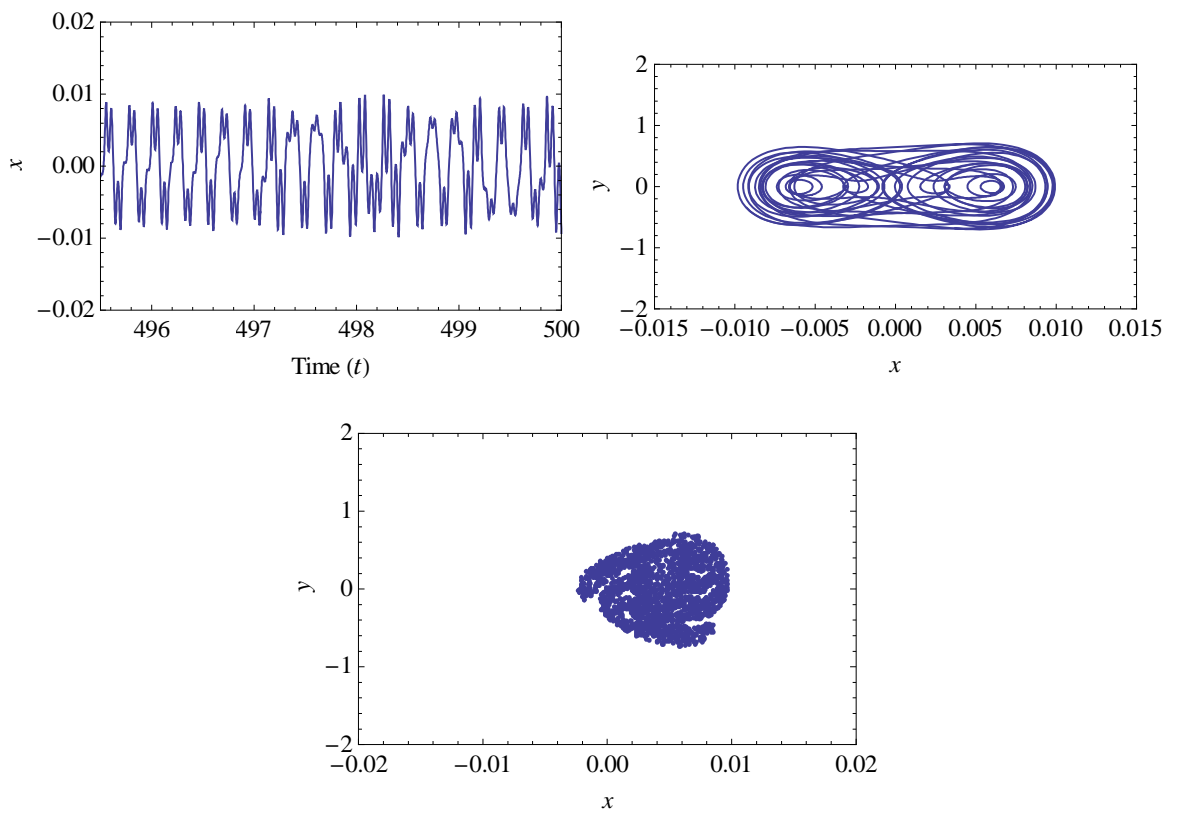
(a) Time plot, phase plane, and Poincaré map for normalised excitation acceleration of 40.50 (Period-1 motion)



(b) Time plot, phase plane, and Poincaré map for normalised excitation acceleration of 41.70 (Period-2 motion)

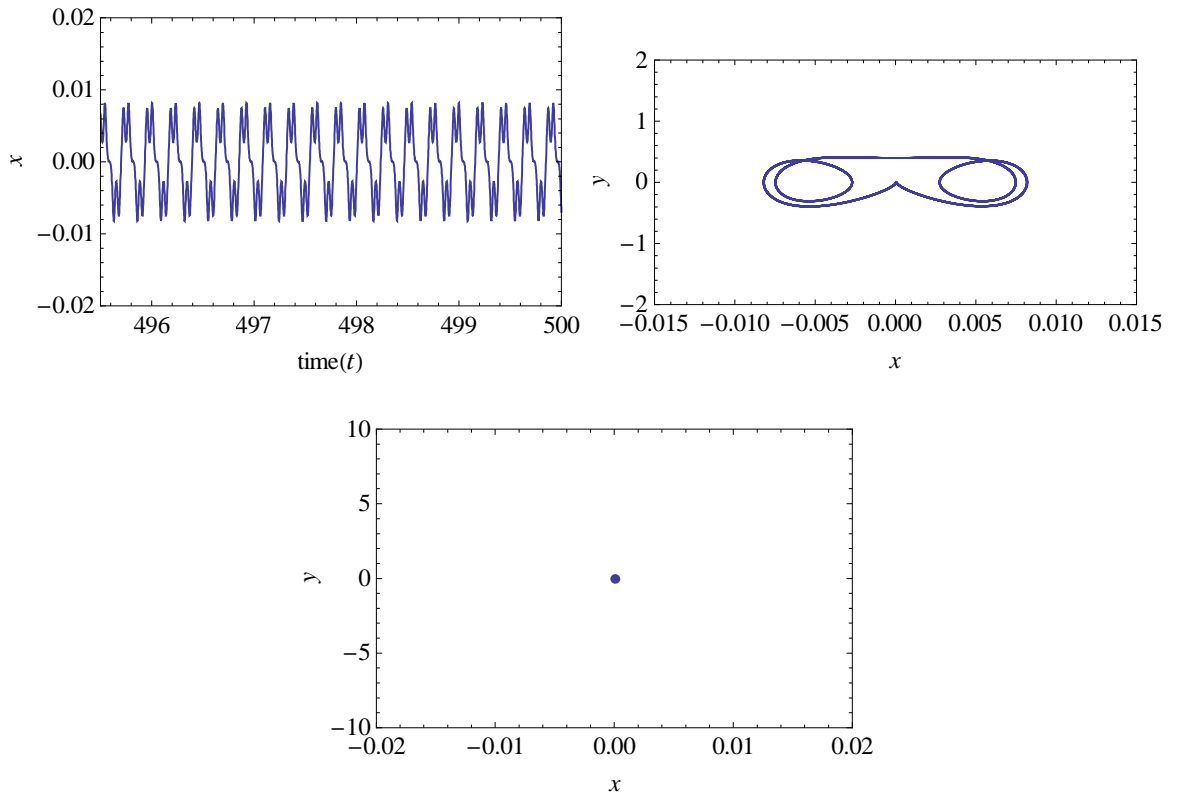


(c) Time plot, phase plane, and Poincaré map for normalised excitation acceleration of 42.10 (Period-4 motion)

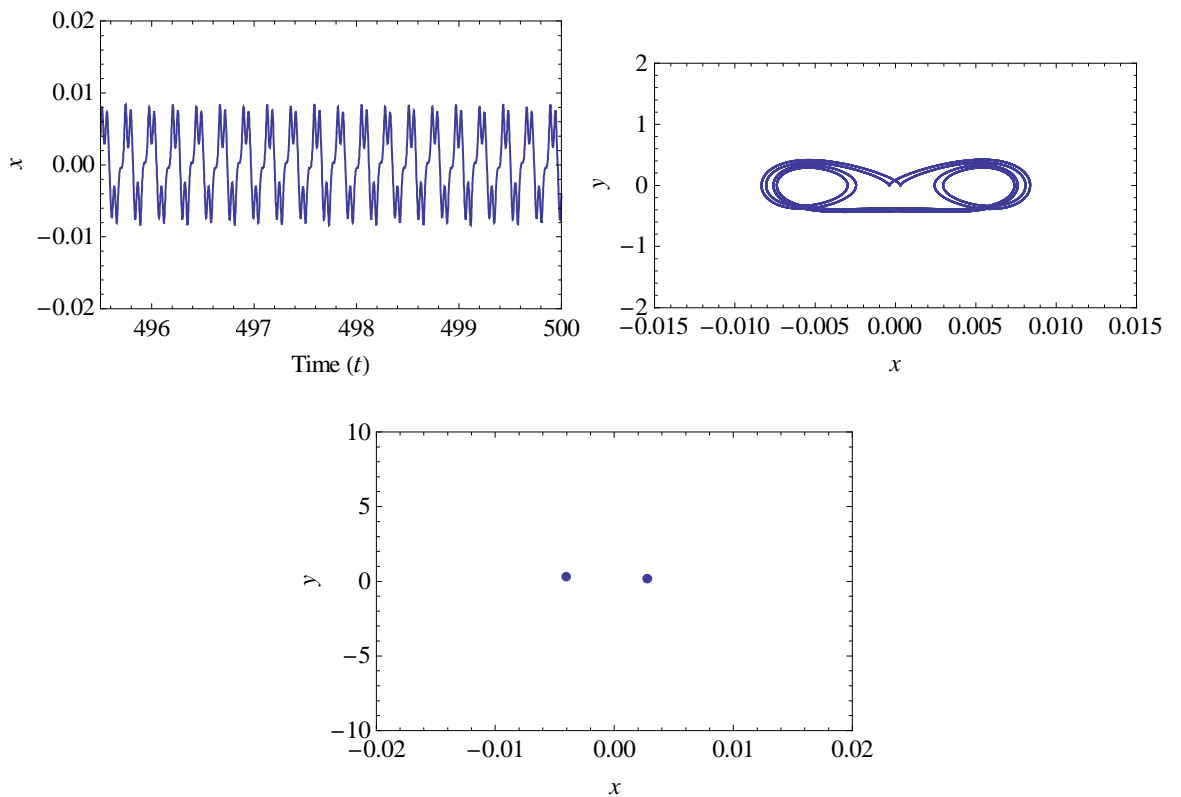


(d) Time plot, phase plane, and Poincaré map for normalised excitation acceleration of 42.30 (Chaotic motion)

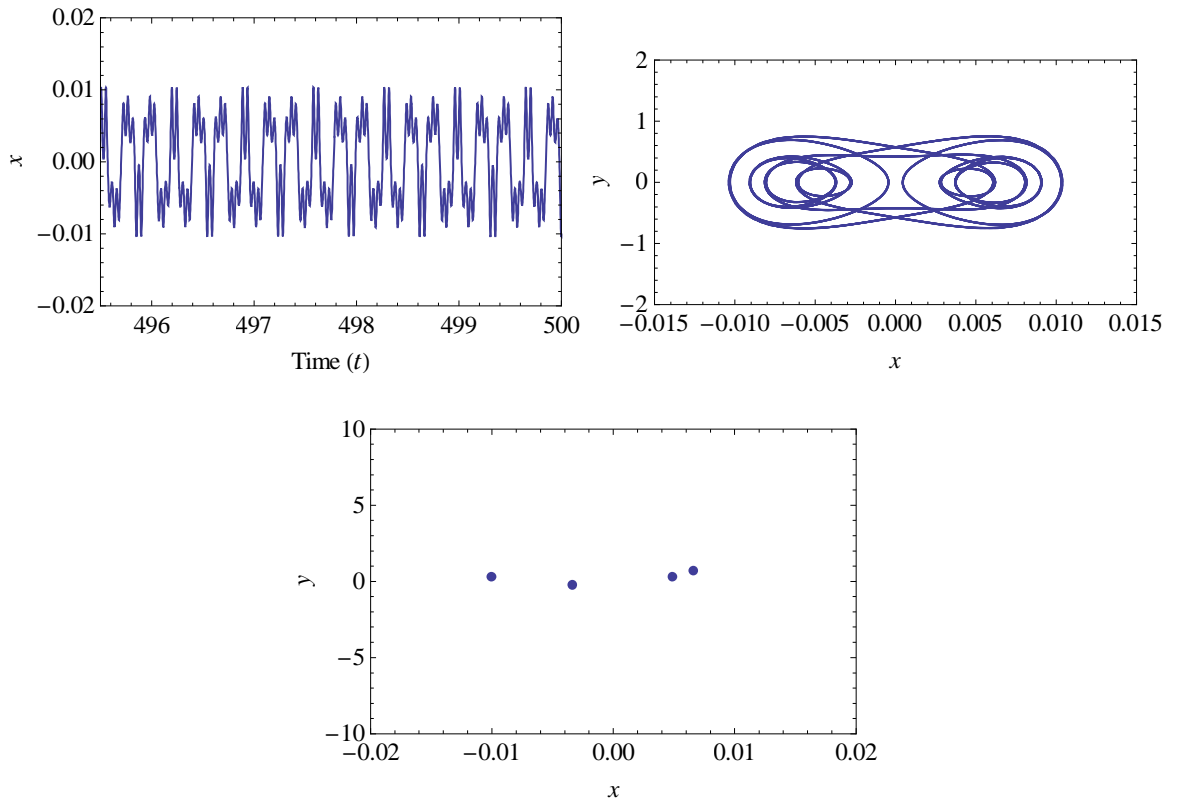
Figure 5-21 : Dynamical systems analysis for an intact plate with CFFF boundary condition



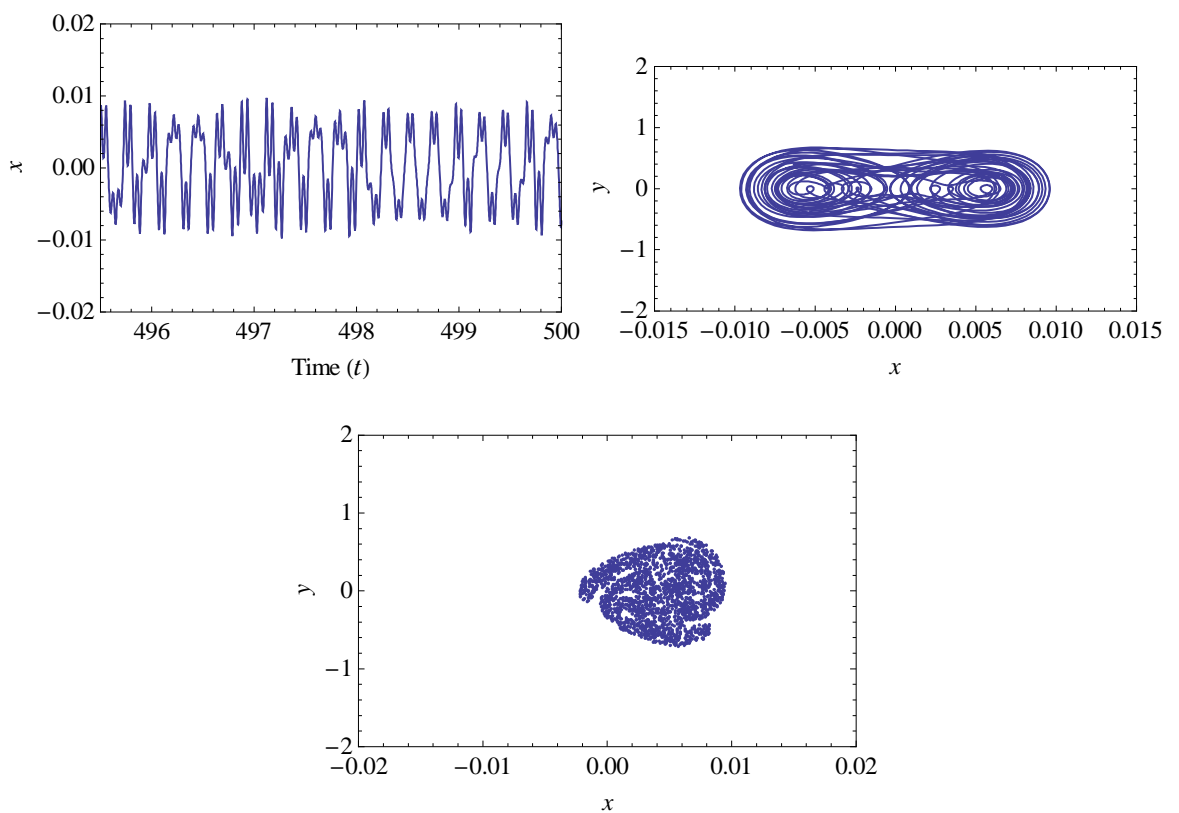
(a) Time plot, phase plane, and Poincaré map for normalised excitation acceleration of 38.50 (Period-1 motion)



(b) Time plot, phase plane, and Poincaré map for normalised excitation acceleration of 39.20 (Period-2 motion)

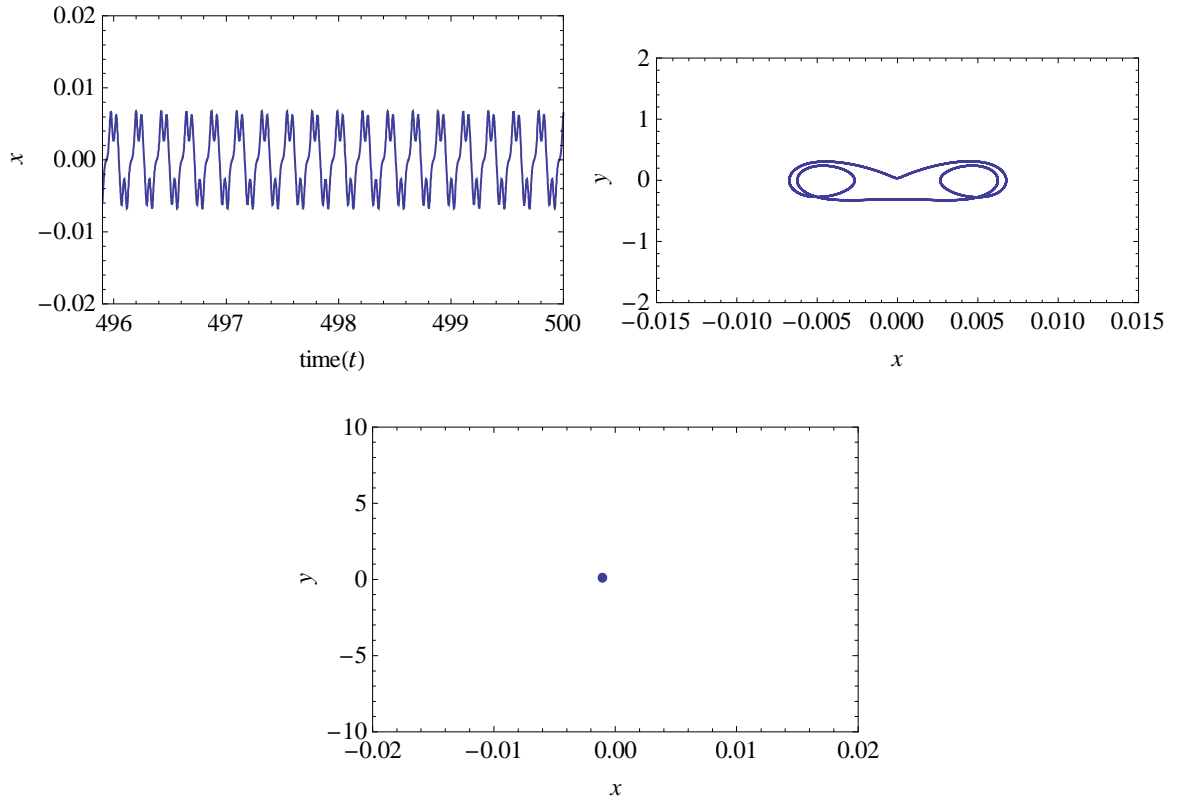


(c) Time plot, phase plane, and Poincaré map for normalised excitation acceleration of 39.55 (Period-4 motion)

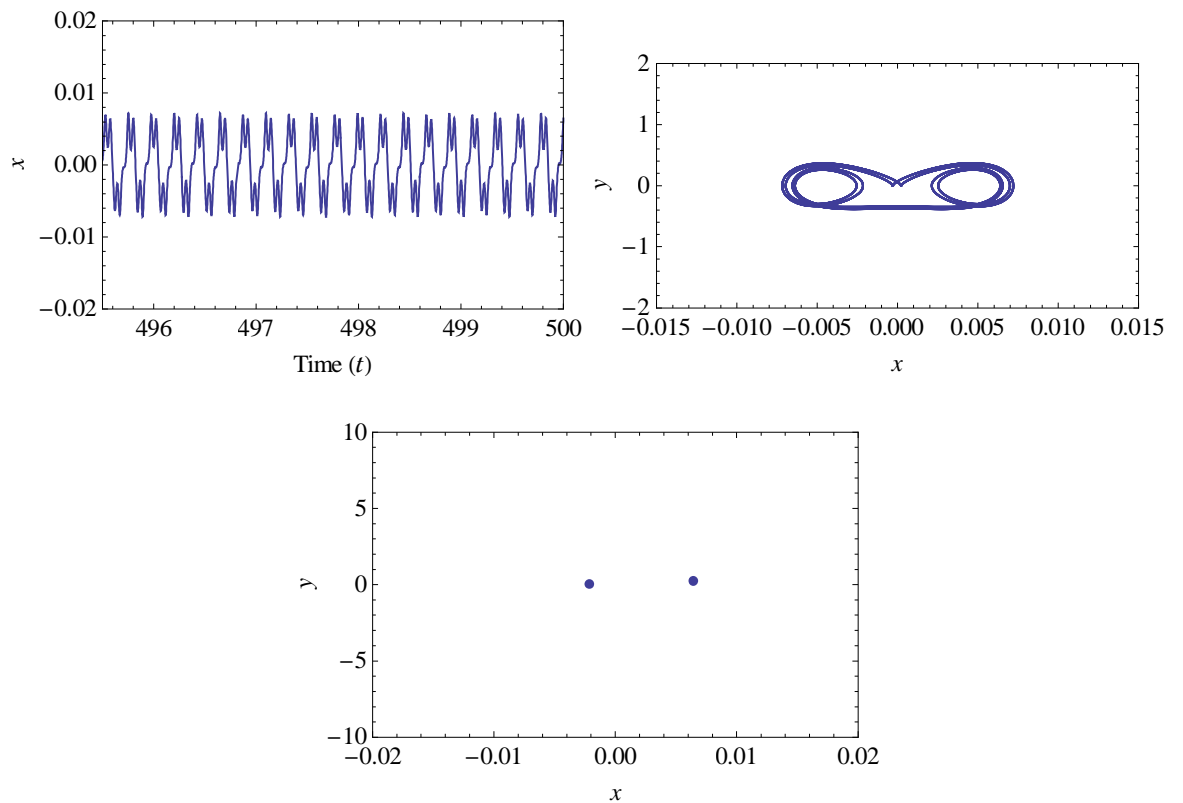


(d) Time plot, phase plane, and Poincaré map for normalised excitation acceleration of 39.80 (Chaotic motion)

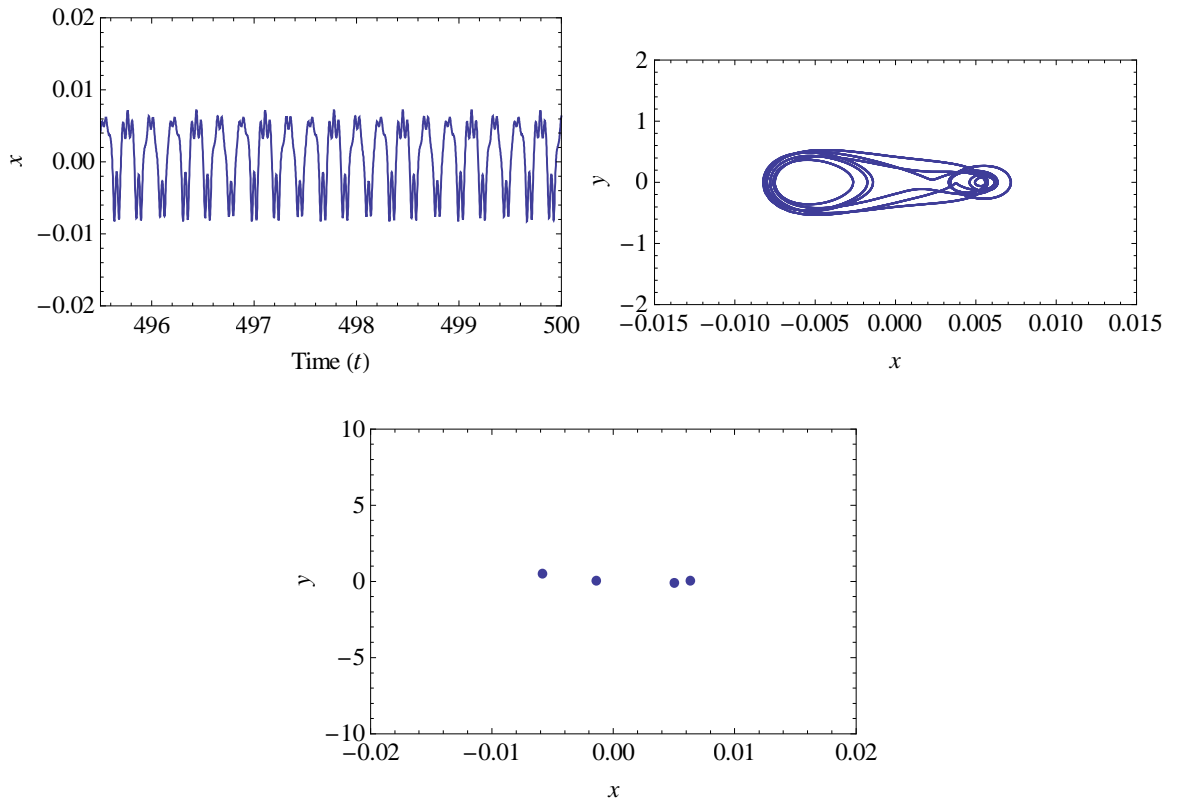
Figure 5-22 : Dynamical systems analysis for a cracked plate with half-crack length of 0.003 m and $\beta = 0^\circ$ with CCFF boundary condition



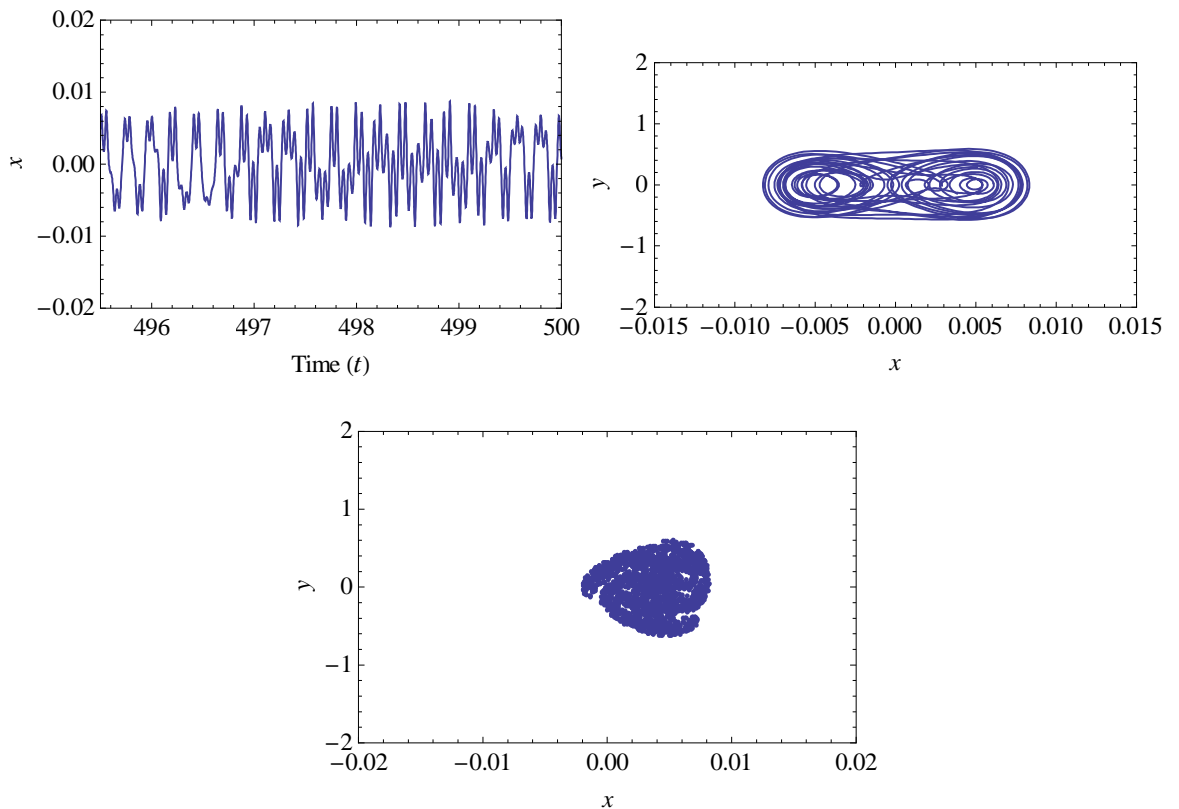
(a) Time plot, phase plane, and Poincaré map for normalised excitation acceleration of 34.50 (Period-1 motion)



(b) Time plot, phase plane, and Poincaré map for normalised excitation acceleration of 35.80 (Period-2 motion)

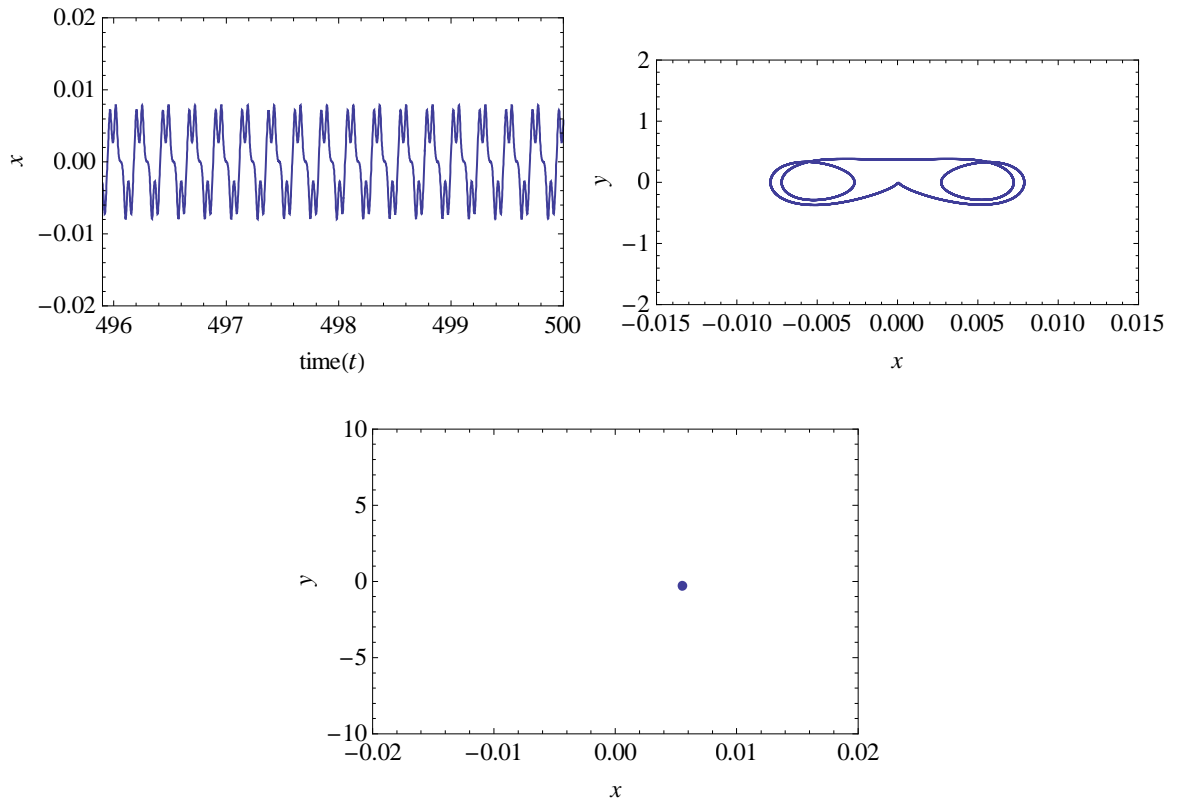


(c) Time plot, phase plane, and Poincaré map for normalised excitation acceleration of 36.15 (Period-4 motion)

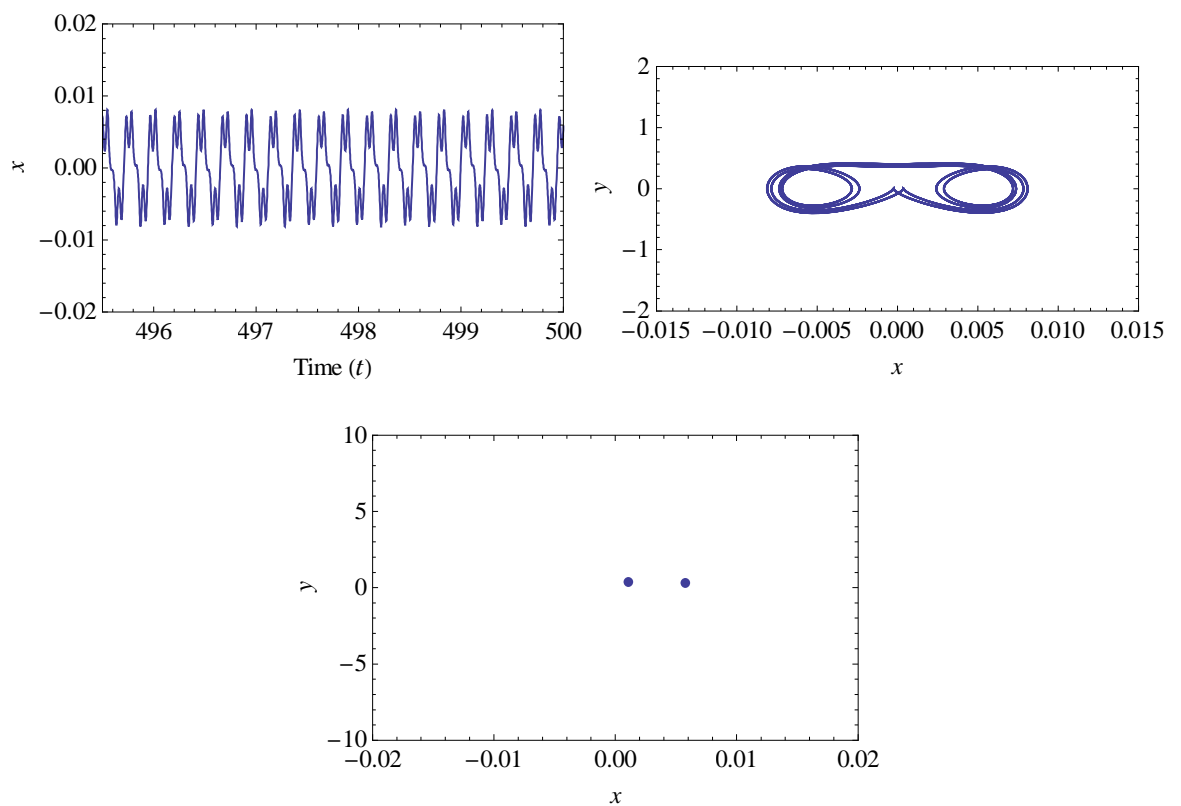


(d) Time plot, phase plane, and Poincaré map for normalised excitation acceleration of 36.50 (Chaotic motion)

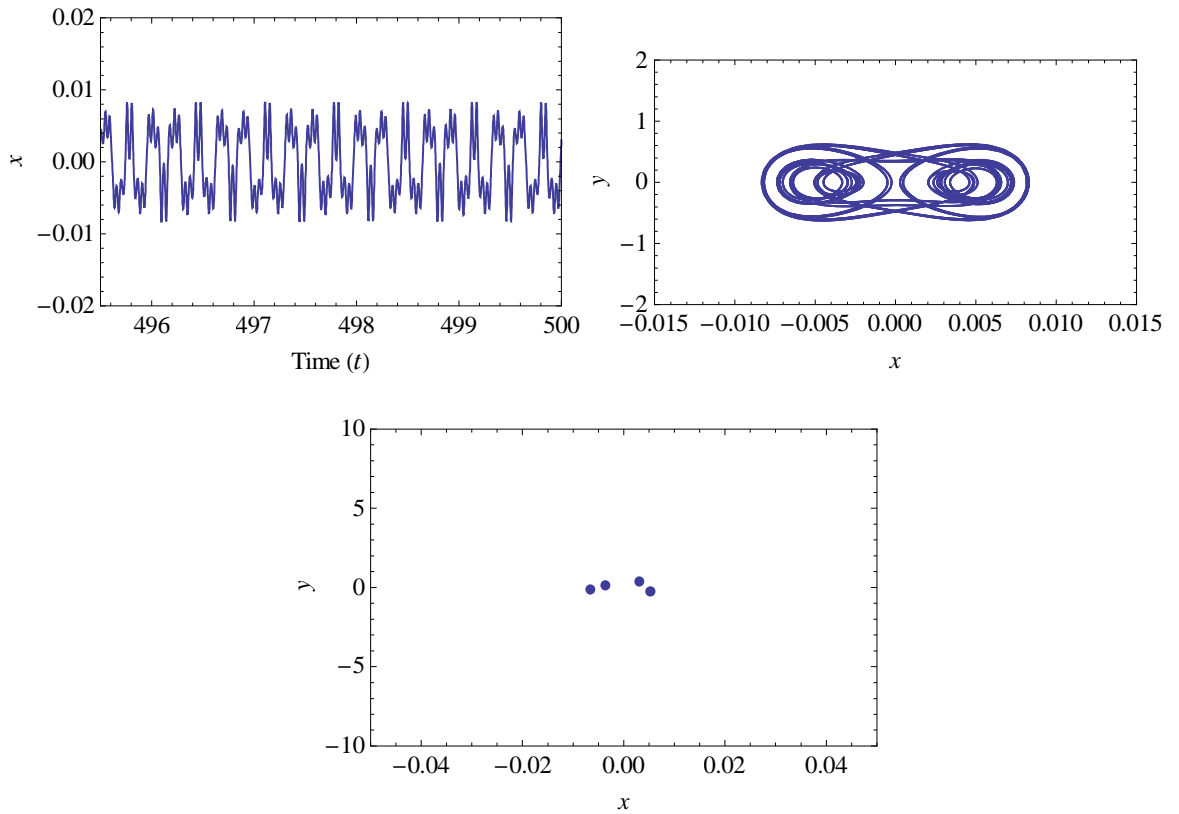
Figure 5-23 : Dynamical systems analysis for a cracked plate with half-crack length of 0.003 m and $\beta = 60^\circ$ with CCFF boundary condition



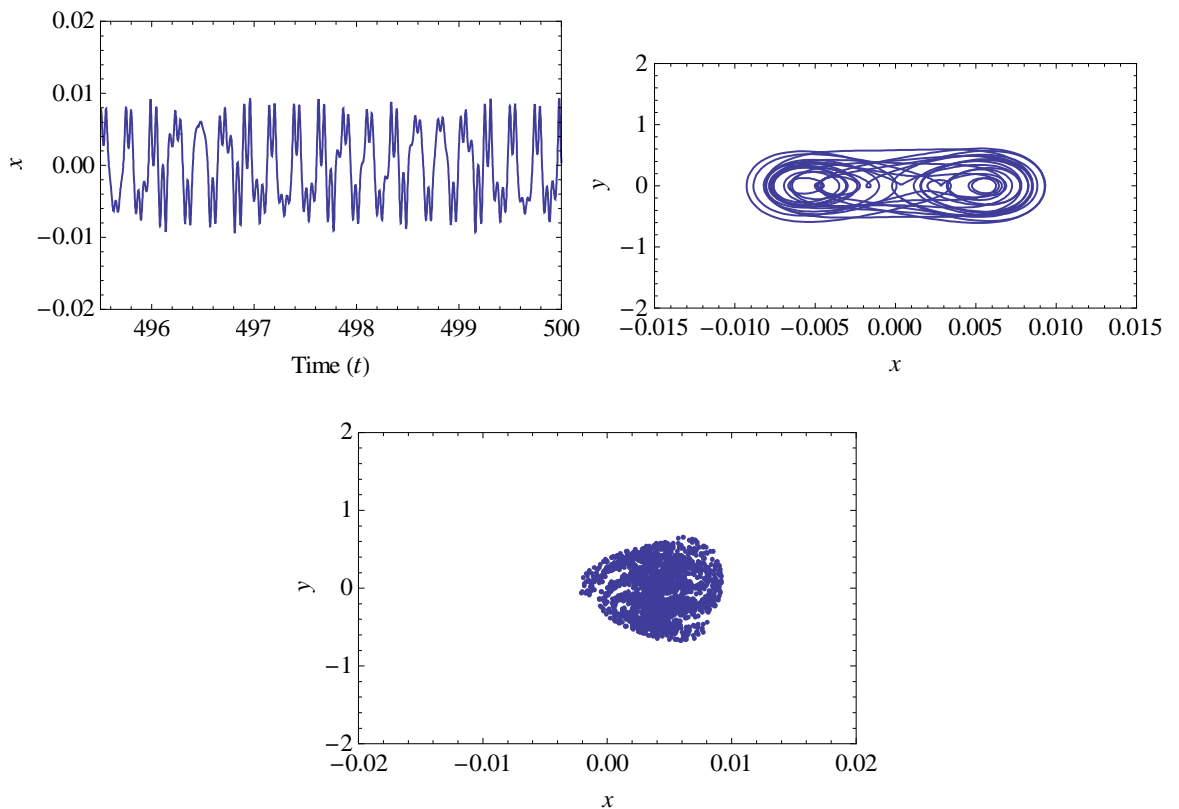
(a) Time plot, phase plane, and Poincaré map for normalised excitation acceleration of 36.15 (Period-1 motion)



(b) Time plot, phase plane, and Poincaré map for normalised excitation acceleration of 36.60 (Period-2 motion)

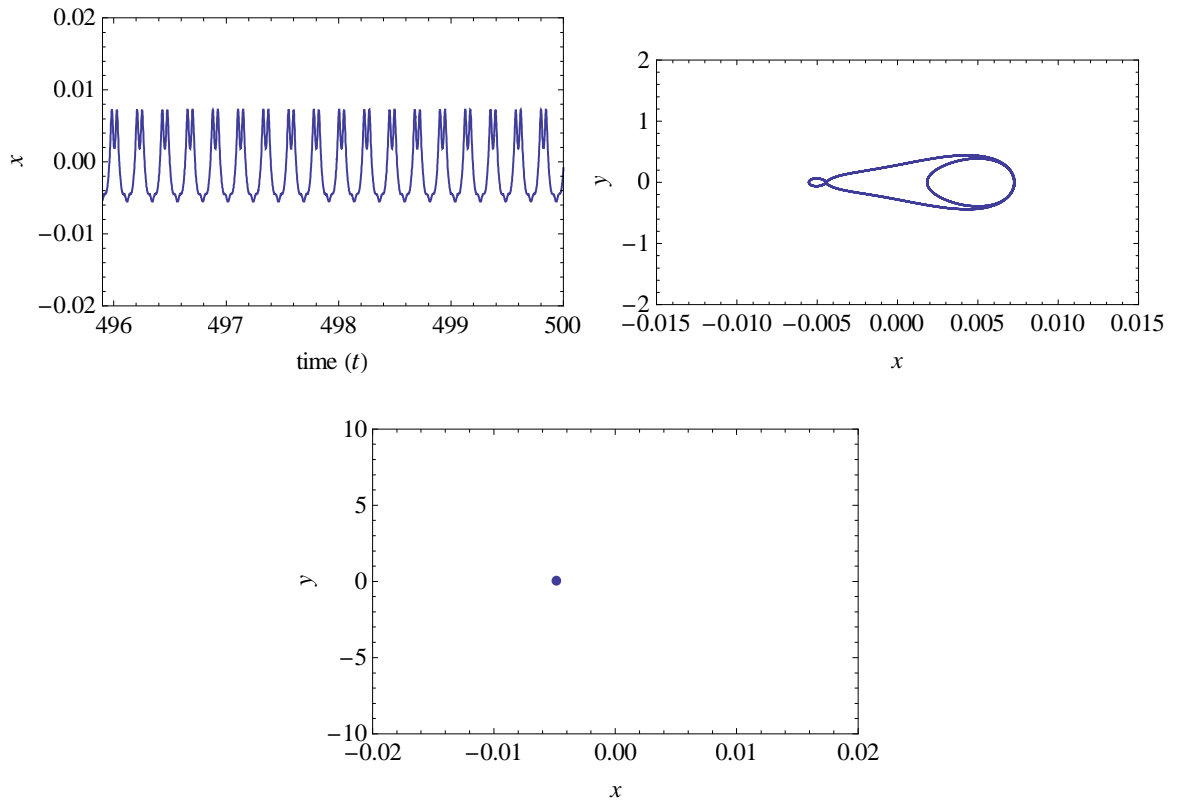


(c) Time plot, phase plane, and Poincaré map for normalised excitation acceleration of 36.93 (Period-4 motion)

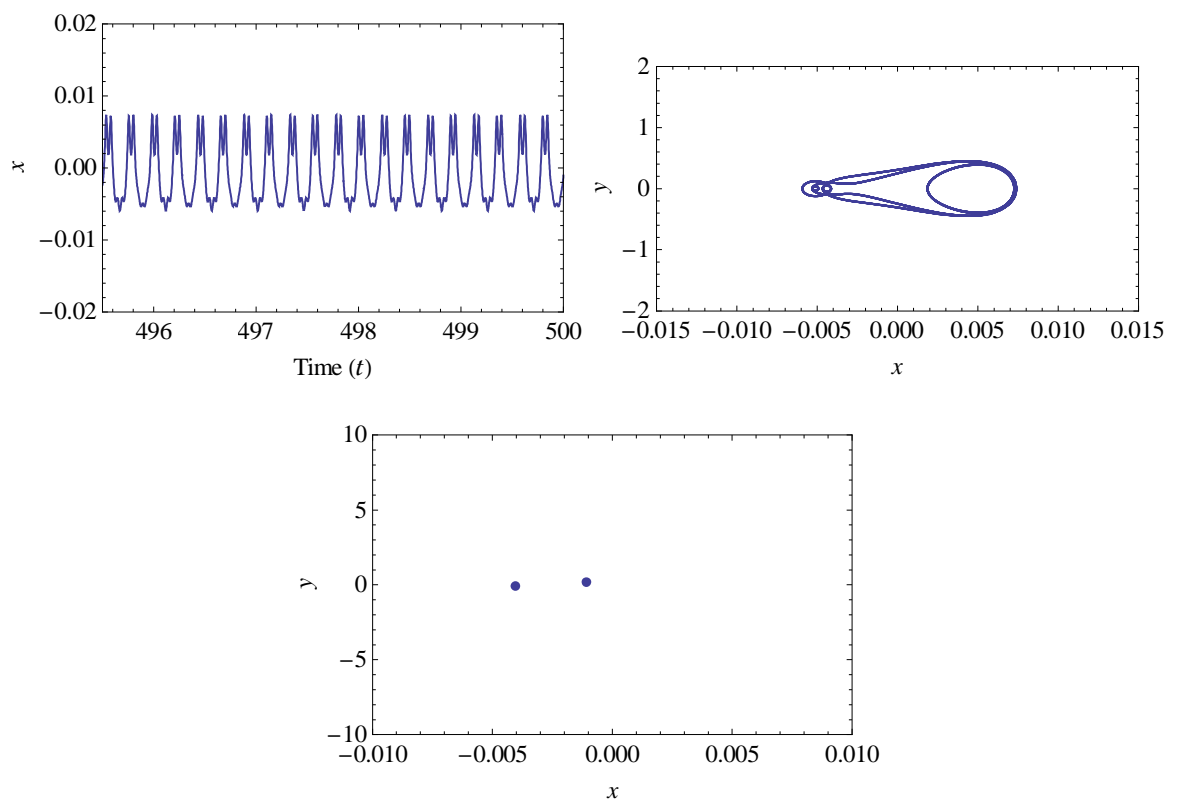


(d) Time plot, phase plane, and Poincaré map for normalised excitation acceleration of 37.71 (Chaotic motion)

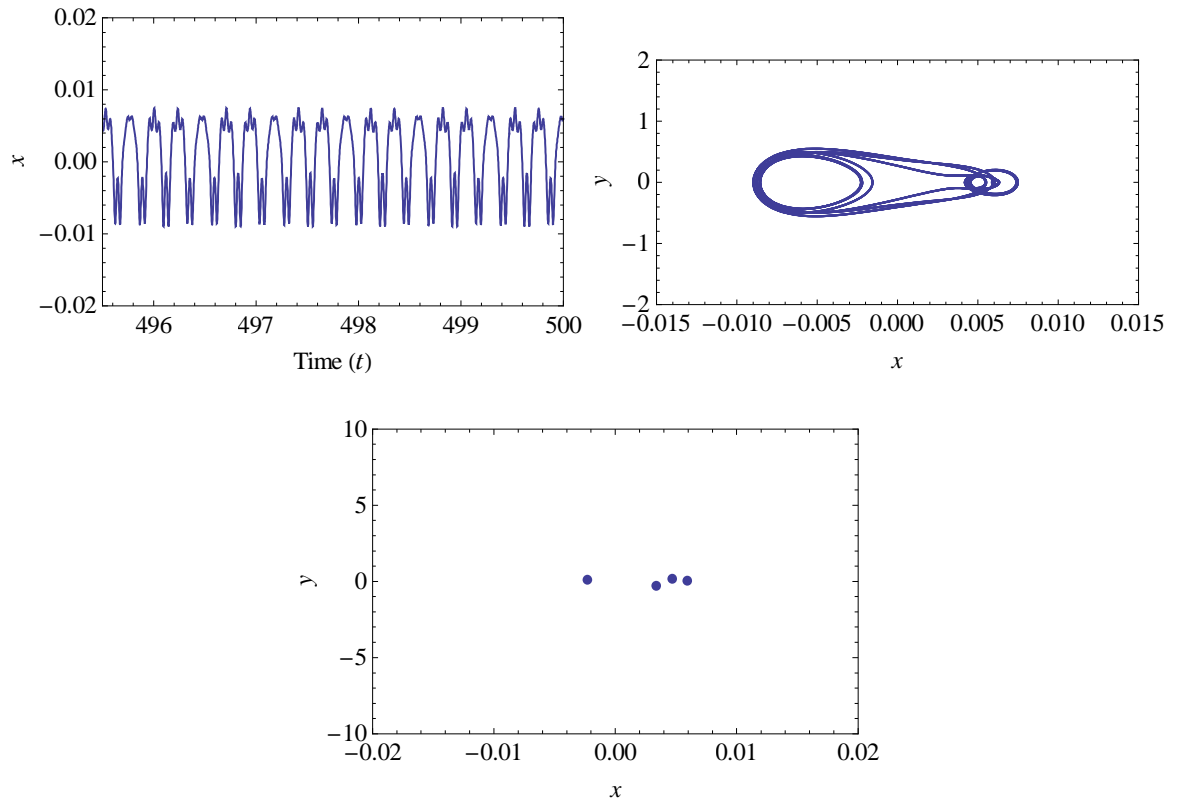
Figure 5-24 : Dynamical systems analysis for a cracked plate with half-crack length of 0.0075 m and $\beta = 0^\circ$ with CFFF boundary condition



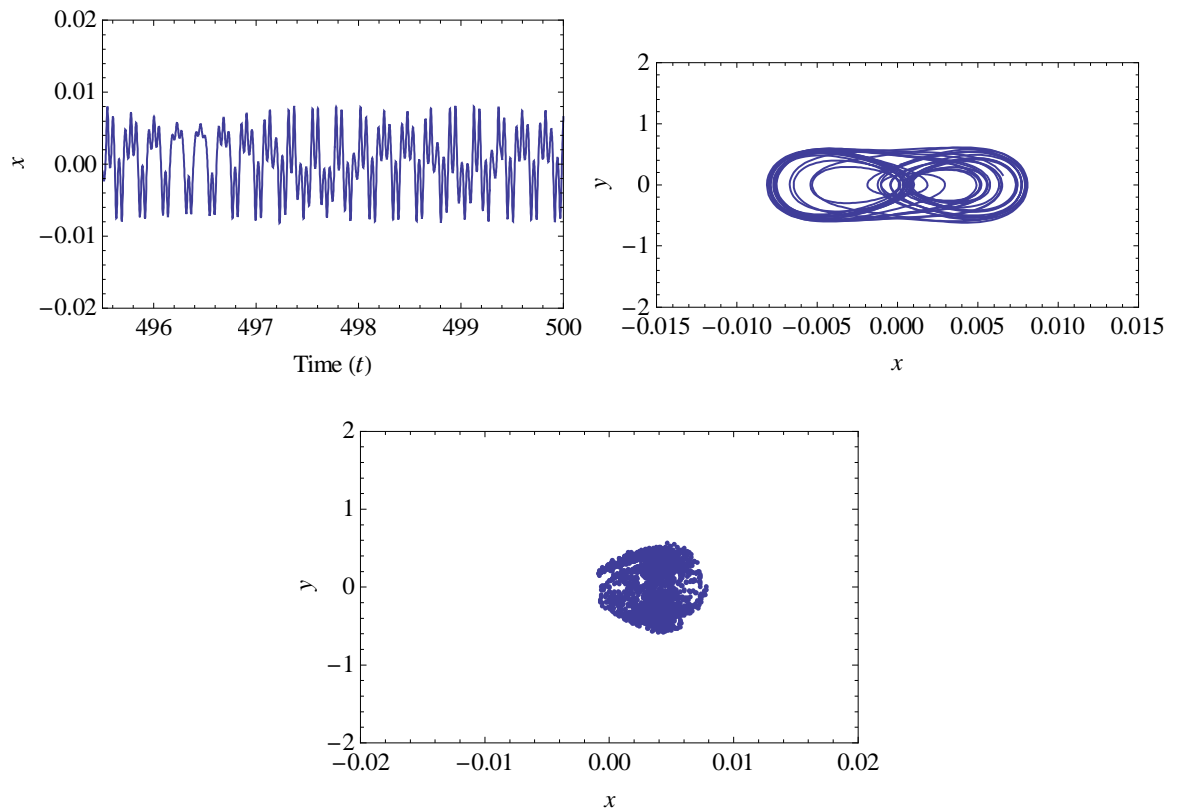
(a) Time plot, phase plane, and Poincaré map for normalised excitation acceleration of 34.50 (Period-1 motion)



(b) Time plot, phase plane, and Poincaré map for normalised excitation acceleration of 35.80 (Period-2 motion)



(c) Time plot, phase plane, and Poincaré map for normalised excitation acceleration of 36.15 (Period-4 motion)



(d) Time plot, phase plane, and Poincaré map for normalised excitation acceleration of 36.50 (Chaotic motion)

Figure 5-25 : Dynamical systems analysis for a cracked plate with half-crack length of 0.0075 m and $\beta = 60^\circ$ with CCFF boundary condition

5.8 Chapter Conclusions

A dynamical analysis of intact and cracked plate models with different crack orientation angles has been presented in this chapter. The linear, nonlinear (period doubling behaviour), and chaotic responses of these systems can be obtained by changing the normalised excitation accelerations. The system is excited at its resonant frequency. Periodic doubling bifurcations can be clearly observed in all the Figures. There are five types of system motion existing over the range of normalised excitation acceleration, namely stable single period motion, stable period-2 motion, stable period-4 motion, stable multiperiod motion, and finally chaotic motion. Besides the types of boundary conditions, the crack length and the crack orientation angle are also found have a significant effect on the system's motion i.e. on the route to chaotic motion. As the crack length is increased, less excitation acceleration is required for the periodic response to become chaotic. This is due to the decrease in the value of the cubic nonlinear coefficient and excitation frequency. However by increasing the orientation angle of the crack, the systems with the SSSS and CCSS boundary conditions are less likely to bifurcate, while for the system with the CCFF boundary condition a similar phenomenon occurs when the angle is more than 40° . In addition, the phase plane plots and Poincaré maps for the selected discrete normalised excitation acceleration values evidently display periodic or chaotic motions corresponding to their bifurcation diagrams.

Chapter 6

Experimental Validation

6.1 Introduction

Chapter 6 presents an experimental study of the dynamics of the cracked plate system, where the crack is located with variable orientation. Experimental measurements of fundamental natural frequency values and vibrational amplitude responses at the resonance frequencies are carried out, and then compared with the theoretical results in order to verify the theoretical model as far as possible. Details of the experimental set up, including the construction of the test rig and the equipment used, are all described here.

6.2 Plate Specimens

Seven aluminium alloy 5083 plate specimens with equal dimensions of 150 mm x 300 mm x 3 mm are used in this investigation. These plate specimens are denoted by A to G inclusive. Plate A represents an intact plate, plate B is a plate with a horizontal centre crack parallel to the x direction of the plate, and plates C to G represent those specimens with various surface crack orientation angles β , with respect to the x direction, specifically at 20° , 40° , 60° , 80° , and 90° . The test cracks machined into the specimens have equal dimensions, i.e. 15 mm x 0.3 mm x 1.8 mm. The cracks are machined in each specimen, as shown in Figure 5-1, by using a three axis milling machine.

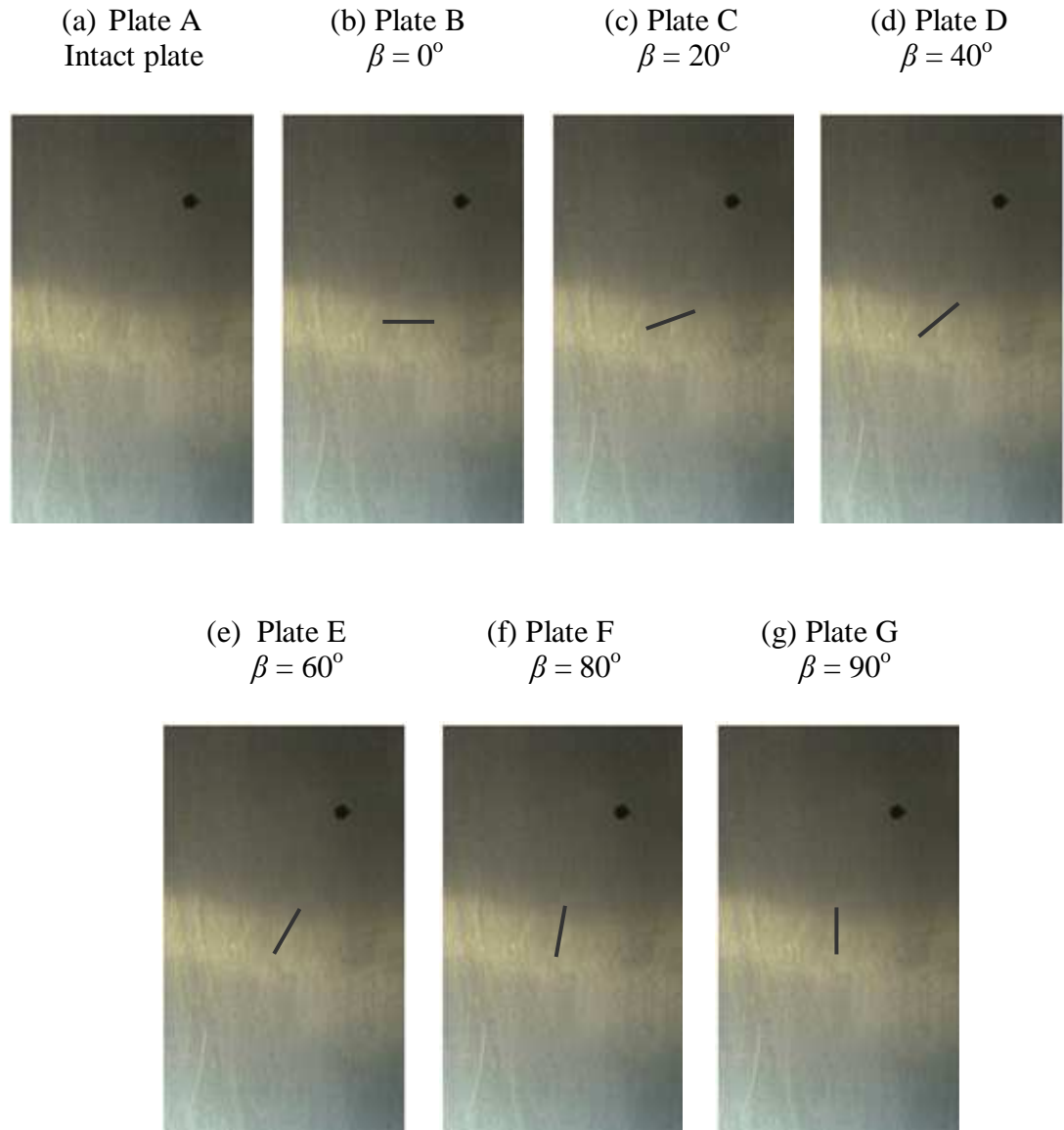


Figure 6-1 : Classification of experimental crack orientations, dark dot denoting excitation location point

6.3 Experimental Setup and Procedure

A schematic layout of the experimental system is given in Figure 6-2. In this Figure, the electro-dynamic exciter is driven by a function generator that is connected through a power amplifier. A vibrometer controller connected to a spectrum analyser enables the identification of plate responses through the signal from the laser vibrometer. Figure 6-3 shows the arrangement of the equipment used for testing and the list of these instruments is included in Appendix D. In this work, the clamped-clamped free-free (CCFF) boundary condition is arbitrarily chosen. In order to obtain this boundary condition a heavy steel rig was designed and fabricated to function as an extremely rigid support for the two adjacent sides of the plate. These two sides were clamped to the support by a sturdy frame. The

whole rig was fitted to a suitably massive base in order to isolate the system from any unwanted ambient vibration. A harmonic excitation was applied to the plate by an electro-dynamic exciter, and this excitation was monitored by means of a calibrated force transducer fitted serially in the shaker rod. The excitation point was arbitrarily chosen at the location of (112.5, 225) mm. This was measured from the clamped end of the plate in the x and y directions, respectively. Generally an excitation signal was taken from a function generator and amplified in order to drive the shaker. A 1D laser vibrometer was used to get the response and to measure the displacement of the plate, and a spectrum analyser was used to monitor this response. In this experiment a mirror was fitted to obtain the response of the plate at any required point of interest on the surface of the plate.

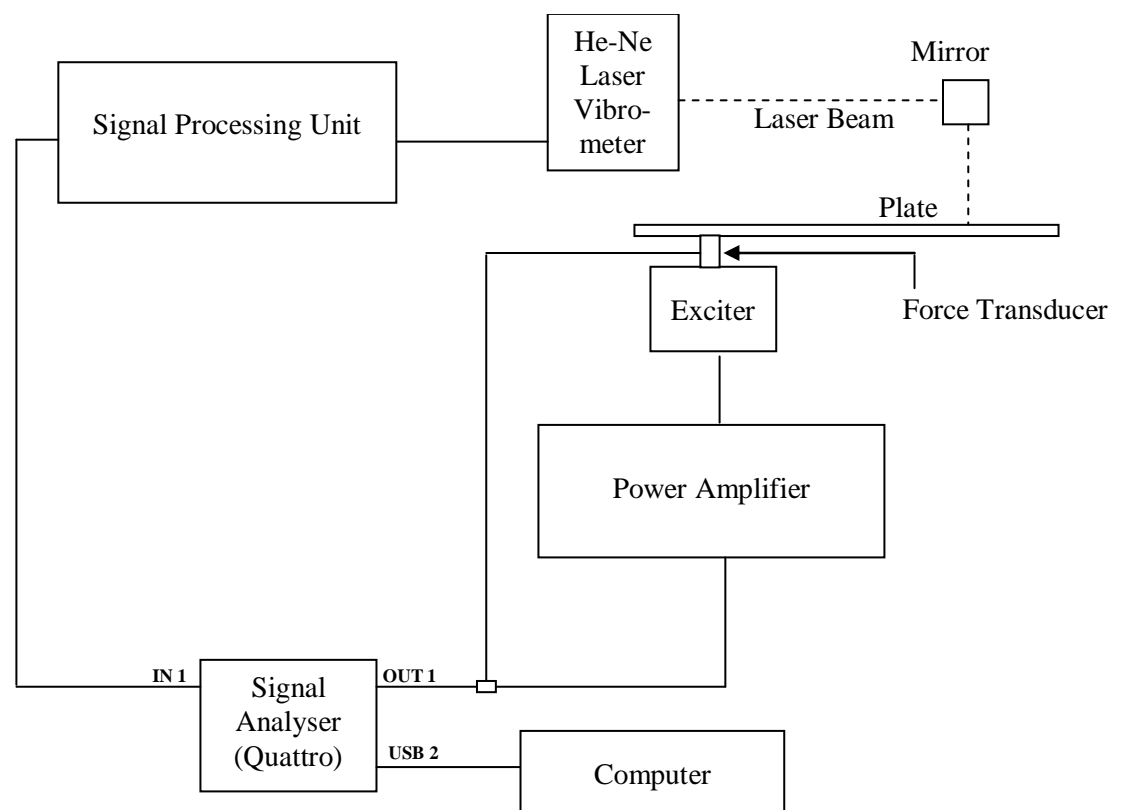


Figure 6-2 : Layout of the experimental setup

Firstly, the test plate was excited with a random excitation signal by the electro-dynamic exciter in order to obtain the fundamental natural frequency of each plate. A true random force signal was generated within the measurement range of 0-1000 Hz with an input voltage level of 0.875V RMS. The excitation level of $V_{\text{rms}} = 0.875\text{V}$ was equivalent to an excitation force of approximately 10N. This was obtained from the sensitivity of the force transducer of 123.78 mV/N. Subsequently a sine test was performed to obtain the maximum vibrational amplitude in the first mode of vibration of the plate. In this test the

resonant frequency was applied, and then the responses at several points on the surface of the tested plate were observed and the maximum amplitude value noted.

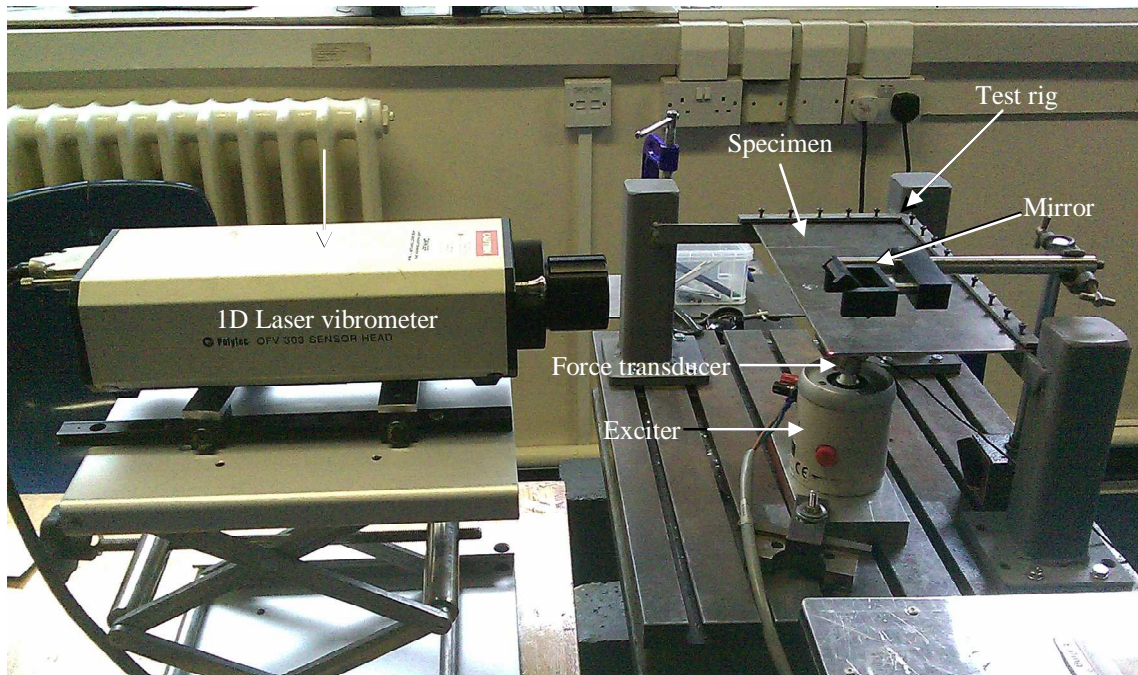


Figure 6-3 : The experimental test rig

6.4 Experimental results

Table 6-1 shows the results obtained from the tests. It can clearly be seen that the frequency decreases with the inclusion of the crack in the plate, for all three modes of vibration. The frequencies of the intact plate obtained were 107.60, 273.40, and 532.80 Hz for the first, second and third mode of vibration, respectively, while they reduce to 99.61, 262.10, and 525.00 Hz for the addition of a crack of length 15 mm. In terms of crack orientation, the same phenomenon was encountered as in the previous chapter, whereby the frequency increases up to an angle of 60° then decreases when the orientation angle exceeds 60° . Figure 6-3 shows the frequency response function curves for the intact plate and the cracked plate specimens, with crack orientation angles of 0° , 20° , 40° , 60° , 80° , and 90° . In addition, the maximum vibrational amplitudes for the first mode of vibration were obtained at the tip of the free end of the plate specimens. However, the results show that the amplitude of the vibration behaves conversely to the natural frequency, and decreases up to 80° , then increases when the crack orientation angle exceeds 80° .

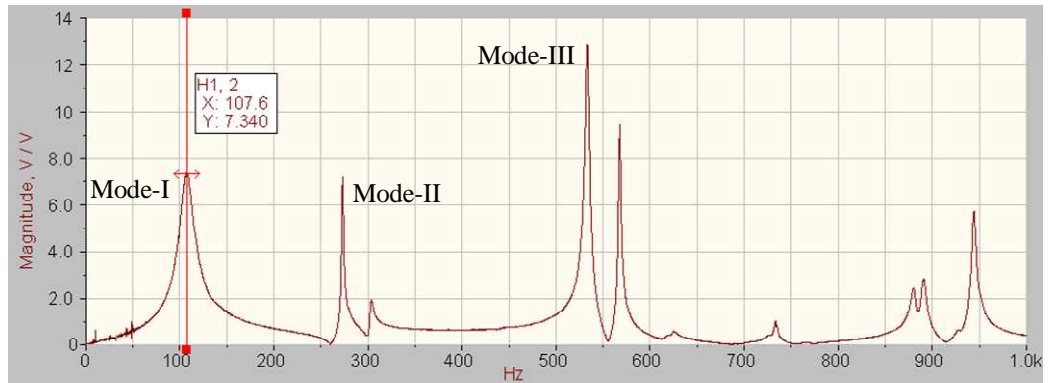
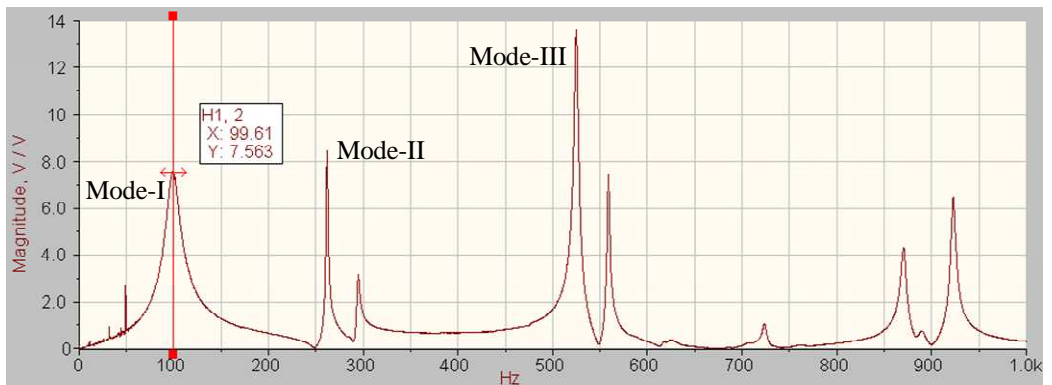
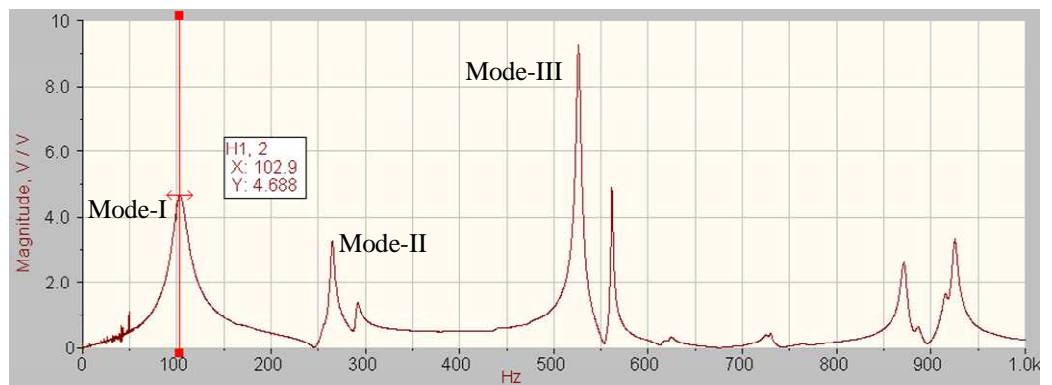
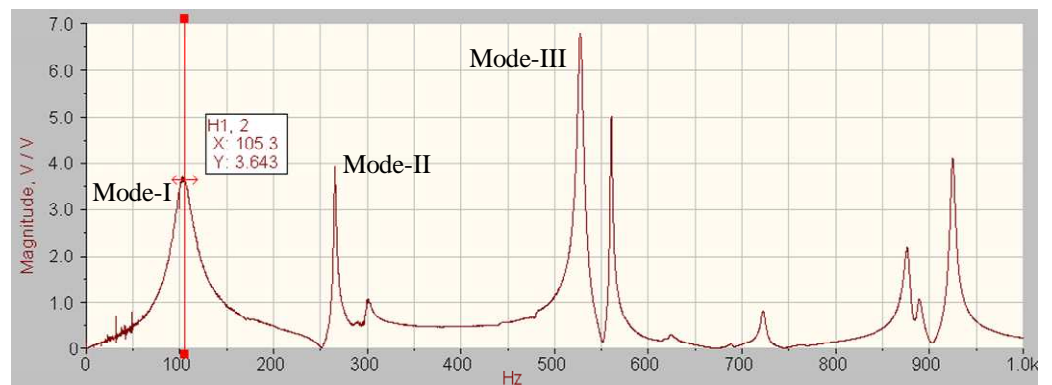
Aluminium Plates	Crack Orientation Angle β (deg)	Frequency (Hz)			Maximum vibrational amplitude (mm)
		First vibration mode	Second vibration mode	Third vibration mode	First vibration mode only
Intact Plate	-	107.60	273.40	532.80	7.056
Cracked Plate	0°	99.61	262.10	525.00	7.498
	20°	102.90	265.60	526.20	7.278
	40°	105.30	266.60	527.30	7.187
	60°	106.40	268.90	529.50	7.176
	80°	104.10	267.80	530.70	7.274
	90°	102.00	265.60	518.20	7.591

Table 6-1 : Experimental results for the first three modes of vibration for intact and cracked aluminium plates with a 7.5 mm half-crack length for a plate aspect ratio of 0.15/0.3

6.5 Chapter Conclusions

Intact and cracked plates (with variably orientated cracks) have been investigated experimentally in this chapter. The insertion of the crack in the plate was found to have a strong influence on the frequency and amplitude responses. The orientation of the crack also has a significant effect on the vibration characteristics of this system. Plate structures undergoing transverse deflection can be categorised as nonlinear systems depending on several factors. One of them is when the deflection is a multiple of the plate thickness but much less than the plate side length (Malatkar, 2003 and Israr, 2008). Therefore, these plate specimens could be exhibiting nonlinear behaviour because the results show that the amplitude response is within this category. Besides that, nonlinear dynamical phenomena for these plate specimens can also be observed when the excitation frequency is increased until a jump phenomenon occurs in the first mode. The comparative study between theoretical and experimental results is discussed in Chapter 7.

(a) Intact Plate

(b) Cracked plate with crack orientation angle, $\beta = 0^\circ$ (c) Cracked plate with crack orientation angle, $\beta = 20^\circ$ (d) Cracked plate with crack orientation angle, $\beta = 40^\circ$ 

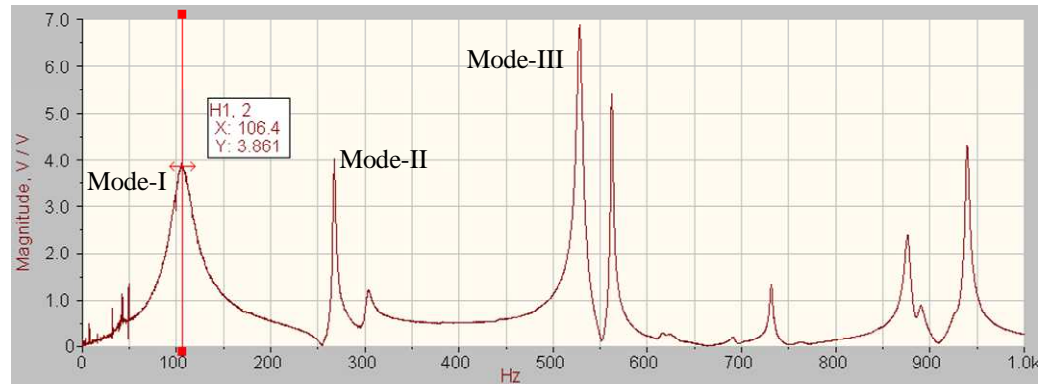
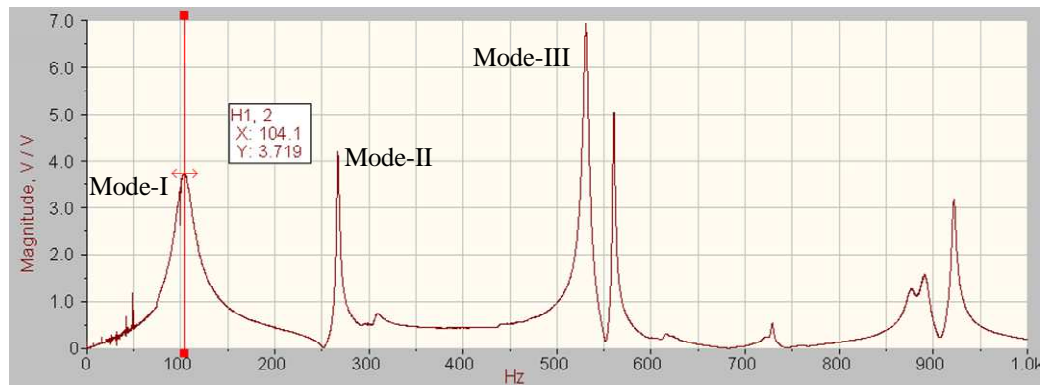
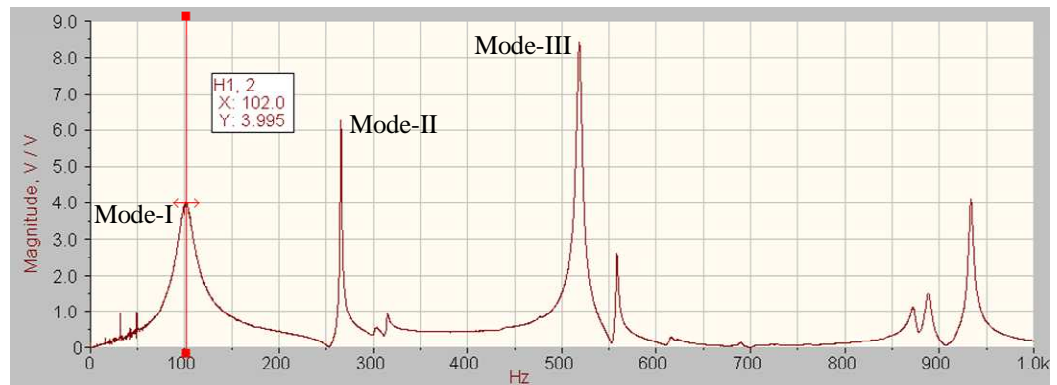
(e) Cracked plate with crack orientation angle, $\beta = 60^\circ$ (f) Cracked plate with crack orientation angle, $\beta = 80^\circ$ (g) Cracked plate with crack orientation angle, $\beta = 90^\circ$ 

Figure 6-4 : Frequency responses for the first three modes of vibration for an aluminium rectangular plate

Chapter 7

Comparative Study and Discussion

7.1 Introduction

The equation of motion of a cracked plate model containing a crack of variable angular orientation was obtained in Chapter 3, and this system has been analysed using theoretical and experimental methods, as discussed in Chapters 3 to 6. For reasons of comparison and validation a finite element model and experiments were undertaken to enable a further modal analysis in order to corroborate the effect of crack length and crack orientation angle on the natural frequency, and also the vibrational amplitude, as predicted by the theory. Thus, the purpose of this chapter is to provide a comparative assessment of these methods, and to extend the discussion, where appropriate, regarding the results obtained from Chapters 3 to 6, including the method of multiple scales, the direct numerical integration method within MathematicaTM, and a numerical study into the system's dynamics, to enable conclusions to be defined for this overall study.

7.2 Comparative Assessment

Comparative studies of the theoretical modelling and finite element approaches, and also the theoretical modelling with experimental measurements are carried out for the arbitrarily chosen boundary condition of CCFF in order to verify the model proposed in this thesis. Intact plate and cracked plates with cracks at orientation angles of 0° , 20° , 40° , 60° , 80° , and 90° , and different half-crack lengths of 3 mm and 7.5 mm are all compared. Tables 7-1 and 7-2 summarise the comparative assessment of the theoretical modelling and the finite element modelling approaches, and the theoretical predictions with the experimental measurements, respectively. The performance of each method is compared in terms of the first mode natural frequency of the cracked plate models and their amplitude responses. In Table 7-1 we can see that the results show good agreement between the finite element-extracted and analytically-calculated results for the frequencies and amplitudes. Both sets of results show a significant change in the natural frequency and response amplitude for the different lengths of the crack and also for the varying orientation angle of the crack. The natural frequencies obtained for both results decrease slightly with an increase in the crack length for every crack inclination angle. In addition, it is apparent that

the finite element predicted frequency and amplitude trends are similar to the analytical results for which the frequency values increase from 0° up to 60° and then decrease when β is more than 60° , while the amplitude responses behave conversely. Very close agreement was obtained between the analytical and finite element results, with the maximum error in the prediction of the frequency value generally at about 7.7 % and the amplitude response at around 7.6 %.

	Crack Orientation Angle	Natural Frequency for first vibration mode (Hz)		Error (%)	Amplitude for first vibration mode (mm)		Error (%)	
		Analy. result	FEA result		Analy. result	FEA result		
Intact Plate	-	122.58	122.94	0.29	7.979	7.372	7.61	
Cracked Plate	3 mm	0°	118.38	122.73	3.67	8.019	7.483	6.68
		20°	121.82	122.77	0.78	7.220	7.379	2.20
		40°	124.57	122.84	1.39	6.993	7.263	3.86
		60°	125.41	123.05	1.88	6.898	7.200	4.38
		80°	123.98	122.82	0.94	7.524	7.727	2.70
		90°	122.58	122.73	0.12	7.979	7.739	3.01
	7.5 mm	0°	113.91	122.69	7.71	8.066	7.564	6.22
		20°	118.18	122.75	3.87	6.951	7.227	3.97
		40°	122.37	122.81	0.36	6.659	6.969	4.66
		60°	124.61	123.04	1.26	6.548	6.796	3.79
		80°	123.95	122.81	0.92	7.336	7.309	0.37
		90°	122.58	122.69	0.09	7.979	7.614	4.57

Analy. = Analytical

Table 7-1 : Comparison of the frequency and amplitude response results for the theoretical and finite element analyses for Mode I only.

A comparison between the results obtained from the proposed cracked plate model and the experimental work was also undertaken and the results are listed in Table 7-2. Similarity can be observed between the trends for the theoretical and experimental results for the CCFB boundary condition, with the maximum error in the prediction of the frequency value showing as around 16.8 % and the amplitude response at about 11.6 %.

	Crack Orientation Angle	Natural Frequency for first vibration mode (Hz)		Error (%)	Amplitude for first vibration mode (mm)		Error (%)	
		Analy. result	Exp. result		Analy. result	Exp. result		
Intact Plate	-	122.58	107.60	12.2	7.979	7.056	11.6	
Cracked Plate	7.5 mm	0°	113.90	99.61	12.5	8.066	7.498	7.0
		20°	118.18	102.90	12.9	6.951	7.278	4.7
		40°	122.37	105.30	13.9	6.659	7.187	7.9
		60°	124.61	106.40	14.6	6.548	7.176	9.6
		80°	123.95	104.10	16.0	7.336	7.274	0.8
		90°	122.58	102.00	16.8	7.979	7.591	4.9

Analy. = Analytical
Exp. = Experimental

Table 7-2 : Comparison between the experimental and theoretical results for the first mode of vibration

7.3 Discussions of Results

Discussion of the results from Chapters 3 to 6 is divided into three categories, namely the analytical results, numerical results and the experimental results.

7.3.1 Analytical Results

A new mathematical model has been proposed for a thin plate with enhanced crack modelling which considers an alternative geometry whereby the crack orientation angle can be varied, and is used for vibration analysis. The dynamic characteristics of the model have been investigated and general observations are summarised from the studies as follows:

- Initially the correctness of the enhanced crack model within an analytical model of the plate has been partially checked by referring to the existing model for a centrally located crack parallel to one side of the plate, as proposed by Israr (2008), and close agreement was found. The values of the differences between the first mode natural frequencies of these two models are small, with a maximum percentage error of approximately 0.012 (Table 3-1).

- The results show generally that the natural frequency reduces with an increase in the half-crack length and it is also influenced by the boundary conditions and when the geometry of the plate is changed.

A plate with a crack of variable angular orientation:

- In comparison with a plate model for a horizontally located centre crack of fixed orientation, the natural frequency results for a plate model with a crack of variable angular orientation show that the presence of a crack at the centre of the plate with variable orientation angle significantly influences the natural frequency of the first mode, in all three boundary condition cases that were investigated. These included SSSS (Table 3-2), CCSS (Table 3-3), and CCFE (Table 3-4).
- The results show that the natural frequency reduces with an increase in the half-crack length, as shown in Figure 3-7, in which the cracked plate model predicts the natural frequency very well for the SSSS and CCSS boundary conditions, but the prediction is rather inaccurate for a half-crack length of less than 0.001m in the case of the CCFE boundary condition.
- The results show that the natural frequency increases with the increase in the crack angle, up to 90° for the SSSS and CCFE boundary conditions. For the case of the CCFE boundary condition the frequency increases up to 60° , and then decreases when the crack angle exceeds 60° (Figure 3-8). This similar trend was also seen by Maruyama and Ichinomiya (1989) and Wu and Law (2004).
- The physical reason that cracks generally lower the natural frequencies of a plate is due to changes to the local flexibility in the vicinity of the crack, which in turn reduces the overall stiffness of the structure.
- In the case of the CCFE boundary condition the orientation angles for which the natural frequency is maximum are affected by crack length, plate thickness, plate aspect ratio, Poisson's ratio, plate density and the modulus of elasticity. Simulation with standard parameter properties showed changes in the natural frequency values at an angle of approximately $59^\circ \approx 60^\circ$.

- In addition to the effect of the half-crack length and the crack orientation angle, the natural frequency is also influenced if the geometry of the plate is changed, particularly in the length of the plate (via the aspect ratio) and the plate thickness.

The analytical developments involved using the perturbation method of multiple scales, a direct numerical integration method, and finite element analysis. In the following points are summarised which emerged from these studies:

- The results from the method of multiple scales are given in Figures 4-1 and 4-2 representing the behaviour of square and rectangular plates containing a crack of variable angular orientation for the three chosen of boundary conditions. The effect of a crack within the plate model produced a global effect on the nonlinear response of the overall system. For the cracked plate model with the SSSS and CCSS boundary conditions, the nonlinearity bends the curves to the right, as for a hardening system, whereas for the CCFF boundary condition the nonlinearity bends the curves to the left as for a softening system.
- The nonlinear hardening effect is much stronger for the SSSS boundary condition compared to the CCSS case. It is evident that for all types of boundary condition the cracked rectangular plate model with an aspect ratio of 1:2 displays a much stronger general nonlinearity than the square plate model.
- The influence of the crack orientation angle on the frequency response was also observed. For the SSSS and CCSS boundary conditions no obvious hardening effects emerged for rectangular plates. However for square plates with an increase in the crack orientation angle, the nonlinear hardening phenomenon clearly increases (Figure 4-1). Similarly, for the CCFF boundary condition the nonlinear softening effect increases up to 60° and then reduces when the crack orientation angles starts to exceed 60° . It should be noted that the amplitude decreases with an increase in the excitation frequency value.
- Changing the location of the applied load on the plate surface slightly affects the nonlinear behaviour of the cracked plate model whereby the width of the nonlinear region becomes narrower as the excitation location moves closer to the constrained area (Figure 4-3). In addition the frequency response curve is also affected by

changing the value of the excitation amplitude such that the amplitude increases when the excitation amplitude increases (Figure 4-4).

- Increasing the damping coefficient results in a decrease in the amplitudes.
- The numerical results calculated by directly integrating the nonlinear ordinary differential equation (3.89) within the Mathematica™ environment qualitatively and quantitative produce a similarly decreasing response in the natural frequency, and an increasing response in the amplitude, both corroborating those of the method of multiple scales (Figure 4-6). Both the responses show a characteristic softening effect, however the overhanging part of the curve in the numerical prediction represents unstable solutions, and this over-prediction of the softening overhang by the multiple scales solution is undoubtedly due to an over-correction to the solution from the first order perturbation contribution.
- The results from the finite element analysis for the CCFB boundary condition also show that a large crack shifts the frequency values of the 1st, 2nd and 3rd modes downwards, as expected, and is due to a reduced plate stiffness. For both crack lengths of 3 mm and 7.5 mm, the frequency values increase monotonously from 0° up to 60°, and then decrease when β is more than 60° (Table 4-3) in which a similar trend from the analytical prediction was exhibited.
- The amplitude responses from the finite element analysis of the cracked plate model produced results that corroborate those of the method of multiple scales. As expected the frequency results show a decreasing trend at the resonance condition, and similarly, the amplitude results show an increasing trend, when using a small crack, again fully in-line with the analytical model (4-4).
- A comparative study of the theoretical modelling and finite element approaches is presented in Table 7-1. Both sets of results show a significant change in the natural frequency and the response amplitude at the resonance condition for the different lengths of the crack and the varying orientation angle of the crack. Very close agreement was obtained between the analytical and finite element results, with a maximum error in the prediction of the frequency value of about 7.7 % and the amplitude response at around 7.6 %. This error might have occurred because in the finite element analysis the crack width is taken to be 0.3 mm, whereas it has been

proposed as a continuous line spring in the derivation of the cracked plate model (chapter 3).

7.3.2 Numerical Results

Subsequent numerical analyses were conducted using the dynamical systems tools within the MathematicaTM environment. From this investigation the following is concluded:

- Bifurcation diagrams for the amplitude response x as a function of the normalised excitation acceleration can be obtained.
- Periodic doubling bifurcation can be observed in all the results with an increase in the normalised excitation acceleration, and when the normalised excitation acceleration value is increased to a high level this periodic response appears to bifurcate to chaos. There are five types of system motion exists over the range of normalised excitation acceleration, namely stable single period motion, stable period-2 motion, stable period-4 motion, stable multiperiod motion, and finally chaotic motion.
- Specific boundary conditions are found to have a strong influence on the route to chaos. Crack length and crack orientation angle also have a significant effect on the system's motion. As the crack length is increased the system appears to get more chaotic. However, as the orientation angle of the crack is increased from 0° to 90° the system with SSSS and CCSS boundary conditions seems to get less chaotic. For the CCFF boundary condition the same phenomenon occurred when the crack orientation angle exceeded 40° .

Detailed analysis of the bifurcation diagrams in Figures 5-2 to 5-10 was extended to the time plots, phase planes, and the Poincaré maps, as shown in Figures 5-11 to 5-25 for discrete normalised excitation acceleration points. The following are general observations:

- Figures 5-11 to 5-25 illustrate the time plots, phase plane, and Poincaré maps for the cracked plate model for the SSSS, CCSS and CCFF boundary conditions.
- All the time plots are for periodic motion.

- The periodic orbits in the phase plane move away from each other as the effect of the predominant system nonlinearity is changed, either by manipulation of the cubic nonlinear coefficient due to the presence of the small crack in the system, or by variations in the normalised excitation acceleration. And therefore the phenomenon behind this behaviour, as shown on the phase plane, could represent a bifurcation to chaos.
- When the normalised excitation acceleration is increased complicated and richer phase plots are obtained which could indicate chaotic motion. However, the orbits repeat themselves in the same way, when the simulation time is extended.
- In the Poincaré maps strange attractors are also obtained for higher value of normalised excitation accelerations, and these are clearly indicative of chaotic motion.

7.3.3 Experimental Results

The theoretical predictions of the vibration characteristics of the cracked plate model have been successfully validated through experiment measurement. The following conclusions are obtained from this work:

- The insertion of the crack in the centre of the aluminium plate was found to have a strong influence on the frequency and amplitude responses.
- The results from the experimental measurement qualitatively produce a similar decreasing trend in the natural frequencies with the insertion of a crack. The frequency value decreases with an increase in the crack length, and increases with an increase in the crack orientation angle up to 60° .
- The results also qualitatively produced a similar increasing trend in the amplitude response with the insertion of a crack as for the theoretical prediction, except for a crack at an orientation angle of 20° .
- Similarity can be observed between the trends for the theoretical and experimental results for the CCFB boundary condition, with a maximum error in the prediction of the frequency value of about 16.8 % and in the amplitude response of about 11.6 %.

However the measured values from the experiments are lower than those predicted by the theoretical calculations based on approximate techniques. This could be because of the fact that microscopic flaws or cracks always exist under normal conditions at the surface and within the interior of the body of a material (Griffith, 1921).

- The plate specimens could be exhibiting nonlinear behaviour because the results show that the deflection is a multiple of the plate thickness, but is much less than the plate side length, as discussed by Malatkar (2003) and Israr (2008).

Chapter 8

Conclusions

This chapter summarises the main conclusions of this thesis and makes recommendations for further work.

8.1 Summary and Conclusions

The equation of motion for an isotropic plate containing a crack of variable angular orientation subjected to transverse harmonic excitations has been derived based on classical plate theory. This equation of motion is a nonlinear ordinary differential equation with a cubic nonlinearity which was generated by the use of Berger's formulation. Berger's formulation was used to assimilate the in-plane forces within this mathematical model and also to reduce the equation to the form of a specialised Duffing equation. This mathematical model has been shown to be capable of detecting and predicting the nonlinear vibration behaviour of the cracked plate, and in showing the trend of the natural frequency values, and the linear and nonlinear frequency curves for the three chosen boundary conditions, namely SSSS, CCSS and CCFF. For a cracked square and rectangular plate the influence of the boundary conditions, crack orientation angles, crack lengths, and location of the point load have all been discussed.

Initially the proposed model was validated through convergence studies for a plate with a horizontally orientated centre crack. The results showed excellent agreement with those obtained by Israr (2008), with the maximum error in the prediction of the first mode natural frequency for the boundary conditions taken, of approximately 0.012%. Then the proposed model was applied to a plate with a variably orientated surface crack. It was found that the vibration characteristics of this plate structure could be greatly affected by the orientation of the crack depending on the type of boundary condition applied. For the SSSS and CCSS boundary conditions, the natural frequency increases with an increase in the crack angle, up to 90° . But it is a different situation for the case of the CCFF boundary condition, where the natural frequency increases up to 60° , and then decreases when β exceeds 60° . This similar trend for the crack orientation effect was also reported by Maruyama and Ichinomiya (1989) and Wu and Law (2004). In terms of crack length effects the results show generally that the natural frequency reduces with an increase in the half-crack length. The derived cracked plate model predicts the natural frequency very well

for cases with SSSS and CCSS boundary conditions. However for the CCFF boundary condition the prediction is rather inaccurate, especially for a half-crack length, a of less than 0.001 m. The physical parameters such as crack length, plate thickness, plate aspect ratio, Poisson's ratio, plate density and modulus of elasticity also contribute to the changes in the orientation angles for which the natural frequency is maximum.

The physical behaviour of this cracked plate model has been explored in Chapter 4 through the approximate solutions that have been obtained based on the perturbation method of multiple scales and the finite element method. For purposes of comparison numerical results were also calculated by directly integrating the nonlinear ordinary differential equation for the model, and the results from this were compared with the results obtained from the multiple scales method. The inclusion of a crack within the plate model produced a global effect on the nonlinear response of the overall system for both solutions. Interesting nonlinear behaviour was observed for the primary resonance condition, and the results obtained from the multiple scales method showed hardening spring behaviour for the SSSS and CCSS boundary conditions and a softening spring phenomenon for the CCFF boundary condition. It was shown conclusively, by using a first order multiple scales approximation solution, that the nonlinear characteristics of the steady-state responses are encoded within the non-autonomous modulation equations.

The dynamics of the cracked plate model are investigated using dynamical systems tools in Chapter 5 to study the relevant bifurcatory phenomena and stability of the system. From the observation of bifurcation diagrams, time plots, the phase plane, and Poincaré maps, this study has shown that additional and highly complex dynamics could be observed, especially in more strongly excited systems. In addition, the amplitude response characteristics for the performance of this system could be effectively achieved by applying different combinations of system parameters.

Finally, the validity of the developed model was shown through a comparison of the results with experimental work, in Chapter 6 and 7. The response of an aluminium cracked plate for the arbitrarily chosen CCFF boundary condition, and when subjected to transverse harmonic excitation, was observed. The insertion of the crack in the plate was found to have a strong influence on the natural frequency and the amplitude responses. The orientation of the crack also had a significant effect on the vibration characteristics of this experimental system in which the same phenomenon was encountered as in the analytical model. The comparison showed that the analytical model was able to predict results

qualitatively similar to the experimental measurements, however the results vary quantitatively. The discrepancies in the results might have arisen because one or more of the factors such as the nonlinear damping, shaker-structure interaction, internal discontinuities within the plate, and initial curvature of the plate were neglected in the analytical model. These factors might be contributing a bigger role than expected, and this could be further investigated. The instability region of the boundary condition of the plate was manipulated by altering the tightness of the clamped edges of the plates. The tightness of the clamped edges can alter the stability characteristics of the system. For a highly excited system careful design and assembly of the experimental system components is crucial for better overall performance.

Overall, this research provides some basic theory and understanding of how inclusion of a crack in a plate structure and the orientation of the crack can both influence significantly the vibration and nonlinear behaviour of a plate structure. It has provided an extension to the development of currently available analytical models of the nonlinear characteristics of a cracked plate structure, particularly for an alternative geometry in which the crack orientation is variable. It can be seen that the new analytical model could constitute a useful tool for subsequent investigation into the development of damage detection methodologies for generalised plate structures.

8.2 Recommendations for further work

Generally antinodally located cracks will have a particular significance for resonant properties. Such insight could be explored further in the future, as could the effects of prescribed wave number and other modal properties. The orientation of travelling waves shows a strong relationship with crack orientation, thus the wave numbers in both the x and y directions could be used to determine this relationship.

The effect of the nonlinearity introduced into the analytical model through the crack analysis is unlikely to have been as faithfully reproduced within the current finite element analysis. This could be a further study in future work.

It would also be interesting to see if one could extend this work for a thick plate by applying Mindlin Plate theory and then investigating the influence of such cracks on the responses of that kind of plate structure. Similarly, the study could also be extended for all-through cracks and elliptical cracks.

The route to chaotic motion of this cracked plate system can be further explored by using other dynamical systems tools to calculate the Lyapunov exponent in order to underpin and provide more evidence of the existing results from the bifurcation diagrams.

List of References

- ABE, A. 2006. On non-linear vibration analyses of continuous systems with quadratic and cubic non-linearities. *International Journal of Non-Linear Mechanics*, 41, 873-879.
- ALHAZZA, K. A. & NAYFEH, A. H. 2001. Nonlinear Vibrations of Doubly-curved Cross-ply Shallow Shells. Proceedings of the 42nd AIAA/ASME/ASCE/AHS/ASC Structures, Structural Dynamics, and Materials Conference, Seattle, Washington.
- AMABILI, M. 2004. Nonlinear vibrations of rectangular plates with different boundary conditions: theory and experiments. *Computers & Structures*, 82, 2587-2605.
- ATEPOR, L. 2008. Vibration analysis and intelligent control of flexible rotor systems using smart materials. *PhD. Thesis, Department of Mechanical Engineering, University of Glasgow, Glasgow, UK.*
- AZRAR, L., BOUTYOUR, E. H. & POTIER-FERRY, M. 2002. Non-linear forced vibrations of plates by an asymptotic-numerical method. *Journal of Sound and Vibration*, 252, 657-674.
- BACHENE, M., TIBERKAK, R. & RECHAK, S. 2009. Vibration analysis of cracked plates using the extended finite element method. *Archive of Applied Mechanics*, 79, 249-262.
- BARDELL, N. S. 1991. Free vibration analysis of a flat plate using the hierarchical finite element method. *Journal of Sound and Vibration*, 151, 263-289.
- BEGHINI, M., BERTINI, L. & FONTANARI, V. 2001. A weight function technique for partially closed inclined edge cracks analysis. *International Journal of Fracture*, 112, 57-68.
- BENAMAR, R., BENNOUNA, M. M. K. & WHITE, R. G. 1993. The Effects of Large Vibration Amplitudes on the Mode Shapes and Natural Frequencies of Thin Elastic Structures, Part II: Fully Clamped Rectangular Isotropic Plates. *Journal of Sound and Vibration*, 164, 295-316.

- BENCHARIF, N. & NG, S. F. 1994. Linear and non-linear deflection analysis of thick rectangular plates—I. theoretical derivation. *Computers & Structures*, 50, 757-761.
- BERGER, H. M. 1955. A new approach to the analysis of large deflections of plates. *Journal of Applied Mechanics*, 22, 465-472.
- BHAT, R. B. 1985. Natural frequencies of rectangular plates using characteristic orthogonal polynomials in Rayleigh-Ritz method. *Journal of Sound and Vibration*, 102, 493-499.
- BHIMARADDI, A. 1987. Nonlinear flexural vibrations of rectangular plates subjected to in-plane forces using a new shear deformation theory. *Thin-Walled Structures*, 5, 309-327.
- CANCHANG, L. & JIANSHE, P. Semi-analytic approach for the nonlinear vibration analysis of beams. Computer, Mechatronics, Control and Electronic Engineering (CMCE), 2010 International Conference on, 24-26 Aug. 2010 2010. 8-11.
- CARTMELL, M. P. 1990. Introduction to Linear, Parametric and Non-Linear Vibrations, *Chapman & Hall, London*.
- CARTMELL, M. P., ZIEGLER, S. W., KHANIN, R. & FOREHAND, D. I. M. 2003. Multiple Scales Analysis of the Dynamics of Weakly Nonlinear Mechanical Systems. *Applied Mechanics Reviews*, 56(5), 455-492.
- CHANG, C.-C. & CHEN, L.-W. 2004. Damage detection of a rectangular plate by spatial wavelet based approach. *Applied Acoustics*, 65, 819-832.
- CHEN, H.-P. & BICANIC, N. 2000. Assessment of damage in continuum structures based on incomplete modal information. *Computers & Structures*, 74, 559-570.
- CHIA, C. Y. 1980. Nonlinear analysis of plates. *McGraw-Hill, New York*.
- CHIA, C. Y. 1982. Large amplitude vibrations of laminated rectangular plates. *Fibre Science and Technology*, 17, 123-131.
- CHU, H. N. & HERMANN, G. 1956. Influence of Large Amplitudes on Free Flexural Vibrations of Rectangular Elastic Plates. *Journal of Applied Mechanics*, 23, 532-540.

- CORDES, R. D. & JOSEPH, P. F. 1994. Crack surface contact of surface and internal cracks in a plate with residual stresses. *International Journal of Fracture*, 66, 1-17.
- CORNWELL, P., DOEBLING, S. W. & FARRAR, C. R. 1999. Application of the strain energy damage detection method to plate-like structures. *Journal of Sound and Vibration*, 224, 359-374.
- DARBYSHIRE, A. G. 1994. Calculating Lyapunov Exponents from a Time Series. *The Institution of Electrical Engineers*, 2, 1-6.
- DATE, K., SHIMADA, H. & IKENAGA, N. 1982. Crack height measurement-an evaluation of the accuracy of ultrasonic timing methods. *NDT International*, 15, 315-319.
- DAWE, D. J. & ROUFAEIL, O. L. 1980. Rayleigh-Ritz vibration analysis of Mindlin plates. *Journal of Sound and Vibration*, 69, 345-359.
- DELALE, F. & ERDOGAN, F. 1981. Line-spring model for surface cracks in a reissner plate. *International Journal of Engineering Science*, 19, 1331-1340.
- DIMAROGONAS, A. D. 1996. Vibration of cracked structures: A state of the art review. *Engineering Fracture Mechanics*, 55, 831-857.
- DOEBLING, S. W., FARRAR, C. R. & PRIME, M. B. 1998. A summary review of vibration-based damage identification methods. *Shock and Vibration Digest*, 30, 91-105.
- DOLBOW, J., MOËS, N. & BELYTSCHKO, T. 2000. Modeling fracture in Mindlin-Reissner plates with the extended finite element method. *International Journal of Solids and Structures*, 37, 7161-7183.
- DUMIR, P. C. & BHASKAR, A. 1988. Nonlinear forced vibration of orthotropic thin rectangular plates. *International Journal of Mechanical Sciences*, 30, 371-380.
- DYSHEL, M. S. 2003. Stability of Plates with an Oblique Edge Crack under Tension. *International Applied Mechanics*, 39, 1081-1083.
- EFTIS, J., SUBRAMONIAN, N. & LIEBOWITZ, H. 1977. Crack border stress and displacement equations revisited. *Engineering Fracture Mechanics*, 9, 189-210.

EL BIKRI, K., BENAMAR, R. & BENNOUNA, M. 2003. Geometrically non-linear free vibrations of clamped simply supported rectangular plates. Part I: the effects of large vibration amplitudes on the fundamental mode shape. *Computers & Structures*, 81, 2029-2043.

EL KADIRI, M. & BENAMAR, R. 2002. Improvement of the semi-analytical method, for determining the geometrically non-linear response of thin straight structures: Part II- First and second non-linear mode shapes of fully clamped rectangular plates. *Journal of Sound and Vibration*, 257, 19-62.

EL KADIRI, M. & BENAMAR, R. 2003. Improvement of the semi-analytical method, based on Hamilton's principle and spectral analysis, for determination of the geometrically non-linear response of thin straight structures. Part III: steady state periodic forced response of rectangular plates. *Journal of Sound and Vibration*, 264, 1-35.

EL KADIRI, M., BENAMAR, R. & WHITE, R. G. 1999. The non-linear free vibration of fully clamped rectangular plates: Second non-linear mode for various plate aspect ratios. *Journal of Sound and Vibration*, 228, 333-358.

EMAM, S. A. & NAYFEH, A. H. 2002. Nonlinear Dynamics of a Clamped-clamped Buckled Beam Proceedings of the 43rd AIAA/ASME/ASCE/AHS/ASC Structures, Structural Dynamics, and Materials Conference, Denver, Colorado.

EWING, P. D., SWEDLOW, J. L. & WILLIAMS, J. G. 1976. Further results on the angled crack problem. *International Journal of Fracture*, 12, 85-93.

FAN, W. & QIAO, P. 2011. Vibration-based damage identification methods: A review and comparative study. *Structural Health Monitoring*, 10 (1), 83-111.

FRISWELL, M. I. & PENNY, J. E. T. 2002. Crack Modeling for Structural Health Monitoring. *An International Journal Structural Health Monitoring*, 1, 139-148.

FUJIMOTO, T., WAKATA, K., CAO, F. & NISITANI, H. 2003. Vibration Analysis of a Cracked Plate Subjected to Tension using a Hybrid Method of FEM and BFM. *Materials Science Forum., Trans. Tech. Publications, Switzerland*, 440-441, 407-414.

GILLICH, G.-R., PRAISACH, Z. & ONHICS, D. M. About the effectiveness of damage detection methods based on vibration measurements. Proceedings of the 3rd WSEAS international conference on Engineering mechanics, structures, engineering geology, 2010 Corfu Island, Greece. 204-209.

GORMAN, D. G., TRENDAFILOVA, I., MULHOLLAND, A. J. & HORÁČEK, J. 2008. Vibration analysis of a circular plate in interaction with an acoustic cavity leading to extraction of structural modal parameters. *Thin-Walled Structures*, 46, 878-886.

GORMAN, D. J. 1976. Free vibration analysis of cantilever plates by the method of superposition. *Journal of Sound and Vibration*, 49, 453-467.

GORMAN, D. J. 1979. Solutions of the Lévy type for the free vibration analysis of diagonally supported rectangular plates. *Journal of Sound and Vibration*, 66, 239-246.

GORMAN, D. J. 1984. An exact analytical approach to the free vibration analysis of rectangular plates with mixed boundary conditions. *Journal of Sound and Vibration*, 93, 235-247.

GORMAN, D. J. 1995. Accurate free vibration analysis of the orthotropic cantilever plate. *Journal of Sound and Vibration*, 181, 605-618.

GORMAN, D. J. 2005. Highly accurate free vibration eigenvalues for the completely free orthotropic plate. *Journal of Sound and Vibration*, 280, 1095-1115.

GRIFFITH, A. A. 1921. The phenomena of rupture and flow in solids. *Philosophical Transactions of the Royal Society of London, Series A, Containing papers of a Mathematical or Physical Character*, 221, 163-198.

GUAN-LIANG, Q., SONG-NIAN, G. & JIE-SHENG, J. 1991. A finite element model of cracked plates and application to vibration problems. *Computers & Structures*, 39, 483-487.

GUTIÉRREZ, J. M. 1998. Mathematica package for analysis and control of chaos in nonlinear systems. *Computers in Physics*, 12, 608-619.

HADJILEONTIADIS, L. J. & DOUKA, E. 2007. Kurtosis analysis for crack detection in thin isotropic rectangular plates. *Engineering Structures*, 29, 2353-2364.

HAN, W. & PETYT, M. 1996(a). Linear vibration analysis of laminated rectangular plates using Hierarchical finite element method I: Forced vibration analysis. *Computers and Structures*, 61(4), 713-724.

HAN, W. & PETYT, M. 1996(b). Linear vibration analysis of laminated rectangular plates using the Hierarchical finite element method I: Free Vibration Analysis. *Computers and Structures*, 61(4), 705-712.

HAN, W. & PETYT, M. 1997. Geometrically nonlinear vibration analysis of thin, rectangular plates using the hierarchical finite element method—I: The fundamental mode of isotropic plates. *Computers & Structures*, 63, 295-308.

HAO, Y. X., ZHANG, W. & YANG, J. 2011. Nonlinear oscillation of a cantilever FGM rectangular plate based on third-order plate theory and asymptotic perturbation method. *Composites Part B: Engineering*, 42, 402-413.

HE, K. & ZHU, W. D. 2011. Structural Damage Detection Using Changes in Natural Frequencies: Theory and Applications. *Journal of Physics: Conference Series*, 305, 012054.

HILBORN, R. C. 2000. Chaos and Nonlinear dynamics: An introduction for scientists and engineers. Oxford University Press, New York.

HIRANO, Y. & OKAZAKI, K. 1980. Vibration of Cracked Rectangular Plates. *Bulletin JSME*, 23, 732-740.

HOSSEINI-HASHEMI, S., ROOHI GH, H. & ROKNI D.T, H. 2010. Exact free vibration study of rectangular Mindlin plates with all-over part-through open cracks. *Computers & Structures*, 88, 1015-1032.

HSU, M.-H. 2003. Vibration Analysis of Isotropic and Orthotropic Plates with Mixed Boundary Conditions. *Journal of Science and Engineering*, 6, 217-226.

- HU, H., WANG, B.-T., LEE, C.-H. & SU, J.-S. 2006. Damage detection of surface cracks in composite laminates using modal analysis and strain energy method. *Composite Structures*, 74, 399-405.
- HU, X. T., QIN, Z. Y. & CHU, F. L. 2011. Damage Detection in Plate Structures Based on Space-time Autoregressive Moving Average Processes. *Journal of Physics: Conference Series*, 305, 012119.
- HUANG, C.-H. & MA, C.-C. 2000. Vibration of cracked circular plates at resonance frequencies. *Journal of Sound and Vibration*, 236, 637-656.
- HUANG, C. S. & LEISSA, A. W. 2009. Vibration analysis of rectangular plates with side cracks via the Ritz method. *Journal of Sound and Vibration*, 323, 974-988.
- HUANG, C. S., LEISSA, A. W. & CHAN, C. W. 2011a. Vibrations of rectangular plates with internal cracks or slits. *International Journal of Mechanical Sciences*, 53, 436-445.
- HUANG, C. S., LEISSA, A. W. & LI, R. S. 2011b. Accurate vibration analysis of thick, cracked rectangular plates. *Journal of Sound and Vibration*, 330, 2079-2093.
- HUANG, C. S., LEISSA, A. W. & LIAO, S. C. 2008. Vibration analysis of rectangular plates with edge V-notches. *International Journal of Mechanical Sciences*, 50, 1255-1262.
- IRWIN, G. R. 1962. Crack Extension Force for a Part through Crack in a Plate. *Journal of Applied Mechanics*, 29, 651-654.
- ISRAR, A. 2008. Vibration analysis of cracked aluminium plates. *PhD. Thesis, Department of Mechanical Engineering, University of Glasgow, Glasgow, UK.*
- ISRAR, A. & ATEPOR, L. 2009. Investigation of the nonlinear dynamics of a partially cracked plate. *Journal of Physics: Conference Series*, 181, 012087.
- ISRAR, A., CARTMELL, M., MANOACH, E., TRENDAFILOVA, I., OSTACHOWICZ, W. L., KRAWCZUK, M. & ARKADIUSZ 2009. Analytical Modeling and Vibration Analysis of Partially Cracked Rectangular Plates With Different Boundary Conditions and Loading. *Journal of Applied Mechanics*, 76 (1), 011005.

JI, W., RONG-XING, W. & JIAN-KE, D. The nonlinear thickness-shear vibrations of an infinite and isotropic elastic plate. *Piezoelectricity, Acoustic Waves, and Device Applications (SPAWDA) and 2009 China Symposium on Frequency Control Technology, Joint Conference of the 2009 Symposium on, 17-20 Dec. 2009* 2009. 85-85.

JOSEPH, P. F. & ERDOGAN, F. 1991. Surface crack in a plate under antisymmetric loading conditions. *International Journal of Solids and Structures*, 27, 725-750.

KANG, J.-H. & SHIM, H.-J. 2004. Exact solutions for the free vibrations of rectangular plates having in-plane moments acting on two opposite simply supported edges. *Journal of Sound and Vibration*, 273, 933-948.

KARPENKO, E. V., WIERCIGROCH, M. & CARTMELL, M. P. 2002. Regular and chaotic dynamics of a discontinuously nonlinear rotor system. *Chaos, Solitons & Fractals*, 13, 1231-1242.

KAZEMI, S., FOOLADI, A. & RAHAI, A. R. 2010. Implementation of the modal flexibility variation to fault identification in thin plates. *Acta Astronautica*, 66, 414-426.

KEER, L. M. & SVE, C. 1970. On the Bending of Cracked Plates. *International Journal of Solids and Structures*, 6, 1545-1559.

KEVORKIAN, J. & COLE, J. D. 1981. *Perturbation Methods in Applied Mathematics*, Springer-Verlag, New York.

KHADEM, S. E. & REZAEI, M. 2000. Introduction of modified comparison functions for vibration analysis of a rectangular cracked plate. *Journal of Sound and Vibration*, 236, 245-258.

KHAN, S. M. A. & KHRAISHEH, M. K. 2000. Analysis of mixed mode crack initiation angles under various loading conditions. *Engineering Fracture Mechanics*, 67, 397-419.

KHANIN, R., CARTMELL, M. & GILBERT, A. 2000. A computerised implementation of the multiple scales perturbation method using Mathematica. *Computers & Structures*, 76, 565-575.

- KIM, T.-W. & KIM, J.-H. 2002. Nonlinear vibration of viscoelastic laminated composite plates. *International Journal of Solids and Structures*, 39, 2857-2870.
- KING, R. B. 1983. Elastic-plastic analysis of surface flaws using a simplified line-spring model. *Engineering Fracture Mechanics*, 18, 217-231.
- KITIPORNCHAI, S., XIANG, Y., WANG, C. M. & LIEW, K. M. 1993. Buckling of thick skew plates. *International Journal for Numerical Methods in Engineering*, 36, 1299-1310.
- KOPMAZ, O. & TELLI, S. 2002. Free vibrations of a rectangular plate carrying a distributed mass. *Journal of Sound and Vibration*, 251, 39-57.
- KRAWCZUK, M. 1993. Natural vibrations of rectangular plates with a through crack. *Archive of Applied Mechanics*, 63, 491-504.
- KRAWCZUK, M. & OSTACHOWICZ, W. M. 1994. A finite plate element for dynamic analysis of a cracked plate. *Computer Methods in Applied Mechanics and Engineering*, 115, 67-78.
- KRAWCZUK, M., PALACZ, M. & OSTACHOWICZ, W. 2004. Wave propagation in plate structures for crack detection. *Finite Elements in Analysis and Design*, 40, 991-1004.
- KRAWCZUK, M., ŻAK, A. & OSTACHOWICZ, W. 2001. Finite element model of plate with elasto-plastic through crack. *Computers & Structures*, 79, 519-532.
- KUO, C. H., KEER, L. M. & CORDES, R. D. 1985. A note on the line spring solution for a part-through crack. *International Journal of Fracture*, 72, 191-195.
- LACARBONARA, W. 1999. Direct Treatment and Discretizations of Non-linear Spatially Continuous Systems. *Journal of Sound and Vibration*, 221, 849-866.
- LEE, H. E. 1992. Fundamental Frequencies of Annular Plates with Internal Cracks. *Computers and Structures*, 43, 1085-1089.
- LEE, H. P. & LIM, S. P. 1992. Free vibration of isotropic and orthotropic rectangular plates with partially clamped edges. *Applied Acoustics*, 35, 91-104.

- LEE, U., CHO, K. & SHIN, J. 2003. Identification of orthotropic damages within a thin uniform plate. *International Journal of Solids and Structures*, 40, 2195-2213.
- LEISSA, A. W. 1973. The free vibration of rectangular plates. *Journal of Sound and Vibration*, 31, 257-293.
- LEISSA, A. W. 1993. Vibration of Plates. NASA SP-160, National Acoustical and Space Administration, Washington, DC.
- LEUNG, A. Y. T. & MAO, S. G. 1995. A symplectic Galerkin method for non-linear vibration of beams and plates. *Journal of Sound and Vibration*, 183, 475-491.
- LEUNG, A. Y. T. & Zhu, B. 2004. Comments on 'Free Vibration of Skew Mindlin Plates by p-version of F.E.M. *Journal of Sound and Vibration*, 278, 699-703.
- LI, Y. Y., CHENG, L., YAM, L. H. & WONG, W. O. 2002. Identification of damage locations for plate-like structures using damage sensitive indices: strain modal approach. *Computers & Structures*, 80, 1881-1894.
- LIEW, K. M., HUNG, K. C. & LIM, M. K. 1994. A solution method for analysis of cracked plates under vibration. *Engineering Fracture Mechanics*, 48, 393-404.
- LIM, F. C. N. 2003. A preliminary investigation into the effects of nonlinear response modification within coupled oscillators. *PhD. Thesis, Department of Mechanical Engineering, University of Glasgow, Glasgow, UK.*
- LIU, B. & XING, Y. 2011. Exact solutions for free vibrations of orthotropic rectangular Mindlin plates. *Composite Structures*, 93, 1664-1672.
- LOENDERSLOOT, R., OOIJEVAAR, T. H., WARNET, L., BOER DE, A. & AKKERMAN, R. 2010. Vibration based structural health monitoring of a composite plate with stiffeners. *International Conference on Noise and Vibration Engineering, ISMA 2010*. Leuven, Belgium.
- LU, C. H. & EVAN-IWANOWSKI, R. M. 1994. Period doubling bifurcation problems in the softening Duffing oscillator with nonstationary excitation. *Nonlinear Dynamics*, 5, 401-420.

- LU, Y.C. & XU, Y. G. 1986. Line-spring model for a surface crack loaded antisymmetrically. National University of Defense Technology Technical Paper. Acta Mechanica Solida Sinica. 1986-01.
- LYNCH, J. P. & LOH, K. J. 2006. A summary review of wireless sensors and sensor networks for structural health monitoring. *The Shock and Vibration Digest*, 38, 91-128.
- LYNN, E. E. & KUMBASAR, N. 1967. Free Vibration of Thin Rectangular Plates having Narrow Cracks with Simply Supported Edges. *In: 10th Midwestern Mechanics Conference, Fort Collins, USA*, 911-928.
- MAESTRELLO, L, FRENDI, A. & BROWN, D. E. 1992. Nonlinear Vibration and Radiation from a Panel with Transition to Chaos. *AIAA Journal*, 30, 2632-2638.
- MALATKAR, P. 2003. Nonlinear vibrations of cantilever beams and plates. *PhD Thesis, Virginia Polytechnic Institute and State University, USA*.
- MARUYAMA, K. & ICHINOMIYA, O. 1989. Experimental study of free vibration of clamped rectangular plates with straight narrow slits. *JSME International Journal, Ser. 3, Vibration, Control Engineering, Engineering for Industry* 32, 187-193.
- MEI, C. 1973. Finite element displacement method for large amplitude free flexural vibrations of beams and plates. *Computers & Structures*, 3, 163-174.
- MINDLIN, R. D. 1951. Influence of Rotatory Inertia and Shear on Flexural Motions of Isotropic Elastic Plates. *Journal of Applied Mechanics*, 18, 31-38.
- MITRA, A., SAHOO, P. & SAHA, K. N. 2010. Large amplitude forced vibration analysis of cross-beam system through energy method. *International Journal of Engineering, Science and Technology*, 2, 113-133.
- MITRA, A., SAHOO, P. & SAHA, K. N. 2012. Effect of in-plane boundary conditions on forced vibration analysis of stiffened plates with a free edge. *Journal of Vibration and Control*, 0, 1-28.
- MIYAZAKI, N. 1989. An application of a line-spring model to a transient analysis of the dynamic stress intensity factor. *International Journal of Fracture*, 39, R77-R80.

MOON, F. C. 1987. Chaotic Vibrations an introduction for applied scientists and engineers. *John Wiley & Sons, New York*.

NAYFEH, A. H. 1973. Perturbation Methods. *Wiley, New York*.

NAYFEH, A. H. 2000. Nonlinear Interactions. *Wiley, New York*.

NAYFEH, A. H. & ARAFAT, H. N. 2002. Nonlinear Responses of Suspended Cables to Primary Resonance Excitations, Denver, Colorado. *Proceedings of the 43rd AIAA/ASME/ASCE/AHS/ASC Structures, Structural Dynamics, and Materials Conference*.

NAYFEH, A. H. & CHIN, C. -M. 1999. Perturbation Methods with Mathematica™, *Dynamic Press, Virginia*.

NAYFEH, A. H. & LACARBONARA, W. 1997. On the Discretization of Distributed-parameter Systems with Quadratic and Cubic Nonlinearities. *Nonlinear Dynamics*, 13, 203-220.

NAYFEH, A. H. & MOOK, D. T. 1979. Nonlinear Oscillations. *John Wiley & Sons, New York*.

NAYFEH, A. H. & SANCHEZ, N. E. 1989. Bifurcations in a forced softening duffing oscillator. *International Journal of Non-Linear Mechanics*, 24, 483-497.

NEWMAN JR, J. C. & RAJU, I. S. 1981. An empirical stress-intensity factor equation for the surface crack. *Engineering Fracture Mechanics*, 15, 185-192.

NEZU, K. 1982. Free Vibrations of a Simple Supported Rectangular Plate with a Straight Through-notch. *Bulletin JSME*, 25, 16-23.

NG, S. F. & ARAAR, Y. 1989. Free vibration and buckling analysis of clamped rectangular plates of variable thickness by the Galerkin method. *Journal of Sound and Vibration*, 135, 263-274.

NIKKHAH-BAHRAMI, M., LOGHMANI, M. & POOYANFAR, M. 2008. Analytical solution for free vibration of rectangular Kirchhoff plate from wave approach. *World Academy of Science, Engineering and Technology*, 39, 221-223.

- NIYOGI, A. K. & MEYERS, B. L. 1981. A Perturbation Solution of Non-Linear Vibration of Rectangular Plates. *International Journal of Non-Linear Mechanics*, 16(5/6), 401-408.
- NOOR, A. K., ANDERSEN, C. M. & PETERS, J. M. 1993. Reduced basis technique for nonlinear vibration analysis of composite panels. *Computer Methods in Applied Mechanics and Engineering*, 103, 175-186.
- PAKDEMIRLI, M., NAYFEH, S. A. & Nayfeh, A.H. 1995. Analysis of One-to-One Autoparametric Resonances in Cables–Discretization vs. Direct Treatment. *Nonlinear Dynamics*, 8, 65-83.
- PAKDEMIRLI, M. & KARAHAN, M. M. F. 2010. A new perturbation solution for systems with strong quadratic and cubic nonlinearities. *Mathematical Methods in the Applied Sciences*, 33, 704-712.
- PARLITZ, U. & LAUTERBORN, W. 1985. Superstructure in the bifurcation set of the Duffing equation $\ddot{x} + d\dot{x} + x + x^3 = f \cos(\omega t)$. *Physics Letters A*, 107, 351-355.
- POOK, L. P. 1971. The effect of crack angle on fracture toughness. *Engineering Fracture Mechanics*, 3, 205-218.
- PRATHAP, G. & PANDALAI, K. A. V. 1978. Non-linear vibrations of transversely isotropic rectangular plates. *International Journal of Non-Linear Mechanics*, 13, 285-294.
- QIAN, G. L., GU, S. N. & JIANG, J. S. 1991. A Finite Element Model of Cracked Plates Application to Vibration Problems. *Computers and Structures*, 39, 483-487.
- RAHMAN, Z. & BURTON, T. D. 1986. Large amplitude primary and superharmonic resonances in the Duffing oscillator. *Journal of Sound and Vibration*, 110, 363-380.
- REGA, G., LACARBONARA, W., NAYFEH, A. H. & CHIN, C. -M. 1999. Multiple Resonances in Suspended Cables: Direct versus Reduced-order Models. *International Journal of Non-Linear Mechanics*, 34, 901—924.
- REHFIELD, L. W. 1973. Nonlinear free vibrations of elastic structures. *International Journal of Solids and Structures*, 9, 581-590.

- RIBEIRO, P. & PETYT, M. 1999. Geometrical non-linear, steady-state, forced, period vibration of plates, Part II: Stability study and analysis of multi-modal response. *Journal of Sound and Vibration*, 226, 985-1010.
- RICE, J. R. 1972. Some remarks on elastic crack-tip stress fields. *International Journal of Solids and Structures*, 8, 751-758.
- RICE, J. R. & LEVY, N. 1972. The part-through surface crack in an elastic plate. *Journal of Applied Mechanics*, 39, 185-194.
- RUCKA, M. & WILDE, K. 2006. Application of continuous wavelet transform in vibration based damage detection method for beams and plates. *Journal of Sound and Vibration*, 297, 536-550.
- SAADATPOUR, M. M. & AZHARI, M. 1998. The Galerkin method for static analysis of simply supported plates of general shape. *Computers & Structures*, 69, 1-9.
- SAADATPOUR, M. M., AZHARI, M. & BRADFORD, M. A. 2000. Vibration analysis of simply supported plates of general shape with internal point and line supports using the Galerkin method. *Engineering Structures*, 22, 1180-1188.
- SAHA, K. N., MISRA, D., GHOSAL, S. & POHIT, G. 2005. Nonlinear free vibration analysis of square plates with various boundary conditions. *Journal of Sound and Vibration*, 287, 1031-1044.
- SAITO, A., CASTANIER, M. P. & PIERRE, C. 2009. Estimation and veering analysis of nonlinear resonant frequencies of cracked plates. *Journal of Sound and Vibration*, 326, 725-739.
- SANCHEZ, N. E. & NAYFEH, A. H. 1990. Prediction of bifurcations in a parametrically excited duffing oscillator. *International Journal of Non-Linear Mechanics*, 25, 163-176.
- SANDRI, M. 1996. Numerical Calculation of Lyapunov Exponents. *The Mathematica Journal*, 6, 78-84.
- SATHYAMOORTHY, M. 1979. Effects of large amplitude, shear and rotatory inertia on vibration of rectangular plates. *Journal of Sound and Vibration*, 63, 161-167.

- SATHYAMOORTHY, M. 1998. *Nonlinear Analysis of Structures*. CRC Press, Boca Raton FL.
- SHEN, J., LIN, K., CHEN, S. & SZE, K. 2008. Bifurcation and route-to-chaos analyses for Mathieu–Duffing oscillator by the incremental harmonic balance method. *Nonlinear Dynamics*, 52, 403-414.
- SHLYANNIKOV, V. N. & TUMANOV, A. V. 2011. An inclined surface crack subject to biaxial loading. *International Journal of Solids and Structures*, 48, 1778-1790.
- SHOOSHTARI, A. & KHADEM, S. E. 2007. A multiple scale method solution for the nonlinear vibration of rectangular plates. *Scientia Iranica*, 14, 64-71.
- SHU, C., WU, W. X., DING, H. & WANG, C. M. 2007. Free vibration analysis of plates using least-square-based finite difference method. *Computer Methods in Applied Mechanics and Engineering*, 196, 1330-1343.
- SHUFRIN, I., RABINOVITCH, O. & EISENBERGER, M. 2009. Elastic nonlinear stability analysis of thin rectangular plates through a semi-analytical approach. *International Journal of Solids and Structures*, 46, 2075-2092.
- SIH, G. C. 1974. Strain-energy-density factor applied to mixed mode crack problems. *International Journal of Fracture*, 10, 305-321.
- SOLARI, H. G., NATIELLO, M. A. & MINDLIN, G. B. 1996. *Nonlinear Dynamics*. IOP Publishing Ltd, Bristol and Philadelphia.
- SOLECKI, R. 1980. Bending vibration of simply supported rectangular plates with internal rigid support. *International Journal of Engineering Science*, 18, 1309-1318.
- SOLECKI, R. 1983. Bending vibration of a simply supported rectangular plate with a crack parallel to one edge. *Engineering Fracture Mechanics*, 18, 1111-1118.
- SOLECKI, R. 1985. Bending vibration of a rectangular plate with arbitrarily located rectilinear crack. *Engineering Fracture Mechanics*, 22, 687-695.

SRINIVASAN, A.V. 1965. Large-amplitude Free Oscillations of Beams and Plates. *AIAA Journal*, 3(10), 1951–1953.

STAHL, B. & KEER, L. M. 1972. Vibration and Stability of Cracked Rectangular Plates. *International Journal of Solids and Structures*, 8, 69-91.

STANIŠIĆ, M. M. & PAYNE, J. G. 1968. A Rapidly Converging Technique for Vibration Analysis of Plates with a Discrete Mass Distribution. *Archive of Applied Mechanics*, 37(3), 189-195.

STASZEWSKI, W. J. & WORDEN, K. An Overview of Optimal Sensor Location Methods for Damage Detection. *In: RAO, V. S., ed. Smart Structures and Materials 2001: Modeling, Signal Processing, and Control in Smart Structures*, 2001 Newport Beach, CA, USA. 179.

STONESIFER, R. B., BRUST, F. W. & LEIS, B. N. 1993. Mixed-mode stress intensity factors for interacting semi-elliptical surface cracks in a plate. *Engineering Fracture Mechanics*, 45, 357-380.

SZILARD, R. 2004. Theories and applications of plate analysis, *John Wiley & Sons, New York*.

THEOCARIS, P. S., PAZIS, D. & KONSTANTELLOS, B. D. 1986. The exact shape of a deformed internal slant crack under biaxial loading. *International Journal of Fracture*, 30, 135-153.

THOMPSON, J. M. T. & STEWART, H. B. 2002. *Nonlinear Dynamics and Chaos*, 2nd ed. John Wiley & Sons, UK.

THOMSEN, J. J. 1997. *Vibrations and Stability – Order and Chaos*, McGrawHill, UK.

THOMSEN, J. J. 2003. *Vibrations and Stability: Advanced theory, analysis, and tools*. 2nd ed. Berlin, Germany: Springer. 225-284.

TIMOSHENKO, S. P. 1921. On the Correction for Shear of the Differential Equation for Transverse Vibrations of Prismatic Bars. *Philosophical Magazine*, 41, 744-746.

- TIMOSHENKO, S. P. & WOINOWSKY-KRIEGER, S. 1959. Theory of plates and shells, *New York, McGraw-Hill*.
- TOMAR, J. S. 1962. On flexural vibrations of isotropic elastic thin square plates according to Mindlin's theory. 29 (2), 169-179.
- TRENDAFILOVA, I. 2005(a). A Study on Vibration-Based Damage Detection and Location in an Aircraft Wing Scaled Model. *Applied Mechanics and Materials, Trans. Tech. Publications, Switzerland*, 3-4, 309-314.
- TRENDAFILOVA, I. 2005(b). An Investigation on Vibration-based Damage Detection in an Aircraft Wing Scaled Model. *Key Engineering Materials*, 293-294, 321-328.
- TRENDAFILOVA, I. 2006. Vibration-based damage detection in structures using time series analysis. *Proceedings of the Institution of Mechanical Engineers, Part C: Journal of Mechanical Engineering Science*, 220, 261-272.
- TRENDAFILOVA, I., CARTMELL, M. P. & OSTACHOWICZ, W. 2008. Vibration-based damage detection in an aircraft wing scaled model using principal component analysis and pattern recognition. *Journal of Sound and Vibration*, 313, 560-566.
- TRENDAFILOVA, I. & MANOACH, E. 2008. Vibration based damage detection in plates by using time series analysis. *Mechanical Systems and Signal Processing*, 25, 1092-1106.
- UGURAL, A. C. 1999. Stresses in Plates and Shells. 2nd ed. *McGraw-Hill*.
- VAN DER POL, B. & VAN DER MARK, J. 1927. Frequency Demultiplication. *Nature*, 120, 363-364.
- VENDHAN, C. P. 1975. A study of Berger equations applied to nonlinear vibrations of elastic plates. *International Journal of Mechanical Sciences*, 17, 461-468.
- VON KARMAN, T. 1910. Festigkeitshprobleme im Maschinenbau. *Encyklopadie der Mathematischen Wissenschaften IV*, 349.
- WAH, T. 1963. Large amplitude flexural vibration of rectangular plates. *International Journal of Mechanical Sciences*, 5, 425-438.

- WANG, F.-Y. 1990. Monte carlo analysis of nonlinear vibration of rectangular plates with random geometric imperfections. *International Journal Solids Structures*, 25, 99-109.
- WANG, L. & CHAN, T. H. T. 2009. Review of Vibration-Based Damage Detection and Condition Assessment of Bridge Structures using Structural Health Monitoring. In: The Second Infrastructure Theme Postgraduate Conference: Rethinking Sustainable Development: Planning, Engineering, Design and Managing Urban Infrastructure, Queensland University.
- WANG, Y. & WANG, Z.-M. 2008. Transverse vibration of viscoelastic rectangular plate with linearly varying thickness and multiple cracks. *Journal of Sound and Vibration*, 318, 1005-1023.
- WANG, Z.-M., WANG, Y. & ZHOU, Y.-F. 2008. Dynamic Stability of Cracked Viscoelastic Rectangular Plate Subjected to Tangential Follower Force. *Journal of Applied Mechanics*, 75, 1-12.
- WANG, Z., WANG, Y. & GUO, X. 2009. Dynamic stability of linearly varying thickness viscoelastic rectangular plate with crack and subjected to tangential follower force. *Applied Acoustics*, 70, 845-856.
- WARBURTON, G. B. The vibration of rectangular plates. *Proceedings of the Institution of Mechanical Engineers*, 1954. 371-384.
- WILLIAMS, J. G. & EWING, P. D. 1984. Fracture under complex stress — The angled crack problem. *International Journal of Fracture*, 26, 346-351.
- WOLF, A., SWIFT, J. B., SWINNEY, H. L. & VASTANO, J. A. 1985. Determining Lyapunov exponents from a time series. *Physica D: Nonlinear Phenomena*, 16, 285-317.
- WU, B. & ERDOGAN, F. 1993. Fracture mechanics of orthotropic laminated plates—III. The surface crack problem. *International Journal of Solids and Structures*, 30, 2393-2406.
- WU, D. & LAW, S. S. 2004a. Anisotropic damage model for an inclined crack in thick plate and sensitivity study for its detection. *International Journal of Solids and Structures*, 41, 4321-4336.

- WU, D. & LAW, S. S. 2004b. Damage-detection-oriented model for a cracked rectangular plate. *Smart Structures and Materials*, 5391, 470-481.
- WU, D. & LAW, S. S. 2004c. Damage localization in plate structures from uniform load surface curvature. *Journal of Sound and Vibration*, 276, 227-244.
- WU, J. H., LIU, A. Q. & CHEN, H. L. 2007. Exact solutions for free-vibration analysis of rectangular plates using Bessel functions. *Journal of Applied Mechanics*, 74, 1247-1251.
- WU, G. Y. & SHIH, Y. S. 2005. Dynamic Instability of Rectangular Plate with an Edge Crack. *Computers and Structures*, 84, 1-10.
- XIAO, Y. -G., FU, Y.-M. & ZHA, X.-D. 2006. Bifurcation and Chaos of Rectangular Moderately Thick Cracked Plates on an Elastic Foundation Subjected to Periodic Load Chaos. *Solitons and Fractals*, 35, 460-465.
- XING, Y. & LIU, B. 2009a. Characteristic equations and closed-form solutions for free vibrations of rectangular mindlin plates. *Acta Mechanica Solida Sinica*, 22, 125-136.
- XING, Y. & LIU, B. 2009b. New exact solutions for free vibrations of rectangular thin plates by symplectic dual method. *Acta Mechanica Sinica*, 25, 265-270.
- YAMAKI, N. 1961. Influence of Large Amplitudes on Flexural Vibrations of Elastic Plates. *ZAMM-Journal of Applied Mathematics and Mechanics*, 41, 501-510.
- YAN, Y. J. & YAM, L. H. 2002. Online detection of crack damage in composite plates using embedded piezoelectric actuators/sensors and wavelet analysis. *Composite Structures*, 58, 29-38.
- YANG, C. Y. 1988. Line spring method of stress-intensity factor determination for surface cracks in plates under arbitrary in-plane stresses. Fracture mechanics: Nine-teenth symposium, ASTM STP, American Society for testing and materials, Philadelphia, 657-668.
- YE, L., LIN, Y. & ZHONGQING, S. 2006. Crack identification in aluminium plates using Lamb wave signals of a PZT sensor network. *Smart Materials and Structures*, 15, 839-849.

- YEH, F. H. & LIU, W. H. 1991. Nonlinear analysis of rectangular orthotropic plates. *International Journal of Mechanical Sciences*, 33, 563-578.
- YEH, H.-Y. & KIM, C. H. 1995. Fracture mechanics of the angled elliptic crack under uniaxial tension. *Engineering Fracture Mechanics*, 50, 103-110.
- YONG-GANG, X., YI-MING, F. & XU-DONG, Z. 2005. Nonlinear vibration for moderate thickness rectangular cracked plates including coupled effect of elastic foundation. *Applied Mathematics and Mechanics*, 26, 963-972.
- ZENG, Z. -J. & DAI, S. H. 1993. A new method of analyzing surface cracks. *Applied Mathematics and Mechanics*, 14, 787-792.
- ZENG, Z. -J. & DAI, S. H. 1994. Stress intensity factors for an inclined surface crack under biaxial stress state. *Engineering Fracture Mechanics*, 47, 281-289.
- ZHOU, D. & JI, T. 2006. Free vibration of rectangular plates with continuously distributed spring-mass. *International Journal of Solids and Structures*, 43, 6502-6520.
- ZHOU, L. & ZHENG, W. X. 2006. Moving least square Ritz method for vibration analysis of plates. *Journal of Sound and Vibration*, 290, 968-990.
- ZHU, Q. & WANG, X. 2011. Free vibration analysis of thin isotropic and anisotropic rectangular plates by the discrete singular convolution algorithm. *International Journal for Numerical Methods in Engineering*, 86, 782-800.

Publications

The work presented in this thesis has led to the following publications:

ISMAIL, R. & CARTMELL, M. P. 2012. An investigation into the vibration analysis of a plate with a surface crack of variable angular orientation. *Journal of Sound and Vibration*, 331, 2929-2948.

RAINAH ISMAIL & CARTMELL, M. P. 2012. An analysis of the effects of the orientation angle of a surface crack on the vibration of an isotropic plate. *Journal of Physics: Conference Series* 382 012007.

Appendices

Appendix A

i. EQUATION OF MOTION -CHAPTER 3(Equation 3.88)

$$\begin{aligned}
 & \psi''_{ij}[t] + 2\mu \varphi'_{ij}[t] + (1/((\rho * h)/D1) \sum_{j=1}^1 \sum_{i=1}^1 A_{i,j} \int_0^{11} \int_0^{12} ((Xi)^2 * (Yj)^2) dx dy) \\
 & \sum_{j=1}^1 \sum_{i=1}^1 A_{i,j} \int_0^{11} \int_0^{12} \left((Xi^4 * Yj) + (2 * Xi^2 * Yj^2) + (Yj^4 * Xi) - \right. \\
 & \left. \left(\frac{a (1 + \cos[2 * \beta]) (v * Xi^2 * Yj^2 + Yj^4 * Xi)}{3 \left(\frac{\alpha_{bt}}{6} + \alpha_{bb} \right) (3 + v) (1 - v) h + 2 a} \right) - \right. \\
 & \left. \left(\frac{2 * a \sin[2 * \beta] (v * Xi^3 * Yj1 + Yj3 * Xi1)}{3 \left(\frac{c_{bt}}{6} + c_{bb} \right) (1 + v) h + 2 a} \right) \right) (Xi * Yj) dx dy \\
 & \left. \right)^2 \varphi_{ij}[t] + \\
 & (1/((\rho * h)/D1) \sum_{j=1}^1 \sum_{i=1}^1 A_{i,j} \int_0^{11} \int_0^{12} ((Xi)^2 * (Yj)^2) dx dy) \\
 & \sum_{i=1}^1 \sum_{j=1}^1 A_{i,j}^3 \left(\int_0^{11} \int_0^{12} \left(\left(- \left(\frac{6}{h^2 * 11 * 12} \right. \right. \right. \right. \\
 & \left. \left. \left. \left(\sum_{i=1}^1 \sum_{j=1}^1 \int_0^{11} \int_0^{12} ((Xi1)^2 * (Yj)^2) + (v * (Yj1)^2 * (Xi)^2) \right) dx dy \right) \right) \right) \\
 & \left. * (Xi2) * (Yj) \right) + \\
 & \left(\left(a (1 + \cos[2 * \beta]) * \left(\frac{6}{h^2 * 11 * 12} \right. \right. \right. \right. \\
 & \left. \left. \left. \left(\sum_{i=1}^1 \sum_{j=1}^1 \int_0^{11} \int_0^{12} ((Yj1)^2 * (Xi)^2) + (v * (Xi1)^2 * (Yj)^2) \right) dx dy \right) \right) \right) \\
 & \left. / ((6 * \alpha_{tb} + \alpha_{tt}) (1 - v^2) h + 2 a) * (Yj2) (Xi) \right) + \\
 & \frac{2 a \sin[2 * \beta]}{(6 * c_{tb} + c_{tt}) (1 + v) h + 2 a} \\
 & \left(\frac{6}{h^2 * 11 * 12} \right. \\
 & \left. \left(\sum_{i=1}^1 \sum_{j=1}^1 \int_0^{11} \int_0^{12} ((Yj1)^2 * (Xi)^2) + (v * (Xi1)^2 * (Yj)^2) \right) dx dy \right) \\
 & \left. * Xi1 * Yj1 \right) (Xi * Yj) dx dy \\
 & \left. \right) \varphi_{ij}^3[t] \\
 & = ((X_i Y_j) / ((\rho * h)/D1) \sum_{j=1}^1 \sum_{i=1}^1 A_{i,j} \int_0^{11} \int_0^{12} ((Xi)^2 * (Yj)^2) dx dy) / D1) q \cos \Omega_{ij}[t]
 \end{aligned}$$

ii. DIRECT INTEGRATION METHOD- SECTION 4.3

```
eqn =  $\psi_{ij}''[t] + \mu * \psi_{ij}' + (\text{Subscript}[\omega, ij])^2 * \psi[t] + \gamma_{ij} * \psi_{ij}^3[t] - \eta_{ij}/D1 * \cos \Omega_{ij}[t]$ 
```

```
Solution=NDSolve[{eqn==0,  $\psi[0]==0, \psi'[0]==0$ },  $\psi[t]$ , {t, 0, 500},  
MaxSteps->Infinity, AccuracyGoal->Automatic,  
PrecisionGoal->Automatic]
```

```
Plot[Evaluate[ $\psi[t]$ /.Solution], {t, 0, 500},  
Frame->True, FrameTicks->Automatic,  
FrameLabel->{Time[t],  $\psi[m]$ }]
```

```
Plot[Evaluate[ $\psi'[t]$ /.Solution], {t, 0, 500},  
Frame->True, FrameTicks->Automatic,  
FrameLabel->{Time[t],  $\psi'[m]$ }]
```

iii. BIFURCATION DIAGRAM - SECTION 5.6

```
M=3000000; step=0.00001; MaxAmp=M*step; a=0; b=0;  
For[i=1, i<=M, i++, A=step*i; pp=NDSolve[  
{ $x'[t]==y[t], y'[t]==-C2*x[t]-C1*y[t]-C3*(x[t])^3+A$   
 $\cos[\omega t]$ ,  
 $x[0]==a, y[0]==b$ }, {x, y}, {t, 0, 2  
Pi/omega}, MaxSteps->Infinity];  
a=Flatten[x[2 Pi/omega] /. pp];  
b=Flatten[y[2 Pi/omega] /. pp]; rampup[i]=Sqrt[a^2]]  
  
p1=ListPlot[Table[Flatten[{m*step, rampup[m]}], {m, 1, M}],  
PlotStyle->PointSize[0.003]];  
Show[{p1}, PlotRange->{{0, 30}, {-0.0001, 0.005}},  
AxesLabel->{"Rho", "x"}, AxesOrigin->{0, -0.0001},  
TextStyle->{FontSize->12}, Ticks->Automatic]  
Quit[];
```

```
Duffing=NDSolve[  
{ $x'[t]==y[t], y'[t]==-C2*x[t]-C1*y[t]-C3*(x[t])^3 + A$   
 $\cos[\omega*t]$ ,  
 $x[0]==0, y[0]==0$ }, {x[t], y[t]}, {t, 0, 500}, MaxSteps->Infinity];
```

iv. PLOTTING OF POINCARÉ MAP - SECTION 5.7

```
ParametricPlot[Evaluate[{x[t],y[t]}/.Duffing],{t,495.5,500},  
FrameLabel→{ x, y},AspectRatio→ 1/2,AxesOrigin→{-0.005,-  
0.4},  
Frame→True,PlotRange→{{-0.005,0.005},{-0.4,0.4}},  
LabelStyle→Directive[FontFamily→"Times New Roman",12]]
```

v. PLOTTING OF PHASE PLANE- SECTION 5.7

```
ListPlot[Table[Flatten[{x[t],y[t]}/.Duffing],{t,495.5,500}],  
PlotStyle→PointSize[0.02],FrameLabel→{x, y},  
AxesOrigin→{-0.005,-1.5},Frame→True,  
PlotRange→{{-0.005,0.005},{-1.5,1.5}},  
LabelStyle→Directive[FontFamily→"Times New Roman",12]]
```

vi. PLOTTING OF TIME PLOT- SECTION 5.7

```
Plot[Evaluate[x[t]/.Duffing],{t,495.5,500},  
FrameLabel→{ "Time(t)",x},  
LabelStyle→Directive[FontFamily→"Times New Roman",12],  
Frame→True,PlotRange→{{495.5,500},{-0.01,0.01}},  
AxesOrigin→{495.5,-0.01}]
```

Appendix B

Experimental Measurement: List of Instruments

The list of instruments used in this research is:

- Power Amplifier- LDS PA25E-CE
- Electro-dynamic Exciter- LING Dynamics Systems LTD Model 201
- 1D Laser Vibrometer (Polytech OFV 303)
- Vibrometer Controller (Polytech OFV 3001: 100/115/230v- 50/60Hz)
- Mirror
- Force Transducer IEPE (B&K 8230)
- Signal Analyser (Quattro)
- Desktop PC using Signal Calc ACE data acquisition software, Data Physics Corp.



(a) Power Amplifier



(b) Electro-dynamics Exciter



(c) 1D Laser Vibrometer



(d) Vibrometer Controller



(e) Force Transducer



(f) Signal Analyser



(g) Computer

Figure B1: Schematic view of the instruments used